

# **Towards the Development of Processable Molecular Imprinted Polymers**

**Azrinawati Mohd Zin**

**MSc. (Chemistry)**

School of Environmental and Life Sciences  
Faculty of Science and Information Technology



**Doctor of Philosophy (Chemistry)**  
February 2015

## Declaration

The thesis contains no material which has been accepted for the award of any other degree or diploma in any university or other tertiary institution and, to the best of my knowledge and belief, contains no material previously published or written by another person, except where due reference has been made in the text. I give consent to the final version of my thesis being made available worldwide when deposited in the University's Digital Repository, subject to the provisions of the Copyright Act 1968.

.....

Azrinawati Mohd Zin

## Dedication

*This thesis is dedicated to my beloved mom.*

## Acknowledgements

All my gratitude and praise goes to Allah, the Almighty, for giving me the strength and His blessing to accomplish this work. This thesis would not have been made possible without the great help of the following people.

First and foremost, I would like to express my deepest gratitude to my supervisors, Prof. Erica Wanless and Dr. Clovia Holdsworth for their guidance, support and encouragement throughout my PhD research work. My heartfelt thanks go to them for their patience and understanding.

I am very thankful for the generous help that I received from the staff members in Chemistry. In particular, I wish to thank Prof. Scott Donne for his generous assistance in getting the BET and BJH data. My thanks also go to Dr. Monica Rossignoli for her invaluable help in NMR as well as Vicki Thompson and Carolyn Freeburn for their continuous assistance in the laboratories. I would also like to thank Dr. Grant Webber for allowing me access to the Zetasizer Nano instrument and Dave Phelan for his kind help in taking the SEM images.

My sincere thanks go to all my friends, group mates and colleagues for their friendship and support: Anang, Sunsan, Edwin, Delfin, Tim, Kate W, Frem, Yuhanis, Diana, Hanadi, Purnama, Azadeh, Yaser, Ahmed and Nor. My special thanks go to Anna and Zara for their endless advice and encouragement.

I wish to thank the Malaysian government for awarding me the scholarship that made the present research possible in the first place and the University of Newcastle for giving me a completion scholarship.

Finally, I would like to thank my family, especially my mother, father, sisters, brothers and not to forget my parents in law for their love, support and encouragement that keeps me going. Special thanks and loves go to my children: Sheereen, Faris and Syameel, who are my greatest source of strength and inspiration.

## Publication

Lim, K. F., Zin, A. M., Romano, E., Wanless, E. J., Holdsworth, C. I. Advances and Challenges in the Design and Synthesis of Molecularly Imprinted Microspheres. In *Molecularly Imprinted Catalyst: Principles, Syntheses and Applications*, Li, S. J., Cao, S. S., Piletsky, S. A., Turner A. P. F., Ed. Elsevier: Amsterdam, 2015; pp 55 – 77.

## Abstract

The synthesis of processable core crosslinked star (CCS) polymers via iniferter and RAFT mediated radical polymerisation has been investigated for their potential application in the field of molecular recognition. Molecular imprinted CCS polymers have potential as delivery systems in solution and, by virtue of its improved processability, may be used to produce thin films with recognition capability for sensing applications.

Synthesis of CCS polymers, consist of poly(ethylene glycol dimethacrylate) core and polystyrene (PS) arms, via the arm-first method proved to be more straightforward than the core-first method. The length of the PS arm could be controlled by varying the ratio of styrene monomer to the iniferter or RAFT agent and polymerisation time. Although lower polydispersity (PDI) of PS arms were produced via RAFT (PDI values between 1.2 – 1.6) compared to those of the iniferter (PDI values between 1.8 – 12.2), synthesis of arm-first CCS polymers via iniferter was more successful than RAFT. Synthesis of CCS polymers via the core-first method was deemed more suitable for the preparation of molecular imprinted CCS since the imprinted core can be accessed for a more comprehensive characterisation and, unlike the CCS via arm-first, there is no contamination from unreacted PS arms.

CCS molecular imprinted polymers (MIPs) were synthesised employing the core-first method. The molecular imprinted microspheric cores were prepared using methacrylic acid as functional monomer and ethylene glycol dimethacrylate as crosslinker at various concentrations of iniferter/RAFT (i.e. 5, 10 and 20 mol % with respect to the total monomer) in the presence of benzylpiperazine (BZP) as template. The large difference in size between the MIPs and their NIP counterparts, which translated to a large difference in the specific surface areas of the microspheres, has implications on the assessment of binding efficiency generally normalised against NIPs with respect to mass. Therefore, the binding efficiency of the MIPs was also expressed with respect to specific surface area. Among the formulations, MIP microspheres prepared with 5% BDDC and MCEBTTC exhibited the best binding performance in their respective series,

with BDDC MIP cores exhibiting higher binding capacity and greater specific binding compared to the RAFT MIPs. Further investigation revealed that the 5%BDDC MIP exhibited higher maximum number of binding sites ( $N$ ) and greater high affinity binding sites (about 90% and 2.5-fold higher, respectively) as well as stronger affinity towards the BZP template (lower  $K_d$  value) compared to those of the 5%RAFT MIP.

Selectivity studies were carried out on the 5%BDDC MIP against 1-phenylpiperazine (PHP) and (1R,2S)-(-)-ephedrine (EPH) having closely related structures to that of BZP. The MIP exhibited better selectivity towards BZP over PHP but better selectivity towards EPH over BZP in the non-competitive binding environment. In the competitive binding environments, the MIP exhibited better selectivity towards BZP over PHP but showed equivalent selectivity towards both BZP and EPH, which was attributed to the smaller size and stronger hydrogen bonding ability of EPH compared to BZP.

Several fractions of CCS MIPs, which differ in their degree of dispersibility in THF, were obtained when polystyrene (PS) arms were grafted to 5%BDDC MIP. Our results show that dispersibility improved with increasing arm length, although it did not necessarily contribute to better binding performance. The presence of PS arms around the imprinted core resulted in a decrease in binding capacity of the CCS MIPs compared to the core precursor in acetonitrile, a bad solvent for the arm. Similar results are obtained in THF, a good solvent for the PS arm. However, contrary to the binding results in acetonitrile where binding capacity seemed to decrease with increasing arm length, greater binding capacity was exhibited by the CCS MIPs with longer arms than those with shorter arms in THF. In this study, we have demonstrated that processability of MIP microspheres can be readily introduced by attaching linear polymeric arms. However, it was difficult to obtain comprehensive binding assessment using the conventional comparison of the MIP with the NIP due to the presence of difference number and/or arm length around the CCS polymers.

## Table of Contents

<b>Declaration</b>	<b>ii</b>
<b>Dedication</b>	<b>iii</b>
<b>Acknowledgements</b>	<b>iv</b>
<b>Publication</b>	<b>v</b>
<b>Abstract</b>	<b>vi</b>
<b>Table of Contents</b>	<b>viii</b>
<b>List of Tables</b>	<b>xiv</b>
<b>List of Figures</b>	<b>xvi</b>
<b>List of Schemes</b>	<b>xxi</b>
<b>Chapter 1 Introduction</b>	<b>1</b>
1.1 Star Polymers	1
1.2 Star Polymer Synthesis	2
1.2.1 Arm-first method	3
1.2.1.1 General Characteristics	3
1.2.1.2 Macroinitiator Approach	4
1.2.1.3 Macromonomer Method	6
1.2.2 Core-first Method	8
1.3 Reversible-Deactivation Radical Polymerisation	10
1.3.1 Atom Transfer Radical Polymerisation	11
1.3.2 Iniferter	14
1.3.3 Reversible Addition-Fragmentation Chain Transfer	19
1.4 CCS Polymer Applications	23

1.4.1	Molecular Imprinting	23
1.5	Project Outline	31
<b>Chapter 2 Core Crosslinked Star Polymers Via a Photoiniferter</b>		<b>33</b>
2.1	Introduction	33
2.2	Experimental	34
2.2.1	Materials	34
2.2.2	Synthesis of BDDC Iniferter	34
2.2.3	Preparation of CCS Polymers via Arm-First	35
2.2.3.1	Synthesis of PS Arm using BDDC Iniferter	35
2.2.3.2	Preparation of Arm-first CCS Polymers	36
2.2.4	Preparation of CCS Polymers via Core-first	36
2.2.4.1	Synthesis of PEGDMA Core using BDDC Iniferter	36
2.2.4.2	Preparation of Core-first CCS Polymers	37
2.3	Characterisation	37
2.3.1	Nuclear Magnetic Resonance	37
2.3.2	Fourier Transform Infrared	37
2.3.3	Gel Permeation Chromatography	37
2.3.4	Dynamic Light Scattering	40
2.3.5	Scanning Electron Microscopy	40
2.4	Results and Discussion	41
2.4.1	Arm-First CCS Polymers via Iniferter	41
2.4.1.1	Preparation of Linear PS Arm Precursor	42
2.4.1.2	PS-DDC End-Group Analysis	43
2.4.1.3	Effect of Monomer to Iniferter Ratio	48
2.4.1.4	Effect of Polymerisation Time	52
2.4.1.5	Arm-first CCS Polymers	54
2.4.1.6	Structural Confirmation and Morphology of CCS Polymers	54
2.4.1.7	Effect of Polymerisation Time	57
2.4.1.8	Effect of EGDMA to PS Arm Ratio	61
2.4.1.9	Effect of Concentration and MW of PS Arm	64

2.4.1.10 Summary	69
2.4.2 Core-first CCS Polymers via Iniferter	70
2.4.2.1 Preparation of PEGDMA Core Precursor	70
2.4.2.2 Core-first CCS Polymers	72
2.4.3 Transmission Electron Microscope	76
2.5 Conclusions	76
<b>Chapter 3 Core Crosslinked Star Polymers Via RAFT</b>	<b>78</b>
3.1 Introduction	78
3.2 Experimental	79
3.2.1 Materials	79
3.2.2 Synthesis of RAFT agent	79
3.2.2.1 Preparation of CCS Polymers via Arm-First	80
3.2.2.2 Synthesis of PS Arm using MCEBTTC RAFT Agent	80
3.2.2.3 Preparation of Arm-first CCS Polymers	81
3.2.3 Preparation of CCS Polymers via Core-First	81
3.2.3.1 Synthesis of PEGDMA Core using MCEBTTC RAFT Agent	81
3.2.3.2 Preparation of Core-First CCS Polymers	82
3.3 Characterisation	82
3.4 Results and Discussion	82
3.4.1 Arm-First CCS Polymers via RAFT	82
3.4.1.2 Preparation of Linear PS Arm Precursor	83
3.4.1.3 PS-TTC End Group Analysis	83
3.4.1.4 Effect of Solvent	87
3.4.1.5 Effect of Monomer to RAFT Agent Ratio	90
3.4.1.6 Arm-first CCS Polymers	96
3.4.1.7 Structural Confirmation of Arm-First CCS Polymers	97
3.4.1.8 Preparation of Arm-First CCS Polymers via RAFT	99
3.4.2 Core-first CCS Polymers via RAFT	101
3.4.2.1 Preparation of PEGDMA Core Precursor	102
3.4.2.2 Core-First CCS Polymers	103

3.4.3	Comparison between RAFT and Iniferter Polymerisation	108
3.5	Conclusion	109
<b>Chapter 4 Reactive MIP Microspheres</b>		<b>111</b>
4.1	Introduction	111
4.2	Experimental	114
4.2.1	Materials	114
4.2.2	Synthesis of MIP Microspheres	115
4.2.2.1	Iniferter Method	115
4.2.2.2	RAFT Method	116
4.2.3	Template extraction	117
4.2.4	Batch Rebinding Studies	117
4.2.4.1	Optimum Binding Time	119
4.2.4.2	Binding Isotherms	120
4.2.5	Selectivity Studies	121
4.2.6	Surface Area and Porosity	124
4.2.7	Other Characterisation Methods	126
4.2.7.1	FTIR	126
4.3	Results and Discussion	127
4.3.1	MIP Design and Synthesis	127
4.3.1.1	Choice of Functional Monomer	128
4.3.1.2	Choice of Crosslinker	130
4.3.1.3	Choice of Porogenic Solvent	131
4.3.2	Molecular imprinted Polymers by the Iniferter Method	131
4.3.2.1	Synthesis and Physical Characterisation	131
4.3.2.2	Binding Performance	138
4.3.2.2.1	Optimum Binding Time	139
4.3.2.2.2	Binding Isotherm Studies	141
4.3.2.2.3	Effect of Iniferter Concentration	150
4.3.2.2.4	Effect of solvent	155
4.3.3	Molecular imprinted Polymers by RAFT	158

4.3.3.1	Synthesis and Physical Characterisation	158
4.3.3.2	Binding Performance	163
4.3.3.2.1	Optimum Binding Time	164
4.3.3.2.2	Binding Isotherm Studies	166
4.3.3.2.3	Effect of RAFT Agent Concentration	172
4.3.3.2.4	Effect of Solvent	176
4.3.4	Comparison between Microspheres Prepared via Iniferter and RAFT	178
4.3.5	Selectivity Studies	183
4.3.6	Non-competitive and Competitive Binding Experiment	183
4.4	Summary	192
<b>Chapter 5 Core Crosslinked Star Molecular imprinted Polymers</b>		<b>194</b>
5.1	Introduction	194
5.2	Experimental	196
5.2.1	Materials	196
5.2.2	CCS MIP Synthesis	196
5.2.3	Characterisation of CCS MIP	200
5.2.3.1	FTIR	200
5.2.4	CCS MIP Composition by FTIR Analysis	200
5.2.5	Determination of $M_n$ of PS Arm by $^1\text{H}$ NMR	203
5.2.6	Batch Rebinding Studies	203
5.3	Results and Discussion	203
5.3.1	Preparation and Characterisation of CCS MIPs and NIPs	203
5.3.1.1	Preparation of CCS MIPs/NIPs	203
5.3.1.2	Particle Size Analysis by SEM and DLS	204
5.3.1.3	FTIR Analysis	207
5.3.1.4	$^1\text{H}$ NMR Analysis.	211
5.3.1.5	Structural Analysis	216
5.3.2	Batch rebinding studies	218
5.4	Conclusion	226

<b>Chapter 6 Summary and Recommendations</b>	<b>227</b>
6.1 Summary of Results	227
6.2 Recommendations for Future Work	231
<b>References</b>	<b>233</b>

## List of Tables

Table 2.1. Photopolymerisation of styrene using various St to BDDC mole ratios. <sup>a</sup>	48
Table 2.2. Relationship between [St]:[BDDC] ratio and molecular weight of PS arm. <sup>a</sup>	51
Table 2.3. Effect of reaction time on the molecular weight of PS arm. <sup>a</sup>	53
Table 2.4. Formation of CCS polymers from iniferter polymerisation at various polymerisation times. <sup>a</sup>	59
Table 2.5. Formation of CCS polymers from iniferter polymerisation at various [EGDMA]:[PS arm] ratios. <sup>a</sup>	63
Table 2.6. Formation of CCS polymers from iniferter polymerisation at various PS arm concentrations. <sup>a</sup>	67
Table 3.1. Influence of solvent on the molecular weight and conversion of PS arm prepared via RAFT. <sup>a</sup>	89
Table 3.2. Relationship between [St]:[RAFT] ratio and molecular weight of PS arm at [RAFT]:[AIBN] = 1:0.01. <sup>a</sup>	92
Table 3.3. Relationship between [St]:[RAFT] ratio and molecular weight of PS arm. <sup>a</sup>	94
Table 3.4. Relationship between [St]:[RAFT] ratio and molecular weight of PS arm at increasing concentration of AIBN with ratio. <sup>a</sup>	95
Table 3.5. Experimental data for preparation of arm-first CCS polymers via RAFT. <sup>a</sup>	100
Table 3.6. Comparison between RAFT and Iniferter Polymerisation of Styrene.	109
Table 4.1. Physical characteristics of the BZP-imprinted polymer microspheres and the NIP prepared by precipitation polymerisation using BDDC iniferter.	136
Table 4.2. Equilibrium dissociation constant ( $K_d$ ) and maximum number of binding sites ( $N$ ) estimated from the binding isotherm (Figure 4.9), and derived from the Langmuir (Figure 4.10) and Scatchard (Figure 4.11) plots for the MIP and NIP prepared using 5% BDDC in acetonitrile.	144
Table 4.3. BZP binding capacity ( $S_B$ ), specific binding ( $\Delta S_B$ ) and imprinting factor (IF) values of microspheres prepared using 5%, 10% and 20% BDDC after 2 hr of contact time in acetonitrile and THF.	151
Table 4.4. Physical characteristics of the BZP-imprinted polymer microspheres and the corresponding NIPs prepared by precipitation polymerisation using RAFT agent.	160
Table 4.5. Equilibrium dissociation constant ( $K_d$ ) and number of binding site ( $N$ ) extracted from the binding isotherm (Figure 4.17), and derived from the Langmuir	

(Figure 4.18) and Scatchard (Figure 4.19) plots for the MIP and NIP prepared using 5% RAFT in acetonitrile.	168
Table 4.6. BZP binding capacity ( $S_B$ ), specific binding ( $\Delta S_B$ ) and imprinting factor (IF) values of microspheres prepared using 5%, 10% and 20% RAFT agent, after 2 hr of contact time in acetonitrile and THF.	173
Table 4.7. Physical characteristics of the BZP-imprinted polymer microspheres and the corresponding NIPs prepared by precipitation polymerisation using BDDC iniferter and MCEBTTC RAFT agent (extracted from Tables 4.1, 4.3, 4.4 and 4.6).	180
Table 4.8. Comparison between the binding dissociation constant ( $K_d$ ) and maximum binding capacity ( $N$ ) normalised with respect to the surface area of the microspheres prepared via iniferter and RAFT	181
Table 4.9. Binding capacity ( $S_B$ ), specific binding $\Delta S_B$ , imprinting factor (IF) and standardised specific selectivity factor (SSF) values normalised with respect to mass in a single-analyte, binary-analyte and tertiary-analyte binding assays of BZP imprinted polymer prepared via iniferter. <sup>a</sup>	185
Table 4.10. Binding capacity ( $S_B$ ), specific binding $\Delta S_B$ , imprinting factor (IF) and standardised specific selectivity factor (SSF) values normalised with respect to surface area in a single-analyte, binary-analyte and tertiary-analyte binding assays of BZP imprinted polymer prepared via iniferter. <sup>a</sup>	186
Table 5.1. Physical characteristics of CCS imprinted and non-imprinted polymers versus the core microspheres.	207
Table 5.2. Proposed dominant structures within the CCS MIP and NIP fractions.	217
Table 5.3. Binding capacities of the CCS MIP and NIP fractions compared to their corresponding core precursors.	218

## List of Figures

Figure 1.1. Schematic diagrams of a (A) homoarm and (B) miktoarm or heteroarm star polymers.	1
Figure 1.2. General structure of a RAFT agent.	19
Figure 1.3. General principle of molecular imprinting.	24
Figure 2.1. An example of a polystyrene calibration curve used for the molecular weight (MW) determination.	39
Figure 2.2. Deconvolution of a GPC curve (CCS-I6, Table 2.4) carried out using the Solver function in Microsoft Excel 2010. G1 and G2 represent the high and low MW polymers, respectively. The solid blue (height) and the black dashed (Y) lines are the measured and fitted GPC curves, respectively.	40
Figure 2.3. FTIR spectrum of linear PS prepared via BDDC iniferter.	44
Figure 2.4. A typical $^1\text{H}$ NMR spectrum of a living linear PS arm prepared via BDDC iniferter. Numbers and letters refer to the end groups and backbone protons, respectively.	45
Figure 2.5. A typical $^{13}\text{C}$ NMR spectrum of a living linear PS arm prepared via iniferter. X denotes peak attributed to $\text{CDCl}_3$ .	46
Figure 2.6. UV-GPC traces of (A) synthesised PS and (B) commercial PS ( $M_n = 3.7$ and 10.5 kDa, respectively).	47
Figure 2.7. Relationship between percent conversion of St and mole ratio of St to BDDC as well as resultant molecular weight ( $M_n$ ) of PS (polymerisation time: 3 h).	49
Figure 2.8. GPC traces of PS arms as a function of different $[\text{St}]:[\text{BDDC}]$ ratios.	50
Figure 2.9. GPC traces of PS arms as a function of different irradiation time.	52
Figure 2.10. $M_n$ -conversion relation for bulk polymerisation of St with BDDC iniferter.	53
Figure 2.11. FTIR spectra of (A) a CCS polymer and (B) the corresponding PS arm precursor.	55
Figure 2.12. $^1\text{H}$ NMR spectrum of a typical arm-first CCS polymer prepared via iniferter.	56
Figure 2.13. SEM and TEM images of arm-first CCS polymers prepared via iniferter: (A and B) and (C and D) respectively. A and C were recorded at 5000X magnification whereas C and D were recorded at 20000X magnification.	57

Figure 2.14. GPC traces of CCS polymers obtained at various polymerisation times compared with that of the PS arm precursor.	58
Figure 2.15. GPC traces of CCS polymers obtained from the polymerisation at various [EGDMA]:[PS arm] ratios.	62
Figure 2.16. GPC traces of CCS polymers obtained from the polymerisation at various PS arm concentrations compared with that of the linear PS arm precursor (PS-I17).	65
Figure 2.17. FTIR spectrum of a PEGDMA core synthesised using BDDC iniferter.	72
Figure 2.18. FTIR spectrum of (A) a core precursor and (B) the corresponding core-first CCS polymer prepared using BDDC iniferter.	73
Figure 2.19. <sup>1</sup> H NMR spectrum of a core-first CCS polymer prepared using BDDC iniferter. X denotes contaminant peak attributed to THF.	74
Figure 2.20. SEM images of (A) a core-first CCS polymer and (B) the corresponding core precursor. A and B were recorded at 10000X and 15000X magnifications respectively.	75
Figure 3.1. Methyl 2-(butylthiocarbonothioylthio) propanoate (MCEBTTC).	79
Figure 3.2. FTIR spectrum of a linear PS arm prepared via MCEBTTC RAFT agent.	84
Figure 3.3. A typical <sup>1</sup> H NMR spectrum of a living linear PS arm prepared via RAFT. Numbers and letters refer to the end groups and backbone protons, respectively.	85
Figure 3.4. <sup>13</sup> C NMR spectrum of a linear PS arm prepared via RAFT.	86
Figure 3.5. UV-GPC traces at 254 and 312 nm of (A) a linear PS synthesised via MCEBTTC RAFT agent and (B) a commercial PS.	87
Figure 3.6. GPC traces of PS arms synthesised at various ratios of St to MCEBTTC.	91
Figure 3.7. Effect of [St]:[MCEBTTC] on $M_n$ and PDI of PS arm.	93
Figure 3.8. Comparison between the effect of St to MCEBTTC mole ratio at constant and various MCEBTTC to AIBN ratios on the MW ( $M_n$ ) of PS arm.	96
Figure 3.9. FTIR spectra of (A) a PS arm precursor and (B) the corresponding arm-first CCS polymer prepared via RAFT.	98
Figure 3.10. <sup>1</sup> H NMR spectrum of a typical arm-first CCS polymer (CCS-R6) prepared via RAFT. (X is attributed to the methine proton peak of styrene adjacent to the trithiocarbonate (Peak H <sub>a</sub> , Figure 3.3) whereas Y denotes a contaminant peak from THF).	99
Figure 3.11. FTIR spectrum of a PEGDMA core synthesised using MCEBTTC RAFT agent.	103

Figure 3.12. FTIR spectra of (A) a core-first CCS polymer via RAFT and (B) the corresponding PEGDMA core precursor	104
Figure 3.13. <sup>1</sup> H NMR spectrum of a typical core-first CCS polymer prepared via RAFT. (Y denotes a contaminant peak from THF).	106
Figure 3.14. GPC curve of a core-first CCS polymer prepared via RAFT.	107
Figure 3.15. DLS intensity particle size distribution of a core-first CCS polymer prepared via RAFT.	107
Figure 4.1. Structure of benzylpiperazine.	113
Figure 4.2. Structures of (1R,2S)-(-)-ephedrine [2], 1-phenylpiperazine [3], ethylene glycol dimethacrylate [4], methacrylic acid [5], benzyl N,N-diethyldithiocarbamate [6] and methyl 2-(butylthiocarbonothioylthio) propanoate [7].	115
Figure 4.3. Calibration curve used for the determination of concentration of BZP.	119
Figure 4.4 Calibration curves used for the determination of concentration of (A) BZP, (B) EPH and (C) PHP analytes.	122
Figure 4.5. Deconvolution of a HPLC curve (MIP-5%BDDC, Table 4.9) carried out using the Solver function in Microsoft Excel 2010. G1 and G2 represent BZP and PHP respectively. The sold blue (height) and the black dashed (Y) lines are the measured and fitted HPLC curves, respectively.	124
Figure 4.6. Comparison of FTIR absorbance spectra of (A) the monomers (EGDMA:MAA = 5:1) and (B) the MIP microsphere (MIP-20%BDDC).	127
Figure 4.7. Molecular modelling image obtained using the molecular simulation software, Spartan '04	129
Figure 4.8. FTIR spectra of (A) MAA, (B) BZP and (C) MAA-BZP complex. The peaks at 1545 and 1404 cm <sup>-1</sup> are attributed to the asymmetric and symmetric stretching vibration of COO <sup>-</sup> of MAA, respectively.	130
Figure 4.9. SEM images of spherical MIP microspheres prepared using (A) 5 mol %, (B) 10 mol % and (C) 20 mol % BDDC and their corresponding NIP microspheres (D), (E) and (F) respectively.	134
Figure 4.10. Incremental pore volume versus pore width plots for MIP-5%BDDC and NIP-5%BDDC.	138
Figure 4.11. Time rebinding results for the MIP and NIP prepared using 5%BDDC in acetonitrile normalised with respect to (A) mass and (B) surface area as well as in THF normalised with respect to (C) mass and (D) surface area.	140
Figure 4.12. Binding isotherms for BZP imprinted polymers prepared using 5% BDDC and the control (NIP) carried out in acetonitrile normalised with respect to (A) mass and (B) surface area.	143

Figure 4.13. Langmuir plots for BZP imprinted polymers prepared using 5% RAFT and the control (NIP) normalised with respect to (A) mass and (B) surface area.	146
Figure 4.14. Scatchard plots for BZP imprinted polymers prepared using 5% RAFT and the corresponding NIP normalised with respect to (A) mass and (B) surface area.	481
Figure 4.15. Types of binding sites in the MIP microspheres.	150
Figure 4.16. Comparison between the binding capacity of MIP microspheres prepared via RAFT in acetonitrile and THF normalised with respect to (A) mass and (B) surface area.	155
Figure 4.17. SEM images of MIP microspheres prepared using various amount of MCEBTTC RAFT agent i.e.	159
Figure 4.18. Incremental pore volume versus pore width plots for MIP-5%RAFT and NIP-5%RAFT.	163
Figure 4.19. Time rebinding results for MIP and NIP prepared using 5%RAFT in acetonitrile normalised with respect to (A) mass and	165
Figure 4.20. Binding isotherms for BZP imprinted polymers prepared using 5% RAFT carried out in acetonitrile normalised with respect to (A) mass and (B) surface area.	167
Figure 4.21. Langmuir plots for BZP imprinted polymers prepared using 5% RAFT and the control (NIP) normalised with respect to (A) mass and (B) surface area.	169
Figure 4.22. Scatchard plots for BZP imprinted polymers prepared using 5% RAFT and the corresponding NIP normalised with respect to (A) mass and (B) surface area.	171
Figure 4.23. Comparison between the binding capacity of MIP microspheres prepared via RAFT in acetonitrile and THF normalised with respect to (A) mass and (B) surface area.	177
Figure 4.24. Comparison between the binding capacity of MIP microspheres prepared via iniferter and RAFT normalised with respect to (A) mass and (B) surface area.	179
Figure 4.25. Single-analyte (A and B), binary-analyte (C - F) and tertiary-analyte (G and H) binding assays of BZP imprinted polymer with BZP, EPH and PHP normalised with respect to mass (A, C, E and G) and surface area (B, D, F and H).	187
Figure 4.26. Computer generated molecular modelling images of (A) EPH:MAA 1:1 and (B) PHP:MAA 1:1 for the geometry optimised T:M clusters.	190
Figure 5.1. Purification steps of (A) CCS MIP and (B) CCS NIP.	199
Figure 5.2. Comparison of FTIR absorbance spectra of the (A) calibration mixture (5% styrene), (B) core precursor (MIP-5%BDDC-B2) and (C) CCS MIP (CCS MIP-F1).	201
Figure 5.3. The calibration curves used for the estimation of the mass fraction of the MAA and EGDMA constituent of the core in the CCS polymer with styrene arms. The y-	

axis indicates the (C=O/aromatic C-H) absorbance ratio of a mixture of EGDMA, MAA and styrene whilst the x-axis is the mass fraction of the EGDMA/MAA mixture with respect to the total mass. (A) used for calibration for C=O/aromatic C-H ratios less than 2, and (B) used for C=O/aromatic C-H ratios greater than 2. 202

Figure 5.4. SEM images of (A) MIP-5%BDDC-B2, (B) CCS MIP-F1, (C) CCS MIP-F2, (D) NIP-5%BDDC-B2, (E) CCS NIP-F1, (F) CCS NIP-F2 and (G) CCS NIP-F3. The images were recorded at 15000X magnifications. 206

Figure 5.5. FTIR spectra of (A) CCS MIP and (B) CCS NIP fractions compared to their corresponding core precursors. 209

Figure 5.6.  $^1\text{H}$  NMR spectrum of CCS MIP-F2. 212

Figure 5.7.  $^1\text{H}$  NMR spectra of CCS NIP-F2. 214

Figure 5.8.  $^1\text{H}$  NMR spectrum of CCS NIP-F3. 215

Figure 5.9. The BZP binding capacity of the (A) CCS MIP and (B) NIP fractions compared with their corresponding core precursors in acetonitrile and THF. 219

Figure 5.10. Computer generated molecular modelling images of BZP and (A) 2, (B) 4 and (C) 8 units of styrene for the geometry optimised BZP:St clusters. 222

## List of Schemes

Scheme 1.1. Synthesis of star-shaped polymers via arm-first methods.	4
Scheme 1.2. Proposed mechanism for the synthesis of CCS polymers from a living macroinitiator and a crosslinker.	5
Scheme 1.3. Preparation of star-shaped polymers by a core-first method.	9
Scheme 1.4. Synthesis of star polymers with a crosslinked core via ATRP by the “star in situ generated core” method. <sup>49</sup>	10
Scheme 1.5. General scheme of the ATRP polymerisation process.	11
Scheme 1.6. Synthesis of star polymers with a crosslinked core via ATRP using the arm-first method.	12
Scheme 1.7. General mechanism of a photoiniferter-mediated polymerisation. X is usually a sulphur radical whilst R may be either a sulphur radical or a carbon radical.	17
Scheme 1.8. Mechanism of RAFT polymerisation.	20
Scheme 1.9. Schematic of the synthesis of CCS polymers using RAFT via the arm-first approach.	21
Scheme 2.1. Reaction scheme for the synthesis of BDDC [1].	34
Scheme 2.2. Synthetic route of CCS polymers via the arm-first iniferter polymerisation.	42
Scheme 2.4. Synthesis of CCS polymer via the core-first approach.	70
Scheme 3.1. Synthetic route of CCS polymers via the arm-first RAFT polymerisation.	83
Scheme 3.2. Synthetic route of CCS polymers via the core-first RAFT polymerisation.	102
Scheme 5.1. Synthesis of core-first CCS MIP by iniferter-mediated precipitation polymerisation.	197

# Chapter 1

## Introduction

### 1.1 Star Polymers

Star polymers are hyperbranched polymers with a large number of arms emanating from a central core.<sup>1</sup> A structurally well-defined star polymer contains only one central branching point (the core of the star) and multiple radial arms (Figure 1.1). Based on the chemical composition of the arm species, star polymers can be further classified into two categories: homoarm star polymer (Figure 1.1a) and miktoarm (or heteroarm) star polymer (Figure 1.1b).<sup>1</sup> While homoarm star polymers consist of a symmetric structure comprising radiating arms with similar molecular weight and identical chemical composition, a miktoarm star molecule contains arm species with different chemical compositions and/or molecular weights.

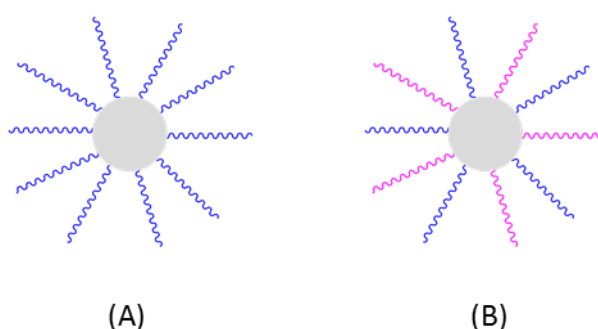


**Figure 1.1.** Schematic diagrams of a (A) homoarm and (B) miktoarm or heteroarm star polymers.

The three-dimensional globular compact structure of star polymers results in a unique set of physical properties, such as high functionality and low viscosity when dispersed

in a solvent as compared to their linear analogues with similar molecular weight.<sup>2</sup> This generates a wide range of potential applications for star polymers, including drug delivery, cosmetics, coatings, membranes, or lithography.<sup>3-7</sup>

## 1.2 Star Polymer Synthesis

The synthesis of well-defined star polymers has become an important field in macromolecular chemistry due to their unique geometry and rheological properties and has been the subject of a number of studies.<sup>8-10</sup> The synthesis of well-defined star polymers with uniform size, desired functionality and various architectures generally involves living polymerisation techniques, and this has been extensively investigated in anionic, cationic, ring opening metathesis and group transfer polymerisations.<sup>1</sup>

Among the drawbacks of ionic and group transfer polymerisations are their stringent synthetic requirements such as high sensitivity to oxygen, moisture, very low temperatures (<-70 °C) and restriction to certain functional groups. In contrast, free radical polymerisation (FRP) is more tolerant to impurities and is capable of polymerizing a great variety of vinyl monomers. Other advantages include fast reaction times, rapid formation of high molecular weight polymers and relatively easy manufacturing techniques. However, due to high termination rates, and combination and disproportionation reactions, free radical polymers have a broad molecular weight distribution and varying macromolecular structure.<sup>11</sup>

One method to attain molecular control of the polymer structure is by creating a living radical polymerisation in which there is little or no termination. The primary definition of a living polymerisation is that termination and chain transfer reactions do not occur. In a free radical polymerisation, it can be very difficult to meet all of these criteria. Realistically, irreversible termination is only minimized, thus these free radical polymerisations are termed controlled or living polymerisations.<sup>12</sup> However, recently the International Union of Pure and Applied Chemistry (IUPAC) task group has recommended the term reversible-deactivation radical polymerisation (RDRP) to describe these types of radical polymerisations.<sup>13</sup> RDRP routes such as atom transfer

radical polymerisation (ATRP), nitroxide mediated polymerisation (NMP) and reversible addition-fragmentation chain transfer (RAFT) have proven to be very promising for the synthesis of low polydispersity linear polymers, block copolymers and star polymers.<sup>14</sup> All these RDRP techniques have a common mechanism, which is the alternating activation–deactivation process, where the dormant but potentially active species can be activated to become a polymer radical.<sup>15</sup>

Preparation of star polymers via RDRP techniques can be divided into two broad approaches namely the ‘arm-first’ and the ‘core-first’ methods.<sup>6, 7</sup> In the arm-first approach, monofunctional, living linear macromolecules are initially synthesized, followed by crosslinking reaction with a divinyl crosslinker to form star polymers with a crosslinked core.<sup>16</sup> In the core-first approach, either multifunctional initiators are used to grow chains from a central core resulting in star polymers with well-defined structures in terms of both arm number and length<sup>17</sup> or a highly cross-linked core containing multiple initiating sites in a statistical distribution was prepared by homopolymerisation of crosslinker before growth of arms to afford the star polymer.<sup>18</sup>

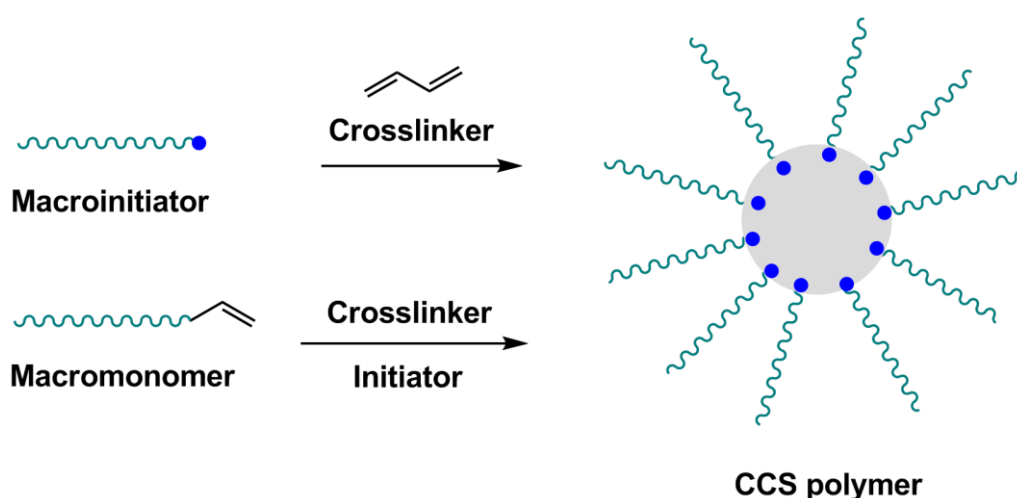
## **1.2.1 Arm-first method**

### **1.2.1.1 General Characteristics**

The arm-first method was first developed via anionic polymerisation<sup>19</sup> followed by group transfer polymerisation in the mid 1980s.<sup>20</sup> The method has been later extensively employed using different RDRP techniques<sup>6</sup> for the synthesis of various functional star polymers due to the straightforward experimental set up and broad range of suitable monomers.

The synthesis of star polymers via the arm-first method involves the reaction of living or macromonomers<sup>20</sup> or macroinitiators<sup>21</sup> with a difunctional monomer to form a densely crosslinked core from which the arms radiate (Scheme 1.1).<sup>18</sup> By using the arm-first approach, star polymers with very large numbers of arms<sup>22</sup> can be produced with relative ease and the star polymers possess a significantly sized crosslinked core

(relative to the overall molecular weight of the macromolecule).<sup>23, 24</sup> Due to the densely crosslinked structure of the cores which typically account for 10–30% of the polymers' molecular weight,<sup>25</sup> this class of star polymer are sometimes referred to as 'core crosslinked star' (CCS) polymers,<sup>6</sup> thus distinguishing them from star polymers which possess discrete and well-defined core moieties of relatively small molecular weight compared to the overall macromolecule molecular weight. Where appropriate, this term will be used throughout the whole thesis.



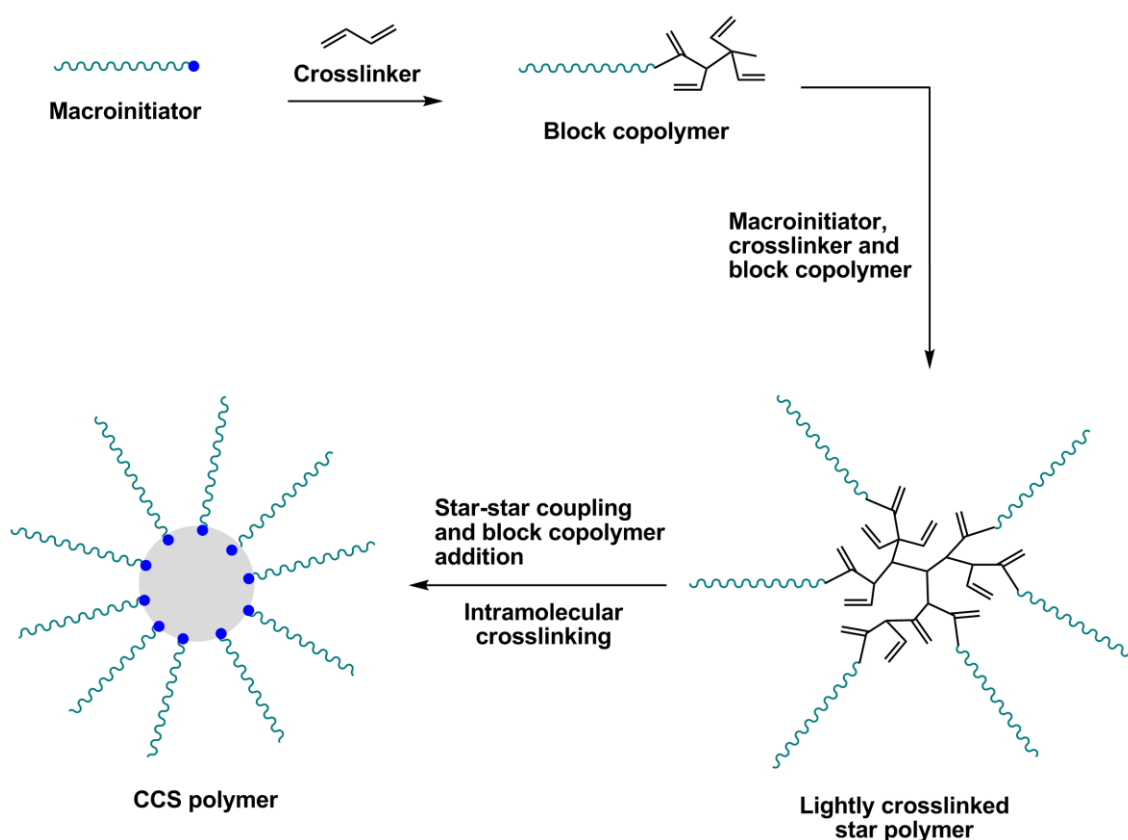
**Scheme 1.1.** Synthesis of star-shaped polymers via arm-first methods.

Among the most popular RDRP techniques that have been applied to the synthesis of CCS polymers by crosslinking living linear chains using a divinyl crosslinker are ATRP,<sup>26</sup> NMP<sup>27</sup> and RAFT.<sup>28</sup> Other RDRP techniques such as degenerative chain transfer mediated by iodine<sup>29</sup> or other groups,<sup>30, 31</sup> transition metal-mediated stable FRP<sup>32</sup> and iniferter<sup>33</sup> have to date focussed on optimizing polymerisation conditions to achieve the synthesis of linear block copolymers with various monomers, well-defined structure and high chain-end functionality.

### 1.2.1.2 Macroinitiator Approach

The arm-first method, based on crosslinking of a linear macroinitiator (MI) with a divinyl compound is the easiest way to synthesize CCS polymers containing multiple arms and functionalities and allows preparation of various miktoarm CCS polymers.<sup>34, 35</sup> The proposed mechanism of CCS polymer formation from living macroinitiators and

a divinyl crosslinker is as follows (Scheme 1.2).<sup>6</sup> Initially, the addition of a crosslinker to a solution containing linear living macroinitiator forms short block copolymers. The block copolymers can then react with more crosslinker, macroinitiators or with the pendant vinyl groups present on other block copolymers. As more of the block copolymers link together, a star polymer with a lightly crosslinked core is formed. Star-star coupling can occur if the cores of these star polymers are sterically accessible to each other which results in the formation of higher molecular weight macromolecules leading to a broader molecular weight distribution (MWD,  $M_w/M_n > 1.5$ ) for the resultant CCS molecules.<sup>36</sup> Simultaneously, block copolymers and macroinitiators could also add to these lightly crosslinked star polymers. Once the majority of the block copolymers have been immobilised into the star structure, intramolecular crosslinking within the stars is likely to dominate producing CCS polymers with denser crosslinked cores.



**Scheme 1.2.** Proposed mechanism for the synthesis of CCS polymers from a living macroinitiator and a crosslinker.

Apart from having a broad MWD due to the significant level of star–star coupling reactions, another drawback to CCS polymer synthesis using a linear macroinitiator as the arm precursor is that caution has to be taken in order to avoid macroscopic gelation<sup>37</sup> when too much star–star coupling occurs. Star–star coupling reactions can be decreased by using less divinyl crosslinker, e.g., a lower molar ratio of crosslinker to arm precursor, and/or carrying out the reaction under dilute solution conditions. However, the molecular weight and the yield of the obtained CCS molecules decrease significantly.<sup>21, 38</sup> In addition, the final CCS product formed via crosslinking the linear macroinitiators is often contaminated by the presence of residual unincorporated linear polymers,<sup>21, 39</sup> which requires an extra purification step such as fractional precipitation or dialysis protocols in order to obtain a CCS polymer with higher purity and narrower MWD.<sup>4</sup>

### 1.2.1.3 Macromonomer Method

Macromonomers (MM), which consists of a combination of a macromolecular chain and a polymerisable end group, have been widely and successfully used as building blocks for the synthesis of an enormous number of branched macromolecular architectures.<sup>40</sup> CCS polymers utilizing the macromonomer method have been synthesised using RDRP techniques such as ATRP<sup>16, 41, 42</sup> and RAFT.<sup>43, 44</sup> Employing ATRP, CCS polymers with high molecular weight and low polydispersity in high yield were synthesised via copolymerisation of linear MM with a divinyl crosslinker in one-pot.<sup>16</sup> The method was then extended to the synthesis of low polydispersity CCS polymers with core functionality by using a low molar mass functional ATRP initiator<sup>41</sup> as well as low polydispersity miktoarm CCS copolymers.<sup>42</sup> RAFT polymerisation was utilised in the synthesis of peptide CCS polymers by crosslinking linear poly(amino acid) MM with divinyl benzene in homogeneous media.<sup>43</sup> By using a multibatch approach, the star yield was found to be increased while maintaining narrow MWD. Very recently, CCS polymers of high yield and low polydispersity were successfully synthesised via a one-step RAFT-mediated emulsion polymerisation in aqueous media.<sup>44</sup> Using this technique, no surfactant was required as the CCS polymers were self-stabilised or dispersed in water.

In the macroinitiator method, both initiating sites and arms in the CCS molecule are derived from the macroinitiator resulting in their identical numbers in each star. On the other hand, in the macromonomer method, the numbers of initiating sites and arms can be independently controlled since they are derived separately from the initiator and the macromonomer. Therefore, the number of initiating sites per star molecule may be much smaller than the number of arms when a low molar ratio of initiator to macromonomer was used. A lower number of initiating sites in the star core decreases the possibility of star-star reactions and results in the formation of CCS polymers with narrower MWD.<sup>16</sup> In addition, since the macromonomer, initiator, and crosslinkers can be added in several steps, the flexibility of star synthesis is increased. An extra advantage of this macromonomer method for the synthesis of CCS polymers is that additional functional groups can be easily introduced into the star core via functional initiators.<sup>41</sup>

The use of macromonomers, however, is accompanied by several drawbacks that emerge from their homo- and copolymerisation characteristics,<sup>45</sup> such as: (a) the polymerisation is performed in a solution of increased viscosity, (b) the concentration of the polymerisable end groups is very low, (c) the polymerisation proceeds through the interaction of polymer chains and, (d) the steric hindrance of the active centre of the developing polymer chain is increased during the polymerisation. All of the above may lead to products of increased compositional and chemical heterogeneity. Although the synthesis of linear macromonomers<sup>46</sup> is not as straightforward or as easy as the synthesis of linear macroinitiators,<sup>36</sup> the macromonomer method could be extended as a general method in conventional radical polymerisation,<sup>47, 48</sup> and other RDRP techniques for the synthesis of CCS polymers with high star yield, high molecular weight and low polydispersity.<sup>16, 44</sup>

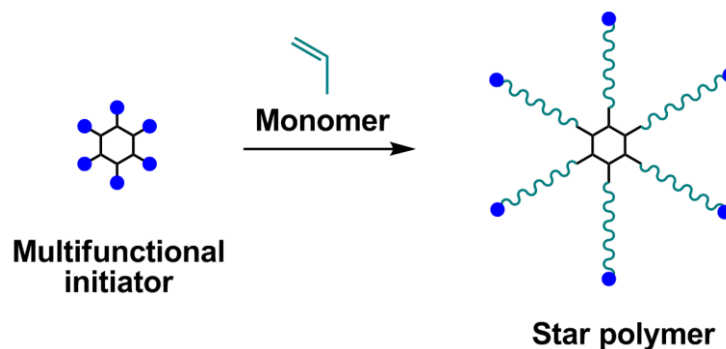
The structure (e.g., number of arms ( $f$ ), radius of gyration ( $R_g$ ), core size and molecular weight) as well as yield of CCS polymers are influenced by a large variety of experimental factors such as the type of macroinitiator/macromonomer and crosslinker used, the degree of polymerisation (DP) of the

macroinitiator/macromonomer, the molar ratio of crosslinker to macroinitiator/macromonomer, the molar ratio of initiator to macromonomer, the concentration of the macroinitiator/macromonomer, the incorporation of a spacer group during core formation and the nature of the solvent.<sup>6</sup> Among them, the three most important factors to consider when preparing CCS polymers via the arm-first method are the concentration and the DP of the macroinitiator, as well as the crosslinker/macroinitiator ratio. However, the structure and reactivity of the crosslinker as well as the structural composition of the macroinitiator also affect these variables to some extent.

Despite the complexity of having a large number of variables to consider in the preparation of CCS polymers via the arm-first method, some general trends can be noted. An increase in the macroinitiator concentration or crosslinker/macroinitiator molar ratio, up to a certain point, leads to an increase in CCS polymer molecular weight and yield.<sup>6</sup> Further increases in the former or latter result in the formation of star–star coupling producing CCS polymers with high polydispersities and even insoluble gels.<sup>39</sup> The molecular weight and yield of the CCS polymers also generally increase with increasing DP of the macroinitiator.<sup>23, 38</sup>

### **1.2.2 Core-first Method**

The core-first method involves the use of a multifunctional initiator (Scheme 1.3), and the number of arms per star polymer is determined by the number of initiating functionalities on each initiator. The initiating sites on the star polymers can be further used for chain extension with a second monomer to form star block copolymers. For the synthesis of well-defined star polymers with uniform arms, controllable molecular weights and low molecular weight distribution using this technique, reactive sites of the multifunctional initiator must be equally reactive and initiation must be rapid relative to propagation.<sup>1</sup>

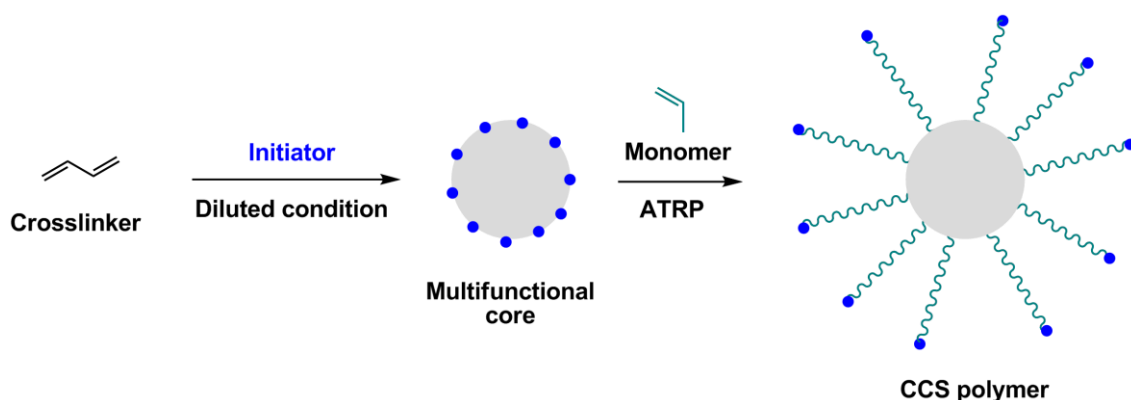


**Scheme 1.3.** Preparation of star-shaped polymers by a core-first method.

Among the most beneficial aspects of the core-first approach are the very high yields and the ease with which the pure star polymer can be isolated, since the crude reaction mixture only requires separation of any unreacted monomers. However, this approach is not well suited to the preparation of miktoarm stars unless specially designed multifunctional initiators with orthogonal initiating functions are employed. In addition, the preparation of stars with high arm number ( $>30$ ) requires the synthesis of complex and highly functionalised initiators. Although the number of arms can be indirectly determined via several methods, including end-group analysis, determination of branching parameters and isolation of the arms after cleavage, the molecular weight of the arms cannot be measured directly. Another drawback that applies when RDRP methods are employed for the core-first approach is the need for special precautions to prevent star–star coupling.<sup>6</sup>

A new method termed as “star from in situ generated core” was reported for the synthesis of CCS polymers containing a highly crosslinked core and many radiating arms via ATRP (Scheme 1.4).<sup>49</sup> The CCS polymers were prepared by sequential polymerisation of crosslinker and monomer. In this synthetic method, a highly cross-linked core was prepared by homopolymerisation of crosslinker (ethylene glycol dimethacrylate) before the growth of arms. Therefore, this method may also be categorised as the core-first method. In this method, large amount of different acrylate monomers was injected into the reaction system at high conversion of the crosslinker to afford CCS polymers with different arm chemical compositions. Compared to the star polymers synthesized from the traditional core-first method, this new strategy

skipped the tedious synthesis of the multifunctional initiator before polymerisation. The CCS polymers synthesised by this core-first method had a similar structural compactness to those formed via the arm-first method. However, in contrast to the latter, where the dormant initiating sites were present in the star core, the initiating sites of the former were preserved at the chain ends, the periphery of the star. Therefore, the chain of the CCS macroinitiator can be extended by polymerisation of a second monomer to form CCS block copolymers.<sup>49</sup>



**Scheme 1.4.** Synthesis of star polymers with a crosslinked core via ATRP by the “star in situ generated core” method.<sup>49</sup>

The applicability of RDRP toward the formation of star polymers via the core-first approach has been demonstrated in several studies.<sup>50-54</sup> However, comparably few studies report the application of RDRP in the synthesis of CCS polymer formation via the core-first approach.<sup>49, 55</sup>

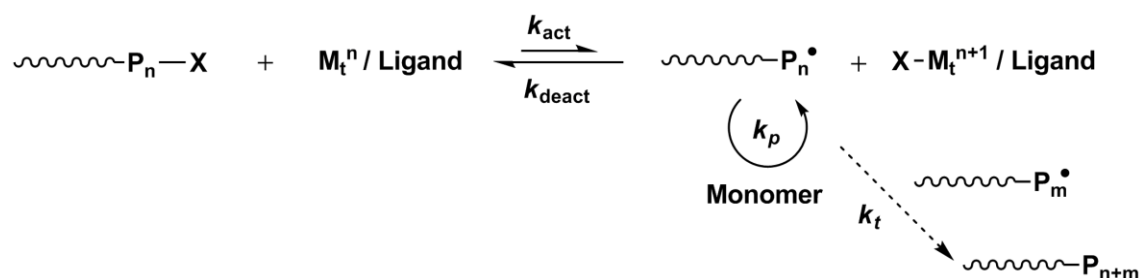
### 1.3 Reversible-Deactivation Radical Polymerisation

Generally, three different mechanisms of intermittent activation are employed in RDRP: dissociation-combination (e.g. NMP or organometallic radical polymerisation); catalytic atom (group) transfer (ATRP) and degenerative chain transfer (e.g. iodine mediated polymerisation or RAFT). During these RDRP processes, the active radicals participate in degenerative transfer reaction in RAFT, but they undergo a reversible activation/deactivation processes in NMP and ATRP. Another method, which is called iniferter, is based on reversible combination of growing chains with a terminator

molecule.<sup>56</sup> Here, however, only the most relevant of these RDRP techniques to this thesis including the most widely applied method for controlling radical polymerisation, ATRP<sup>57-59</sup> will be discussed.

### 1.3.1 Atom Transfer Radical Polymerisation

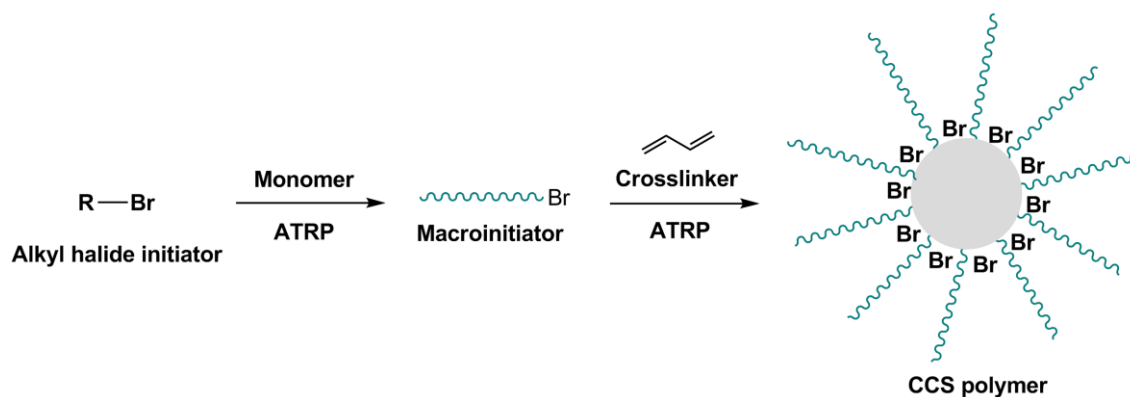
Atom transfer radical polymerisation (ATRP) involves the reversible activation of dormant alkyl halides (R-X) to form radicals via halogen abstraction by low-oxidation state transition metal complexes ( $M_t^n/\text{Ligand}$ ).<sup>60, 61</sup> The dynamic equilibrium between the alkyl halides and radicals is greatly shifted toward the dormant alkyl halides. The low concentration of radicals suppresses the contribution of radical termination reactions and maintains a constant number of propagating polymer chains (Scheme 1.5).



**Scheme 1.5.** General scheme of the ATRP polymerisation process.

The construction of CCS polymers via ATRP generally involves the preparation of a living macroinitiator followed by crosslinking with a divinyl (or higher) crosslinker in either a one-pot or two-pot strategy (Scheme 1.6).<sup>62</sup> The one-pot strategy involves the addition of crosslinkers to the macroinitiator formation reaction at a certain monomer conversion, whilst the two-pot strategy involves the synthesis and isolation of the macroinitiator followed by a second reaction with crosslinkers. The synthesis of the macroinitiator is stopped prior to complete consumption of the monomer in order to maintain a high proportion of living polymer chains in the initial stage. This is due to the fact that side reactions become apparent at low monomer concentrations.<sup>62</sup> As a result of the incorporation of a spacer group (the remaining monomer from the

macroinitiator synthesis) in the one-pot strategy, the one-pot and two-pot strategies lead to CCS polymers with slightly different crosslinking densities within the core.



**Scheme 1.6.** Synthesis of star polymers with a crosslinked core via ATRP using the arm-first method.

The first synthesis of star polymers with a crosslinked core by ATRP was reported in 1999 by Xia *et al.*<sup>21</sup> Star-shaped polystyrenes were prepared by the coupling of polystyrene macroinitiators in the presence of divinylbenzene (DVB) using copper-mediated ATRP. They discovered that using DVB as a crosslinker led to the formation of CCS polymers with the best controlled structure as compared to other crosslinkers such as ethylene glycol diacrylate (EGDA) and ethylene glycol dimethacrylate (EGDMA). However, the star product was contaminated with residual linear chains and exhibited a broad MWD due to star–star coupling reactions. Following the same approach, poly(*tert*-butyl acrylate) (PtBA) CCS polymers were synthesized through the use of functional ATRP initiators for the synthesis of linear PtBA macroinitiators.<sup>63</sup> Various functional groups such as epoxy, amino, cyano or bromo, were introduced into the chain end of each arm, the periphery of the star.

(PolytBA)*n*-poly(DVB-co-tBA) CCS polymers were successfully prepared in a one-pot reaction in high yield without the need to isolate and purify the linear PtBA macroinitiators.<sup>62</sup> The timing of addition of the subsequent DVB at different tBA conversions significantly affected the structure of the CCS polymers formed in these reactions. The addition of DVB at lower tBA conversion caused the incorporation of more monovinyl monomer into the star core, which decreased the crosslinking density

of the core, facilitated incorporation of more arms into each star molecule, and increased the star size and star yield. Employing shorter arm lengths and using more crosslinker produced CCS polymers of higher molecular weight and yield, having more arms per star and exhibited a more compact structure. One of the significant findings was that the CCS copolymer with a core containing both DVB and *t*BA units, from the one-pot process, had a higher star molecular weight and yield when compared to the CCS copolymer with a core containing the same number of pure DVB units from the two-pot process. This confirmed that the introduction of monovinyl monomer units during the star core formation decreased the steric congestion of the core and facilitated the incorporation of more arms into each CCS molecule.

ATRP via the macromonomer method was recently applied to the high-yield synthesis of low-polydispersity CCS polymers by means of copolymerisation of a linear macromonomer and divinyl crosslinker, using a low molar mass ATRP initiator in a homogeneous solution.<sup>16, 64</sup> Employing the copolymerisation of a linear macromonomer with a crosslinker to incorporate arms into a star completely bypassed the requirement of chain extension of linear macroinitiator.<sup>21, 62</sup> The incorporation of linear macromonomers into the preformed CCS polymer increased the star yield but kept a low polydispersity of the resultant stars.<sup>16</sup> The CCS polymer continued to grow until the core was fully covered by the linear arms and reached a steric saturation state, thus further star growth ceased. Addition of another batch of crosslinker and initiator at this stage introduced more pendant vinyl groups and initiating sites to the star core, expanding its size and functionality. This expansion decreased core congestion and made further incorporation of linear chains into the star polymer possible. With appropriate amounts of additional crosslinker and initiator, it is possible to conduct star-linear macromonomer reactions with limited star–star coupling reactions. Therefore, the newly added crosslinker and initiator increased the star yield and star molecular weight while avoiding broadening of the MWD. Star-linear macromonomer reactions stopped when the CCS polymer reached its new saturated size. However, the addition of a second batch of crosslinker and initiator expanded the

core and allowed further star growth. This process could be repeated until the star yield essentially reaches 100% incorporation of the initially added macromonomer.<sup>16</sup>

Several researchers have described the use of ATRP for synthesis of star polymers by the core-first approach.<sup>65-67</sup> In addition to the necessary high initiation efficiency required for the core-first approach,<sup>68</sup> synthesis of high-molecular-weight star polymers demands a low extent of chain transfer and termination reactions<sup>69</sup> while maintaining a moderate reaction rate. ATRP has also been applied to the synthesis of CCS polymers by using a new core-first method, where the crosslinker was polymerised first to form a star core, followed by addition of monomer to grow the arms.<sup>49</sup>

ATRP is a very versatile technique for preparing polymers with predefined structures<sup>70, 71</sup> and is among the most popular techniques to synthesise CCS polymers.<sup>6, 7</sup> However, any parameters in ATRP such as the structures and concentrations of the utilized monomers, catalysts (metals/ligands) and initiators, solvents, reactant ratios, and reaction temperatures can significantly influence the controllability of polymerisations. This makes the optimization of reaction conditions very time consuming, in particular when a new reaction system is investigated.<sup>72</sup> Another disadvantage of ATRP is that a high concentration of a catalyst is usually required<sup>61</sup> and thus has to be removed from the obtained polymers typically by a manual chromatographic process prior to their characterization (e.g. the determination of the molecular weights and polydispersity indices of the polymers by size exclusion chromatograph) and application.<sup>73</sup>

### 1.3.2 Iniferter

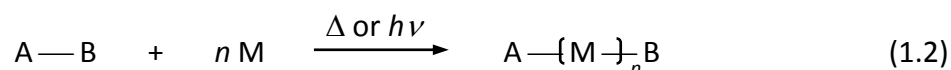
Iniferters are initiators that induce radical polymerisation that proceeds via initiation, propagation, primary radical termination, and transfer to initiator. The term iniferter (initiator-transfer agent-terminator) was proposed by Otsu *et al.* in 1982.<sup>74</sup> The concept was introduced for the radical polymerisation of monofunctional and bifunctional oligomers and polymers. The use of well-designed iniferters would give polymers or oligomers bearing controlled end groups. If the end groups of the

polymers obtained by a suitable iniferter serve further as a polymeric iniferter, these polymerisations proceed in a living radical polymerisation mechanism in a homogeneous system. Initiators containing carbon-sulphur or sulphur-sulphur bonds were discovered to serve as excellent photoiniters by Otsu and Kuriyama.<sup>75</sup>

There are two types of iniferter: A-B and B-B types. A-B type iniferters can be either thermally or photochemically dissociated into two different radicals:



where A• is the reactive radical, which participates only in initiation, and B• is the less or non-reactive radical which cannot participate in initiation and acts as a primary radical termination. Examples of this type of iniferter are benzyl *N,N*-diethyldithiocarbamate (BDDC), and 1-(*N,N*-diethyldithiocarbamyl) ethylbenzene (StDC). These iniferters thermally or photochemically dissociate at the weak bonds, and then monomer molecules are inserted by propagation, followed by primary radical termination and/or chain transfer to give polymers which also contain iniferter bonds at the chain end:



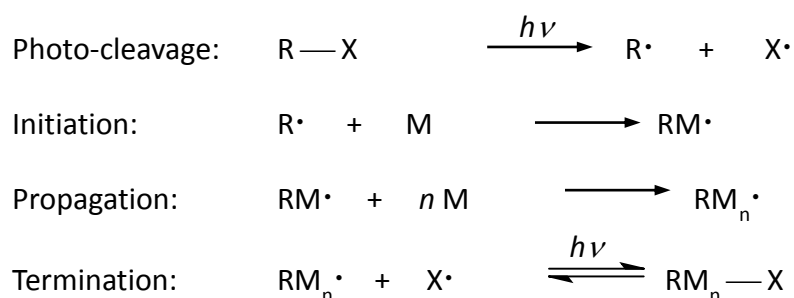
On the other hand, the B-B type iniferters such as tetraethylthiuram disulphide (TED), *p*-xylene bis(*N,N*-diethyldithiocarbamate) (XDC) and mercaptobenzothiazole disulphide (MBTS) dissociate into two identical radicals as follows:



where B• is a radical which can participate in both initiation and primary radical termination. As a result, these radicals yield polymers having iniferter fragments at both chain ends. For a more efficient synthesis of polymers with controlled structure, the A-B type iniferters have proved to be more useful than the B-B type.<sup>76</sup> The functionality of the iniferters can be controlled by changing the number of A-B bonds introduced into an iniferter molecule, for instance using B-A-B as a bifunctional iniferter.

From the viewpoint of controlled polymer synthesis, iniferters can be classified into several types: thermal or photoiniferters; monomer or macromonomer iniferters; monofunctional, difunctional, trifunctional, or polyfunctional iniferters as well as monomeric, polymeric, or gel iniferters.<sup>33</sup> These lead to the synthesis of various monofunctional, telechelic, block, graft, star, and crosslinked polymers. Very few structures exhibit photoiniferter properties, among these benzyl dithiocarbamate (BDC) is the most popular one.<sup>75, 77</sup> In contrast with thermal iniferters, polymerisation using compounds having a photodissociable dithiocarbamate (DC) group as photoiniferters can be performed at low temperature, such as room temperature. Many DC derivatives with various structures can be readily prepared, demonstrating that the functionalization and molecular structure design are relatively straightforward.<sup>78</sup>

The ideal mechanism of the photoiniferter-mediated polymerisation proposed by Otsu *et al.*<sup>77</sup> is shown in Scheme 1.4.<sup>79</sup> The key to this polymerisation is that the polymer chain must photodissociate into a reactive, carbon-centred radical and a less reactive sulphur radical. This then allows for successive insertion of monomer molecules. In general, photoiniferters dissociate into reactive ( $R\cdot$ ) and less reactive ( $X\cdot$ ) radicals. Reactive radical  $R\cdot$  can react with a given vinyl monomer to initiate the polymerisation reaction. The recombination of the less reactive radical  $X\cdot$  with the propagating radical is photochemically reversible and provides a living character to the reaction. In comparison to the propagation process, the exchange between the propagating radical  $R-M_n\cdot$  and the dormant species  $R-M_n-X$  must be rapid. The photodissociation of the polymer chain end and further propagation occur repeatedly. As a result, molecular weight of the resulting polymer increases with monomer conversion (the total number of chains is expected to be constant).<sup>33, 79</sup>



**Scheme 1.7.** General mechanism of a photoiniferter-mediated polymerisation. X is usually a sulphur radical whilst R may be either a sulphur radical or a carbon radical.

There are several important features for polymerisations initiated by iniferters such as: (i) the molecular weight of the polymer increases with time; (ii) the DP increases linearly with conversion of monomer; (iii) the rate of polymerisation decreases with time and then later remains unchanged after reaching a limiting value; (iv) starting from a certain instant, the number of iniferter fragments in the polymer does not alter with conversion (v) polymerisation products are macroinitiators capable of continuous growth of their molecular weight.<sup>80</sup>

After the first attempt by Otsu to polymerise methyl methacrylic acid (MMA) in the presence of phenylazotriphenylmethane and benzyl dithiocarbamate,<sup>81</sup> his route has been followed by many researchers to synthesize complex macromolecular architectures,<sup>76</sup> such as block<sup>78, 82, 83</sup> and graft<sup>84, 85</sup> copolymers, hyperbranched,<sup>86</sup> crosslinked<sup>87</sup> as well as star polymers,<sup>75, 88, 89</sup> using dithiocarbamate iniferters. The studies, however, were mostly focused on the living radical graft polymerisation.<sup>90-92</sup> For example, Mijangos *et al.* developed a new polymeric macroinitiator and used it for grafting of monomers such as AA, MA and EGDMA onto poly(trimethylolpropane trimethacrylate) (polyTRIM) particles using 2,2-diethyl dithiocarbamic acid benzyl ester (DDCABE) as an initiator.<sup>92</sup> The living nature of the iniferter modified macroradicals was found to permit easy consecutive grafting of multiple polymeric layers, allowing straightforward functionalisation of particles. However, the effectiveness of the grafted initiator decreased with each cycle of polymerisation.

So far, only a few papers have been published on the synthesis of star polymers via the iniferter technique.<sup>75, 77, 93</sup> For example, four-arm methyl methacrylate star polymers have been synthesized by Kuriyama and Otsu using a tetrafunctional iniferter, 1,2,4,5-tetrakis(*N,N*-diethyldithiocarbamylmethyl)benzene.<sup>75</sup> Later, Doi *et al.* synthesized a star polymer of methyl methacrylate using a two-component iniferter by combining benzyl *N,N*-diethyldithiocarbamate and tetraethylthiuram disulfide (TD), but the resultant star polymer had a very broad molecular weight distribution.<sup>93</sup> Recently, the synthesis of star block copolymers with a crosslinked core using dithiocarbamate iniferter under ultraviolet (UV) irradiation has been reported by Ishizu *et al.*<sup>88</sup> The CCS block copolymers (PtBA-block-PMMA arm) were synthesized by the radical polymerisation of the corresponding diblock initiator initiated by (4-cyano-4-diethyldithiocarbamyl)pentanoic acid (CDPA) with EGDMA under UV irradiation. However, the star yield was low possibly due to the slow and incomplete initiation of alkyl dithiocarbamate under UV irradiation and loss of chain-end functionality via the potential dimerization of dithiocarbamyl mediating radicals.

The polymers synthesized using a DC iniferter have an unstable terminal DC group. Stabilization of the chain end of the polymers, i.e. decomposition or removal of the DC group may be carried out using one of the following methods: hydrolysis of the DC group with sodium hydroxide as a nucleophile, thermal decomposition of the DC group e.g. at 230 °C and removal of the group through a photoinduced transfer to thiol e.g. mercaptan.<sup>94</sup> However, only the third method (chain transfer to thiol) is found to be suitable for the polymer design because both the hydrolysis and decomposition methods involved the undesired coupling between the polymer chains leading to an increase in the molecular weight of the polymer.

One of the advantages of iniferter radical polymerisation compared to other RDRP techniques is that the polymerisation can be initiated photo-chemically which is a faster process than thermal initiation. Apart from that, the polymerisation can be carried out at room temperature and might be useful considering some functional monomers that are thermally unstable. In addition, the dithiocarbamate end group is

easily convertible to the thiol ( $-\text{SH}$ ) functionality that could be used for further transformations.<sup>95</sup>

### 1.3.3 Reversible Addition-Fragmentation Chain Transfer

The reversible addition-fragmentation chain transfer (RAFT) is a relatively new RDRP technique discovered by researchers at Commonwealth Scientific and Industrial Research Organisation (CSIRO) in Australia,<sup>96</sup> which involves the use of a chain transfer agent (RAFT agent or CTA). The general structure of a common thiocarbonylthio RAFT agent is shown in Figure 1.2. Z denotes the activating/stabilizing group that controls the reactivity of the  $\text{C}=\text{S}$  bond toward radical and fragmentation,<sup>97</sup> whereas R is the free radical homolytic leaving group that is responsible for re-initiating the polymerisation.<sup>98</sup>

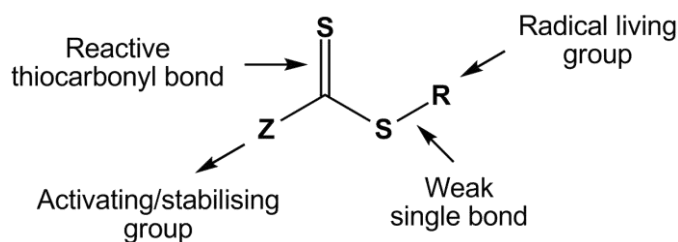
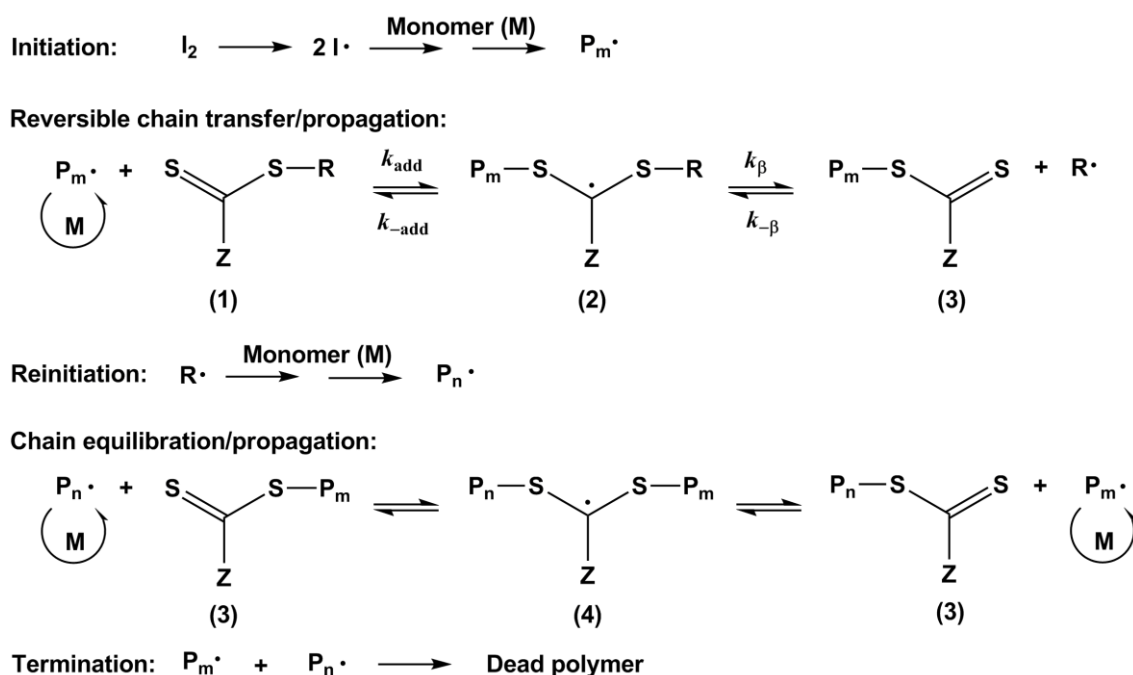


**Figure 1.2.** General structure of a RAFT agent.

The currently accepted mechanism for the RAFT process is outlined in Scheme 1.8.<sup>99, 100</sup> Its overall kinetics and polymerisation rate resemble a conventional radical polymerisation process with slow initiation and fast termination reactions.<sup>60</sup> Although conventional initiator is used for radical initiation, the chain transfer agent employed is present at a much higher concentration than the radical initiator and quickly exchanges a group/atom among all growing chains. Thus, the transfer agent plays the role of the dormant species to provide control over molecular weight and polydispersity. As illustrated in the reaction scheme, the initiator radical  $\text{I}\cdot$  reacts with monomer molecules to form a propagating radical  $\text{P}_m\cdot$ , which further adds to the thiocarbonylthio compound ( $\text{RSC}(\text{Z})=\text{S}$ ) (1) yielding a carbon-centered intermediate RAFT radical (2). Fragmentation of these intermediate radicals produces a polymeric

thiocarbonylthio compound ( $P_mS(Z)C=S$ ) (3) and a new radical  $R\cdot$ , which is able to reinitiate polymerisation by reacting with monomer molecules, thus forming a new propagating radical ( $P_n\cdot$ ). Ultimately, the existence of a rapid equilibrium between the active propagating radicals ( $P_m\cdot$  and  $P_n\cdot$ ) and the dormant polymeric thiocarbonylthio compounds (3) provides equal probability for all chains to grow and allows for the production of narrow polydispersity polymers with a thiocarbonylthio end group. The desired product of a RAFT polymerisation is typically a linear polymer with an R group at one end and a thiocarbonylthio moiety at the other end. However, since free radical intermediates are involved in RAFT polymerisation, some radical-radical termination could not be avoided resulting in an amount of dead polymer.<sup>101</sup>

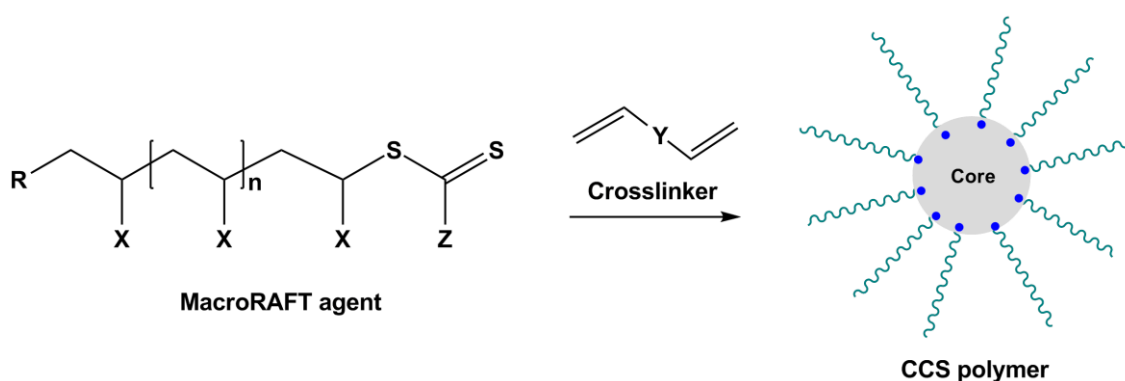


**Scheme 1.8.** Mechanism of RAFT polymerisation.

Depending on the nature of the activating (Z) group, the thiocarbonylthio RAFT agents can be classified into four classes: (i) dithioesters (Z = aryl or alkyl), (ii) dithiocarbamates (Z = substituted nitrogen), (iii) dithiocarbonates (xanthates) (Z = substituted oxygen) and (iv) trithiocarbonates (Z = substituted sulfur).<sup>102, 103</sup> With appropriate choice of RAFT agent and reaction conditions, RAFT polymerisation can be used to produce polymers with narrow polydispersity and predetermined molecular weights. These can be controlled by the extent of conversion and concentration of the

RAFT agent. It has been reported that the effectiveness of RAFT agents depend strongly on (a) the nature of the Z and R groups, (b) the monomer and (c) the polymerisation conditions.<sup>97, 104</sup>

In an arm-first CCS polymerisation, a simple approach to carry out the chain extension of the preformed arm (a macroRAFT agent) may be utilized.<sup>105</sup> The thiocarbonylthio end groups can be reactivated in a polymerisation using divinyl compounds. This leads to the formation of star-shaped structures or microgels with a branch length determined by the size of the macroRAFT agent (Scheme 1.6).



**Scheme 1.9.** Schematic of the synthesis of CCS polymers using RAFT via the arm-first approach.

The possibility of using the arm-first method in RAFT polymerisation for the synthesis of star polymers with a crosslinked core was first proposed by Moad *et al.*<sup>106</sup> but the first experimental proof of the synthesis was reported by Lord *et al.*,<sup>107</sup> followed by Zhang and Chen.<sup>108</sup> The CCS polymers were synthesized from dithiobenzoate terminated living polystyrene and DVB as the crosslinker. However, the resultant polystyrene CCS polymers were poorly controlled with low star yield and high polydispersity as a result of side reactions involving the intermediate radicals<sup>53</sup> and potentially, core and chain shielding effects.<sup>109</sup> Crosslinker concentration and reaction time have to be carefully adjusted to avoid the formation of a broad range of products with a varying number of branches. Better-defined products are usually obtained when CCS with amphiphilic block structures in each arm are prepared.<sup>105, 110</sup> Amphiphilic block copolymers can self-assemble in micelles using a selective solvent. The

subsequent crosslinking captured the well-defined structure of the micelle, leading to CCS polymers with narrower molecular weight distributions.<sup>100</sup> Macromonomer approach has also been applied in the synthesis of CCS polymers via the arm-first RAFT polymerisation.<sup>43</sup> The star yield increased while maintaining narrow MWD when a multi batch approach (step-wise addition of initiator and crosslinker) was applied in the synthesis. Very recently, cleavable miktoarm CCS copolymers containing three different arm compositions (hydrophobic, hydrophilic and cationisable) were successfully synthesised by RAFT polymerisation via the arm-first approach.<sup>35</sup> The star assembly and crosslinking occurred in a single step, which involved copolymerisation of a multiolefinic monomer mediated by a macroinitiator or macro-transfer agent. Both the molecular weight and MWD of the CCS polymers were found to be influenced by the proportion of the hydrophobic arms and amount of crosslinker used. Recent advancement in the synthesis of CCS polymers via arm-first RAFT is based on heterogeneous polymerisation (either emulsion or dispersion polymerisation) in order to afford low-dispersity CCS polymers.<sup>44, 111</sup>

The particular strength of RAFT chemistry lies in its high tolerance to functional monomers such as acid (e.g. acrylic acid), acid salt (e.g. styrenesulfonic acid sodium salt), hydroxy (e.g. hydroxyethyl methacrylate) or tertiary amino (e.g. dimethylaminoethyl methacrylate) groups,<sup>96</sup> and the non-demanding reaction conditions (e.g., tolerance to oxygen and low temperatures) under which the polymerisations can be carried out.<sup>53</sup> In addition, a wide range of monomers with varying reactivity including vinyl acetate and *N*-vinyl pyrrolidone can be polymerized in a controlled manner.<sup>53, 112</sup> RAFT polymerisation offers substantial versatility when it comes to the synthesis of complex architectures<sup>105, 113-115</sup> and is also applicable to emulsion-polymerisation processes.<sup>116, 117</sup> Moreover, it can be performed at low temperatures,<sup>118</sup> in water,<sup>117, 119</sup> and using either UV<sup>120</sup> or  $\gamma$  irradiation<sup>121</sup> as an initiation source.

## 1.4 CCS Polymer Applications

The combination of unique rheological properties and the ability to employ RDRP techniques to obtain well-defined structures make CCS polymers very attractive for use in a variety of applications such as catalysis,<sup>122</sup> drug delivery,<sup>123</sup> polyelectrolytes<sup>124</sup> and molecular imprinting.<sup>122</sup> In this thesis, the focus is on molecular imprinting and thus is discussed in the subsequent section.

### 1.4.1 Molecular Imprinting

Molecular imprinting is a method of inducing molecular recognition properties into synthetic polymers in response to the presence of a target species (template) during formation of the three-dimensional structure of a polymer.<sup>125, 126</sup> Compared to biomolecules such as antibodies and enzymes, molecular imprinted polymers (MIPs) possess advantages of physical robustness, rigidity, resistance to elevated temperatures and pressures, and inertness towards acids, bases, metal ions and organic solvents.<sup>125, 127-129</sup>

Molecular imprinting<sup>126, 128</sup> involves arranging polymerisable functional monomers around a template and is described schematically in Figure 1.3. The arrangement is achieved either by utilizing non-covalent interactions such as hydrogen bonds or ion-pair interactions (non-covalent imprinting) or reversible covalent interactions (covalent imprinting) between the template and the functional monomers. The complexes formed are then incorporated by polymerisation into a highly crosslinked macroporous polymer matrix. Extraction of the template leaves sites in the polymer with specific shape and functional group complementary to the original template. In that way, a molecular memory is introduced into the polymer, which is now capable of selectively rebinding the target.

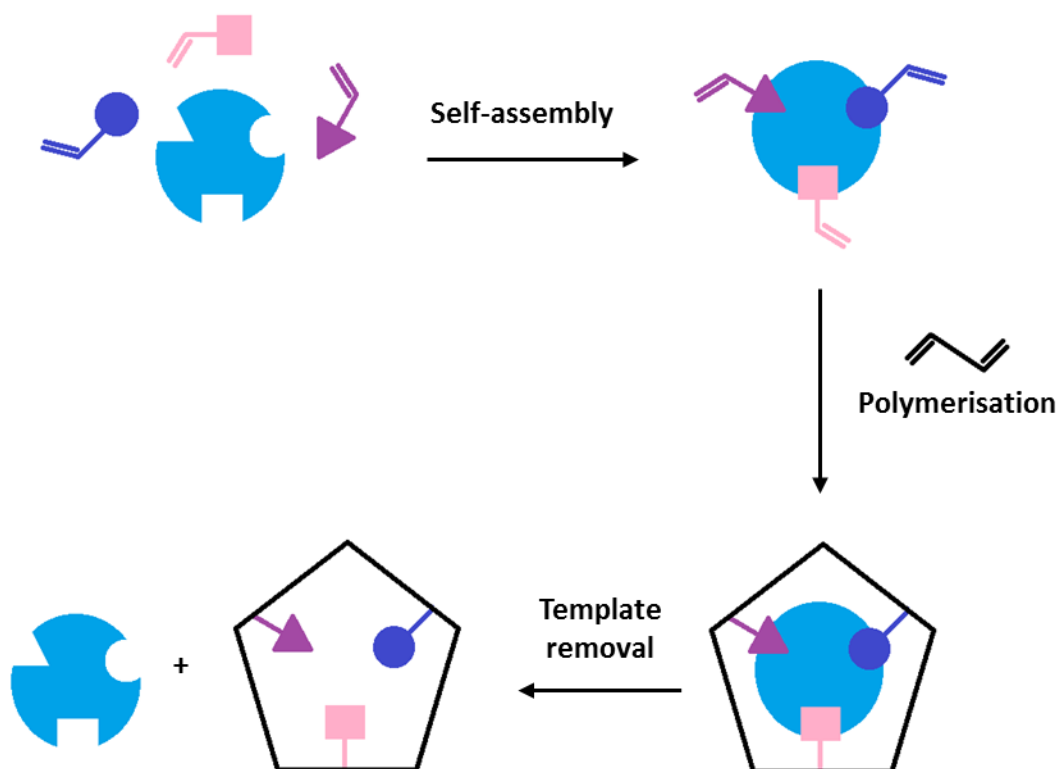


**Figure 1.3.** General principle of molecular imprinting.

The methodologies available for molecular imprinting are both flexible and robust and imprints can now be made against a wide variety of small molecules as well as some large molecules such as oligopeptides<sup>130, 131</sup> and proteins<sup>132-134</sup> with confidence that the resulting polymers will have a high affinity and selectivity for the template.<sup>125, 135</sup> As a generalization, covalent imprinting gives better defined and more homogeneous binding sites, but non-covalent imprinting is much more flexible in the range of functionalities which can be targeted and thus the range of templates which can be used. The latter is also much easier practically, since little or no chemical derivatization is required.

Studies have shown that enantiomeric and substrate selective recognition properties of molecular imprinted polymers are largely dependent on the size, shape, the physical or chemical properties and relative position of the functional groups of the recognition sites and the sample molecule.<sup>136</sup> In organic media, polar interactions (hydrogen bonding, ionic interactions, etc.) are mainly responsible for the binding and

recognition, whereas in aqueous media, hydrophobic interactions play an important role.<sup>137-139</sup>

As mentioned above, a MIP is a recognition tool that can be targeted to specific molecular species. The recognition event can be coupled to a range of detection technologies and the more complex the target species, the more specific and exclusive the recognition event. The important processes in creating a recognition based polymer are (1) creating well-defined sites during the polymerisation by the design of relevant interactions; (2) preserving the structure of imprinted sites intact; and (3) allowing for ease of diffusion of solutes into and out of the network.<sup>122</sup> The ideal imprinting effect, although difficult to achieve, would be one in which the imprinting creates an on/off switch such that only the template is bound and all other molecules are rejected. Among the major factors affecting the creation of specific sites are the interaction between the monomers and the template and having an increased number of point interactions.

Since the molecular imprinting process involves the generation of cavities containing functional sites within a highly crosslinked polymer matrix and is based on the initial formation of a template-functional monomer pre-polymerisation complex, it is very important to strengthen this pre-polymerisation complex. It is the polymerisation of this complex that will yield a defined spatial configuration within the highly crosslinked polymer matrix, leaving behind the cavities that are complementary in shape and chemical functionality to the template after its removal. There are three important factors that affect the formation of the pre-polymerisation complex:<sup>140</sup>

- (i) The type of functional monomer employed during the polymerisation
- (ii) The relative ratio of the functional monomer to the template
- (iii) The solvent (porogen).

In the non-covalent approach, the functional monomer should be able to interact with the template either via hydrogen bonding, electrostatic, or hydrophobic interactions to form special binding sites before the crosslinked co-polymerisation occurs.<sup>141</sup> The

degree of complexation of the template is determined by the relative ratio of the functional monomer to the template<sup>142</sup> and on the strength and the number of the interactions between the functional monomer and the template.<sup>143</sup>

The porogen should be able to dissolve all the reagents and allow the formation of the pre-polymerisation complex. The latter can be enhanced by choosing a porogen that is capable of facilitating the interactions required for the template-monomer pre-polymerization complex to reduce the interferences during the template-monomer pre-polymerisation complex formation.<sup>144, 145</sup> Apart from that, the pore size and surface area are also influenced by the porogen used during polymerisation. Porosity, which affects the mass transfer of template molecules, arises from phase separation of the porogen and the growing polymer during polymerisation.

MIPs have been used in many different applications, such as affinity separation, for directed synthesis, catalysis and slow drug release, as selective solid-phase extraction media, antibody mimics in immunoassays, as well as the recognition elements in biosensors.<sup>146-150</sup> Compared with their natural counterparts (antibodies or enzymes), MIPs possess several advantages such as having a superior chemical and physical stability, which facilitates their storage and handling as well as their integration in standard industrial fabrication procedures.<sup>151</sup> In addition, they can be regenerated and are potentially reusable, and may thus be less costly than biomacromolecules.

The majority of reports on MIPs described organic polymers synthesized from vinyl or acrylic monomers by conventional free-radical polymerisation<sup>152</sup> due to the rather straightforward synthesis of these materials and to the vast choice of available monomers with different functional groups. The lack of control over chain propagation and termination in the conventional FRP has resulted in the formation of polymer networks with heterogeneous structures, which affect the quality of the binding sites formed within the networks and also leads to a broad distribution of binding sites.<sup>153</sup> RDRP methods such as iniferter, RAFT and ATRP offer the ability to create imprinted polymers having more homogeneous network structures and thus enhanced binding

properties.<sup>154-159</sup> However, these techniques have not been extensively applied in the field of molecular imprinting.

The iniferter method was mainly used to achieve the synthesis of thin MIP films on supports by surface-initiation.<sup>160</sup> The application of iniferter-initiated polymerisation in MIP was first demonstrated by Wang *et al.*, who photografted a crosslinking polymeric layer of *N,N'*-methylenebisacrylamide (MBAA) and acrylic acid in the presence of a theophylline template on a polyacrylonitrile membrane modified with a diethyldithiocarbamate iniferter.<sup>155</sup> The resultant membrane was found to exhibit high selectivity towards theophylline template compared to caffeine. Recently, iniferter-induced “living” radical polymerisation (ILRP) mechanism has been introduced into precipitation polymerisation in the one-pot synthesis of molecular imprinted microspheres.<sup>161</sup> The resultant MIP microspheres exhibited obvious molecular imprinting effects towards the template (either 2,4-Dichlorophenoxyacetic acid (2,4-D) or 2-chloromandelic acid (CMA) template rebinding kinetics, and appreciable selectivity over structurally related compounds. More recently, combination of iniferter polymerisation with post dilution proposed by Wulff *et al.*<sup>162</sup> has been reported, which produced higher yield of molecular imprinted nanoparticles than using UV irradiation alone.<sup>163</sup> Using this technique, high monomer and template concentrations could be employed, thus the probability of forming highly specific binding sites is maximised.

RAFT polymerisation has been used to successfully synthesise MIPs with different formats, where the focus was on surface-imprinted polymer preparation. The immobilization of RAFT agent on the surface of supports such as silica nanoparticles was found to allow the growth of uniform MIP shells with adjustable thicknesses.<sup>164</sup> Similar to iniferter, RAFT polymerisation has also been used in combination with precipitation polymerisation which is known as RAFT precipitation polymerisation (RAFTPP) to synthesise molecularly imprinted polymer microspheres.<sup>165</sup> The RAFT polymerised microspheres were reported to exhibit higher binding capacity per unit surface area over the conventionally synthesised MIP microspheres. Recently, the

RAFTPP method was applied in the synthesis of narrowly dispersed pure-water-compatible MIP microspheres with surface-grafted hydrophilic polymer brushes. The obtained MIP microspheres showed significantly enhanced surface hydrophilicity and excellent template recognition ability in pure aqueous solutions. Liu *et al.* compared the separation efficiency of monolithic MIP columns synthesized by conventional FRP and RAFT.<sup>157, 166</sup> The separation on the RAFT MIP was found to be improved owing to an increased specific surface area. More recently, Gonzato *et al.* compared the imprinting of S-propranolol acrylic and methacrylic matrices via RAFT and FRP.<sup>167</sup> It was found that more homogeneous networks were achieved by RAFT compared to FRP which led to higher affinity for the template.

One of the characteristics of MIPs is that they are crosslinked polymers. This crosslinking is necessary in order to maintain the conformation of the three-dimensional binding sites obtained through the molecular imprinting process, and thus the ability of the polymer to specifically and selectively recognize its target molecule. The insolubility of these crosslinked polymers, however, limits the applicability of MIPs by imposing tedious or difficult processes for their inclusion in organic electronic devices such as organic light emitting diodes (OLEDs), photovoltaic cells (OPVCs) and organic field-effect transistors (OFETs).<sup>168, 169</sup> They have to be either prepared as monoliths and ground into powders or are prepared *in situ* on a support. New nanoparticle-based MIPs and new dispersible MIPs may be suitable for potential application in detection methods.<sup>170, 171</sup> This can be achieved via a CCS polymer where the central core is imprinted and crosslinked while the arms of the star provide solubility.

Only a few papers have been published on the application of star polymers in molecular imprinting.<sup>122, 172-175</sup> For example, Oral and Peppas reported the synthesis of responsive and recognitive polymeric networks based on custom made polyethylene glycol (PEG) star polymers.<sup>122</sup> By imprinting the star polymer building blocks with the desired template, D-glucose, polymeric networks that could distinguish between the template and a similar sugar; D-fructose were obtained. Using copolymerisation with

methacrylic acid, star polymer networks with pH-sensitivity, which showed a sharp transition in swelling around a pH of 4.5 were obtained. Later, Southard *et al.* have developed dispersible and processable MIP technologies with good sensitivity and very high selectivity.<sup>173</sup> The MIPs have been prepared using RAFT polymerisation followed by ring-closing metathesis (RCM). Crosslinking of the polymer core which consisted of a dithiobenzoate-substituted tris( $\beta$ -diketonate)-europium(III) complex, was performed using a second generation Grubbs catalyst. The high polydispersity of the three arm star polymers due to inter star crosslinking was improved by crosslinking in very dilute solution. Although an imprinting effect was not clearly demonstrated and a non-imprinted control polymer was not prepared, the polymer was found to be selective for dicotophos over the related compounds dichlorvos, diazinon, and dimethyl methylphosphonate. Recently, the first example of using a MIP to amplify a surface plasmon resonance signal for analyte detection was reported by Izenberg *et al.*<sup>172</sup> They have synthesised water-soluble processable star polymers using RAFT polymerisation via the core first method. Biotin-imprinted 3-arm star polymers were prepared by crosslinking the polymers with 1,4-diaminobutane using *N*-(3-dimethylaminopropyl)-*N'*-ethylcarbodiimine (EDC) / *N*-hydroxysuccinimide (NHS) coupling which were then coupled to a SPR analyte capture method for the detection of low molecular weight amines.

The synthesis of CCS MIPs however has not yet been extensively investigated and thus may be worth exploring. The only report on the synthesis of a CCS MIP was via the arm-first method using benzyl diethyldithiocarbamate iniferter.<sup>174</sup> The CCS MIP, intended as a drug carrier was prepared by crosslinking linear poly(methyl methacrylate) (PMMA) with arylamide *N*,*N*-methylenebisacrylamide in the presence of methacrylic acid (MAA) as well as L-phenylalanine (PA) as the functional monomer and the template respectively.<sup>175</sup> A liquid membrane experiment was conducted and the result showed that less than 3% of the PA template was transported during 120 hr operation of the experiment. They concluded that the star MIP was suitable for extremely slow administration of drug delivery system.

Comparing the above RDRP techniques in the context of MIP, the major limitation for ATRP is the small choice of monomers with suitable functional groups.<sup>151</sup> Typical monomers used for molecular imprinting (e.g. methacrylic acid and trifluoromethyl acrylic acid) are incompatible with the metal–ligand complex involved in ATRP. Moreover, with certain monomers such as methacrylamide and vinylpyridine, it is difficult to achieve high monomer conversion. Template molecules also often carry functional groups that may inhibit the catalyst. In addition, the ATRP method is complicated by the fact that the catalysts need to be removed at the end of the polymerisation. Hence, ATRP may not be the best choice for molecular imprinting due to the difficulty of obtaining high conversion in the presence of certain functional groups on monomer and template. On the other hand, iniferter-initiated and RAFT polymerisations have the advantage of being compatible with the majority of functional monomers and template commonly used in molecular imprinting. In particular, the dithiocarbonyl reagents and the dormant macroradicals of RAFT are non-reactive towards polar and ionic groups, thus RAFT is best suited for polymerisation involving polar species especially in the imprinting system where template/monomer interaction is based on hydrogen bonding or ionic interactions.<sup>176</sup> As for the iniferter polymerisation, since the polymerisation can be initiated photochemically, the iniferter radical polymerisation process is faster than thermal initiation and can be carried out at room temperature, which is also very useful in the molecular imprinted polymer (MIP) preparation where the template/monomer complexes are stable at low temperature.<sup>136, 177</sup>

In view of the above evidence in the literature pertaining to the synthesis of CCS polymers and molecular imprinting, iniferter and RAFT are among the two RDRP techniques that have the potential to be employed in the synthesis of CCS MIPs. Since the aim of this study is to synthesise dispersible and processable CCS MIPs using a simple and robust method, iniferter and RAFT techniques therefore seem to be a more satisfactory choice.

## 1.5 Project Outline

The aim of this project is to synthesise CCS MIPs that are readily dispersible by reversible-deactivation radical polymerisation (RDRP) techniques, i.e. iniferter and RAFT so that they can then be processed to become thin films, via a simple method such as drop coating or spin casting the MIP solution onto a substrate, and has the potential to improve the quality, capacity or ease of synthesis of the films for their inclusion in sensing devices.

We begin our investigation with the synthesis of CCS non-imprinted polymers via iniferter and RAFT, which are discussed in Chapter 2 and Chapter 3, respectively. For this purpose, a series of CCS polymers were synthesised via both the arm-first and the core-first methods. A two-pot strategy was employed in the preparation of the arm-first CCS polymers, where the linear PS arm was synthesised and isolated before being crosslinked by EGDMA to form the arm-first CCS polymers. The effect of changing several parameters such as polymerisation time, ratio of crosslinker to linear arm, concentration of arm as well as arm length on the CCS formation were investigated. The core-first CCS polymers were also synthesised by utilising the two-pot strategy in which the core was synthesised and isolated before being subjected to further polymerisation in the presence of styrene to afford the CCS polymers. A comparison between the iniferter and RAFT methods in the synthesis of CCS polymers are presented at the end of Chapter 3.

Based on the results presented in Chapters 2 and 3, core-first method was chosen as the best method to prepare the CCS MIPs. One of the most important aspects in the synthesis of CCS MIPs via the core-first method was the preparation of the MIP core precursors as the imprinting sites were created during their preparation. Hence, it is crucial to prepare MIP cores with optimised binding properties such as binding capacity, optimum binding time as well as type and number of binding sites. For this purpose, Chapter 4 is dedicated to the preparation of MIP microspheres using iniferter-induced “living” radical polymerisation (ILRP) and RAFT precipitation

polymerisation (RAFTPP). Benzylpiperazine has been chosen as the model template. Binding properties, particle size, morphology, surface area and porosity of the polymers were investigated and compared between the microspheres prepared via iniferter and RAFT methods. The selectivity of the BZP imprinted polymer towards the BZP template was then investigated under non-competitive and competitive environments over other structurally related drugs such as (1R,2S)-(-)-ephedrine (EPH) and 1-phenylpiperazine (PHP).

Based on the results presented in Chapter 4, i.e. preparation of MIP microspheres, iniferter was chosen as a better method to prepare the CCS MIPs over RAFT. Thus, a pilot study was carried out to synthesise CCS MIPs using the best formulation obtained during the preparation of the MIP microspheres as the core precursor. The CCS MIP preparation and assessment of their binding performance are presented in Chapter 5. To the best of my knowledge, this work is first on the CCS MIP synthesis via the two-pot core-first method for benzylpiperazine (BZP) template and, thus, is novel.

## Chapter 2

### Core Crosslinked Star Polymers Via a Photoiniferter

#### 2.1 Introduction

This chapter deals with the preparation of core-crosslinked star (CCS) polymers via the iniferter technique. The focus is on the CCS polymers prepared via the arm-first method, although some preliminary results on the CCS polymers preparation via the core-first method are also included. As mentioned in Chapter 1 (see §1.2), there are several methods that can be used to prepare star polymers which involve the use of macroinitiators, macromonomers, multifunctional linking agents, difunctional monomers or multifunctional initiators.<sup>1, 6</sup> Employing the two-pot approach, we prepared our arm-first CCS polymers using the macroinitiator method i.e. by crosslinking living linear chains endcapped with diethyldithiocarbamate using a divinyl crosslinker (Scheme 1.1, §1.2.1), whereas the core-first CCS polymers were prepared by growing arms from a highly crosslinked core with an active surface (Scheme 1.4, §1.2.2).

The use of diethyldithiocarbamate-mediated living radical polymerisation techniques has been reported in the synthesis of star block copolymers<sup>88, 178</sup> and benzyl *N,N*-diethyldithiocarbamate (BDDC) iniferter was employed in the preparation of CCS polymers via the arm-first method.<sup>174, 175</sup> The synthesis of CCS polymers via the core-first ATRP technique in one-pot has also been reported,<sup>49</sup> however, the use of BDDC

iniferter in the formation of CCS polymers via the two-pot core-first method, to the best of my knowledge, has never been reported.

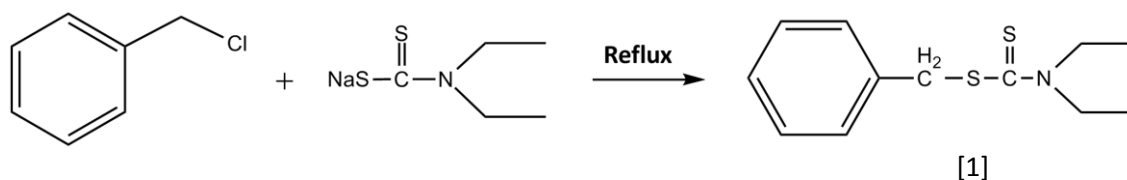
## 2.2 Experimental

### 2.2.1 Materials

Sodium *N,N*-diethyldithiocarbamyl trihydrate and benzyl chloride (99%) were obtained from Sigma-Aldrich and used as received. Styrene (St) and ethylene glycol dimethacrylate (EGDMA) were obtained from Sigma-Aldrich ( $\geq 98\%$  purity), and were passed through a column of activated basic alumina (Aldrich, Brockmann I, standard grade,  $\sim 150$  mesh, 5.8 nm) to remove radical inhibitors. Bulk grade methanol and ethanol were obtained from Merck and were distilled prior to use. All water was purified by reverse osmosis prior to use. Deuterated chloroform ( $\text{CDCl}_3$ , 99.6 atom %), for NMR analysis, was obtained from Aldrich. HPLC grade tetrahydrofuran (THF) was obtained from Scharlau and used for synthesis and GPC analysis. HPLC grade acetonitrile was obtained from Merck and used for synthesis and HPLC analysis. Potassium bromide (KBr) was obtained from Sigma-Aldrich and used for FTIR analysis. Benzyl *N,N*-diethyldithiocarbamate (BDDC, [1]) was synthesised following the procedure described in §2.2.2.

### 2.2.2 Synthesis of BDDC Iniferter

BDDC [1] is classified as a photoiniferter and was synthesised according to the following proposed reaction scheme:<sup>179</sup>



**Scheme 2.1.** Reaction scheme for the synthesis of BDDC [1].

A solution of sodium *N,N*-diethyldithiocarbamyl trihydrate (10.3 g, 0.046 mol) and distilled ethanol (50 mL) were placed in a 200-mL three-necked flask equipped with a stirrer, a dropping funnel, and a reflux condenser. To this solution, 10 mL of ethanol solution of benzyl chloride (4.8 g, 0.038 mol) was added dropwise at 0 °C. The solution was stirred for 24 h at ambient temperature. Then 150 mL of water was added and extracted with diethyl ether (200 mL, 3 times). The organic phase was washed with water, dried on anhydrous sodium sulphate (Na<sub>2</sub>SO<sub>4</sub>), filtered, and evaporated under vacuum. The residue was then recrystallized three times from methanol. Yield of benzyl *N,N*-diethyldithiocarbamate (BDDC [1]: 8.36 g (92%). <sup>1</sup>H-NMR (CDCl<sub>3</sub>, 400 MHz, ppm): δ 7.40-7.2 (m, 5H, C<sub>6</sub>H<sub>5</sub>), 4.54 (s, 2H, CH<sub>2</sub>S), 4.05 (q, 2H, N(CH<sub>2</sub>CH<sub>3</sub>)<sub>2</sub>), 3.73 (q, 2H, N(CH<sub>2</sub>CH<sub>3</sub>)<sub>2</sub>), 1.28 (m, 6H, -N(CH<sub>2</sub>CH<sub>3</sub>)<sub>2</sub>). <sup>13</sup>C-NMR (CDCl<sub>3</sub>, 400 MHz, ppm): δ 195.2, 136.0, 129.4-127.4, 49.4, 46.7, 42.2, 12.5, 11.6. FTIR (cm<sup>-1</sup>): 3028 (aromatic C-H), 2924 (aliphatic C-H), 2000–1665 (aromatic overtones), 1600 and 1452 (C-C), 1485 (C-N), 1267 (S-C=S), 1008 (C-S), 750 and 700 (aromatic C-H).

### 2.2.3 Preparation of CCS Polymers via Arm-First

#### 2.2.3.1 Synthesis of PS Arm using BDDC Iniferter

A typical polymerisation procedure for the synthesis of linear PS with diethyldithiocarbamate (DDC) end functionality is as follows. Styrene (6 mL, 52.2 mmol) and BBDC (240 mg, 1.00 mmol) were mixed in a test tube. The mixture was deoxygenated by purging with nitrogen for 30 minutes, sealed and then placed under UV irradiation (on either an Efos Acticure A4000 with a high pressure 100 Watt mercury vapour short arc bulb and a liquid-filled light guide or a 450 W medium pressure mercury vapour, quartz UV lamp (Ace glass, No. 7825-34) in a photochemical reaction cabinet) at ambient temperature. After polymerisation for the desired time, the polymerisation was quenched by immersing the test tubes in an ice-water bath. The resulting products were diluted with THF and the polymers were precipitated by adding the polymerisation mixtures dropwise into an excess of methanol under vigorous stirring. The polymers obtained were then purified twice by reprecipitation

from THF into methanol, followed by drying in a vacuum oven at 40 °C. The yield of the polymers was determined gravimetrically.

### **2.2.3.2 Preparation of Arm-first CCS Polymers**

For the synthesis of a CCS polymer via the arm-first method, a typical experimental procedure is as follows: Previously synthesised linear PS arm (200 mg) and EGDMA (0.163 mL, 0.862 mmol) were dissolved in THF (11.5 mL) in a test tube. The reaction mixture was purged with nitrogen for 30 min, sealed and placed under UV irradiation from a 450 W medium pressure mercury vapour, quartz UV lamp (Ace glass, No. 7825-34) in a photochemical reaction cabinet at room temperature. After polymerisation for 5 h, the polymerisation was quenched by immersing the test tubes in an ice-water bath. The polymer was precipitated by adding the polymerisation mixture dropwise into an excess amount of methanol under vigorous stirring. The polymer obtained was then purified twice by reprecipitation from THF into methanol, followed by drying in a vacuum oven at 40 °C. The yield of the star polymers was determined gravimetrically.

## **2.2.4 Preparation of CCS Polymers via Core-first**

### **2.2.4.1 Synthesis of PEGDMA Core using BDDC Iniferter**

For the PEGDMA core synthesis, a typical experimental procedure is as follows: EGDMA (2.5 mL, 13.3 mmol) and BDDC (127 mg, 0.530 mmol) were mixed in THF (40.0 mL) in a test tube. The reaction mixture was purged with nitrogen for 30 min, sealed and placed under UV irradiation using a similar set up described in §2.2.3.2 at room temperature. After polymerisation for 24 h, the polymerisation was quenched by immersing the test tubes in an ice-water bath. The viscous reaction mixture was then added dropwise into a large amount of methanol to obtain a white solid, washed twice in methanol followed by drying in a vacuum oven at 40 °C. The core yield was determined gravimetrically.

#### **2.2.4.2 Preparation of Core-first CCS Polymers**

The previously synthesised PEGDMA core from §2.2.4.1 was then used as the core precursor to prepare the CCS polymer. A typical experimental procedure is as follows: PEGDMA core (30 mg), St (3.0 mL, 26.1 mmol) and THF (1.5 mL) were added to a test tube. The reaction mixture was purged with nitrogen for 30 min, sealed and placed under UV irradiation using a similar set up described in §2.2.3.2 at room temperature. After polymerisation for 24 h, the polymerisation was quenched by immersing the test tubes in an ice-water bath. The non-dispersible polymer (fraction 1) was removed by centrifugation and washed with methanol whereas the dispersible polymer (fraction 2) was precipitated by adding the supernatant dropwise into an excess amount of methanol under vigorous stirring. The resultant polymer was then purified twice by reprecipitation from THF into methanol, followed by drying in a vacuum oven at 40 °C.

### **2.3 Characterisation**

#### **2.3.1 Nuclear Magnetic Resonance**

$^1\text{H}$  and  $^{13}\text{C}$  Nuclear Magnetic Resonance (NMR) spectra of the polymers were measured using a Bruker Avance 400 MHz spectrometer in  $\text{CDCl}_3$ .

#### **2.3.2 Fourier Transform Infrared**

Fourier Transform Infrared (FTIR) spectra were recorded on a Shimadzu FTIR 8400S spectrophotometer using IR Solution software and a PIKE technologies 30SPEC EasiDiff diffuse reflectance accessory. The FTIR spectra of mixed powders of sample and KBr were obtained by scanning between  $4000 - 600 \text{ cm}^{-1}$ .

#### **2.3.3 Gel Permeation Chromatography**

The average molecular weight and molecular weight distribution of the polymers were measured with a Shimadzu Gel Permeation Chromatography (GPC) instrument equipped with a pump, refractive index (RI) and photodiode array (PDA) detectors, and

two Waters Styragel columns (HR5E and HR3), operating at 40°C, using THF as an eluent at a rate of 1.0 mL·min<sup>-1</sup>. Approximately 2 mg of a sample was dissolved in 1 mL of THF and the mixture was filtered using a 0.45 micron polytetrafluoroethylene (PTFE) syringe filter. Then 100 µL of the filtered solution was injected using the auto sampler. Linear polystyrene standards (Shodex®) in the molecular weight ( $M_n$ ) range 530 - 505 kDa were used for calibration (Figure 2.1) and the data were analysed using Shimadzu LCsolution 10A software. The area fractions of both the CCS and linear polymers were determined by deconvolution of the GPC curves using the Solver function (non-linear curve fitting)<sup>180</sup> in Microsoft Excel 2010 software. In the literature, the Gaussian function with modifications has been used for deconvolution of chromatograms.<sup>181-184</sup> In this study, for simplicity, the following Gaussian function has been used for this purpose:<sup>185</sup>

$$y(x) = h_m \cdot e^{-\ln 2 \left[ \frac{(x-x_{max})}{(w/2)} \right]^2} \quad (2.1)$$

where  $y$  = amplitude of the peak at point  $x$ ,  $h_m$  is the peak height,  $x$  is point  $x$  with amplitude  $y$ ,  $x_{max}$  is  $x$  at  $h_m$  and  $w$  is the peak width. An example of the deconvoluted GPC curve is shown in Figure 2.2 and the mathematical function to describe the chromatogram is as follows:

$$h(t) = h_m \cdot e^{-\ln 2 \left[ \frac{(t-t_R)}{(w/2)} \right]^2} \quad (2.2)$$

where  $h(t)$  is the intensity of the peak at time  $t$ ,  $h_m$  is the peak height,  $t$  is the time with height  $h$ ,  $t_R$  is the retention time (at  $h_m$ ) and  $w$  is the peak width.

Solver uses iterative numerical methods beginning with starting values (also called initial values) for the adjustable parameters (i.e.  $h_m$ ,  $t_R$  and  $w$ ). These values are changed during every regression step, and the similarity between the measured and calculated values is analysed and compared with the preceding iteration in order to make changes in the parameters for the subsequent iteration. In some cases, where the curve fitting did not yield good results, the position of the peak maxima ( $t_R$ ) had to be fixed so that it was equal or close to its position in the measured GPC curves. As

shown in Figure 2.2, the best fit between the measured GPC curve and the fitted GPC curve (sum of the deconvoluted curves) was obtained using the Solver function by minimising the sum of the squares of the differences between the measured and the fitted GPC curves ( $\Sigma\Delta^2$ ). The percentage of fractions of polymer with different MW was determined by dividing the area under each curve (G1 or G2) with the total areas of the two curves.

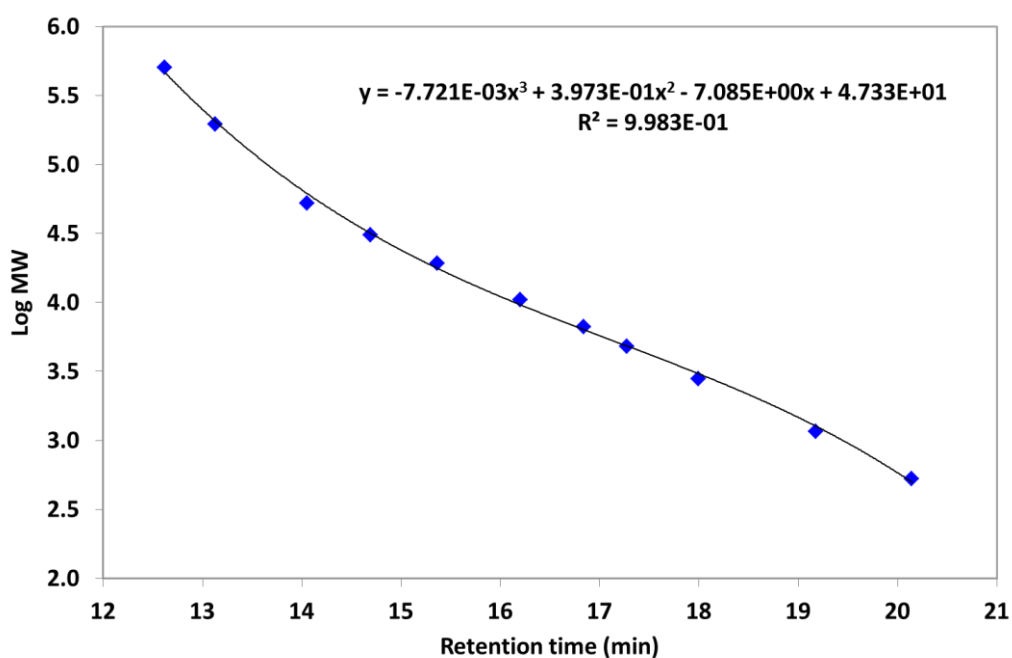


**Figure 2.1.** An example of a polystyrene calibration curve used for the molecular weight (MW) determination.

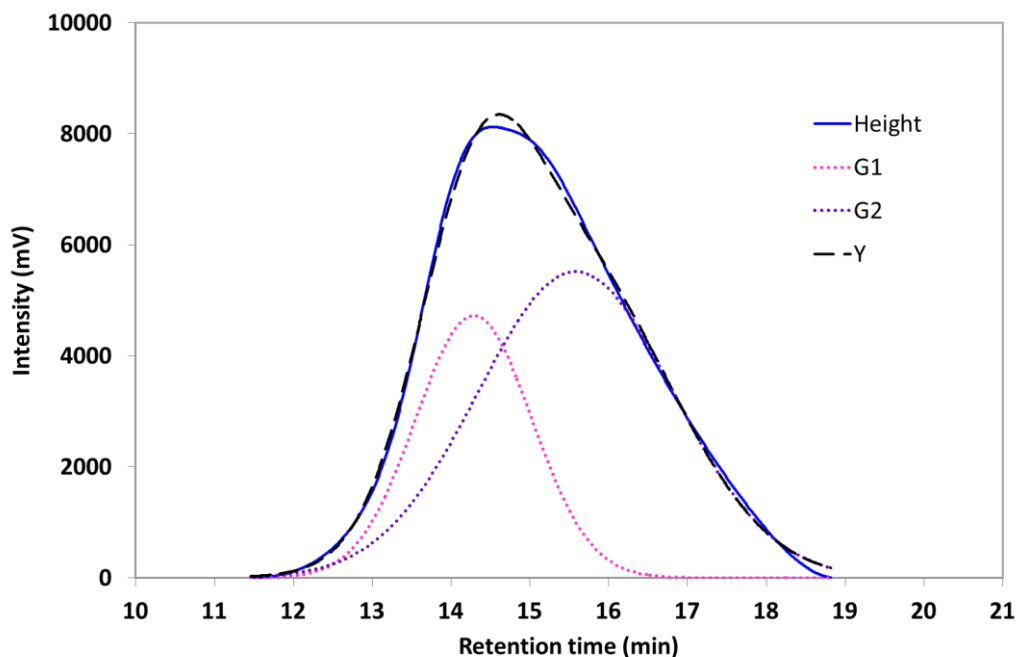


**Figure 2.2.** Deconvolution of a GPC curve (CCS-I6, Table 2.4) carried out using the Solver function in Microsoft Excel 2010. G1 and G2 represent the high and low MW polymers, respectively. The solid blue (height) and the black dashed (Y) lines are the measured and fitted GPC curves, respectively.

### 2.3.4 Dynamic Light Scattering

The particle size of the polymers was determined by dynamic light scattering (DLS, Malvern Zetasizer Nano ZS) with a detection angle of  $175^\circ$  via the in-built non-invasive back scatter technology using a glass cuvette. The DLS experiment was performed at  $20^\circ\text{C}$  with a He-Ne laser system tuned at a wavelength of 632.8 nm in THF and a mixture of THF and methanol (60:40, vol%). The size distribution calculated by the Nano software is derived from a non-negative least squares (NNLS) analysis. To avoid any possible dust contamination during preparation of the solutions, the dispersants were filtered using syringe filters with pore size of 200 nm. The samples were then filtered through a 450 nm membrane filter prior to measurement. Three repeat measurements were performed on each sample to check count rate reproducibility.

### 2.3.5 Scanning Electron Microscopy

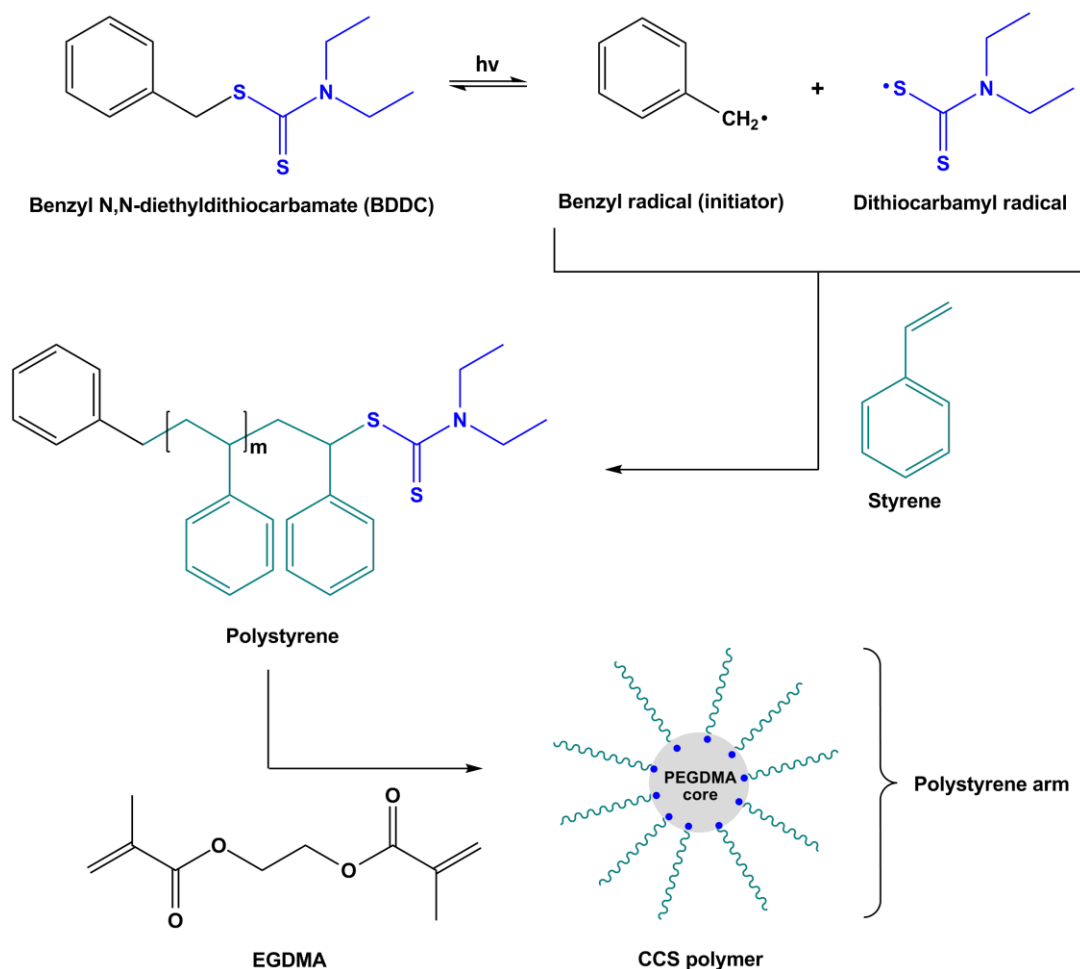
Scanning electron microscope images of the arm-first CCS polymers were generated using a Philips XL30 SEM and Oxford ISIS EDS (1997) software. The SEM images of the

core-first CCS polymer and its core precursor were generated using Zeiss Sigma VP FE-SEM. Surface micrographs were taken at various magnifications ranging from 5000 – 30000X.

## **2.4 Results and Discussion**

### **2.4.1 Arm-First CCS Polymers via Iniferter**

The synthesis of CCS polymers via the arm-first method using BDDC iniferter was carried out in a two-pot reaction as shown in Scheme 2.2. As can be seen from the scheme, the first step in the synthesis the CCS polymer was the preparation of linear PS, which was then isolated before undergoing further polymerisation with EGDMA to afford the CCS polymers. For this purpose, a series of PS arms were prepared by varying parameters such as polymerisation time and the mole ratio of styrene monomer to BDDC iniferter. The results are discussed in the subsequent sections.



**Scheme 2.2.** Synthetic route of CCS polymers via the arm-first iniferter polymerisation.

#### 2.4.1.1 Preparation of Linear PS Arm Precursor

The linear PS was prepared using the previously synthesised BDDC iniferter and then further used as the arm precursor for the preparation of CCS polymers. The photopolymerisation of styrene in the presence of BDDC iniferter is expected to proceed as proposed in reaction Scheme 2.2.

Among the *N,N*-diethyldithiocarbamate (DDC) derivatives, benzyl *N,N*-diethyldithiocarbamate (BDDC, [1]), was found to serve as an excellent photoiniferter in the bulk polymerisation of styrene (St) as it produced a benzyl radical similar to the propagating radicals of St.<sup>77</sup> As can be seen from Scheme 2.2, under the UV irradiation, BDDC photoiniferter dissociates through the C-S bond into two radicals: the active benzyl radical that can initiate propagation and the unreactive dithiocarbamyl radical

that reacts reversibly with the growing radicals to form dormant species.<sup>33, 78</sup> The polymerisation is expected to proceed via a living radical mechanism through the insertion of monomer in between the C-S bond of the iniferter,<sup>76, 78</sup> which leads to PS with two iniferter fragments as shown in Scheme 2.2. The obtained linear PS molecules are macroiniferters that can be used for further polymerisation with styrene leading to chain extension,<sup>186</sup> or with other monomers to form block copolymers.<sup>186-188</sup> In this study, the purified linear PS with DDC end functionality was crosslinked with EGDMA to afford the CCS polymers (Scheme 2.2). By using this method, the DDC moiety was preserved at the core of the CCS polymers.

#### 2.4.1.2 PS-DDC End-Group Analysis

The end group of the synthesised linear PS was characterized by FTIR, UV-GPC as well as <sup>1</sup>H and <sup>13</sup>C NMR spectroscopic analyses. Figure 2.3 shows a typical FTIR spectrum of the linear PS arm (PS-I17, Table 2.6). The characteristic peak of the DDC end group can be observed in the spectrum at 1266 and 1004 cm<sup>-1</sup>, which are attributed to the C=S and C-S stretching, suggesting the successful incorporation of the end group in the arm. The bands with peak locations at 3081, 3058 and 3023 cm<sup>-1</sup> are attributed to the C-H stretching of the aromatic rings of PS, whereas the bands with peak positions of 2917 and 2848 cm<sup>-1</sup> are assigned to the aliphatic C-H stretching. The absorption peaks at 1600, 1492, and 1451 cm<sup>-1</sup> are attributed to the C=C stretching, whilst the peaks at 757 and 698 cm<sup>-1</sup> are assigned to the out-of-plane C-H bending vibration of the aromatic rings of PS. Some of these peaks are also observed in the FTIR spectrum of pure BDDC (see the peak assignment in §2.2.2), which are attributed to the benzyl moiety in the structure.

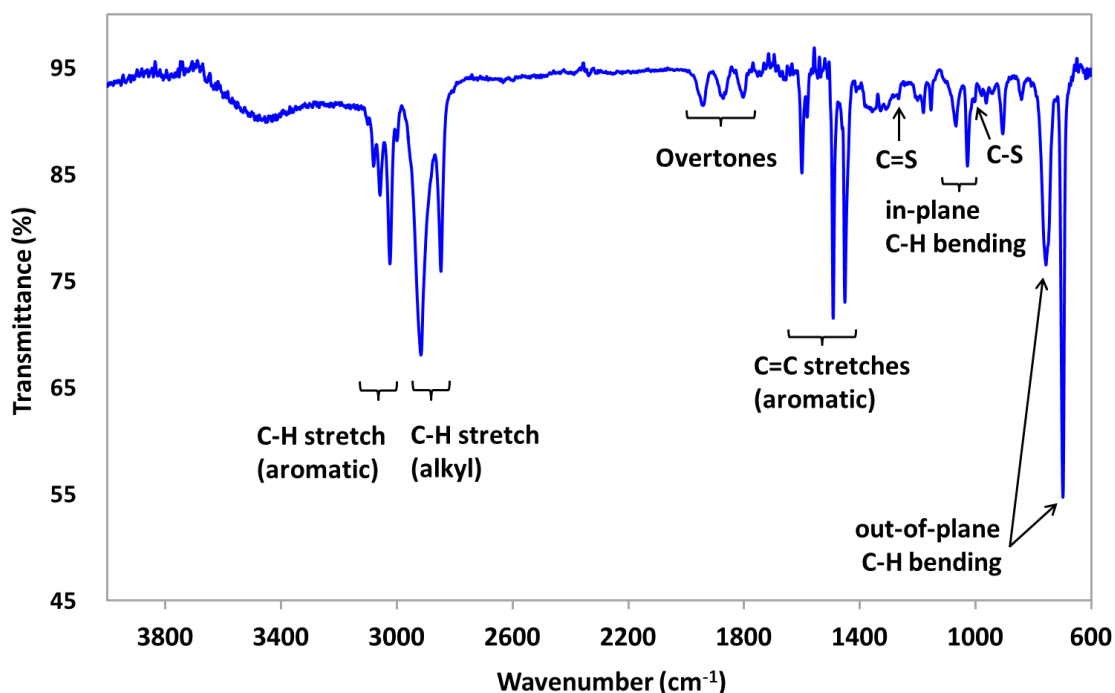


**Figure 2.3.** FTIR spectrum of linear PS prepared via BDDC iniferter.

A typical  $^1\text{H}$  NMR spectrum of a linear PS arm (PS-I19, Table 2.6) synthesised using the BDDC iniferter is depicted in Figure 2.4. In this spectrum, the peaks assigned to the methyl and methylene protons of the terminal DDC group can be clearly seen at about 1.25 ppm ( $\text{H}_4$ ) and between 3.4 – 4.2 ppm ( $\text{H}_3$ ), respectively, confirming the presence of *N,N*-diethyl dithiocarbamate (DDC) at the end of the chains (Scheme 2.2, §2.4.1). Peaks in between 4.7 – 5.3 ppm ( $\text{H}_g$ ) were attributed to the methine proton in the PS unit adjacent to the terminal DDC group, whereas the peak centred at 2.3 ppm ( $\text{H}_2$ ) was assigned to the methylene protons of the benzyl group of the BDDC iniferter. The peaks attributed to the backbone aromatic protons of PS are observed between 6.4 – 7.4 ppm ( $\text{H}_c$ ), which overlapped with the aromatic protons of the iniferter ( $\text{H}_1$ ). Finally, the peaks at about 1.5 and 1.9 ppm ( $\text{H}_d$ ) and ( $\text{H}_e$ ) respectively) are assigned to the backbone methylene and methine protons of PS. These results suggest that BDDC induced living radical polymerisation where the DDC end groups bond to the head position of the terminal styrene units.

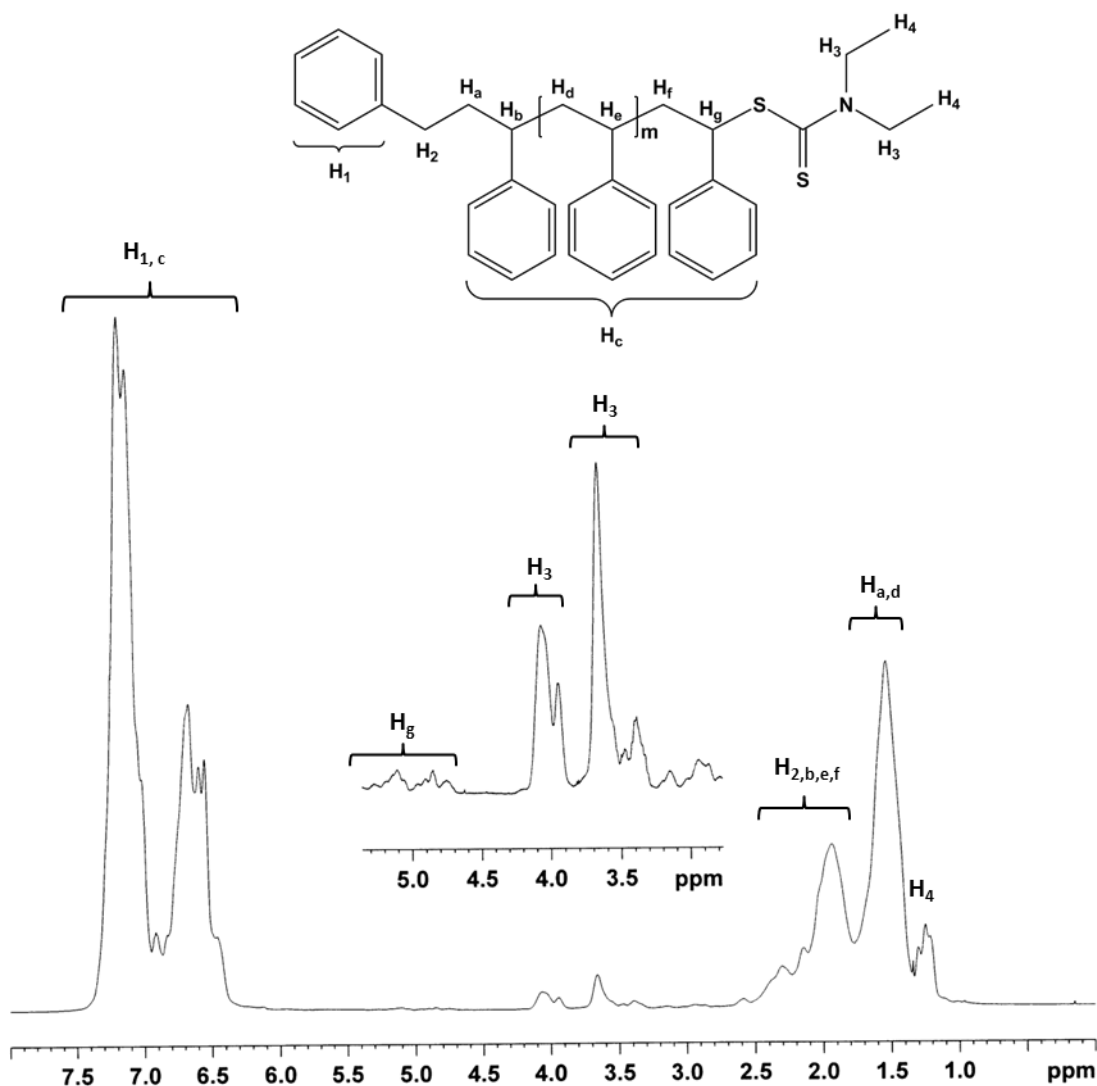


**Figure 2.4.** A typical  $^1\text{H}$  NMR spectrum of a living linear PS arm prepared via BDDC iniferter. Numbers and letters refer to the end groups and backbone protons, respectively.

The corresponding  $^{13}\text{C}$  NMR of the linear PS arm (PS-I19, Table 2.6) is depicted in Figure 2.5. The signals assigned to the backbone methylene and methine carbon of polystyrene are observed between 40 - 41 ppm ( $\text{C}_f$ ) and 41.5 - 45 ppm ( $\text{C}_e$ ) respectively. The characteristic signals of aromatic carbon of PS could be seen between 125 - 146 ppm ( $\text{C}_{c,d}$ ), which overlapped with that of the benzyl moiety ( $\text{C}_{1,2}$ ) of the iniferter. Signals between 11 - 13 ppm ( $\text{C}_6$ ) and 49.5 ppm ( $\text{C}_5$ ) are attributed to the methyl and methylene carbon of DDC end group, respectively, which suggests the incorporation of the end group in the linear PS arm. The signal between 194 - 196 ppm ( $\text{C}_4$ ) attributed to the quaternary carbon ( $\text{CS}_2$ )<sup>189</sup> of DDC end group strongly support the

successful incorporation of the BDDC iniferter. This is confirmed by the appearance of signals at 54 ppm ( $C_h$ ), attributed to the terminal carbon adjacent to sulphur and signal at 38 ppm ( $C_g$ ), which is assigned to the backbone carbon next to it. A signal attributed to the methylene protons of benzyl moiety of the BDDC iniferter could also be observed at about 34 ppm ( $C_3$ ).

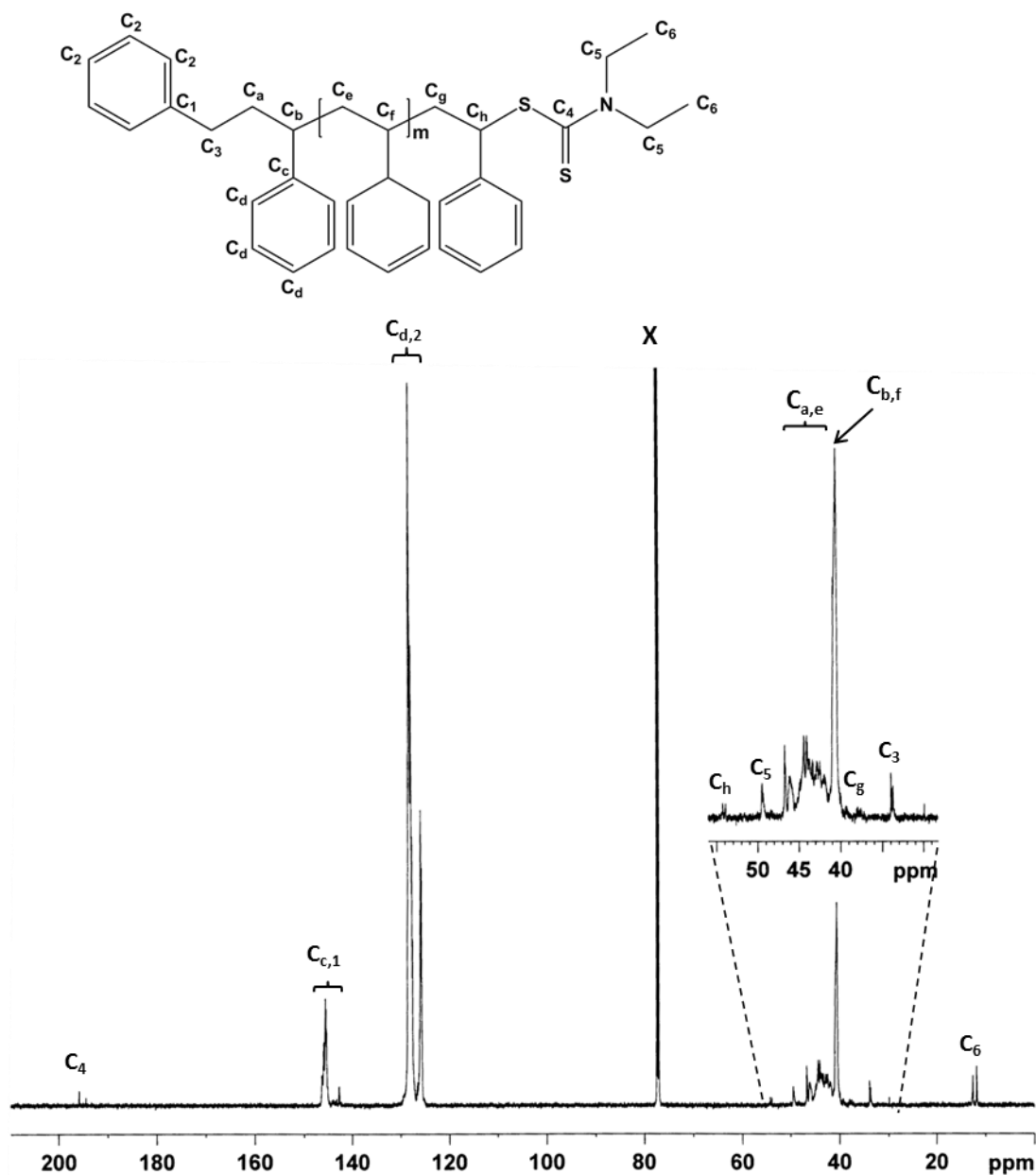


**Figure 2.5.** A typical  $^{13}\text{C}$  NMR spectrum of a living linear PS arm prepared via iniferter. X denotes peak attributed to  $\text{CDCl}_3$ .

Apart from FTIR and NMR, GPC with a photodiode array UV detector was also used for the analysis of the photosensitive DDC end group. Figure 2.6(A) and (B) shows the UV-GPC traces of the synthesised PS (PS-I18) compared to that of a commercial PS at 254 and 282 nm. The absorption observed at 282 nm in the GPC curve of the synthesised PS (Figure 2.6(A)) is attributed to the presence of DDC end group  $(-C(=S)-N)^{81}$  in the functionalised chains since PS obtained from conventional thermal polymerisation does not show any significant UV absorption above 260 nm (Figure 2.6(B)).<sup>190</sup> This result confirmed the successful incorporation of DDC moiety at the end of the linear PS chain.

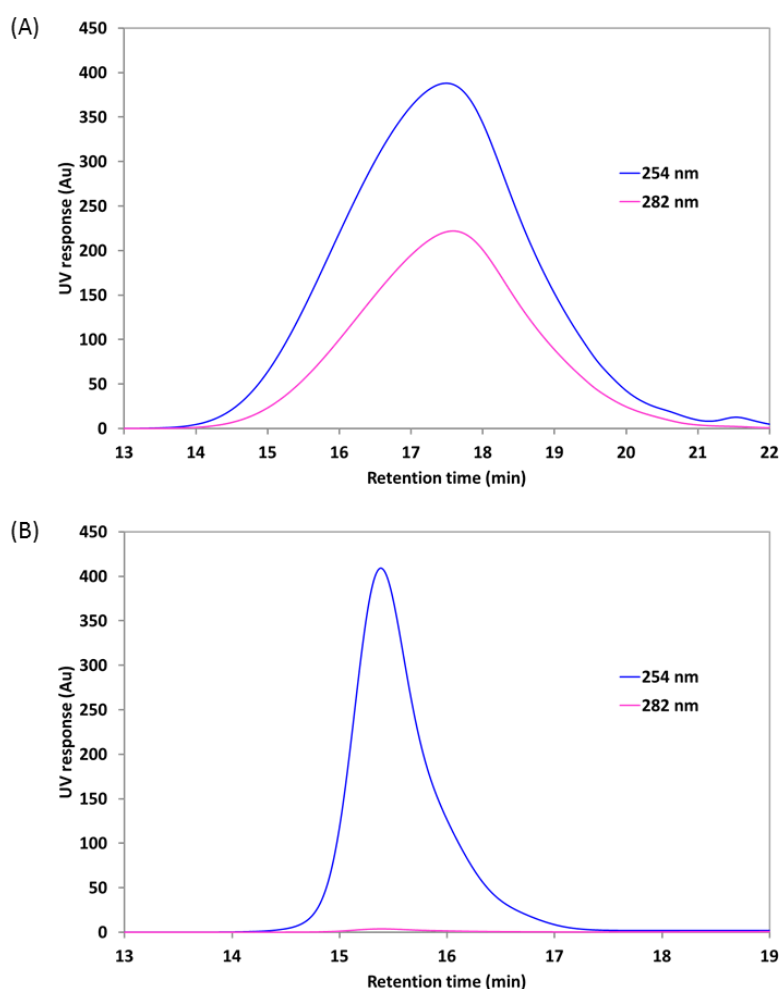


**Figure 2.6.** UV-GPC traces of (A) synthesised PS and (B) commercial PS ( $M_n = 3.7$  and 10.5 kDa, respectively).

### 2.4.1.3 Effect of Monomer to Iniferter Ratio

Preliminary experiments were carried out to study the effect of using different mole ratio of St monomer to BDDC iniferter in the polymerisation of styrene. Following the polymerisation procedure in §2.2.3.1, six different St to BDDC mol ratios (30:1, 50:1, 155:1, 625:1, 1040:1 and 1560:1) were used in polymerisation conducted in bulk for 3 hours using an Efos Acticure A4000 UV/Visible Spot Cure System. GPC analysis was then run to determine the  $M_n$  (number average molecular weight),  $M_w$  (weight average molecular weight),  $M_p$  (peak molecular weight) and PDI (polydispersity index, PDI) of the linear PS and the results are presented in Table 2.1.

**Table 2.1.** Photopolymerisation of styrene using various St to BDDC mole ratios.<sup>a</sup>

PS arm	[St]:[BDDC]	Conversion <sup>b</sup> (%)	$M_n^c$ (kDa)	$M_w^c$ (kDa)	$M_p^c$ (kDa)	PDI <sup>d</sup>
PS-I1	30	2.2	3.5	6.5	4.2	1.87
PS-I2	50	8.0	3.7	7.2	5.1	1.93
PS-I3	155	7.0	5.1	9.7	6.8	1.91
PS-I4	625	5.0	12.0	39.4	21.2	3.28
PS-I5	1040	4.4	19.2	75.2	39.1	3.91
PS-I6	1560	3.0	32.4	87.9	44.5	2.72

<sup>a</sup> Polymerisation conditions: bulk; reaction time: 3 h (Efos Acticure A4000 UV/Visible Spot Cure System)

<sup>b</sup> Monomer conversion (%) was calculated based on the gravimetric method.

<sup>c</sup> Number average molecular weight ( $M_n$ ), weight average molecular weight ( $M_w$ ) and peak molecular weight ( $M_p$ ) obtained by GPC.

<sup>d</sup> Polydispersity index (PDI) =  $M_w/M_n$ .

To further investigate the relationship between the ratio of St to the BDDC iniferter and the conversion of the monomer, a plot of percent conversion versus [St]:[BDDC] used in the polymerisation was then drawn and compared with the molecular weight ( $M_n$ ) of the PS arms obtained (Figure 2.7). From Table 2.1 and Figure 2.7, it can be seen that the number average molecular weight ( $M_n$ ) of the PS arm and hence the degree of polymerisation (DP) increased with increasing [St]:[BDDC] ratio. On the contrary, the percent monomer conversion initially increased as the [St]:[BDDC] ratio was increased

from 30:1 to 50:1, but tended to decline as the [St]:[BDDC] ratio was further increased to 1560:1. This suggested that there was a critical value of the St to BDDC mole ratio for the maximum conversion, which is consistent with the reported result for the polymerisation of isoprene<sup>191</sup> and methyl methacrylate<sup>192</sup> using BDDC iniferter. Increasing the concentration of BDDC iniferter (or decreasing the [St]:[BDDC] ratio) resulted in a higher number of benzyl radicals that can initiate the polymerisation, thus producing a higher number but shorter PS chains. However, as the BDDC concentration was further increased, more DDC end capping agents were available to cap the propagating chains, thus reducing the probability of the propagating chains reacting with the monomers.<sup>192</sup> This could lead to the formation of relatively even shorter chains of PS, some of which were readily soluble in the precipitating solvent and thus were not isolated in the final product. This could explain the lower percentage of conversion at [St]:[BDDC] ratio of 30:1 compared to that of 50:1.

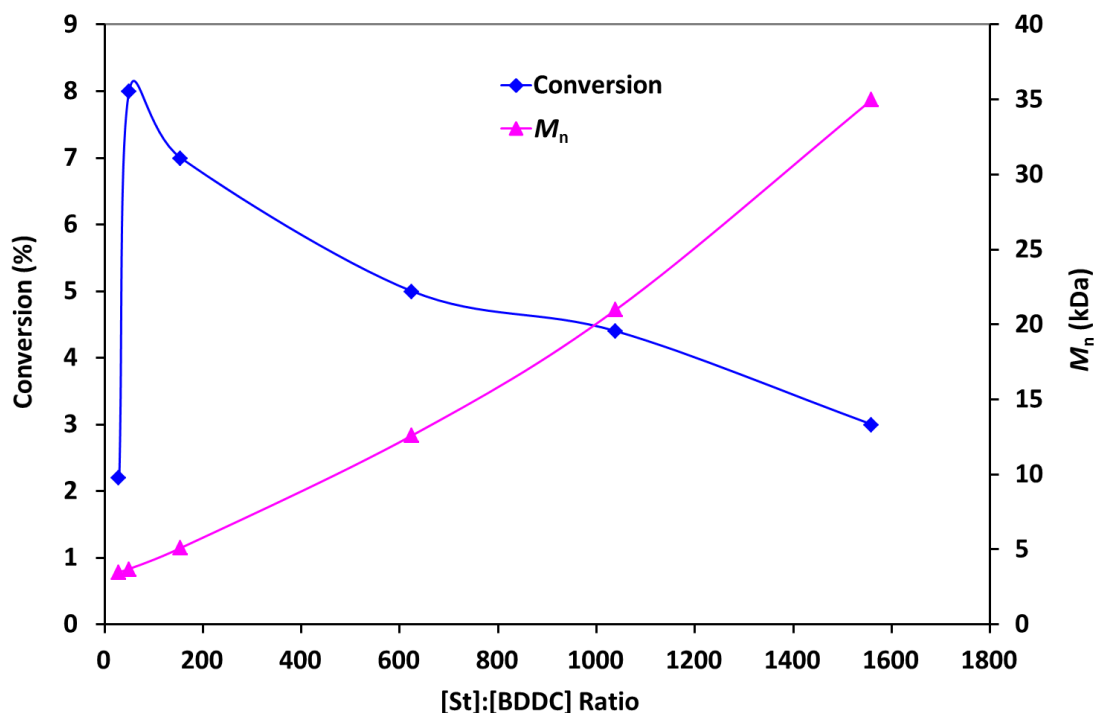


**Figure 2.7.** Relationship between percent conversion of St and mole ratio of St to BDDC as well as resultant molecular weight ( $M_n$ ) of PS (polymerisation time: 3 h).

From Figure 2.7, it can also be noticed that when the experiment was stopped after 3 h, the percent conversion of the monomer was quite low (the highest was only about

8%, when a [St]:[BDDC] ratio of 50:1 was used). This indicates that a longer polymerisation time is required to increase the percent conversion of the monomer, which will in turn result in a higher yield of the polymer.

The effect of the monomer:iniferter ratio was then re-investigated at longer polymerisation times using the UV photoreactor (Ace glass, No. 7825-34) and from this stage onwards, all the polymerisations involved were carried out using this set up. The polymerisation was undertaken at a fixed amount of styrene while the amount of BDDC was varied. Following the polymerisation procedure in §2.2.3.1, four different St to BDDC mol ratios (i.e. 155:1, 390:1, 625:1 and 6250:1) were prepared and the polymerisation was conducted for 24 h. The resulting polymers were characterized by GPC and the results are presented in Table 2.2. Their GPC traces are shown in Figure 2.8, where the retention time is inversely proportional to the molecular weight of the polymers.

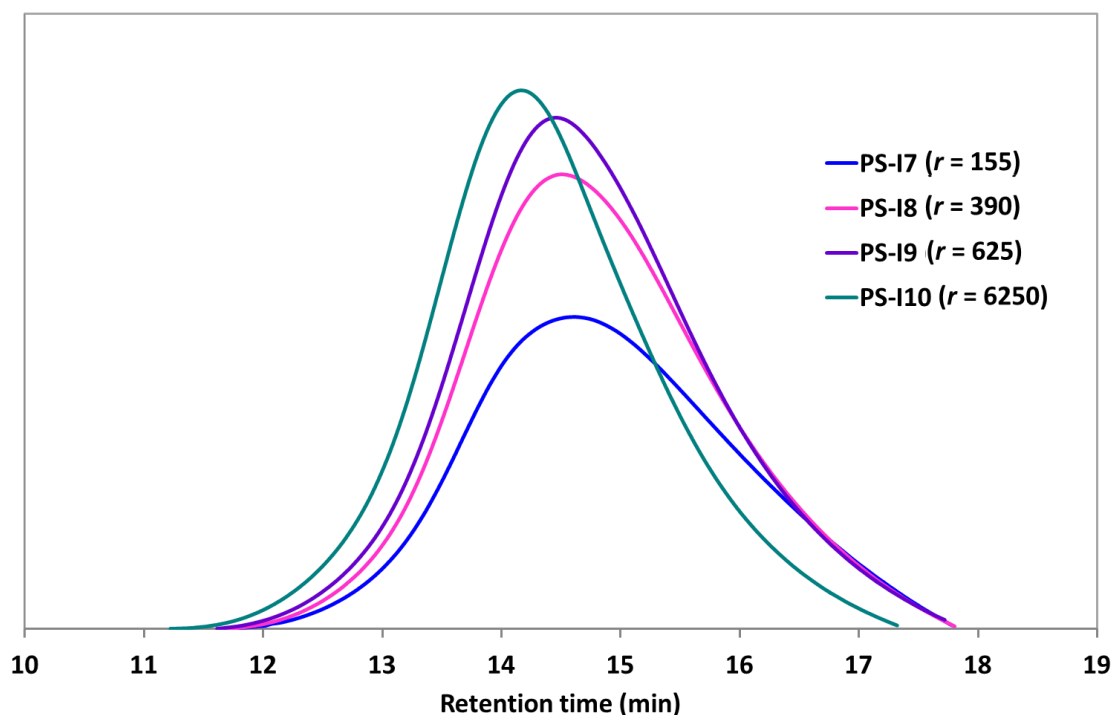


**Figure 2.8.** GPC traces of PS arms as a function of different [St]:[BDDC] ratios.

**Table 2.2.** Relationship between [St]:[BDDC] ratio and molecular weight of PS arm.<sup>a</sup>

PS arm	[St]:[BDDC]	Conversion <sup>b</sup> (%)	$M_n^c$ (kDa)	$M_w^c$ (kDa)	$M_p^c$ (kDa)	PDI <sup>d</sup>
PS-I7	155	47	33.2	251	63.5	7.6
PS-I8	390	39	37.3	268	76.9	7.2
PS-I9	625	25	39.6	332	83.6	8.4
PS-I10	6250	17	59.2	723	130	12.2

<sup>a</sup> Polymerisation conditions: bulk; reaction time: 24 h (450 W medium pressure mercury vapour, quartz UV lamp (Ace glass, No. 7825-34)).

<sup>b</sup> Monomer conversion (%) was calculated based on the gravimetric method.

<sup>c</sup> Number average molecular weight ( $M_n$ ), weight average molecular weight ( $M_w$ ) and peak molecular weight ( $M_p$ ) obtained by GPC.

<sup>d</sup> Polydispersity index (PDI) =  $M_w/M_n$ .

As can be seen from Figure 2.8, the elution peaks shifted to higher molecular weight (shorter retention time) with increasing [St]:[BDDC] ratio. From Table 2.2, it can be seen that increasing the molar ratio of styrene to BBDC from 155 to 6250 results in decreasing percentage conversion of monomer but increasing MW of the PS arm, which is consistent with the polymerisation trend obtained at 3 h. In other words, using a lower amount of BDDC iniferter resulted in a longer chain length of the PS arm. This was because at a lower concentration of BDDC, fewer initiating species, having a relatively long propagating chain length were created, which contributed to the higher viscosity of the reaction tube. Hence, each propagating chains has more chance to react with the monomers, which results in higher molecular weight or kinetic chain length.<sup>191, 192</sup> Fewer initiating sites also lead to a reduced monomer conversion since the number of propagating chains was also decreased. Nevertheless, the percentage conversion was higher when the experiment was conducted for 24 h, where the highest conversion (47%) was obtained at [St]:[BDDC] ratio of 155:1, which is about 6-fold higher compared to that obtained at 3 h (7%, Table 2.1). It can also be noted that the polydispersity tended to increase with increasing ratio of styrene to BDDC iniferter. In other words, using a lower concentration of BDDC resulted in PS arms with higher polydispersity. This could be attributed to the increase in the viscosity of the reaction mixture due to the increase in the propagating chain length,<sup>193</sup> thus reducing the

diffusion rate of radicals and monomers.<sup>194</sup> As a result, the interaction between the propagating chains and the end-capping agent was reduced, resulting in higher polydispersity.<sup>192</sup>

#### 2.4.1.4 Effect of Polymerisation Time

To study the effect of reaction time, four tubes containing the same mole ratio of styrene to BDDC (155:1) were prepared and polymerized at different reaction times (i.e. 3, 6, 12 and 24 h), following the polymerisation procedure in §2.2.3.1. The resulting polymers were characterized by GPC (as shown in Figure 2.9) and the results are summarized in Table 2.3. From the figure, it can be seen that the elution peaks shifted to high-molecular weight (low retention time) with increasing polymerisation time.

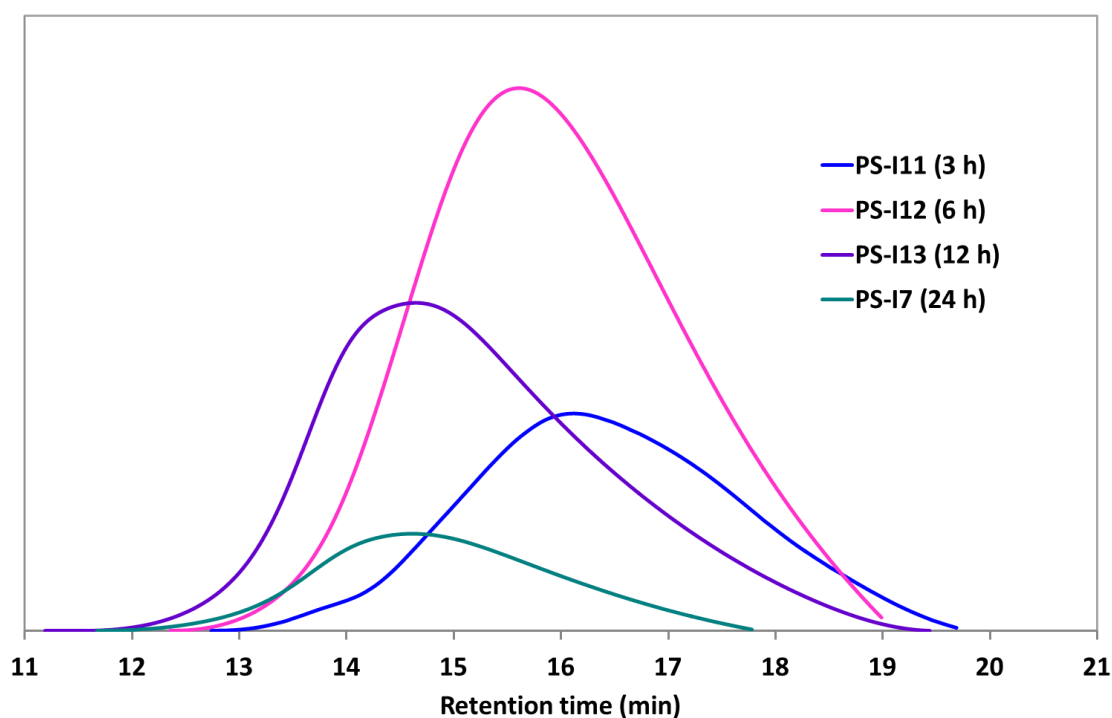


**Figure 2.9.** GPC traces of PS arms as a function of different irradiation time.

As can be seen in Table 2.3, the percentage conversion of monomer, the molecular weight ( $M_n$ ) and polydispersity of the PS arms increased with increasing reaction time. To emphasise this polymerisation behaviour, a plot of  $M_n$  versus monomer conversion was plotted as shown in Figure 2.10. From the plot, it can be observed that  $M_n$

increases approximately linearly with conversion. The results suggested that the polymerisation proceeded via a living mechanism.<sup>195</sup> In living polymerisation, propagating chains are expected to be free from bimolecular termination and more monomers are consumed by the reactive propagating chains at longer reaction time.

**Table 2.3.** Effect of reaction time on the molecular weight of PS arm.<sup>a</sup>

PS arm	Time (h)	Conversion (%) <sup>b</sup>	$M_n$ (kDa) <sup>c</sup>	$M_w$ (kDa) <sup>c</sup>	$M_p$ (kDa) <sup>c</sup>	PDI <sup>d</sup>
PS-I11	3	20	10.1	27.3	15.1	2.7
PS-I12	6	24	13.0	43.6	23.1	3.4
PS-I13	12	37	18.8	117	51.8	6.2
PS-I7	24	47	33.2	251	63.5	7.6

<sup>a</sup> Polymerisation conditions: bulk; [St]:[BDDC] ratio = 155:1.

<sup>b</sup> Monomer conversion (%) was calculated based on the gravimetric method.

<sup>c</sup> Number average molecular weight ( $M_n$ ), weight average molecular weight ( $M_w$ ) and peak molecular weight ( $M_p$ ) obtained by GPC. <sup>d</sup> Polydispersity index (PDI) =  $M_w/M_n$ .

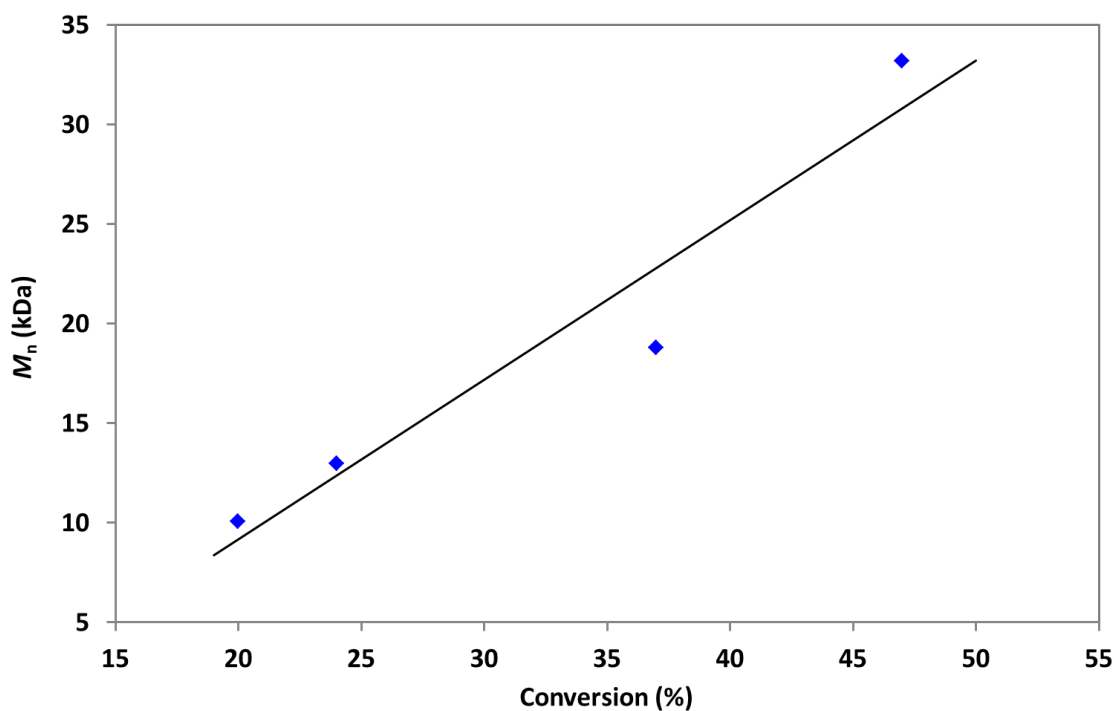


**Figure 2.10.**  $M_n$ -conversion relation for bulk polymerisation of St with BDDC iniferter.

These results are similar to those observed by Otsu and Kuriyama,<sup>94</sup> who found that bulk polymerisation of styrene with BDDC proceeded via the living mechanism as shown by an increase in molecular weight as well as conversion with reaction time. It should also be noted that the highest percentage yield of the polystyrene arm obtained was only about 47%, even after 24 h of polymerisation. This may be attributed to the slower propagation rate of styrene due to the stability of its propagating radical by resonance.<sup>102</sup> As the reaction time was increased from 3 to 24 h, the length of the propagating chains and the viscosity of the mixture in the reaction tube also increased,<sup>193</sup> which in turn reduced the interaction between the propagating chains and the end-capping agent. The BDDC iniferter therefore could not act as a transfer agent and/or a terminator effectively at high conversion, resulting in high polydispersity.<sup>192</sup> This increase in polydispersity with reaction time suggested that polymerisation at a relatively short time, i.e. up to 6 h, is advantageous with regard to producing low polydispersity PS arms.

#### **2.4.1.5 Arm-first CCS Polymers**

The preparation of CCS polymers were carried out following the procedure in §2.2.3.2 by crosslinking the linear PS samples prepared beforehand with EGDMA, as shown in Scheme 2.2. The influence of several parameters such as polymerisation time, [EDGMA]:[PS] arm ratio, concentration of PS arm as well as chain length of PS arm on the formation of the CCS polymers were investigated as these parameters dictate the structure and yield of CCS polymers.<sup>6</sup>

#### **2.4.1.6 Structural Confirmation and Morphology of CCS Polymers**

FTIR and <sup>1</sup>H NMR spectroscopic analyses were carried out to confirm the structure of the synthesised arm-first CCS polymer. A typical FTIR spectrum of an arm-first CCS polymer (CCS-I8, Table 2.4) is shown in Figure 2.11 and compared with that of the PS arm precursor (PS-I15). The strong peak at 1730 cm<sup>-1</sup> and the broad peak at 1154 cm<sup>-1</sup> in the spectrum of the CCS polymer (Figure 2.11(B)) are assigned to the carbonyl (C=O) and C-O-C stretching vibrations of the EGDMA unit in the core, respectively. These peaks which are not present in the spectrum of the PS arm precursor (Figure 2.11(A))

indicate the successful formation of the CCS polymer. However, the characteristic peak of the DDC group at  $1003\text{ cm}^{-1}$  (C-S) is barely observed in the spectrum of the CCS polymer (Figure 2.11(B)), possibly due to its very low intensity.

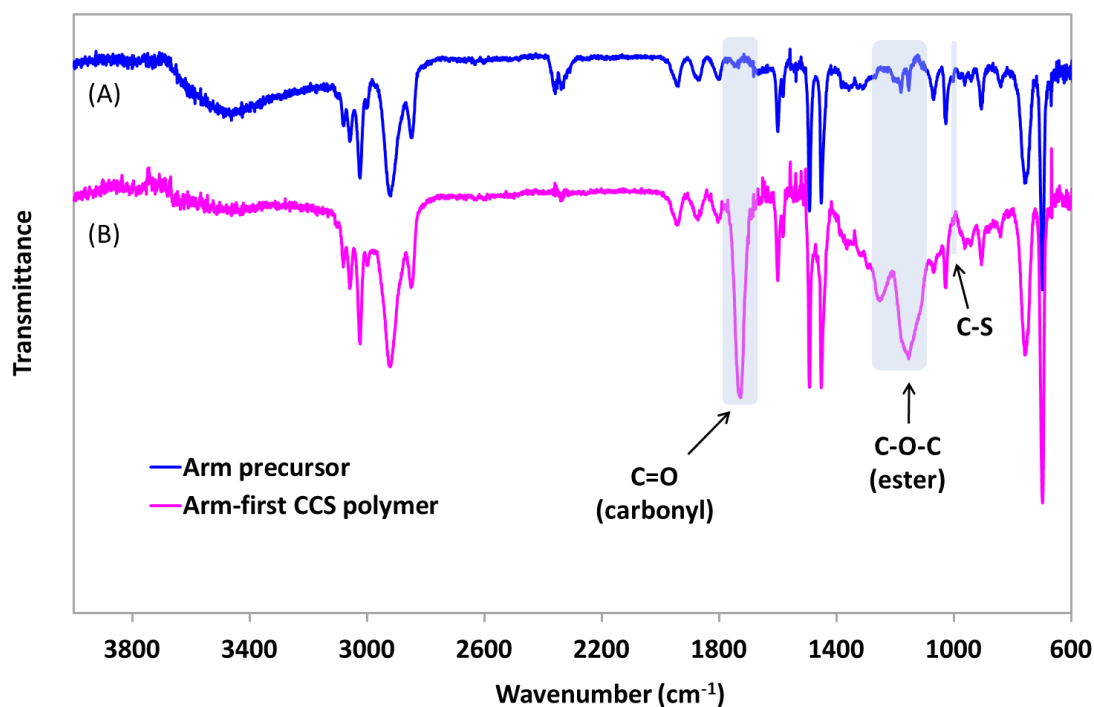


**Figure 2.11.** FTIR spectra of (A) a CCS polymer and (B) the corresponding PS arm precursor.

Figure 2.12 shows a typical  $^1\text{H}$  NMR spectrum of an arm-first CCS polymer (CCS-I14, Table 2.6). As can be seen in the spectrum, the peak between 4.0 - 4.5 ppm is assigned to four protons of PEGDMA (e), which confirms the crosslinking of PS arm by EGDMA to form the core of the CCS polymer. The low intensity observed for these protons in the spectrum illustrates the low mobility of the core in solution due to the highly crosslinked network. The signals between 0.5 to 2.3 ppm ( $\text{H}_a$ ,  $\text{H}_b$  and  $\text{H}_d$ , respectively) were attributed to the backbone methylene protons of both PS and PEGDMA, methine protons of PS and methyl protons of PEGDMA. Since the sample was purified three times, the broad peaks at 5.6 and 6.1 ppm ( $\text{H}_f$ ) are attributed to the methacrylate double bonds rather than vinyl protons of unreacted styrene monomers, which indicate the presence of unreacted pendant carbon-carbon double bonds in the core due to incomplete crosslinking. The characteristic signals for the phenyl protons of PS

arms appear between 6.6 – 7.2 ppm ( $H_c$ ). It is interesting to note that although the methylene protons of the DDC moiety are located at the core of the CCS polymer, signals attributed to them are visible between 3.7 and 4.0 ppm ( $H_1$ ), possibly due to the short linear PS arm precursor (PS-I19,  $M_n = 3.6$  kDa) employed during the CCS polymer preparation (PS-I18,  $M_n = 3.6$  kDa).

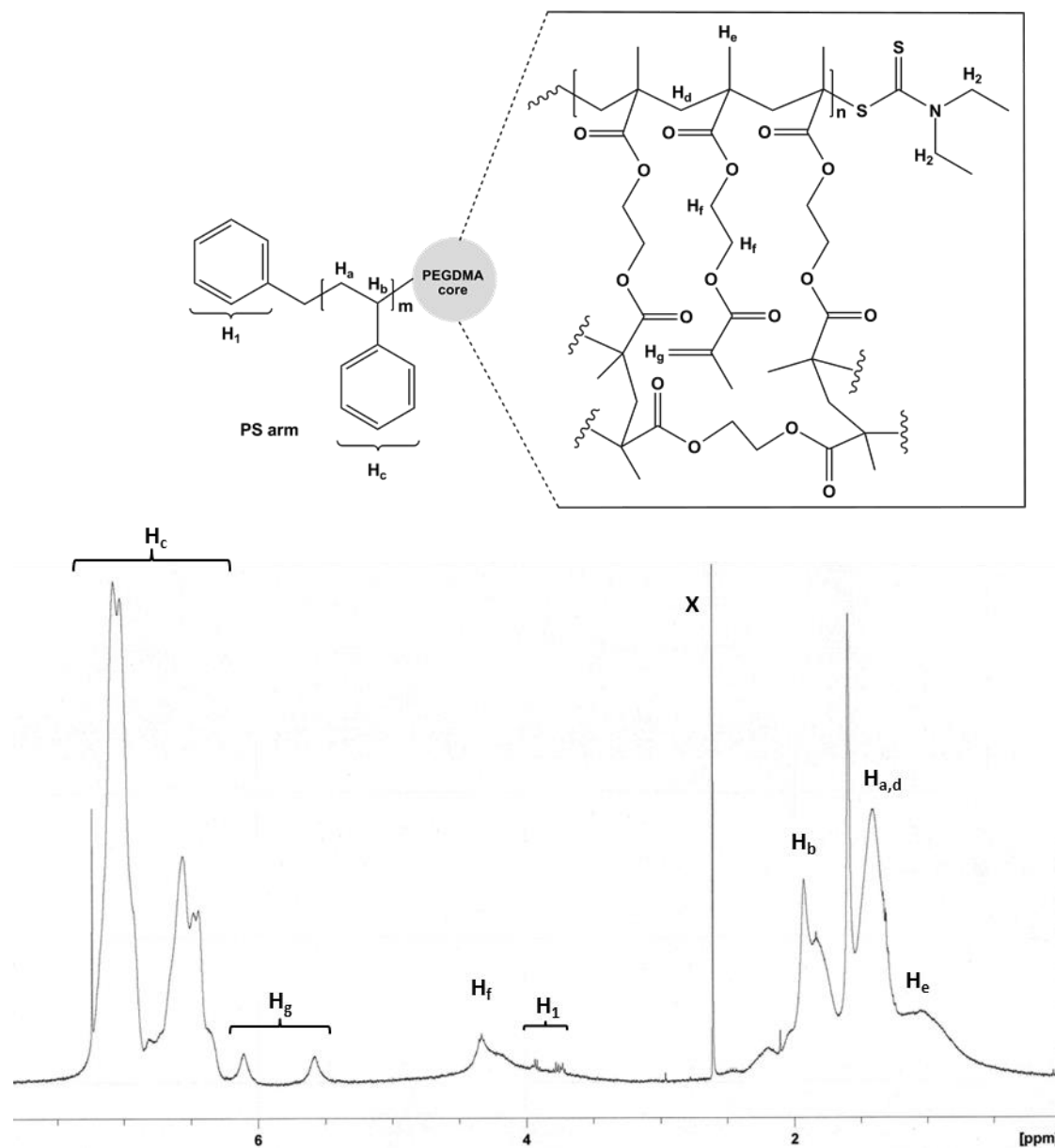


**Figure 2.12.**  $^1\text{H}$  NMR spectrum of a typical arm-first CCS polymer prepared via iniferter.

SEM and TEM were used to view the morphologies of the synthesised arm-first CCS polymer. As an example, the SEM and TEM images of CCS-I14 (Table 2.6) are depicted

in Figure 2.13(A and B) and (C and D), respectively. As can be seen in the SEM images in Figure 2.13(A and B), the synthesized CCS polymer exhibited a spherical shape and appeared polydisperse. This is confirmed by its TEM images (Figure 2.13 (C and D)), which shows globular particles having an average size of  $260 \pm 55$  nm. Additionally, the hydrodynamic particle sizes of these CCS samples after filtration (using a  $0.45 \mu\text{m}$  membrane filter) measured by DLS in THF and THF:MeOH (40:60, vol%) were about  $58 \pm 1$  nm and  $46 \pm 1$  nm, respectively.

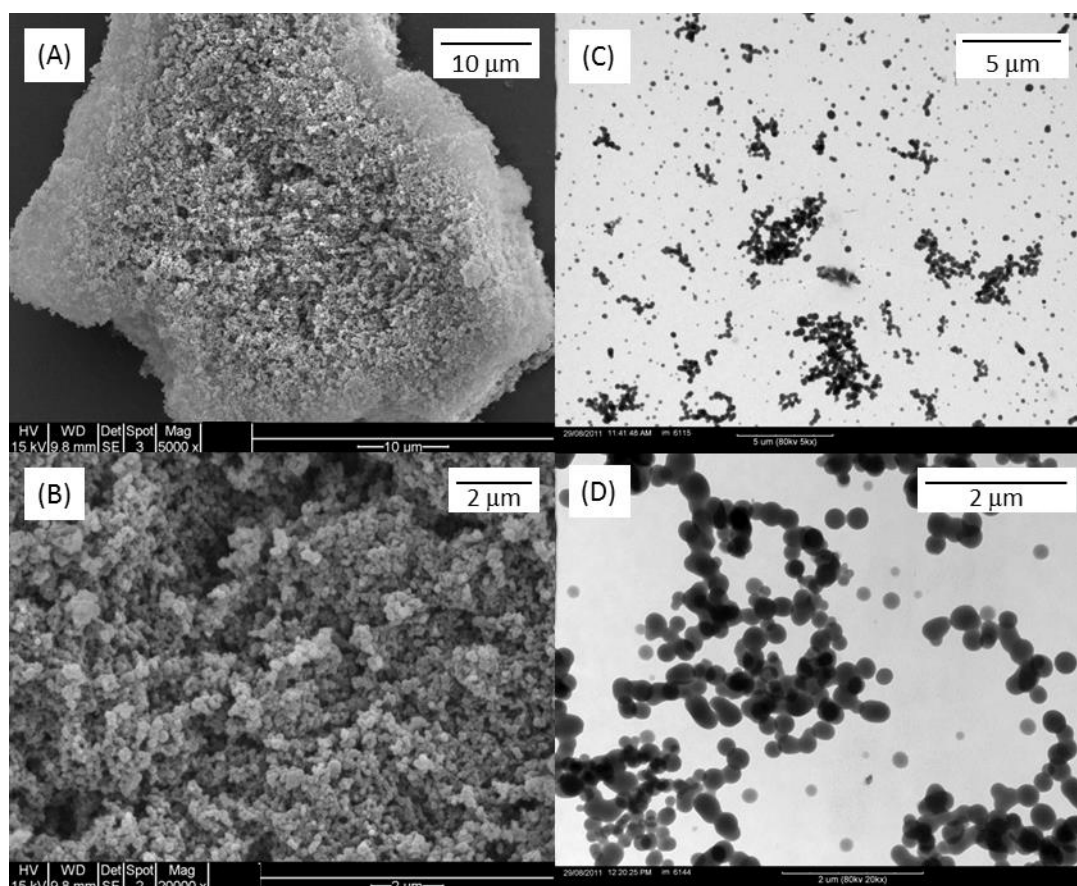


**Figure 2.13.** SEM and TEM images of arm-first CCS polymers prepared via iniferter: (A and B) and (C and D) respectively. A and C were recorded at 5000X magnification whereas B and D were recorded at 20000X magnification.

#### 2.4.1.7 Effect of Polymerisation Time

The effect of reaction time on the formation of the CCS polymer was studied using a linear PS arm (PS-I15) with  $M_n$  of 5.1 kDa, which was synthesized following the procedure in §2.4.1.1. This linear PS arm was prepared based on the previous studies

on the photopolymerisation of St and the formulation was modified to produce linear PS arm with a controlled MW at high yield. A mixture of styrene (6 mL) and BDDC iniferter was mixed at [St]:[BDDC] ratio of 155:1 and then polymerised for 5 h. After the PS arms were isolated and purified, four tubes containing the same mole ratio of EGDMA to the synthesized PS arm (15:1) in THF (3.6 mL) were then prepared and polymerized at different reaction times (3, 6, 12 and 24 h), following the procedure in §2.2.3.2. The resultant CCS polymers were then characterized using GPC and DLS to determine their molecular weight and particle size values, respectively, and the results are tabulated in Table 2.4. The GPC curves of the CCS polymers obtained after various polymerisation times were then compared with that of the original arm precursor, as shown in Figure 2.14.

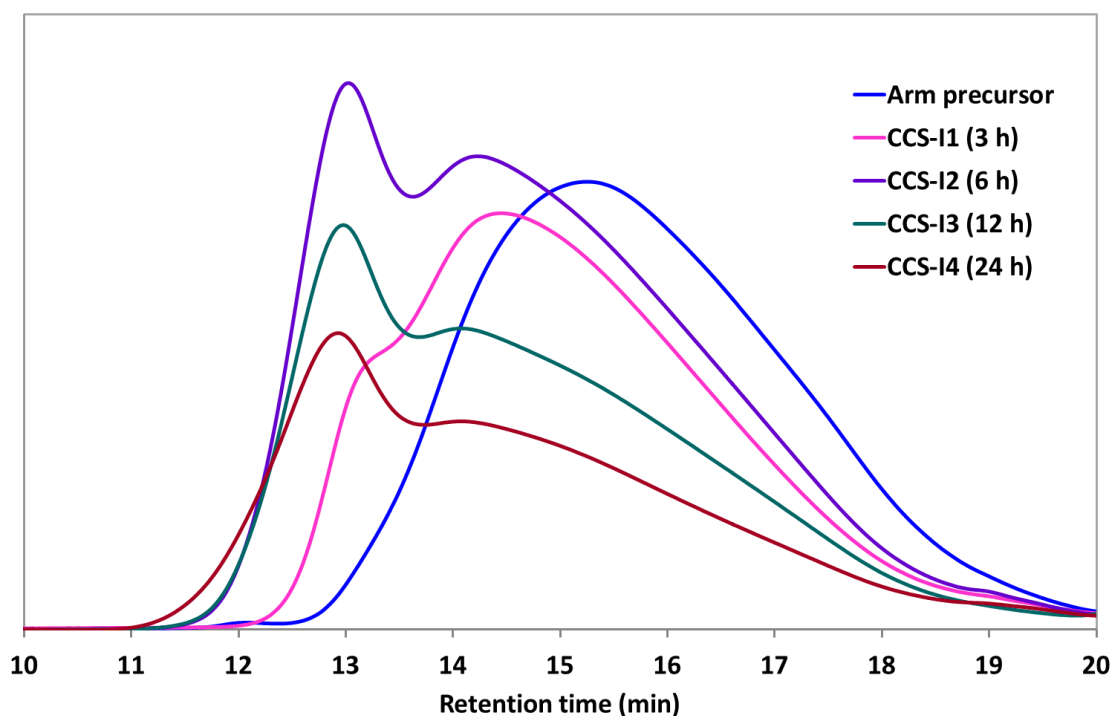


**Figure 2.14.** GPC traces of CCS polymers obtained at various polymerisation times compared with that of the PS arm precursor.

From Figure 2.13, it can be seen that all the GPC curves of the CCS polymers displayed two broad overlapping peaks and the peaks shifted to the lower retention time (higher MW) with increasing polymerisation time. The peaks at lower retention time indicated the successful formation of CCS polymers whilst those observed at higher retention time were attributed to the presence of residual unincorporated PS arm precursor. The

presence of these high-retention peaks in the GPC curves of the CCS polymers even after 24 h of polymerisation indicates the incomplete incorporation of the linear arms into the CCS polymers, which is a common problem encountered in the formation of CCS polymers via the arm-first method.<sup>7, 21, 24, 39, 196</sup> The reason might be attributed to the lower chain mobility, increased solution viscosity and possible chain termination/chain transfer.<sup>197</sup>

To further analyse the formation of these high MW polymers and determine their yield relative to the residual unincorporated PS arm precursor, the GPC curves were deconvoluted using Excel's Solver routine to give the most probable fit for two molecular weight components. The areas under the two Gaussian curves are used to estimate the fractions of CCS polymers and the unincorporated PS arm precursor. The deconvolution process was carried out according to the procedure described in §2.3.3 (Equation 2.2) without fixing any of the peak retention time of the polymers and the results are also tabulated in Table 2.4.

**Table 2.4.** Formation of CCS polymers from iniferter polymerisation at various polymerisation times.<sup>a</sup>

CCS polymer	Reaction time (h)	$M_p$ (GPC) (kDa) <sup>b</sup>	$M_p$ (arm) (kDa) <sup>c</sup>	$M_p$ (CCS) (kDa) <sup>c</sup>	CCS Yield (%) <sup>d</sup>	$D_h$ (nm) <sup>e</sup>		
						THF	THF-MeOH	$\Delta D_h$
CCS-I1	3	24.5	6.8	29.3 <sup>f</sup>	38 <sup>f</sup>	14.2	13.6	0.6
CCS-I2	6	114	13.6	99.6	15	30.5	27.0	3.5
CCS-I3	12	121	13.7	105	19	33.5	27.5	6.0
CCS-I4	24	128	15.3	119	20	86.0	82.4	3.6

<sup>a</sup> Polymerisation conditions: room temperature in THF;  $M_{n(\text{arm})}$  and  $M_{p(\text{arm})}$  = 5.1 and 12.4 kDa respectively; [PS arm] = 11 mM; [PS]:[EGDMA] ratio = 7:1;  $D_h$  (PS arm) in THF = 4.9 nm.

<sup>b</sup> Peak value of the apparent MW measured by GPC in THF, calibrated with linear PS standards.

<sup>c</sup> Peak values of the resultant deconvoluted peaks by Excel Solver.

<sup>d</sup> Calculated from the area of the deconvoluted CCS polymer peak relative to the total area of the deconvoluted polymer peaks as follows: CCS yield (%) =  $\frac{A_{\text{CCS polymer}}}{A_{\text{CCS polymer}} + A_{\text{unreacted PS arm}}} \times 100$ .

<sup>e</sup> Hydrodynamic diameter of filtered sample of polymers (using a 450 nm membrane filter) determined by DLS with distribution analysis at 20 °C in THF and THF-MeOH (methanol) (60/40, vol %).

<sup>f</sup> The peak is attributed to the linear PS-b-polyEGDMA block polymers.

From Table 2.4, it can be seen that in general, the peak MW of the polymers increases as the polymerisation time is increased. From the GPC analysis of the GPC curve after 3 h of polymerisation, the peak MW of the polymer at the high-retention-time side was found to be about 2-fold higher than that of the linear arm precursor, which could indicate the formation of styrene-EGDMA block copolymers,<sup>198</sup> as shown in Scheme 1.2 in §1.2.1.2. These short block copolymers were formed during the initial stage of polymerisation when EGDMA crosslinker was added to a solution containing linear PS with active end group.<sup>6, 199</sup> Deconvolution of the overlapping GPC peaks of CCS-I1 however, resulted in lower peak MW of the unincorporated linear PS arm compared to that obtained from GPC analysis of the linear PS arm precursor (about 45% lower). On the other hand, the deconvoluted peak MW of PS-EGDMA block copolymer was about 20% higher than the original value. It can also be observed that about 38% of these block copolymers were formed after 3 h. As more of the block copolymers linked together, the presence of CCS polymers with lightly crosslinked cores<sup>6</sup> could be observed after 6 h and from this point onwards, the peak MW of the CCS polymer (at the lower retention side) as well as the CCS polymer yield also increased. Note that the peak MW of the unincorporated linear arm precursor was now higher than that of the linear PS arm precursor (between 10 – 20% higher). Although the CCS yield increased with increasing polymerisation time, about 80% of the linear arm precursor was still left even after 24 hr of polymerisation, which could be because of other experimental parameters such as [EGDMA]:[PS arm] ratio and/or concentration of the linear PS arm were not under the optimised conditions.

It can also be observed that the hydrodynamic size of the CCS polymers in THF increased with increasing time (Table 2.4). The difference in sizes when the CCS polymers were dispersed in THF compared to that in THF-methanol mixture was attributed to the relatively more extended structure of the arms in good solvents compared to the bad solvents. THF is a good solvent for the PS arms whereas methanol is a poor solvent for the arms. Therefore the arms are expected to be more extended in THF and somewhat collapsed in the presence of methanol. The almost similar size of the CCS-I1 in THF compared that in THF-methanol ( $D_h \approx 14$  nm) confirms

that it was a block copolymer rather than a CCS polymer. Furthermore, this size is only about 3-fold higher than that of the size of linear PS arm precursor, measured in THF; the good solvent for the arm. It can also be observed that although the hydrodynamic size values of CCS-I2 and CCS-I3 measured in THF-methanol are comparable, the latter exhibited a slightly higher  $D_h$  value when the measurement was carried out in THF (about 10% higher), indicating that its PS arms were more extended compared to those of the former. Although the peak MW values of CCS-I4 are only about 5 and 13 % higher than those of CCS-I3 (before and after being deconvoluted, respectively), the hydrodynamic size of the former was found to be about 2.5-fold higher than that of the latter. Given the little change in the CCS yield and the much bigger size of CCS-I4 compared to that of CCS-I3 (about 2.5-fold bigger), this could indicate the occurrence of star-star coupling, leading to a broader MW distribution of CCS polymer.<sup>6, 63</sup> Since CCS polymers have a more compact structure than the corresponding linear polymers of the same MW, the peak MW obtained from GPC equipped with RI detector calibrated based on linear PS standards was only the apparent value and thus is expected to be smaller than the true value.<sup>111, 200</sup>

#### 2.4.1.8 Effect of EGDMA to PS Arm Ratio

To study the influence of the amount of EGDMA added to the reaction mixture on the formation of CCS polymers,  $r$ , which is defined as the molar ratio of EGDMA to PS arm, was varied while keeping the molar concentration of the PS arm constant. For this purpose, another batch of linear PS arms were prepared (PS-I16,  $M_n = 16.0$  kDa) by mixing a mixture of St (9 mL) and BDDC at [St]:[BDDC] ratio of 230:1 and then polymerised for 5 h, following the procedure in §2.2.3.1. After the PS arms were isolated and purified, five tubes containing the same molar concentration of the synthesized PS arm (5 mM) at various ratio of EGDMA to PS arm (i.e. 5:1, 9:1, 12:1 and 16:1) were then prepared in THF (2.75 mL) and polymerized for 5 hr, following the procedure in §2.2.3.2. The resultant CCS polymers were then characterized using GPC (Figure 2.15) and DLS to determine their molecular weight and particle size values, respectively, and the results are tabulated in Table 2.5.

Figure 2.15 shows the GPC traces of CCS polymers prepared using various EGDMA to PS arm molar ratios. Initially, when the [EGDMA]:[PS arm] ratio ( $r$ ) of 5:1 was used, the appearance of a second peak at higher MW (lower retention time) is hardly observed because it closely overlapped with that of the unincorporated PS arm precursor at lower MW (higher retention time). As the  $r$  value was increased, two peaks can be clearly seen although they still overlapped. The peaks at higher MW indicate the formation of CCS polymers and it can be seen that these peaks shifted to the higher MW side with increasing ratio of EGDMA to PS arm. To further analyse the formation of these high MW polymers and determine their yield relative to the residual unincorporated PS arm precursor, the GPC curves were deconvoluted using Excel's Solver routine to give the most probable fit for two molecular weight components (§2.3.3). The areas under the two Gaussian curves are used to estimate the fractions of CCS polymers and the unincorporated PS arm precursor. The results are tabulated in Table 2.5.

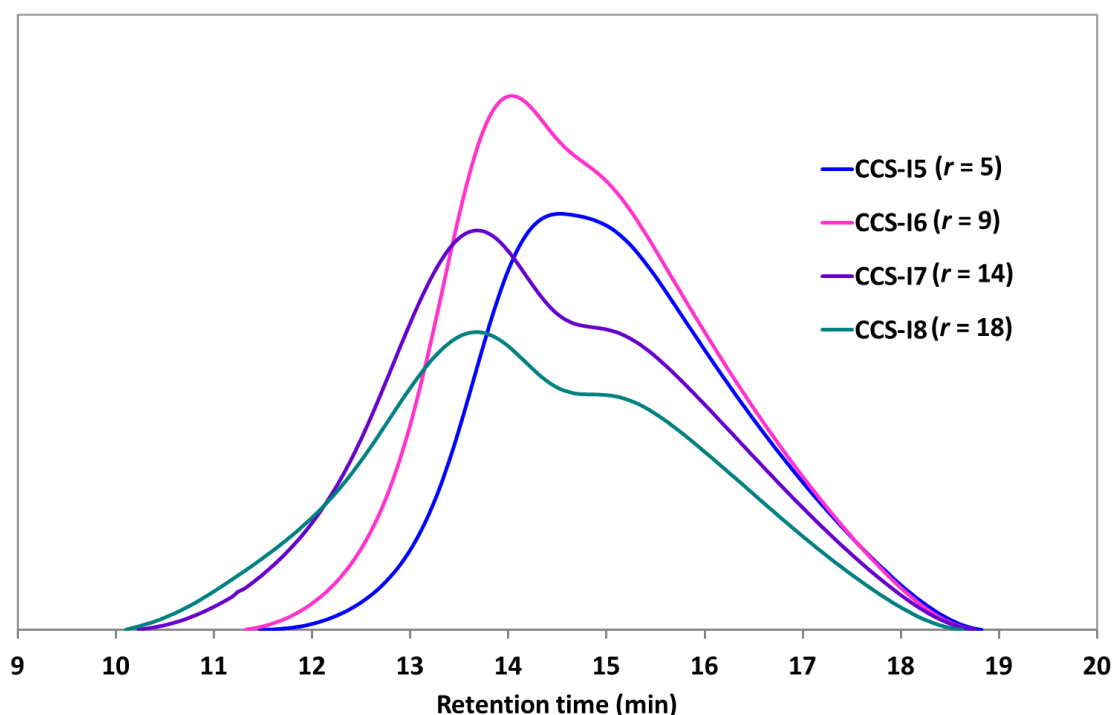


**Figure 2.15.** GPC traces of CCS polymers obtained from the polymerisation at various [EGDMA]:[PS arm] ratios using arm precursor of  $M_p = 21.5$  kDa. The chromatogram of the arm was run in a different condition hence not included here.

**Table 2.5.** Formation of CCS polymers from iniferter polymerisation at various [EGDMA]:[PS arm] ratios.<sup>a</sup>

CCS polymer	[EGDMA]/ [PS arm] ratio ( <i>r</i> )	$M_p$ (GPC) (kDa) <sup>b</sup>	$M_p$ (arm) (kDa) <sup>c</sup>	$M_p$ (CCS) (kDa) <sup>c</sup>	CCS Yield (%) <sup>d</sup>	$D_h$ (nm) <sup>e</sup>		
						THF	THF- MeOH	$\Delta D_h$
CCS-I5	5	74.6	22.8	118	54	18.5	16.9	1.6
CCS-I6	9	164	22.8	181	62	25.6	21.3	4.3
CCS-I7	14	203	18.4	297	37	69.1	57.8	11.3
CCS-I8	18	298	22.2	395	72	98.2	86.6	11.6

<sup>a</sup> Polymerisation conditions: room temperature in THF; reaction time = 5 h;  $M_{n(\text{arm})}$  and  $M_{p(\text{arm})}$  = 16.0 and 21.5 kDa respectively; [PS arm] = 5 mM;  $D_h(\text{PS arm})$  in THF = 6.2 nm.

<sup>b</sup> Peak value of the apparent MW measured by GPC in THF, calibrated with linear PS standards.

<sup>c</sup> Peak values of the resultant deconvoluted peaks by Excel Solver.

<sup>d</sup> Calculated from the area of the deconvoluted CCS polymer peak relative to the total area of the deconvoluted polymer peaks as follows: Yield (%) =  $\frac{A_{\text{CCS polymer}}}{A_{\text{CCS polymer}} + A_{\text{unreacted PS arm}}} \times 100$ .

<sup>e</sup> Hydrodynamic diameter of filtered sample of polymers (using a 450 nm membrane filter) determined by DLS with distribution analysis at 20 °C in THF and THF-MeOH (methanol) (60/40, vol %).

As can be seen from Table 2.5, as the amount of EGDMA added to the reaction mixture was increased, the peak molecular weight of the CCS polymers also increased. This was because in general, a higher molar ratio of EGDMA to PS arm (*r*) produced longer chain length of PEGDMA segment, which in turn, resulted in larger crosslinked cores with more PS arms. It can also be seen that the peak MW values of the CCS polymers after being deconvoluted by Excel's Solver routine were much higher compared to those obtained by GPC, whereas those of the unincorporated PS arms were comparable to those measured by GPC. It can be noted that there was no trend in the CCS polymer yield with increasing *r*. However, the highest CCS polymer yield (72%) was obtained when *r* value of 18 was used in the formulation, which is in agreement with the literature reports in which high crosslinker to linear arm ratio was found to be necessary in order to increase CCS yield and minimise the presence of residual linear arm polymers in the overall polymer products.<sup>24, 38, 63, 196</sup>

From Table 2.5, the hydrodynamic size of the CCS polymers in THF was found to increase with increasing EGDMA to PS arm ratio. The hydrodynamic size also seemed

to decrease when the measurement was carried out in THF-methanol, suggesting the shrinkage of the PS arms in the presence of poor solvent (methanol). It can also be noted that the difference in sizes when the CCS polymers were dispersed in THF compared to that in THF-methanol mixture also increased with increasing  $r$  value. The almost similar size of CCS-I5 in THF compared to that in THF-methanol indicates that it was a block copolymer rather than a CCS polymer. This size is only about 3-fold higher than that of the size of linear PS arm precursor, measured in THF, the good solvent for the arm. On the other hand, the high peak MW value, which was about 5- and 6-fold higher, respectively, compared to that of the linear PS arm precursor before and after deconvolution, as well as the high yield of CCS-I5, could also suggest the formation of lightly crosslinked CCS polymers.<sup>196, 201</sup> When the  $r$  value was increased to 9 (CCS-I6), the  $D_h$  value of the CCS polymer increased by 40%, which was accompanied by twice an increase in the peak MW. The large hydrodynamic size of CCS-I7 and CCS-I8 along with the high peak MW could indicate the formation of star-star coupling, which led to broad MW distribution of CCS polymers.<sup>6, 39, 63</sup>

#### 2.4.1.9 Effect of Concentration and MW of PS Arm

To study the effect of PS arm concentration on the formation of CCS polymer, the molar concentration of linear PS arm was varied while keeping the molar ratio of EGDMA to PS arm ( $r$ ) constant. For this purpose, another batch of linear PS arm was prepared (PS-I17,  $M_n = 15.2$  kDa). These linear PS arms were prepared by mixing a mixture of St and BDDC at different [St]:[BDDC] ratios of 155:1, 105:1 and 50:1 and then polymerised for 5 h, following the procedure in §2.2.3.1. After the PS arms were isolated and purified, four tubes containing the same molar ratio of EGDMA to PS arm (15:1 for PS-I17) at various molar concentration of PS arm (i.e. 2, 5, 9 and 14 mM) were then prepared in THF. This was done by varying the volume of the solvent (ranging from 1 – 6 mL) whilst keeping the mass of the PS arm constant (200 mg) and the mixture was then polymerized for 5 hr, following the procedure in §2.2.3.2. The influence of PS arm concentration on the CCS formation was also studied using PS arms having shorter chain length (lower  $M_n$  values). For this purpose, two batches of PS arms (PS-I18 and PS-I19) were prepared by mixing a mixture of St and BDDC at

different [St]:[BDDC] ratios of 105:1 and 50:1 and then polymerised for 5 h, following the procedure in §2.2.3.1. After the PS arms were isolated and purified, two tubes containing the same molar ratio of EGDMA to PS arm (15:1) at various molar concentration of PS arm (i.e. 14 and 19 mM for PSI-18 and PS-I19, respectively) were then prepared in THF. This was done by fixing the amount of polymers and volume of solvent at 200 mg and 3 mL, respectively and the mixture was then polymerized for 5 h, following the procedure in §2.2.3.2. The resultant CCS polymers were then characterized using GPC and DLS to determine their molecular weight and particle size values, respectively, and the results are tabulated in Table 2.6. Figure 2.16 shows the GPC curves of the CCS polymers synthesized at various PS arm concentrations compared with that of the linear arm precursor (PS-I16).

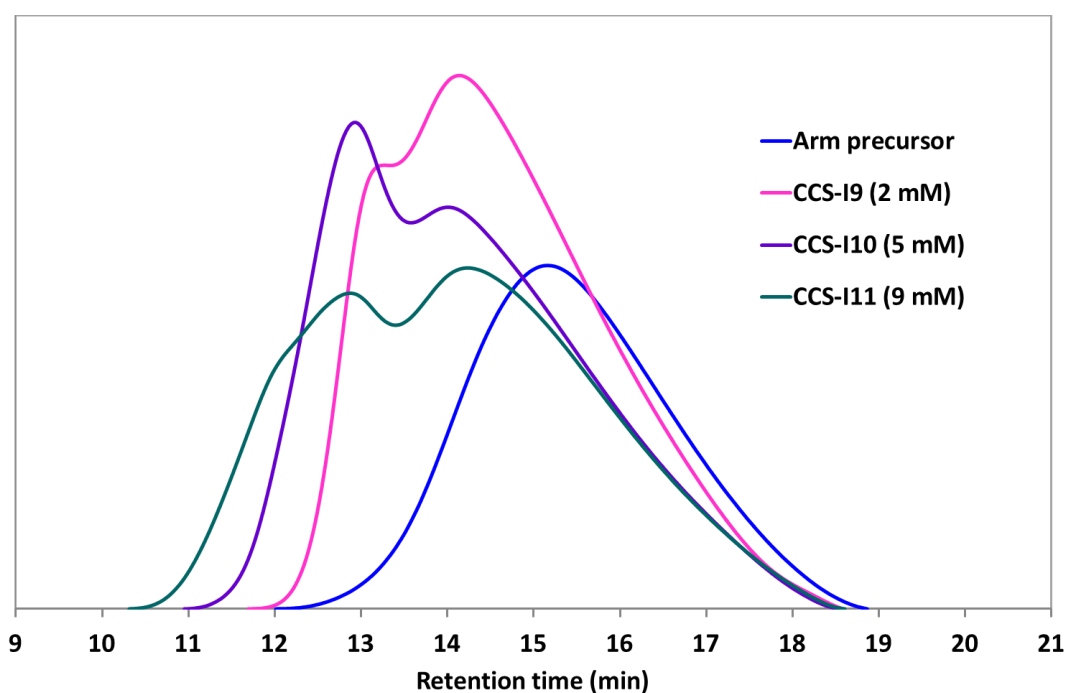


**Figure 2.16.** GPC traces of CCS polymers obtained from the polymerisation at various PS arm concentrations compared with that of the linear PS arm precursor (PS-I17).

As shown in Figure 2.16, when the molar concentration of PS arm was 2 mM, two overlapping peaks could clearly be observed. Note that the lower MW peak (higher retention time) shifted towards the higher MW side compared to that of the linear PS arm precursor, which could indicate the formation of short block copolymers and

lightly crosslinked CCS polymers (see Scheme 1.2, §1.2.1.2). As the concentration was increased, the appearance of the second peak at the higher MW side was more pronounced indicating the formation of higher MW CCS polymer. At the highest concentration of PS arm (9 mM), a shoulder peak was observed at the higher MW side of the GPC curve of CCS-I11, which could indicate possible star-star coupling. In general, the CCS polymer peak shifted to the higher MW side with increasing PS arm concentration. The GPC curves were then deconvoluted using the Excel's Solver routine to give the most probable fit for two or three molecular weight components, without fixing any of the peak retention times. The areas under the two Gaussian curves are used to estimate the fractions of CCS polymers and the residual unincorporated PS arm precursor. The results from GPC analysis are tabulated in Table 2.6 and compared with those of DLS.

From Table 2.6, comparing the peak MW and hydrodynamic diameter values of CCS-I9, CCS-I10 and CCS-I11, which were prepared using the same PS arm, it can be seen that in general, both values increase with increasing PS arm concentration. This is because at higher PS arm concentration and hence higher concentration of EGDMA, there is a greater probability of intermolecular collision between the PS-PEGDMA block copolymers, thus producing larger cores and higher arm numbers around the cores. In other words, more crosslinking reactions occurred at higher PS arm concentration, leading to high MW CCS polymers, which is consistent with the reported results in the literature.<sup>24, 196</sup> Note that further increase in the PS arm concentration (i.e. 14 mM) led to gelation (CCS-I12), possibly due to faster crosslinking reaction with decreasing volume of solvent,<sup>196</sup> thus particles were no longer formed at this high concentration.

**Table 2.6.** Formation of CCS polymers from iniferter polymerisation at various PS arm concentrations.<sup>a</sup>

CCS polymer	[PS arm] (mM)	$M_p$ (GPC) (kDa) <sup>e</sup>		$M_p$ (kDa) <sup>f</sup>		CCS Yield (%) <sup>g</sup>	$D_h$ (nm) <sup>h</sup>		
		Arm	CCS	Arm	CCS		THF	THF-MeOH	$\Delta D_h$
CCS-I9 <sup>b</sup>	2	32.4	71.2	33.0	97.4	9	18.1	17.7	0.4
CCS-I10 <sup>b</sup>	5	36.7	127	31.0	137.9	28	42.3	33.1	9.2
CCS-I11 <sup>b</sup>	9	29.4	135	27.0	123.8 392.8	5 18	95.8	87.0	8.8
CCS-I12 <sup>b</sup>	14	N/A	N/A	N/A	N/A	Gelation	N/A	N/A	N/A
CCS-I13 <sup>c</sup>	14	N/A	114	6.5	45.5 116.5	18 28	32.1	26.8	5.3
CCS-I14 <sup>d</sup>	19	N/A	120	3.7	38.9 124.8	26 37	57.5	46.4	11.1

<sup>a</sup> Polymerisation conditions: room temperature in THF; [PS]:[EGDMA] ratio = 15:1; polymerisation time = 5 h.

<sup>b</sup>  $M_{n(\text{arm})}$  and  $M_{p(\text{arm})}$  = 15.2 and 27.3 kDa respectively;  $D_h$  (PS arm) in THF = 7.6 nm.

<sup>c</sup>  $M_{n(\text{arm})}$  and  $M_{p(\text{arm})}$  = 4.9 and 5.7 kDa respectively;  $D_h$  (PS arm) in THF = 3.6 nm.

<sup>d</sup>  $M_{n(\text{arm})}$  and  $M_{p(\text{arm})}$  = 3.6 and 4.6 kDa respectively;  $D_h$  (PS arm) in THF = 3.4 nm.

<sup>e</sup> Peak value of the apparent MW measured by GPC in THF, calibrated with linear PS standards.

<sup>f</sup> Peak values of the resultant deconvoluted peaks by Excel Solver.

<sup>g</sup> Calculated from the area of the deconvoluted CCS polymer peak relative to the total area of the deconvoluted polymer peaks as follows: CCS yield (%) =  $\frac{A_{\text{CCS polymer}}}{A_{\text{CCS polymer}} + A_{\text{unreacted PS arm}}} \times 100$ .

<sup>h</sup> Hydrodynamic diameter of filtered sample of polymers (using a 450 nm membrane filter) determined by DLS with distribution analysis at 20 °C in THF and THF-MeOH (methanol) (60/40, vol %).

N/A: not available.

The similar size of CCS-I9 in THF compared to that in THF-methanol confirms that it was a block copolymer of poly(styrene-EGDMA) rather than a CCS polymer. This size is only about 2.5-fold higher than that of the size of linear PS arm precursor, measured in THF, the good solvent for the arm. As the PS arm concentration was increased to 5 mM, the difference in sizes when the CCS polymer (CCS-I10) was dispersed in THF compared to that in THF-methanol mixture also increased. However, the difference seemed to be constant when the PS arm concentration was increased to 9 mM, which could indicate that the decrease in the  $D_h$  value was due to the shrinkage of the PS

arms around the CCS polymer core (CCS-I11) in the presence of methanol. The appearance of an additional peak in the GPC curve of CCS-I11, having deconvoluted peak MW of about three times of that of CCS-I10 ( $M_p = 392.8$  and  $137.9$  kDa respectively) as well as the much bigger size of the former (about twice) compared to that of the latter confirms the occurrence of star-star coupling reactions. Star-star coupling could occur if the cores of the CCS polymers are sterically accessible and is enhanced in the presence of higher number of initiation sites in the core.<sup>16</sup> When the PS arm concentration was further increased to  $14$  mM, gelation (CCS-I12) occurred. From the table, it can also be observed that when the PS arm concentration was increased from  $2$  to  $5$  mM, the CCS yield increased about  $3$  times. However, no increase in the CCS yield can be observed when the PS arm concentration was further increased to  $9$  mM.

The effect of using PS arm precursor with lower  $M_n$  values was also investigated using PS arms with  $M_n$  values equal to  $4.9$  and  $3.6$  kDa, respectively. As can be seen in Table 2.6, the preparation of CCS polymer (CCS-I13) using the same PS arm concentration (i.e.  $14$  mM) as that when preparing CCS-I12 did not produce any gelation when PS arm with a lower  $M_n$  value (about three times lower) was used. Similarly when PS arm with four times lower value of  $M_n$  than that of CCS-I12 was employed as the arm precursor, no gelation occurred even when a higher PS arm concentration was used (i.e.  $19$  mM). From Table 2.6, it can be observed that the resultant polymers (CCS-I13 and CCS-I14) consisted of two different MW of CCS polymers where the higher MW polymers were attributed to the result of star-star coupling, which resulted in about  $2.5$ - and  $3$ -fold higher MW values compared to the lower MW polymers of CCS-I13 and CCS-I14 respectively. Nevertheless, the peak MW of both CCS polymers as well as their hydrodynamic diameter were less than those of CCS-I11, which was prepared at lower PS arm concentration ( $9$  mM). This result could indirectly suggest that using lower MW of PS arm led to CCS polymer with lower MW and smaller size, as reported in the literature.<sup>24, 201</sup> However, it is quite difficult to relate the CCS yield of both polymers since they were prepared at different PS arm concentrations ( $14$  and  $19$  mM respectively). Although the  $D_h$  values of the arms were almost similar, the reduction in

the size of CCS-I14 when it was dispersed in THF compared to that in THF–methanol mixture was about twice of that of CCS-I13, indicating that the latter was more compact than the former.

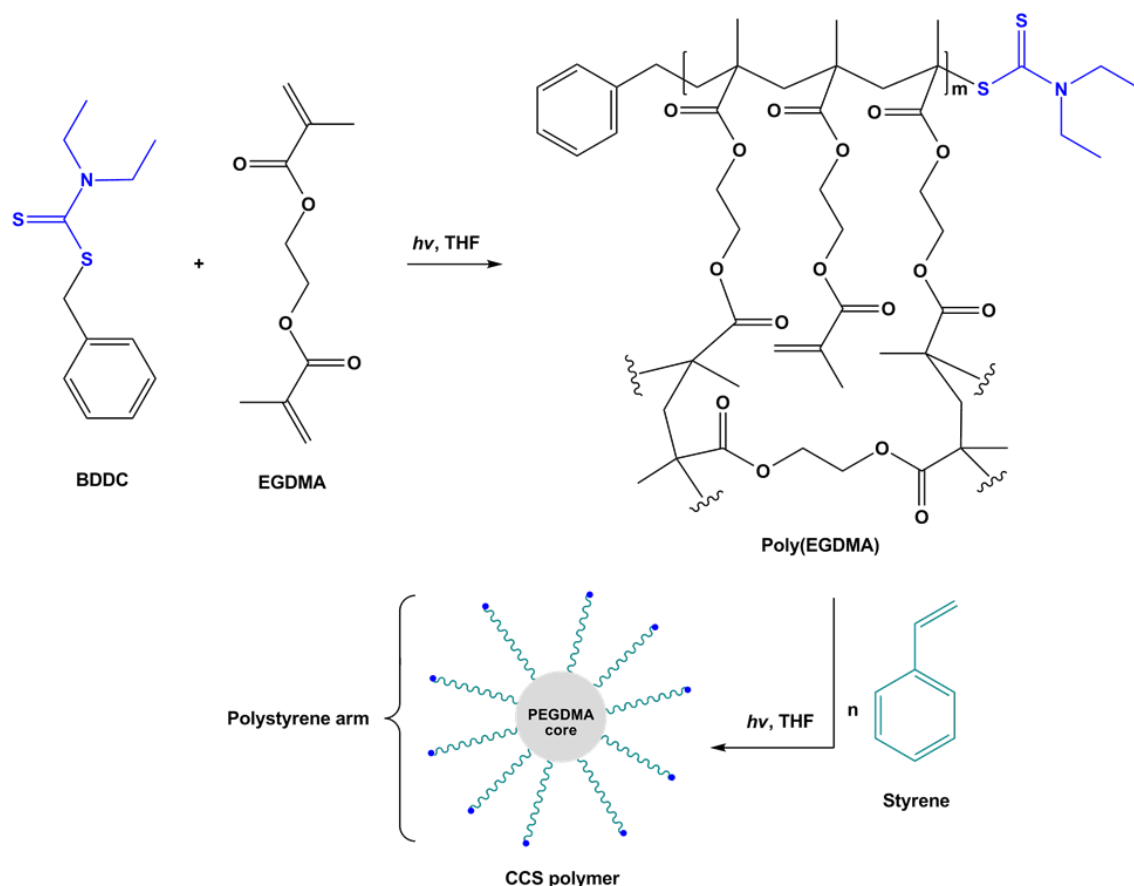
#### 2.4.1.10 Summary

The GPC curves of all the CCS polymers presented in the previous sections exhibited broader MW distribution compared to that of the linear PS arm precursor, which is a characteristic of CCS polymers synthesised via the arm-first method.<sup>36, 39</sup> Evidence of a peak attributed to the residual unincorporated PS arm precursor could be observed in all of the GPC curves of the CCS polymers, which means that the linear arm precursor was not all incorporated into the CCS polymers and hence extra purification steps are necessary in order to separate the CCS polymer from the residual unincorporated arm.<sup>4</sup>

From the results of varying several reaction parameters such as polymerisation time, [EGDMA]:[PS arm] ratio, concentration as well as MW (or chain length) of PS arm precursor in the synthesis of CCS polymers, it can be concluded that all the parameters significantly influenced the MW, size and yield of CCS polymer to a certain degree. It was found that conducting the reaction at longer polymerisation time, using higher [EGDMA]:[PS arm] and molar concentration of PS arm as well as employing a longer chain length (or longer MW) of PS arm resulted in higher MW and bigger size of CCS polymer. Higher yield of CCS polymer was also obtained when higher [EGDMA]:[PS arm] ratio and lower PS arm concentration were used during the polymerisation reaction. However, employing too high [EGDMA]:[PS arm] ratio and PS arm concentration in a very small volume of solvent could lead to gelation. Using PS arm with  $M_n$  value, [EGDMA]:[PS arm] ratio and PS arm concentration of 16.0 kDa, 18:1 and 5 mM respectively, CCS polymer with the highest MW, size and yield (300 kDa, 98 nm and 75% respectively) was synthesised. These results could be used as a guide to tailor-make a CCS polymer with a desired arm length and MW in high yield and hence should be taken into account during the preparation of CCS MIP.

## 2.4.2 Core-first CCS Polymers via Iniferter

The core-first CCS polymer was prepared by employing a two-pot approach, where the core was firstly synthesised and isolated, before being subjected to further photopolymerisation in the presence of styrene to form the CCS polymer by growing PS arms from the active core surface as shown in Scheme 2.3.



**Scheme 2.3.** Synthesis of CCS polymer via the core-first approach.

### 2.4.2.1 Preparation of PEGDMA Core Precursor

The PEGDMA microsphere which will be used as the core precursor was synthesised following the procedure described in §2.2.4.1 using THF as the polymerisation solvent. In the first attempt, the core was prepared by photopolymerisation of EGDMA at a molar ratio of EGDMA to iniferter of 80: 1 in THF (EGDMA:THF = 1:1 v/v) for 2 h, which resulted in gelation. The free flow portion of the gel was separated from the hard gel and vigorously stirred in methanol to precipitate out the polymer (PE-I1). Based on this result, the next polymerisation was carried out using a lower molar ratio of EGDMA to

iniferter of 25:1 at a much lower concentration of EGDMA (EGDMA:THF = 1:16 v/v) and although the reaction mixture turned out to be very viscous after 24 h, no gelation was observed. This indicates that gelation was suppressed at lower ratio of EGDMA to iniferter and conducting the polymerisation in high dilution. The reaction mixture was then stirred in methanol to precipitate out the polymer (PE-I2). After undergoing purification, both PEGDMA microspheres classes were sent for FTIR analysis for structural confirmation. NMR analysis could not be carried out since the microspheres were not dispersible in any organic solvents.

A typical FTIR spectrum of the PEGDMA microsphere (PE-I1) is shown in Figure 2.17. The strong peak at  $1721\text{ cm}^{-1}$  and the broad peak at  $1164\text{ cm}^{-1}$  are assigned to the carbonyl (C=O) and ester (C-O-C) stretching vibration of EGDMA respectively. The peak at  $1636\text{ cm}^{-1}$  is attributed to the pendant unreacted C=C double bond in the microsphere, which indicates the incomplete conversion of pendant double bonds, suggesting a low crosslinking efficiency. The characteristic peaks of the DDC end group can be observed at  $1264$  and  $1005\text{ cm}^{-1}$  (C=S and C-S respectively). In addition, two peaks which are attributed to the out-of-plane C-H bending vibration of the aromatic rings of the benzyl moiety of the iniferter could also be clearly observed at  $747$  and  $700\text{ cm}^{-1}$ , respectively. These results showed that the BDDC iniferter was successfully incorporated into the resulting PEGDMA microsphere.

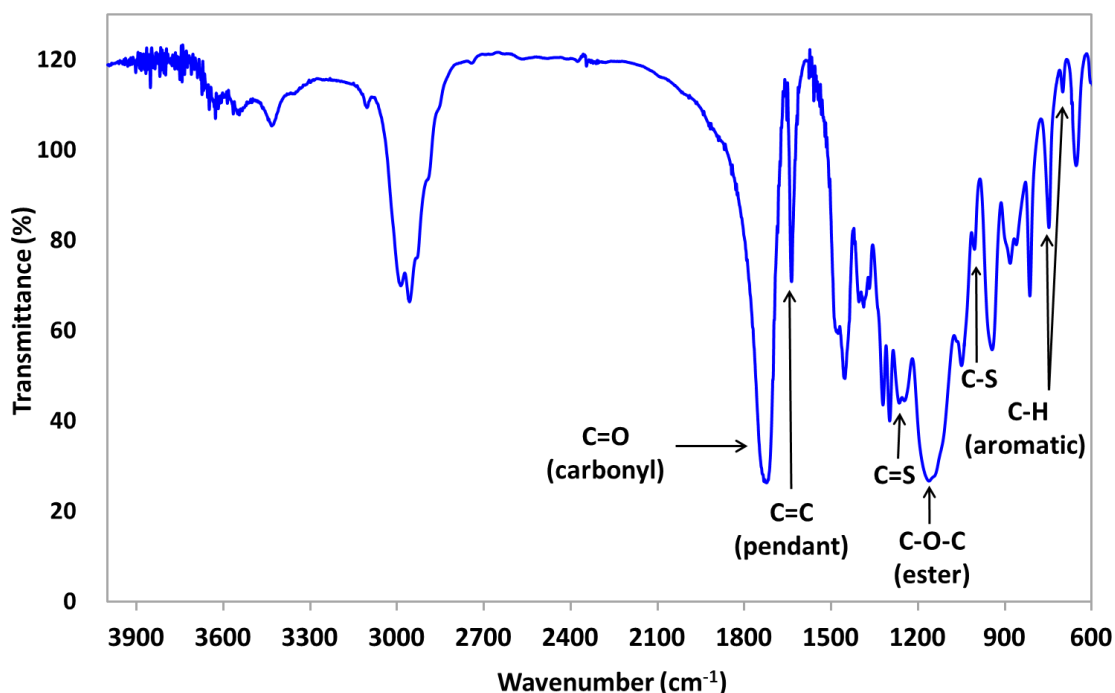


**Figure 2.17.** FTIR spectrum of a PEGDMA core synthesised using BDDC iniferter.

#### 2.4.2.2 Core-first CCS Polymers

The core-first CCS polymer was prepared using the PEGDMA core (PE-I1) synthesised beforehand following the procedure in §2.2.4.2. This was done by preparing a mixture of PEGDMA core (30 mg) and styrene (13.0 mmol) in THF (styrene:THF = 1:1 v/v) followed by photopolymerisation for about 24 h. The purified core-first CCS polymer (CCS-I16) was dispersible in the NMR solvent (deuterated chloroform) and thus was subjected to FTIR as well as NMR spectroscopic analyses for structural confirmation. A typical FTIR spectrum of the core-first CCS polymer (CCS-I16) is shown in Figure 2.18 and compared with that of the core precursor (PE-I1).

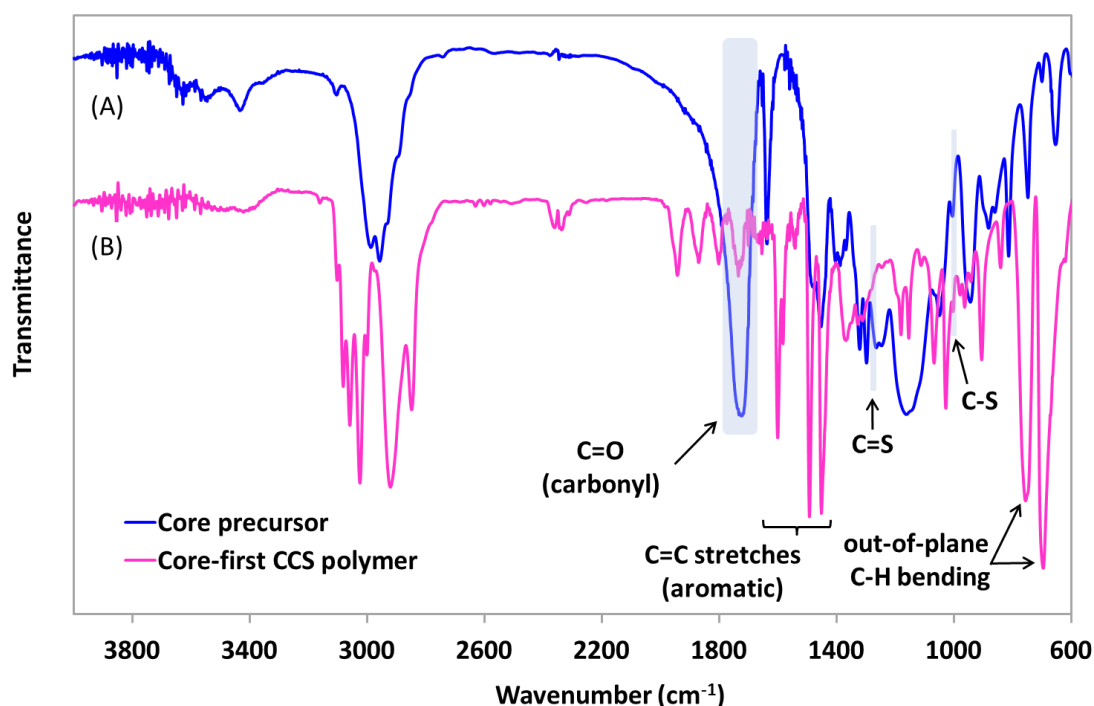


**Figure 2.18.** FTIR spectrum of (A) a core precursor (PE-I1) and (B) the corresponding core-first CCS polymer (CCS-I16) prepared using BDDC iniferter.

In the FTIR spectrum of CCS polymer (Figure 2.18(B)), the strong peaks at 1600, 1491 and 1452  $\text{cm}^{-1}$  are assigned to the C-C stretching of aromatic rings, whilst the peaks at 747 and 699  $\text{cm}^{-1}$  are characteristic of the aromatic C-H out-of-plane bending modes of polystyrene, which indicates the successful growth of PS arm from the DDC moiety on the core surface. The carbonyl C=O stretching vibration of the EGDMA unit in the core can be seen at 1728  $\text{cm}^{-1}$ . Although the intensity of this carbonyl peak is much weaker compared to that of the arm-first CCS polymer (Figure 2.11(A)), possibly due to the fact that the core was surrounded by very long chain of PS arms, the absent of this peak in the FTIR spectrum of a PS arm prepared via BDDC iniferter (Figure 2.3), indicates that the crosslinked core is responsible for the peak. The characteristic peak of the DDC group can be observed at 1279 and 1003  $\text{cm}^{-1}$  (C=S and C-S, respectively).

Figure 2.19 shows a typical proton NMR spectrum of a core-first CCS polymer (CCS-I16) prepared using PE-I1 as the core precursor. Unlike the core precursor, the core-first CCS polymer was dispersible in the NMR solvent, which indicates the growth of PS around the PEGDMA core precursor. This is confirmed by the presence of multiplet

peaks between 7.70 ppm and 7.23 ppm ( $H_c$ ) in the spectrum of CCS polymer, which are assigned to the aromatic protons of styrene. This is supported by the presence of signals between 1.2 – 1.6 ppm ( $H_e$ ) and 1.6 - 2.0 ppm ( $H_f$ ), which are assigned to the backbone methylene and methine protons of PS, respectively. Note that although the DDC moiety is preserved at the CCS periphery, signals attributed to its methylene protons could not be observed possibly due to the presence of a long chain PS arm, which supports the presence of weak carbonyl band in its FTIR spectrum (Figure 2.18(B)). In addition, the absence of signals attributed to the four protons of the EGDMA units ( $H_c$ ) in this spectrum compared to that of the arm-first CCS polymer (Figure 2.12), further confirms the presence of a long chain PS arm around the core.

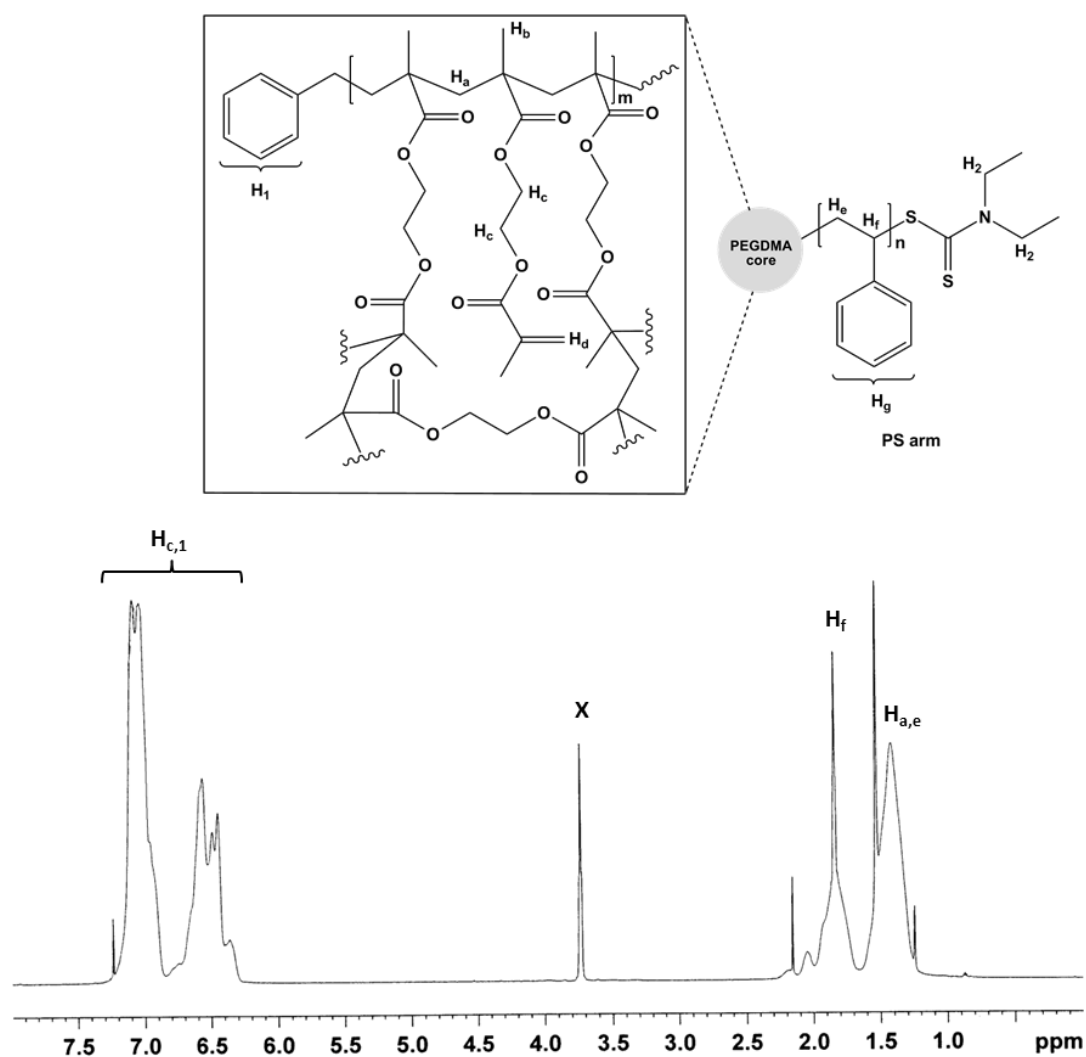


**Figure 2.19.**  $^1\text{H}$  NMR spectrum of a core-first CCS polymer prepared using BDDC iniferter. X denotes contaminant peak attributed to THF.

The SEM images of a core-first CCS polymer (CCS-I15) and the corresponding core precursor (PE-I1) are shown in Figure 2.20(A) and (B) respectively. From the SEM image (Figure 2.20(A)), it can be observed that the core-first CCS polymer did not form spherical particles, unlike those of the arm-first CCS polymer (Figure 2.13(A) and (B)). This could be attributed to the nonspherical core precursor of the core-first CCS polymer (Figure 2.20(B)), which formed soft gel during the polymerisation, as discussed in §2.4.2.1.

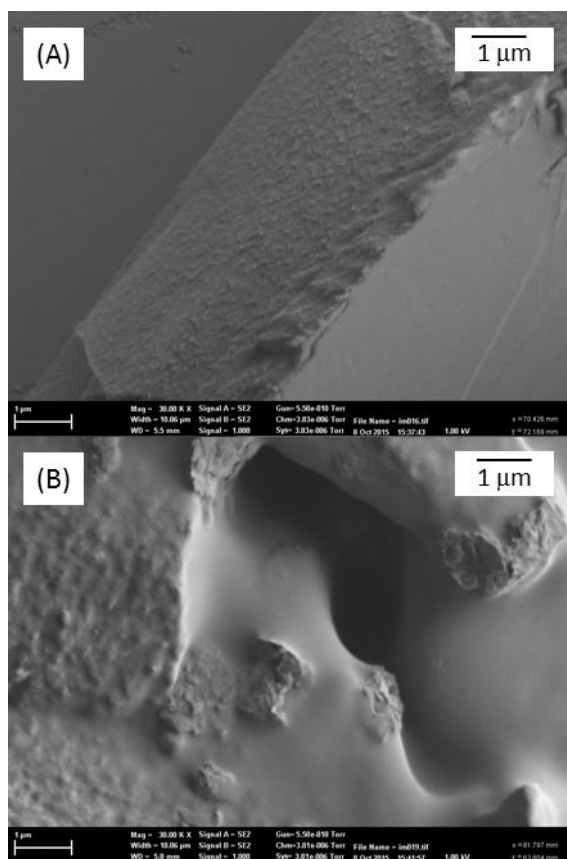


**Figure 2.20.** SEM images of (A) a core-first CCS polymer (CCS-I15) and (B) the corresponding core precursor (PE-I1). Both A and B were recorded at 30000X magnifications.

The above results showed that a core-first CCS polymer was successfully synthesised using BDDC iniferter by employing the two-pot approach. In the preparation of the core precursor, it was found that employing lower ratio of crosslinker to iniferter and conducting the polymerisation in high dilution (about 6 vol % of monomer relative to the reaction medium) are necessary to suppress gelation. Although NMR and FTIR

analysis of the CCS polymer showed evidence of the presence of PS arm respectively, the length of the arm could not be estimated from the former since the end-group was not visible in the NMR spectrum, which indicates the long chain length of the PS arm. Based on the result of the synthesis of the arm (§2.4.1.4), the length of the PS arm could be adjusted by varying the polymerisation time during the synthesis of the CCS polymer. However, further investigations are required to optimise the parameters involved during the preparation of the core precursor (such as ratio of crosslinker to iniferter, crosslinker concentration, type and of solvent and polymerisation time) as well as the CCS polymer (such as core precursor to styrene ratio, concentration of styrene and polymerisation time).

### **2.4.3 Transmission Electron Microscope**

Transmission electron microscope (TEM) analysis was conducted by dispersing about 1 mg of sample in a 1.0 mL mixture of methanol and THF (60/40, vol %). Methanol was added dropwise until the solution became slightly turbid and the solution was left on the shaker overnight. Two drops of the solution were then deposited on the carbon-coated copper grid, followed by evaporation of the solvent at room temperature. The grid was examined using a JEOL JEM-1200EXII instrument, operated at an acceleration voltage of 80 kV with digital imaging software at various magnifications.

## **2.5 Conclusions**

In this study, core-crosslinked PS star polymers were successfully synthesized by using a controlled free radical polymerisation, namely the iniferter technique. In the arm-first method, linear PS arms with reactivatable chain-end initiating sites were synthesized using BDDC iniferter before undergoing a crosslinking reaction with EGDMA to afford CCS polymer with the initiating sites confined at the core. On the other hand, the core-first method involves the polymerisation of EGDMA crosslinker in the presence of BDDC iniferter to generate a multifunctional crosslinked core before addition of styrene monomer to grow the arms from the active core surface. By using

this method, in contrast to the arm-first method, the initiating sites are preserved at the periphery of the CCS polymer.

The effect of changing several parameters on the formation of CCS polymer via the arm-first method was investigated. The results showed that increasing the polymerisation time, concentration of the PS arm, molar ratio of EGDMA to PS arm and arm length resulted in the formation of CCS polymers with higher molecular weight and bigger particle size. Although the arm-first approach allows the length of the arms to be well-controlled since they were synthesised independently, the final products were contaminated by the residual unreacted PS arm precursors, which requires extra purification step in order to obtain high purity CCS polymers. In the core-first approach, it is found that gelation could be suppressed by conducting the photopolymerisation at low ratio of crosslinker to iniferter in high dilution. Although further investigation is required to optimise the parameters involved during the preparation of the core precursor as well as the CCS polymer, initial investigation showed that CCS polymer could be successfully synthesised with ease using this approach. Unlike the CCS polymer via the arm-first method, extra purification step was not required to obtain the pure CCS polymer via the core-first approach. These results can be used as guidelines to design molecular imprinted polymer in the form of core crosslinked star (CCS MIP) with the desired particle size as well as number and length of arms for imprinting purposes.

The above results showed that CCS polymers have been successfully prepared using the RDRP technique, namely iniferter. The synthesis of CCS polymers using other RDRP technique, i.e. RAFT was also investigated and discussed in great details in Chapter 3. A comparison between these two methods is also presented at the end of the chapter.

## Chapter 3

### Core Crosslinked Star Polymers Via RAFT

#### 3.1 Introduction

The CCS polymers were successfully prepared via iniferter polymerisation and discussed in great length in Chapter 2. Apart from iniferter, reversible addition-fragmentation chain transfer (RAFT) polymerisation is another RDRP technique and has been one of the popular techniques to prepare CCS polymers.<sup>6, 202</sup> RAFT offers the benefit of being able to synthesise well-defined polymers for a wider range of monomers under mild conditions.<sup>96</sup> In addition, it can be used in variety of free radical polymerisation modes such as solution,<sup>203</sup> suspension,<sup>204</sup> emulsion<sup>205</sup> and precipitation<sup>206</sup> polymerisations.

Herein, the synthesis of CCS polymers by the arm-first (Scheme 3.1, §3.4.1) and core-first (Scheme 3.2, §3.4.2) methods, via the RAFT technique is presented using methyl 2-(butylthiocarbonothioylthio)propanoate (MCEBTTC) as the RAFT agent. MCEBTTC has been used to prepare grafted silica nanoparticles,<sup>207</sup> thermoresponsive (PNIPAM) and cationic (PDMAEA) diblock copolymer nanoparticles<sup>208</sup> as well as polystyrene nanoparticles in a well-controlled miniemulsion system.<sup>209</sup> The use of MCEBTTC in the synthesis of CCS polymers however, has not yet been reported.

Using an analogous approach to that used in Chapter 2, the CCS polymers were then prepared utilising MCEBTTC as the RAFT agent. The difference between RAFT and iniferter polymerisations is that the former was carried out thermally whereas the

latter was performed photochemically. Apart from that a small amount of AIBN initiator was added during RAFT polymerisation as required and the reaction was also carried out at a much higher temperature compared to that of the iniferter. The results from these two polymerisations will be compared at the end of this chapter.

## 3.2 Experimental

### 3.2.1 Materials

1-butanethiol, triethylamine, carbon disulfide, dichloromethane and diethyl ether and acetonitrile were all used as received. Styrene (St), methacrylic acid (MAA) and ethylene glycol dimethacrylate (EGDMA) were obtained from Sigma-Aldrich ( $\geq 98\%$  purity), and were passed through a column of activated basic alumina (Aldrich, Brockmann I, standard grade,  $\sim 150$  mesh,  $58 \text{ \AA}$ ) to remove radical inhibitors. Azobisisobutyronitrile (AIBN) was recrystallised twice from acetone prior to use. Deuterated chloroform ( $\text{CDCl}_3$ , 99.6 atom %) was obtained from Aldrich and HPLC grade tetrahydrofuran (THF) was obtained from Scharlau. Bulk grade solvents methanol and ethanol were distilled prior to use. All water was purified by reverse osmosis prior to use. Methyl 2-(butylthiocarbonothioylthio) propanoate [1] (MCEBTTC, Figure 3.1) was synthesised following the procedure described in §3.2.2.

### 3.2.2 Synthesis of RAFT agent

The RAFT agent, MCEBTTC (Figure 3.1, [1]) was synthesised according to the literature procedure.<sup>210</sup>

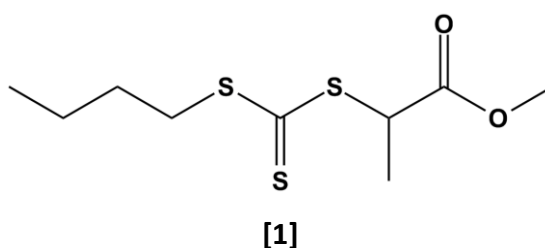


**Figure 3.1.** Methyl 2-(butylthiocarbonothioylthio) propanoate (MCEBTTC).

Carbon disulfide (6.18 mL, 0.103 mol) in dichloromethane (50 mL) was added dropwise to a stirred solution of 1-butanethiol (10 mL, 0.093 mol) and triethylamine (14.3 mL, 0.103 mol) in dichloromethane (100 mL) under nitrogen atmosphere over a period of 30 min at 0 °C. The solution gradually turned yellow during the addition. After complete addition the solution was stirred at room temperature for 1 h. Methyl bromopropionate (11.46 mL, 0.103 mol) in dichloromethane (50 mL) was then added dropwise to the solution over a period of 30 min and the solution was stirred for 2 h. The dichloromethane was removed under vacuum and the residue dissolved in diethyl ether. The solution was then washed with cold 10 % HCl solution (3 x 50 mL) and MilliQ water (3 x 50 mL) and then dried over anhydrous MgSO<sub>4</sub>. The diethyl ether was removed under vacuum and the residual yellow oil was purified by column chromatography (9:1 petroleum ether/ethyl acetate on silica, second band). The structure of the synthesised RAFT agent (MCEBTTC) was confirmed by NMR and FTIR. <sup>1</sup>H NMR (CDCl<sub>3</sub>, δ): 0.87 (tr, 3H, CH<sub>3</sub>CH<sub>2</sub>), 1.37 (mult, 2H, CH<sub>2</sub>), 1.53 (d, 3H, CH<sub>3</sub>), 1.61 (quin, 2H, CH<sub>2</sub>), 3.29 (tr, 2H, CH<sub>2</sub>), 3.67 (s, 3H, CH<sub>3</sub>), 4.77 (quad, 1H, CH); <sup>13</sup>C NMR (CDCl<sub>3</sub>, δ) 13.59, 16.93, 22.06, 29.94, 36.93, 47.67, 52.77, 171.48 (CH-C(=O)-O), 221.99 (S-C(=S)-S). FTIR (cm<sup>-1</sup>): 1735 (s, C=O), 1248 (w, C=S stretching), 1058 (w, C=S vibration), 664 (w, C-S).

### 3.2.2.1 Preparation of CCS Polymers via Arm-First

### 3.2.2.2 Synthesis of PS Arm using MCEBTTC RAFT Agent

Linear PS with trithiocarbonate (TTC) end functionality was synthesised via solution polymerisation of styrene with MCEBTTC as the chain transfer agent. A typical polymerization procedure for the synthesis of PS arm was as follows. Styrene (9 mL, 78.3 mmol), MCEBTTC (65.8 mg, 0.260 mmol) and AIBN (4.3 mg, 0.026 mmol) were mixed in DMSO (6.00 mL) in a test tube. The mixture was deoxygenated by purging with nitrogen for 30 minutes and then heated in an oil bath at 80 °C. The polymerisation was then quenched by immersing the test tubes in an ice-water bath after 24 hours. The polymers were precipitated by adding the polymerization mixture dropwise into an excess amount of methanol under vigorous stirring. The polymers

obtained were then purified twice by reprecipitation from THF into methanol, followed by drying for a day in a vacuum oven at 40 °C. The yield of the PS arm (5 – 40%) was determined gravimetrically and the molecular weights of the produced arm precursors were determined by GPC.

### **3.2.2.3 Preparation of Arm-first CCS Polymers**

A typical RAFT polymerization procedure for the synthesis of a CCS polymer via the arm-first method was as follows. 300 mg of the previously synthesised arm, EGDMA (25  $\mu$ L, 0.13 mmol) and AIBN (0.043 mg,  $2.63 \times 10^{-4}$  mmol) were mixed in a test tube containing THF (5.25 mL). The reaction mixture was stirred, purged with nitrogen for 30 mins and heated in an oil bath at 60 °C for 24 hr. The polymerisation was then quenched by immersing the test tubes in an ice-water bath. The polymer was precipitated by adding the polymerization mixture dropwise into an excess amount of methanol under vigorous stirring. The polymer obtained was then purified twice by reprecipitation from THF into methanol, followed by drying in a vacuum oven at 40 °C. The yield of the PS CCS polymer was determined gravimetrically.

## **3.2.3 Preparation of CCS Polymers via Core-First**

### **3.2.3.1 Synthesis of PEGDMA Core using MCEBTTC RAFT Agent**

A typical polymerization procedure for the synthesis of PEGDMA core was as follows. EGDMA (1.50 mL, 7.95 mmol), MCEBTTC (0.401 g, 1.59 mmol) and AIBN (26.1 mg, 0.159 mmol) were dissolved in THF (35.00 mL) in a test tube. The mixture was deoxygenated by purging with nitrogen for 30 minutes and then heated in an oil bath at 60 °C for 3 hours. The viscous solution was then added dropwise into an excess of methanol under vigorous stirring. After washing in large amount of methanol twice, the precipitate was collected and dried in the vacuum oven at 40°C overnight. The yield of the PEGDMA core was determined gravimetrically.

### **3.2.3.2 Preparation of Core-First CCS Polymers**

The purified PEGDMA core from §3.2.4.1 was then used to form the CCS polymer. The following is a typical polymerisation procedure. Styrene (1.0 mL, 8.7 mmol) was added to the PEGDMA cores (50 mg) in THF (3 mL), stirred and degassed for 30 mins before being heated at 60°C for 24 hrs. The mixture was then added dropwise into a large amount of methanol under vigorous stirring. The precipitates were then dissolved in THF and the solution was centrifuged at 6 000 rpm. The sediments were rinsed with methanol, collected and kept for future use. The supernatant was added dropwise into a large amount of methanol. The precipitate formed was then purified once more by reprecipitation from THF into methanol, followed by drying in a vacuum oven at 40 °C. The yield of the PS CCS polymer was determined gravimetrically.

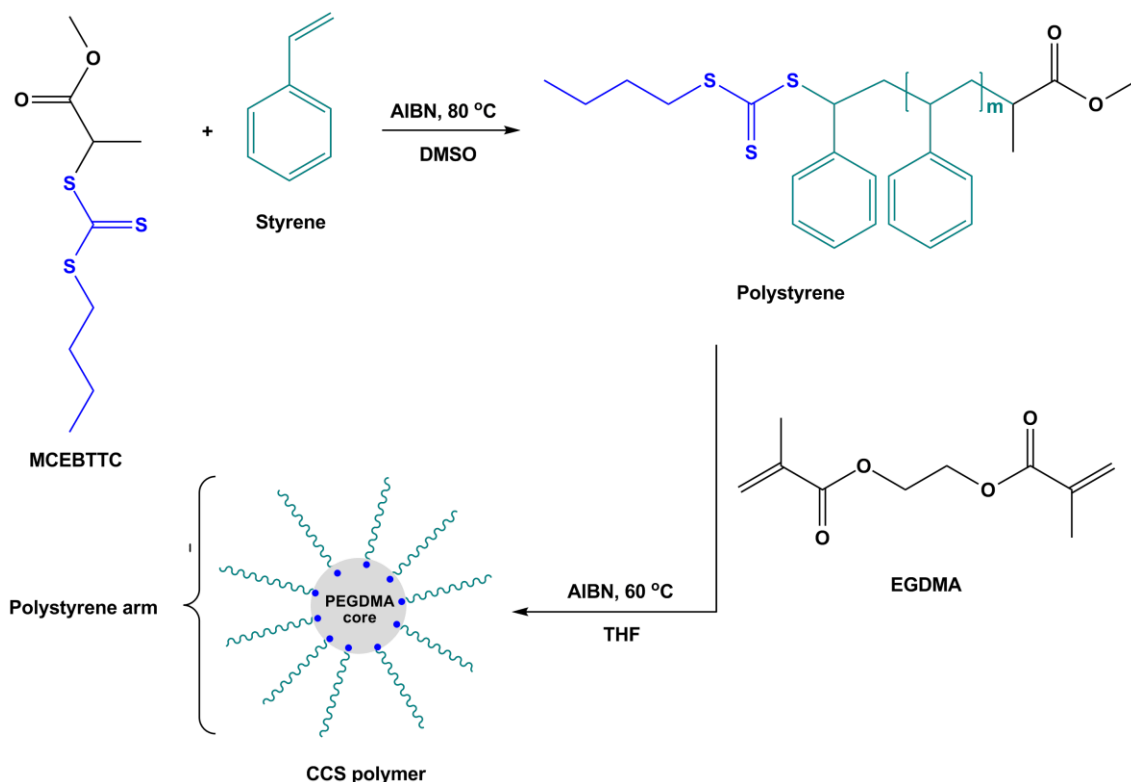
## **3.3 Characterisation**

NMR, FTIR, GPC, DLS, SEM and TEM analyses were carried out following the same procedures outlined in Chapter 2 (§2.2.2).

## **3.4 Results and Discussion**

### **3.4.1 Arm-First CCS Polymers via RAFT**

The synthesis of CCS polymers via the arm-first using MCEBTTC as the RAFT agent was carried out in a two-pot reaction as shown in Schemes 3.1. Using this approach, linear PS arm with trithiocarbonate (TTC) end group was firstly synthesised using the MCEBTTC RAFT agent and was isolated before subjected to further polymerisation with EGDMA to form a CCS polymer.



**Scheme 3.1.** Synthetic route of CCS polymers via the arm-first RAFT polymerisation.

#### 3.4.1.2 Preparation of Linear PS Arm Precursor

The linear PS was prepared using the previously synthesised MCEBTTC RAFT agent and then further used as the arm precursor for the synthesis of CCS polymer, as shown in Scheme 3.1. The synthesised linear PS arm was then characterized by FTIR, UV-GPC as well as  $^1\text{H}$  and  $^{13}\text{C}$  NMR spectroscopic analyses to confirm the incorporation of trithiocarbonate end group at the end of the linear chain.

#### 3.4.1.3 PS-TTC End Group Analysis

A typical FTIR spectrum of a linear PS arm (PS-R2, Table 3.1) synthesised using MCEBTTC is shown in Figure 3.2. The appearance of peaks in the spectrum at 1734 (C=O stretching), 1384 ( $\text{CH}_3$  deformation), 1156 (C-O-C stretching) and  $1030\text{ cm}^{-1}$  (C-O vibration) indicates the presence of the ester functional group of the MCEBTTC RAFT agent. The peak at  $1068\text{ cm}^{-1}$ , which is attributed to the C=S vibration confirms the successful incorporation of TTC end groups into the PS arm. The characteristic of aromatic rings in styrene could be observed between  $3120 - 3010\text{ cm}^{-1}$  (C-H stretches)

and between  $2000 - 1800 \text{ cm}^{-1}$  (weak aromatic overtone and combination bands). A pair of strong peaks at  $758$  and  $698 \text{ cm}^{-1}$  is attributed to the out of plane C-H bending of monosubstituted aromatic ring. The peaks attributed to the aromatic C-C stretching vibration of styrene could be observed at  $1602$ ,  $1494$  and  $1452 \text{ cm}^{-1}$ .

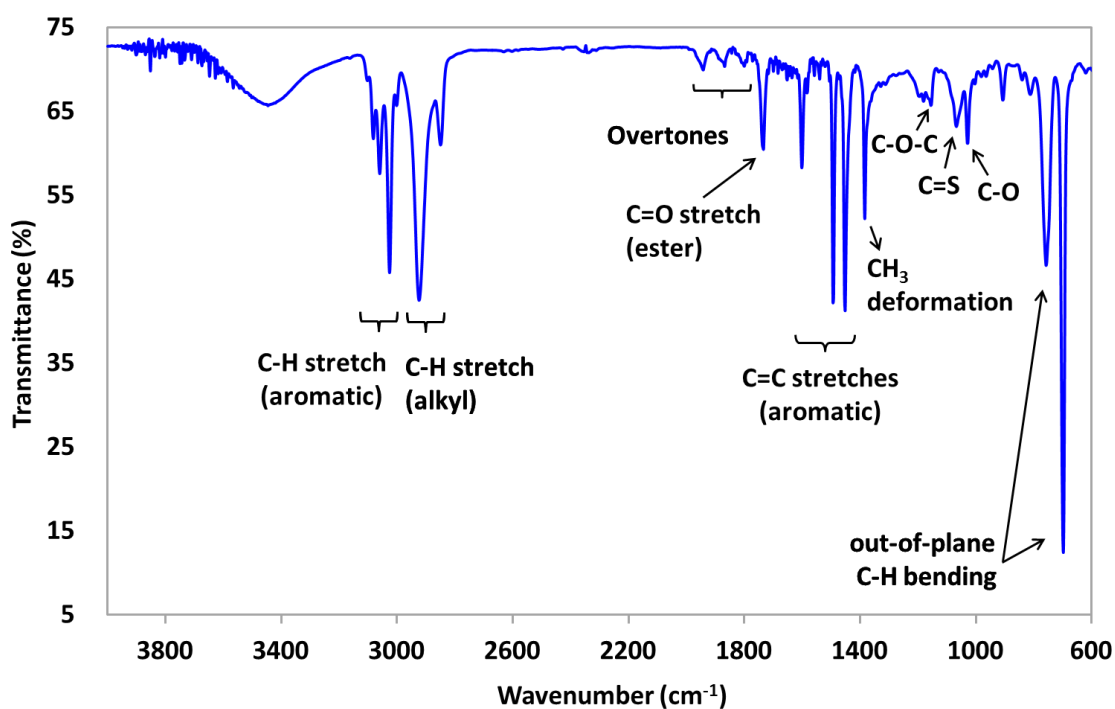


**Figure 3.2.** FTIR spectrum of a linear PS arm prepared via MCEBTTC RAFT agent.

Figure 3.3 shows a typical  $^1\text{H}$  NMR spectrum of a linear PS arm (PS-R2, Table 3.1) synthesised using MCEBTTC. The appearance of peaks at 3.3 ppm ( $\text{H}_4$ ) which was assigned to the methylene protons adjacent to the sulphur atom of the trithiocarbonate moiety, suggest its successful incorporation at the chain end of the linear PS chain. Signals between 4.7 - 5.1 ppm ( $\text{H}_a$ ) assigned to the methine proton of styrene adjacent to the sulphur atom of TTC strongly confirm the incorporation of the group into the polymer chain. The presence of peaks at about 3.4 - 3.6 ppm ( $\text{H}_7$ ) were attributed to the methyl ester, which suggests the incorporation of the RAFT ester group at the other end of the linear PS chain. This is supported by the presence of peaks at about 1.0 ppm attributed to the methylene protons of the RAFT ester group ( $\text{H}_6$ ), which overlapped with that of the trithiocarbonate moiety ( $\text{H}_1$ ). Finally, the signals between 6.7 - 7.2 ppm ( $\text{H}_b$ ) were ascribed to the aromatic protons of the

styrene unit whilst the signals at 1.9 (H<sub>d</sub>) and 1.5 ppm (H<sub>e</sub>), which overlapped with the signals of protons of the TTC end group (H<sub>2</sub> and H<sub>3</sub>), were attributed to the backbone methine and methylene protons of the polystyrene, respectively.

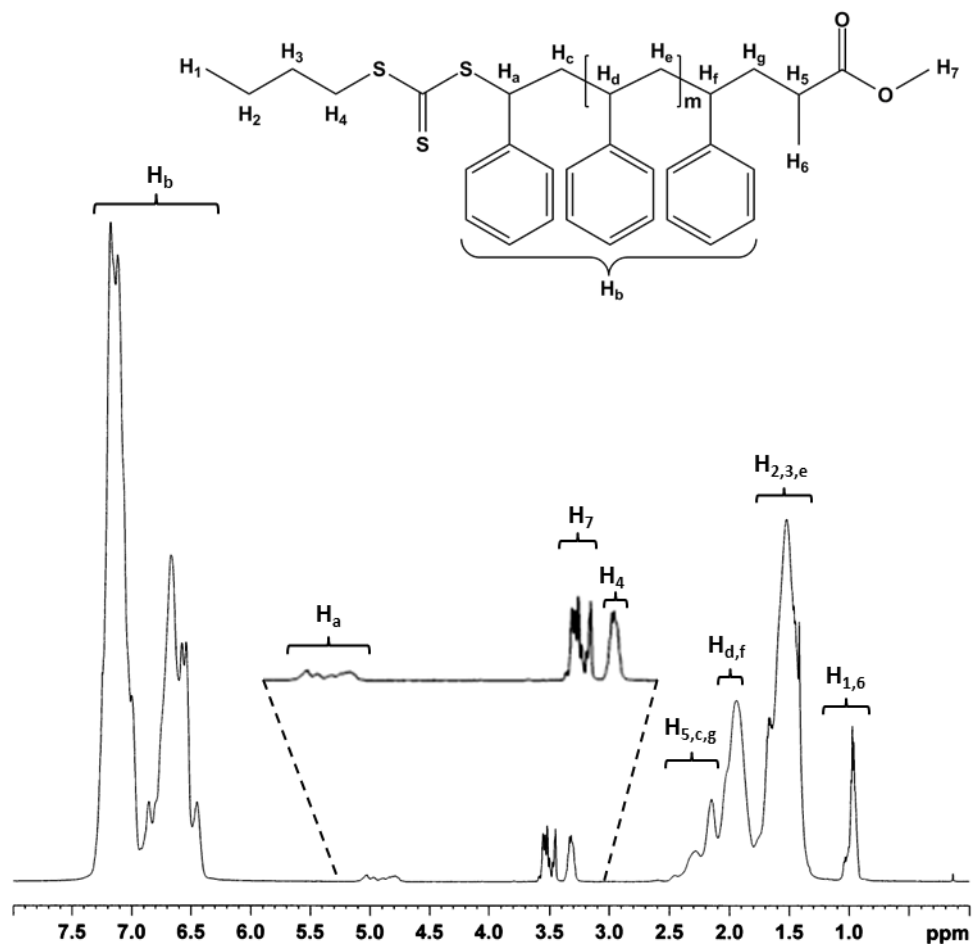


**Figure 3.3.** A typical <sup>1</sup>H NMR spectrum of a living linear PS arm prepared via RAFT. Numbers and letters refer to the end groups and backbone protons, respectively.

A typical <sup>13</sup>C NMR spectrum of the linear PS arm (PS-R2) is shown in Figure 3.4. As can be seen in the figure, the characteristic C=S peak observed at 222 ppm (C<sub>5</sub>) confirms the presence of TTC end group in the linear chain. This is supported by the presence of peak at 53 ppm (C<sub>a</sub>), which was attributed to the methine proton of styrene unit adjacent to S atom. Peaks assigned to the alkyl protons of TTC could also be observed at 13.6 ppm (C<sub>1</sub>), 22.2 ppm (C<sub>2</sub>), 30 ppm (C<sub>3</sub>) and 36.6 ppm (C<sub>4</sub>). The peaks at 177 ppm (C<sub>8</sub>) and 51.5 ppm (C<sub>9</sub>), which were assigned to the carbonyl carbon and methoxy carbon respectively, confirm the presence of ester group at the other end. This is supported by the presence of peaks between 16.3 – 18.2 ppm (C<sub>7</sub>), which was

attributed to the methyl carbon of the ester adjacent to the styrene unit. The peaks observed between 125 – 146 ppm ( $C_{c-e}$ ) and 41 and 44 ppm ( $C_{f-j}$ ) were attributed to the aromatic and aliphatic carbons of the PS backbone, respectively.

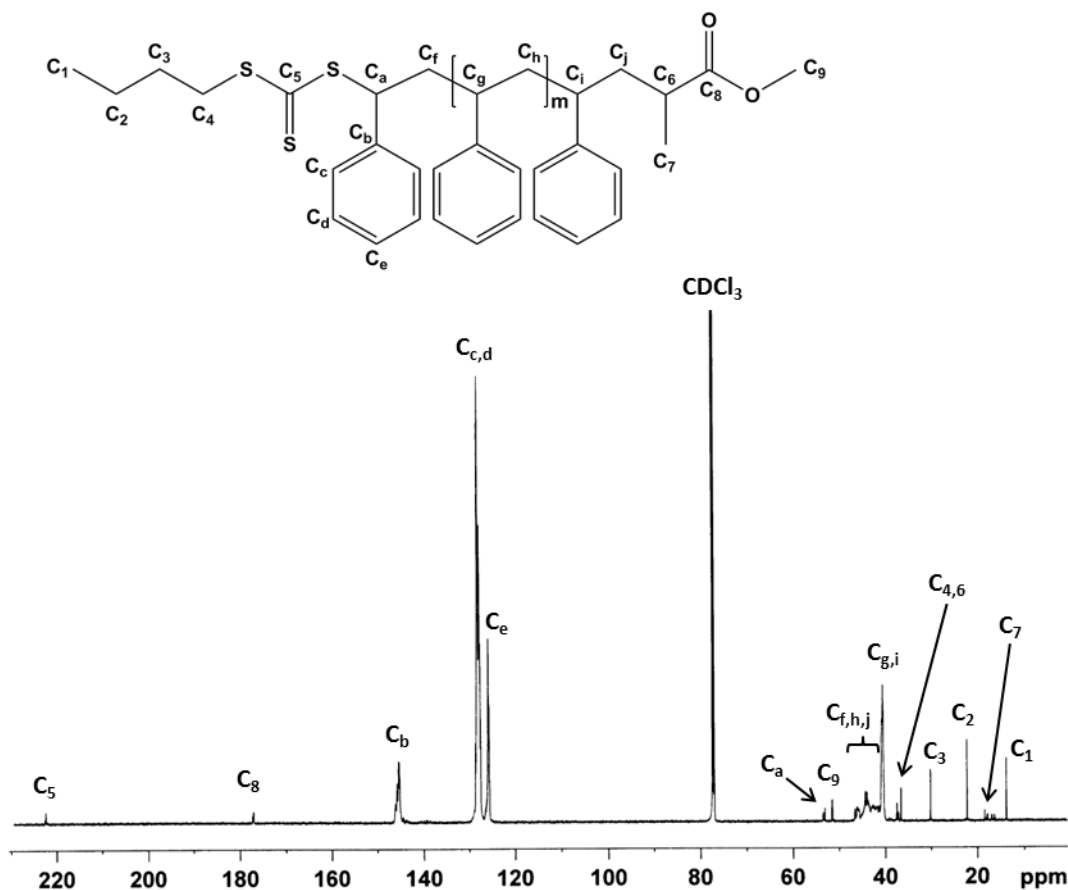


**Figure 3.4.**  $^{13}\text{C}$  NMR spectrum of a linear PS arm prepared via RAFT.

GPC with a photodiode array UV detector was also used for the analysis of the trithiocarbonate end group. Figure 3.5(A) and (B) shows the UV-GPC traces of the synthesised linear PS with trithiocarbonate end group (PS-R1, Table 3.1) and a commercial PS, respectively, at 254 nm compared to those at 312 nm. The absorption at 312 nm is due to the  $\pi \rightarrow \pi^*$  transition of the butyl trithiocarbonate end group ( $-\text{S}-\text{C}(=\text{S})-\text{S}$ )<sup>211</sup> in the polymerization chains since PS obtained from conventional thermal polymerization does not show any significant UV absorption above 260 nm.<sup>190, 212</sup> This result further confirmed the successful incorporation of the trithiocarbonate moiety at the end of the linear chain.

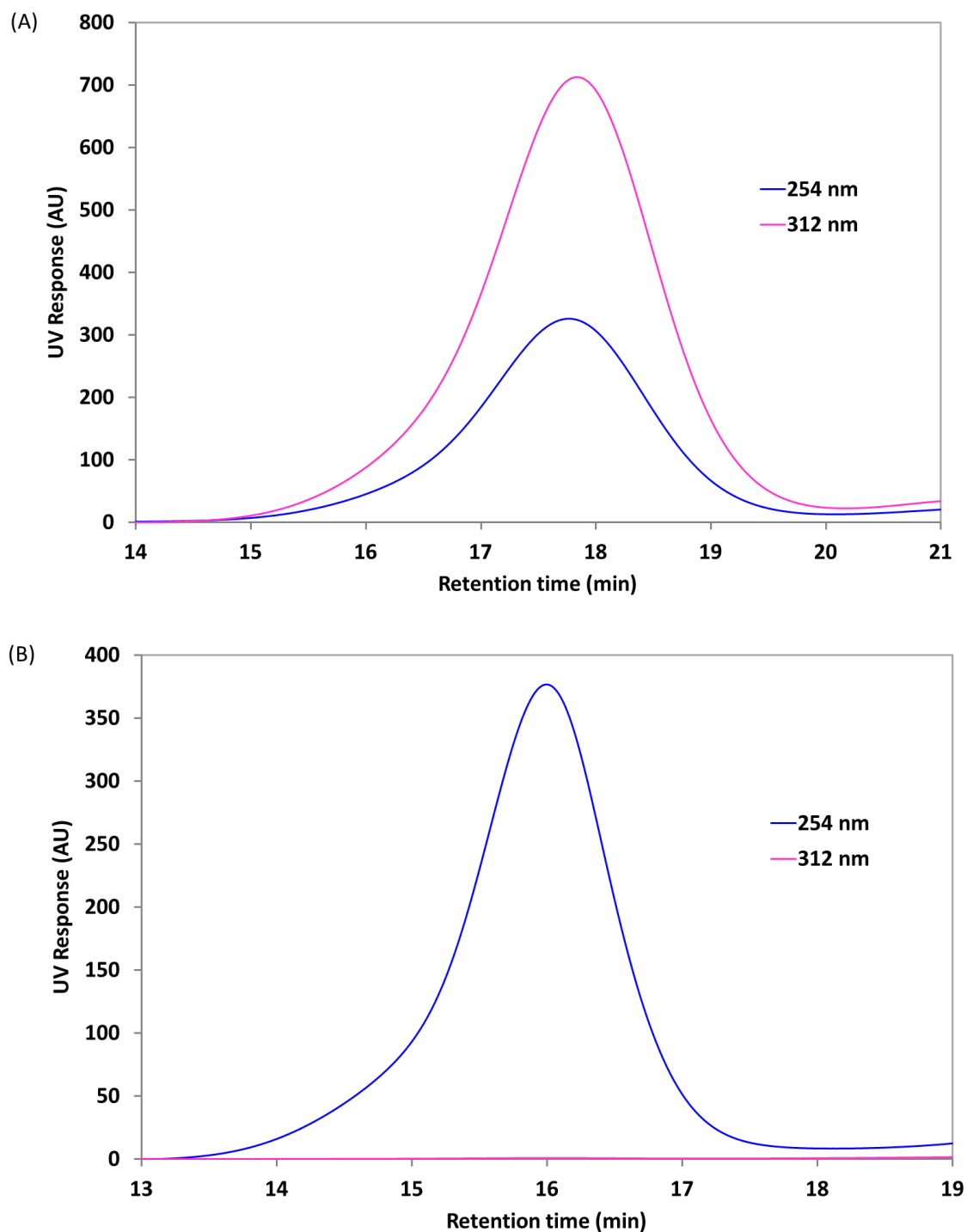


**Figure 3.5.** UV-GPC traces at 254 and 312 nm of (A) a linear PS synthesised via MCEBTTC RAFT agent and (B) a commercial PS.

#### 3.4.1.4 Effect of Solvent

To study the influence of solvent on the polymerisation of styrene monomer in the presence of MCEBTTC, the polymerisation reaction was carried out for 24 h in bulk,

THF as well as DMSO. The styrene to MCEBTTC ratio was fixed at 300:1 (except for PS-R1 and PS-R4) and the ratio of MCEBTTC to AIBN was fixed at 1:0.10. The resulting polymers were characterised by GPC and the results are tabulated in Table 3.1.

As can be seen in Table 3.1, polymerisation of styrene using MCEBTTC in bulk, THF and DMSO resulted in PS arms having different MW. Polymerisation of St in bulk resulted in PS arms (PS-R1 and PS-R2) having  $M_n$  values higher than the calculated theoretical values (about 35% and 20% higher respectively). Comparing between PS-R1 and PS-R2, when the St to MCEBTTC ratio was tripled, the  $M_n$  value increased by about 2-fold whilst the percent monomer conversion seemed to be decreased, which is consistent with the reported result for the RAFT polymerisation of p-acetoxystyrene in bulk.<sup>213</sup> The decrease in the monomer conversion was attributed to the decrease in the polymerisation rate due to the decrease in the number of propagating chains at higher St to MCEBTTC ratio.

From Table 3.1, it can also be observed that the  $M_n$  values of the PS arms prepared in bulk and DMSO (PS-R2 and PS-R3, respectively) were similar and quite close to the theoretical values, which was quite surprising as one would expect slower kinetics for a diluted system. The reason could be attributed to the better solubility of the MCEBTTC RAFT agent in DMSO. A study on the effect of solvents which include DMSO on the homopolymerisation of styrene showed minimal effect on  $K_p$  and no evidence of reduction in  $K_p$  was observed.<sup>214</sup> On the contrary, the  $M_n$  value of PS arm prepared in THF (PS-R4) was much higher (about 2-fold higher) than the theoretical predicted  $M_n$  value, suggesting poor control of polymerisation in THF.

**Table 3.1.** Influence of solvent on the molecular weight and conversion of PS arm prepared via RAFT.<sup>a</sup>

PS arm	Solvent	Temp. (°C)	[Styrene] mM	[St]:[RAFT]	Conversion <sup>b</sup> (%)	$M_{n,theory}^c$ (kDa)	$M_n^d$ (kDa)	$M_w^d$ (kDa)	$M_p^d$ (kDa)	PDI <sup>e</sup>
PS-R1	Bulk	80	8.7	100:1	39	4.32	5.8	7.4	5.5	1.26
PS-R2	Bulk	80	8.7	300:1	29	9.23	11.3	15.1	11.0	1.33
PS-R3	DMSO	80	5.2	300:1	35	11.3	10.8	15.6	12.6	1.44
PS-R4	THF	60	5.2	290:1	10	3.24	7.1	9.2	6.9	1.30

<sup>a</sup> Polymerisation conditions: [RAFT]:[AIBN] = 1:0.10; reaction time: 24 h.

<sup>e</sup> Monomer conversion (%) was calculated based on the gravimetric method.

<sup>f</sup> Theoretical  $M_n$  was calculated according to the following equation:  $M_n = ([St]_0/[RAFT]_0 \times \text{conversion} \times 104) + 252$ .

<sup>g</sup> Number average molecular weight ( $M_n$ ), weight average molecular weight ( $M_w$ ) and peak molecular weight ( $M_p$ ) obtained by GPC.

<sup>h</sup> Polydispersity index (PDI) =  $M_w/M_n$ .

As can be seen in Table 3.1, all the PS arms exhibited narrow polydispersity values (PDI < 1.5), although the values were quite higher than the very narrow polydispersities reported on RAFT polymerisation (typically PDI < 1.2).<sup>96, 202</sup> It can also be seen that the monomer conversion for the polymerisation of styrene in THF (PS-R4) was much lower (about 65 % lower) than that of bulk (PS-R2). This result is consistent with the results of polymerisation of styrene under UV-Vis irradiation at 30 °C, which was attributed to the high chain transfer effect in THF.<sup>215</sup> In our study, the lower monomer conversion obtained in THF compared to that of bulk could also be attributed to the decrease in the polymerisation rate when lower temperature was employed in the former (60 and 80 °C respectively). Polymerisation rate was found to increase with increasing polymerisation temperature, which was attributed to the faster decomposition of AIBN at higher temperature.<sup>216</sup> The reported propagation rate coefficient of styrene at 60 °C was 341 L mol<sup>-1</sup> s<sup>-1</sup>,<sup>102</sup> which means that its polymerisation takes place at a very slow rate at this temperature due to the stability of its propagating radical by resonance. The monomer conversion of the PS arm prepared in DMSO (PS-R3) was higher than that prepared in bulk (PS-R2) at the same St to MCEBTTC ratio, albeit exhibiting the higher PDI value. In addition, the experimental  $M_n$  value of the former closely matched the theoretical value (about 4% difference in  $M_n$  value), which indicates that a better control of polymerisation was achieved in DMSO, hence further preparation of PS arms was carried out in DMSO at 80 °C.

#### 3.4.1.5 Effect of Monomer to RAFT Agent Ratio

As mentioned in §3.1 and already discussed in §1.3.3, initiation process in a RAFT mechanism occurs via the decomposition of the free radical initiator (e.g. AIBN) resulting in the formation of propagating chains, followed by addition of the propagating radicals to the RAFT agent. Since polymers that do not contain the trithiocarbonate end group originate from initiator derived chains, a high MCEBTTC to AIBN ratio was used to study the effect of monomer to RAFT agent molar ratio on the control of MW of the resulting linear PS. This was done by varying the ratio of St to MCEBTTC while keeping the MCEBTTC to AIBN molar ratio constant (i.e. 1 mol % AIBN with respect to MCEBTTC). Following the polymerization procedure in §3.2.3.1, four

different St to MCEBTTC mol ratios ( $[St]:[MCEBTTC]$  or  $r = 200:1, 300:1, 400:1$  and  $500:1$  respectively) were prepared in DMSO and the polymerisation was conducted for 24 hours. The resulting polymers were characterised by GPC and the results are tabulated in Table 3.2.

Fig. 3.6 shows the GPC curves of the PS arms prepared by varying the styrene to MCEBTTC ratios. From the figure, it can be seen that the elution peaks shifted to high-molecular weight (low retention time) with increasing ratio of St to MCEBTTC.

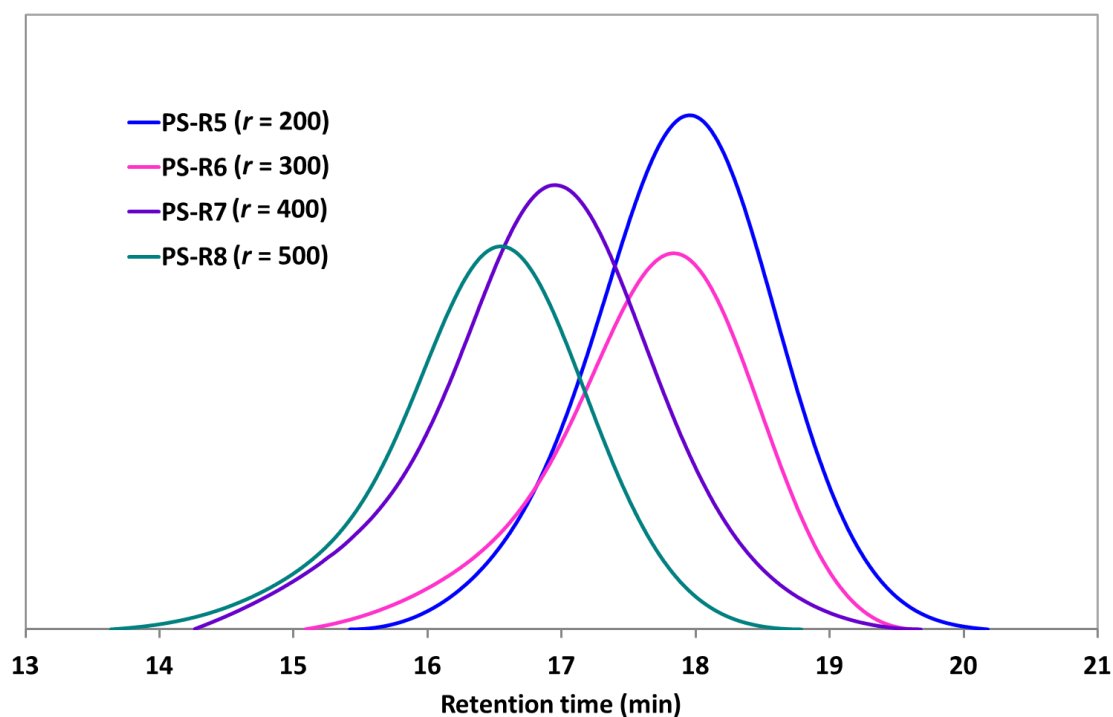


**Figure 3.6.** GPC traces of PS arms synthesised at various ratios of St to MCEBTTC.

**Table 3.2.** Relationship between [St]:[RAFT] ratio and molecular weight of PS arm at [RAFT]:[AIBN] = 1:0.01.<sup>a</sup>

PS arm	[St]:[RAFT]	Conversion <sup>b</sup> (%)	$M_{n,theory}^c$ (kDa)	$M_n^d$ (kDa)	$M_w^d$ (kDa)	$M_p^d$ (kDa)	PDI <sup>e</sup>
PS-R5	200:1	16	3.59	2.8	3.6	3.1	1.25
PS-R6	300:1	15	4.95	3.3	4.2	3.4	1.26
PS-R7	400:1	13	5.41	5.4	7.4	5.9	1.37
PS-R8	500:1	12	6.78	7.4	9.7	7.6	1.32

<sup>a</sup> Polymerisation conditions: 80 °C in DMSO; polymerisation time = 24 h; [St] = 4.6 M; [RAFT]:[AIBN] = 1:0.01.

<sup>b</sup> Monomer conversion (%) was calculated based on the gravimetric method.

<sup>c</sup> Theoretical  $M_n$  was calculated according to the following equation:  $M_n = ([St]_0/[RAFT]_0 \times \text{conversion} \times 104) + 252$ .

<sup>d</sup> Number average molecular weight ( $M_n$ ), weight average molecular weight ( $M_w$ ) and peak molecular weight ( $M_p$ ) obtained by GPC.

<sup>e</sup> Polydispersity index (PDI) =  $M_w/M_n$ .

To further illustrate the effect of styrene to MCEBTTTC molar ratio on the polymerisation reaction, a plot of  $M_n$  versus [St]:[MCEBTTTC] used in the polymerisation was then drawn and compared with the molecular weight distribution (PDI) of the PS arms obtained (Figure 3.7). As can be seen from Figure 3.7 and Table 3.2, in general, when the ratio of styrene to MCEBTTTC was increased from 200 to 500, the MW of the PS arms increased whilst the percent conversion of styrene slightly decreases. In another words, using a smaller amount of RAFT agent resulted in a longer chain of PS. Decreasing the concentration of MCEBTTTC (or increasing the [St]:[MCEBTTTC] ratio) resulted in a lower number of liberated radicals from the RAFT agent that can reinitiate the polymerisation, thus producing longer PS chains. The very low conversion of monomer (< 20%) in each case might be caused by the low amount of AIBN initiator used. The  $M_n$  value of PS-R7 closely matched the theoretical value, whereas that of PS-R8 was slightly higher than the theoretical  $M_n$  value. Both the  $M_n$  values of PS-R5 and PS-R6 however, were slightly lower than the theoretical values. Nevertheless, the narrow polydispersity values (PDI < 1.4) of all the polymers confirms that they were synthesised via a controlled mechanism.

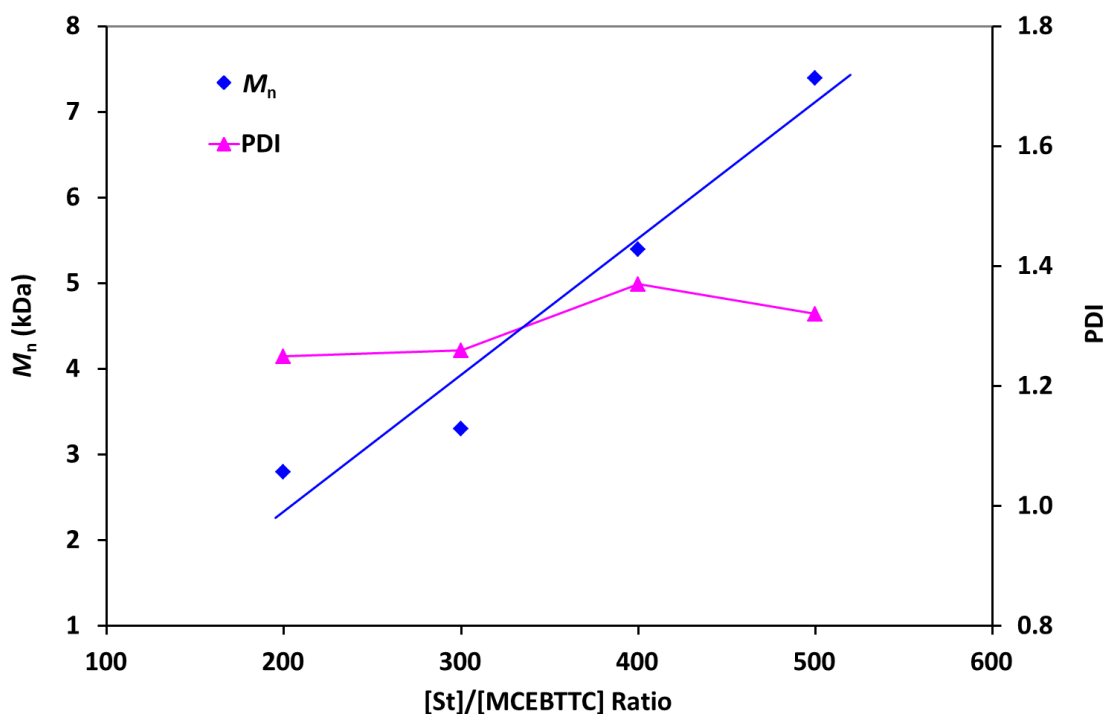


**Figure 3.7.** Effect of [St]:[MCEBTTC] on  $M_n$  and PDI of PS arm.

A second set of experiments was carried out using a lower ratio of MCEBTTC to AIBN to investigate whether this ratio can cause an increase in the monomer conversion, yet still provide a good control over the RAFT polymerisation as has been demonstrated by the previous ratio. Following the procedure in §3.2.3.1, the polymerisation was carried out at various molar ratio of St to MCEBTTC by keeping a constant MCEBTTC to AIBN ratio (this time using 10% of AIBN with respect to MCEBTTC). The MW of the polymers was determined by GPC and the results are tabulated in Table 3.3.

**Table 3.3.** Relationship between [St]:[RAFT] ratio and molecular weight of PS arm.<sup>a</sup>

PS arm	[St]:[RAFT]	Conversion <sup>b</sup> (%)	$M_{n,theory}$ <sup>c</sup> (kDa)	$M_n$ <sup>d</sup> (kDa)	$M_w$ <sup>d</sup> (kDa)	$M_p$ <sup>d</sup> (kDa)	PDI <sup>e</sup>
PS-R9	100:1	29	3.30	4.3	5.4	4.0	1.27
PS-R10	200:1	25	5.50	6.7	8.5	6.5	1.27
PS-R3	300:1	36	11.3	10.8	15.6	12.6	1.44
PS-R11	600:1	32	20.2	20.5	33.5	25.6	1.63

<sup>a</sup> Polymerisation conditions: 80 °C in DMSO; [RAFT]:[AIBN] = 1:0.1; [St] = 5.2 M except for PS-R9, where [St] = 5.8 M.

<sup>b</sup> Monomer conversion (%) was calculated based on the gravimetric method.

<sup>c</sup> Theoretical  $M_n$  was calculated according to the following equation:  $M_n = ([St]_0/[RAFT]_0 \times \text{conversion} \times 104) + 252$ .

<sup>d</sup> Number average molecular weight ( $M_n$ ), weight average molecular weight ( $M_w$ ) and peak molecular weight ( $M_p$ ) obtained by GPC.

<sup>e</sup> Polydispersity index (PDI) =  $M_w/M_n$ .

As shown in Table 3.3, the MW of the PS arm showed a similar trend when the polymerisation was carried out using a lower RAFT agent to initiator ratio ([MCEBTTC]:[AIBN] = 1:0.1) as when higher RAFT agent to initiator ratio ([MCEBTTC]:[AIBN] = 1:0.01) was used (Table 3.2). It was found that the MW of the PS arm increased with increasing St to MCEBTTC ratio. However, higher PDI values were obtained at higher St to MCEBTTC ratio (PDI > 1.4 for PS-R3 and PS-R11). Despite having higher PDI values, the experimental  $M_n$  values of both PS-R3 and PS-R11 were close to the theoretical  $M_n$  values compared to those of PS-R9 and PS-R10 where their experimental  $M_n$  values were higher than the theoretical values, suggesting better control of MW at higher St to MCEBTTC ratios.

Based on the above results, the MW of the PS arm was found to be influenced by the molar ratio of St to MCEBTTC RAFT agent as well as the RAFT agent to AIBN molar ratio. To further investigate the influence of AIBN concentration on the resultant MW of PS another set of experiment was carried out by increasing both the molar ratios of styrene to MCEBTTC as well as the amount of AIBN relative to MCEBTTC by the same increasing ratio and the results are tabulated in Table 3.4. For this purpose, the

polymerisation was conducted at low amount of AIBN initiator with respect to the MCEBTTC RAFT agent (1.5 – 3.5% AIBN with respect to MCEBTTC) and the result are compared with the series in Table 3.2.

**Table 3.4.** Relationship between [St]:[RAFT] ratio and molecular weight of PS arm at increasing concentration of AIBN with ratio.<sup>a</sup>

PS arm	[St]:[RAFT]: [AIBN]	Conversion <sup>b</sup> (%)	$M_{n,theory}$ <sup>c</sup> (kDa)	$M_n$ <sup>d</sup> (kDa)	$M_w$ <sup>d</sup> (kDa)	$M_p$ <sup>d</sup> (kDa)	PDI <sup>e</sup>
PS-R12	200:1:0.015	13	2.99	3.0	3.8	3.2	1.27
PS-R13	350:1:0.027	13	5.03	5.0	6.1	6.6	1.23
PS-R14	450:1:0.035	16	7.98	8.0	10.5	8.4	1.32

<sup>a</sup> Polymerisation conditions: 80 °C in DMSO; [St] = 5.2 M; reaction time = 24 h.

<sup>b</sup> Monomer conversion (%) was calculated based on the gravimetric method.

<sup>c</sup> Theoretical  $M_n$  was calculated according to the following equation:  $M_n = ([St]_0/[RAFT]_0 \times \text{conversion} \times 104) + 252$ .

<sup>d</sup> Number average molecular weight ( $M_n$ ), weight average molecular weight ( $M_w$ ) and peak molecular weight ( $M_p$ ) obtained by GPC.

<sup>e</sup> Polydispersity index (PDI) =  $M_w/M_n$ .

A plot of St to MCEBTTC ratio versus the experimental and theoretical  $M_n$  values for the series of polymers in Table 3.4 was depicted in Figure 3.11 and compared with those of the polymer series in Table 3.2. The polymer series in Table 3.2 was prepared by fixing the ratio of MCEBTTC to AIBN (1% AIBN with respect to MCEBTTC). As for the polymer series in Table 3.4, the amount of MCEBTTC was kept constant whilst both the amount of St and AIBN was increased by the same ratio relative to the amount of MCEBTTC. From Figure 3.8, it can be observed that the  $M_n$  value of the PS arm increases with increasing St to MCEBTTC ratio regardless of whether the amount of AIBN was fixed or increased. However, it is interesting to note that the experimental  $M_n$  values obtained when both the amount of St and AIBN with respect to MCEBTTC were increased by the same ratio closely matched the theoretical calculated values. As for the polymer series in Table 3.2, only when the St to MCEBTTC ratio of 400 was used resulted in PS arm (PS-R7) having experimental  $M_n$  value matched the theoretical value. It can also be seen observed that the  $M_n$  values were higher for the polymer series in Table 3.4, compared to those of Table 3.2, where the former was obtained at

lower MCEBTTC to AIBN molar ratio (> 1% AIBN with respect to MCEBTTC) compared to the latter (1% AIBN with respect to MCEBTTC).

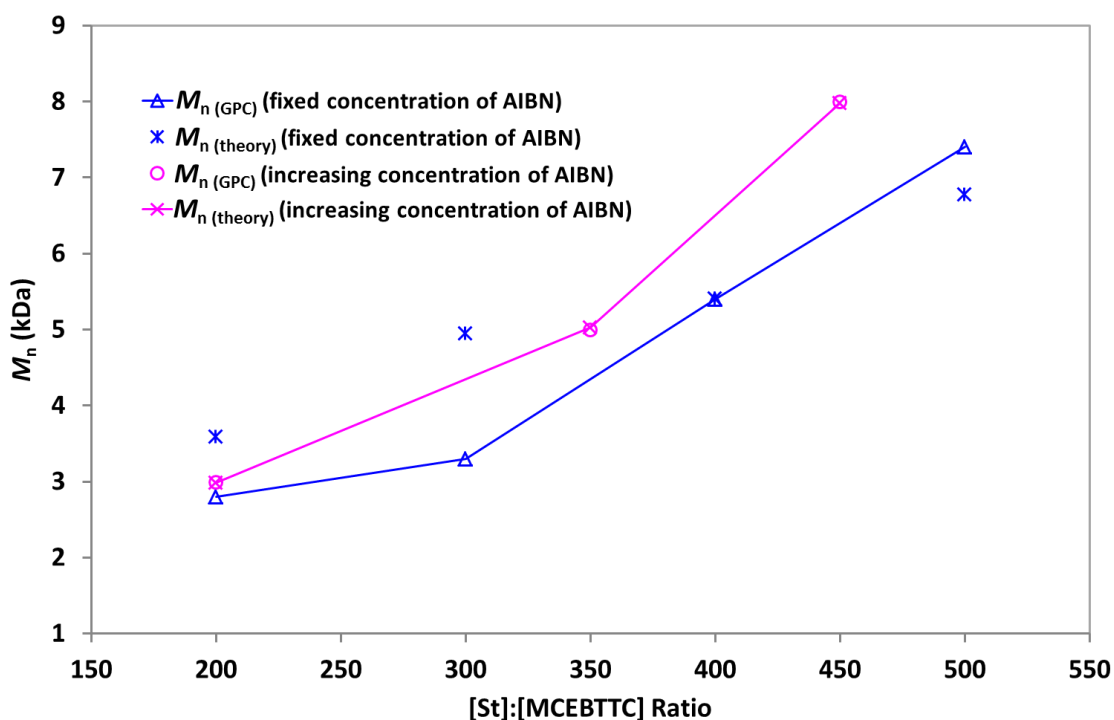


**Figure 3.8.** Comparison between the effect of St to MCEBTTC mole ratio at constant and various MCEBTTC to AIBN ratios on the MW ( $M_n$ ) of PS arm.

From Tables 3.2 and 3.4, it can also be observed that the percent monomer conversion was low ( $\leq 16\%$ ) for both polymer series and showed an opposite trends. As the St to MCEBTTC ratio was increased, the percent monomer conversion seemed to be decreased when the amount of AIBN was fixed. On the other hand, the conversion of monomer tended to slightly increase with increasing ratio of both St and AIBN with respect to MCEBTTC. Both polymer series exhibited narrow polydispersity indices (PDI < 1.4). The results showed that the desired MW of PS arm with low polydispersity could be obtained by careful selection of St to MCEBTTC as well MCEBTTC to AIBN ratios.

#### 3.4.1.6 Arm-first CCS Polymers

The optimal conditions for the preparation of arm-first CCS polymers via RAFT are still not fully understood. Preparation of CCS polymers via the aforementioned method in homogeneous solution usually suffers from a low star yield, low rate of star formation

and relatively high polydispersity of CSS polymers.<sup>107</sup> Among the efforts that have been made to solve these problems are by crosslinking the arm polymers with crosslinkers of low solubility in organic solvents<sup>28</sup> and conducting the RAFT polymerisation in heterogeneous aqueous media such as emulsion or dispersion polymerisation.<sup>111, 201, 217</sup> CCS polymers with low polydispersity have been synthesised in high polymerisation rate and yield by utilising these methods.<sup>28, 218</sup> For the arm-first method, we have decided to prepare the CCS polymers in homogeneous solution. The arm-first CCS polymers were prepared by crosslinking the synthesised linear PS arms with EGDMA following the procedure in §3.2.3.2, as shown in Scheme 3.1. Although the PS arm was prepared in DMSO, the CCS polymer synthesis was carried out in THF at 60 °C. This was due to the insolubility of the isolated linear PS arm in the former. <sup>1</sup>H NMR and FTIR analyses were then carried out to confirm the structure of the CCS polymers obtained.

#### 3.4.1.7 Structural Confirmation of Arm-First CCS Polymers

A typical FTIR spectrum of a CCS polymer (CCS-R4, Table 3.5) obtained via the arm-first RAFT polymerisation is shown in Figure 3.9. The strong peak at 1734 cm<sup>-1</sup> and the broad peak at 1154 cm<sup>-1</sup> in the spectrum of the CCS polymer (Figure 3.12(B)), are assigned to the carbonyl (C=O) and C-O stretching vibrations of the ester group of the EGDMA core, respectively. The increase in the intensity of the carbonyl peak of the CCS polymer compared to that of the PS arm precursor ((Figure 3.9(A)) indicates the successful formation of the CCS polymer. The characteristic peak of the TTC group can be observed at 1068 cm<sup>-1</sup> (C=S).

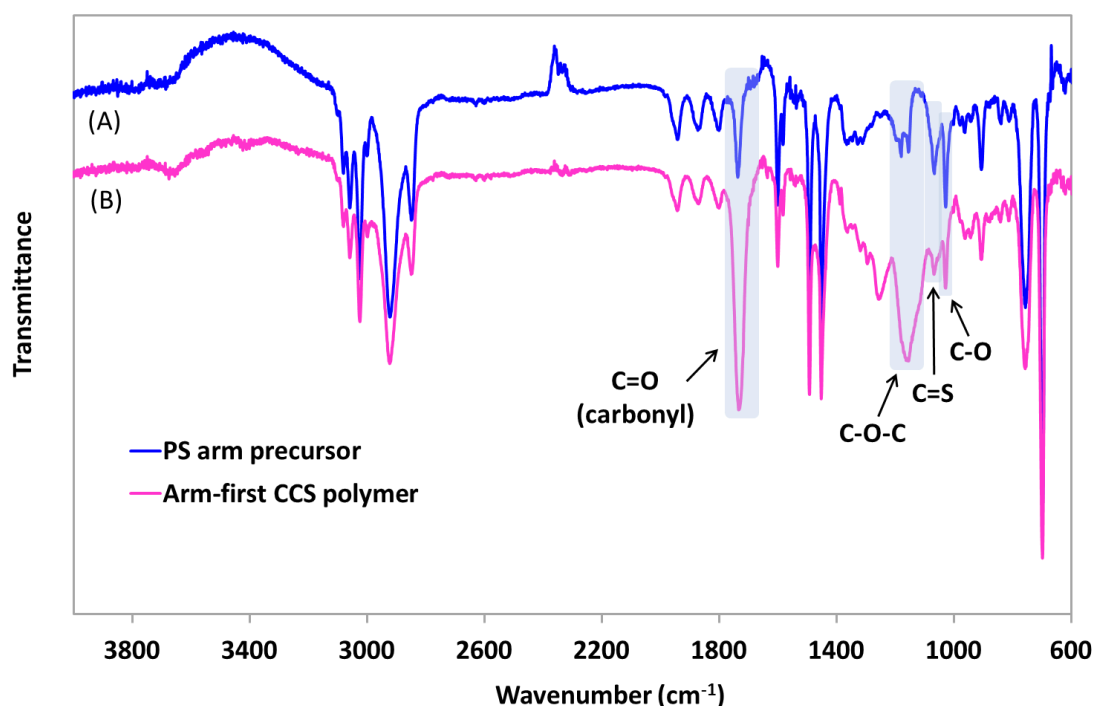


**Figure 3.9.** FTIR spectra of (A) a PS arm precursor and (B) the corresponding arm-first CCS polymer prepared via RAFT.

Figure 3.10 shows a typical  $^1\text{H}$  NMR spectrum of an arm-first CCS polymer (CCS-R6, Table 3.5) prepared via RAFT. As shown in Figure 3.10, the characteristic signals for phenyl protons can be seen between 6.5 – 7.5 ppm ( $\text{H}_c$ ). The peaks assigned to the RAFT moiety could be seen between 0.8 – 1.0, 3.2 – 3.3 and 3.4 – 3.5 ppm ( $\text{H}_3$ ,  $\text{H}_2$  and  $\text{H}_1$  respectively). A new peak is observed between 3.8 – 4.4 ppm ( $\text{H}_f$ ) and was assigned to the protons of EGDMA units. Two more new peaks observed at 5.6 and 6.1 ppm ( $\text{H}_g$ ) were attributed to the pendant double bond of PEGDMA core, suggesting the incomplete crosslinking of the core. A peak between 4.6 – 5.0 ppm (X) was attributed to the methine proton of styrene unit adjacent to the trithiocarbonate, as shown in Figure 3.3 (§3.4.1.2). The presence of this peak in the  $^1\text{H}$  NMR spectrum of arm-first CCS polymer suggested that the CCS polymer was not properly separated from its linear PS arm precursor and thus the NMR sample consisted of a mixture of both.

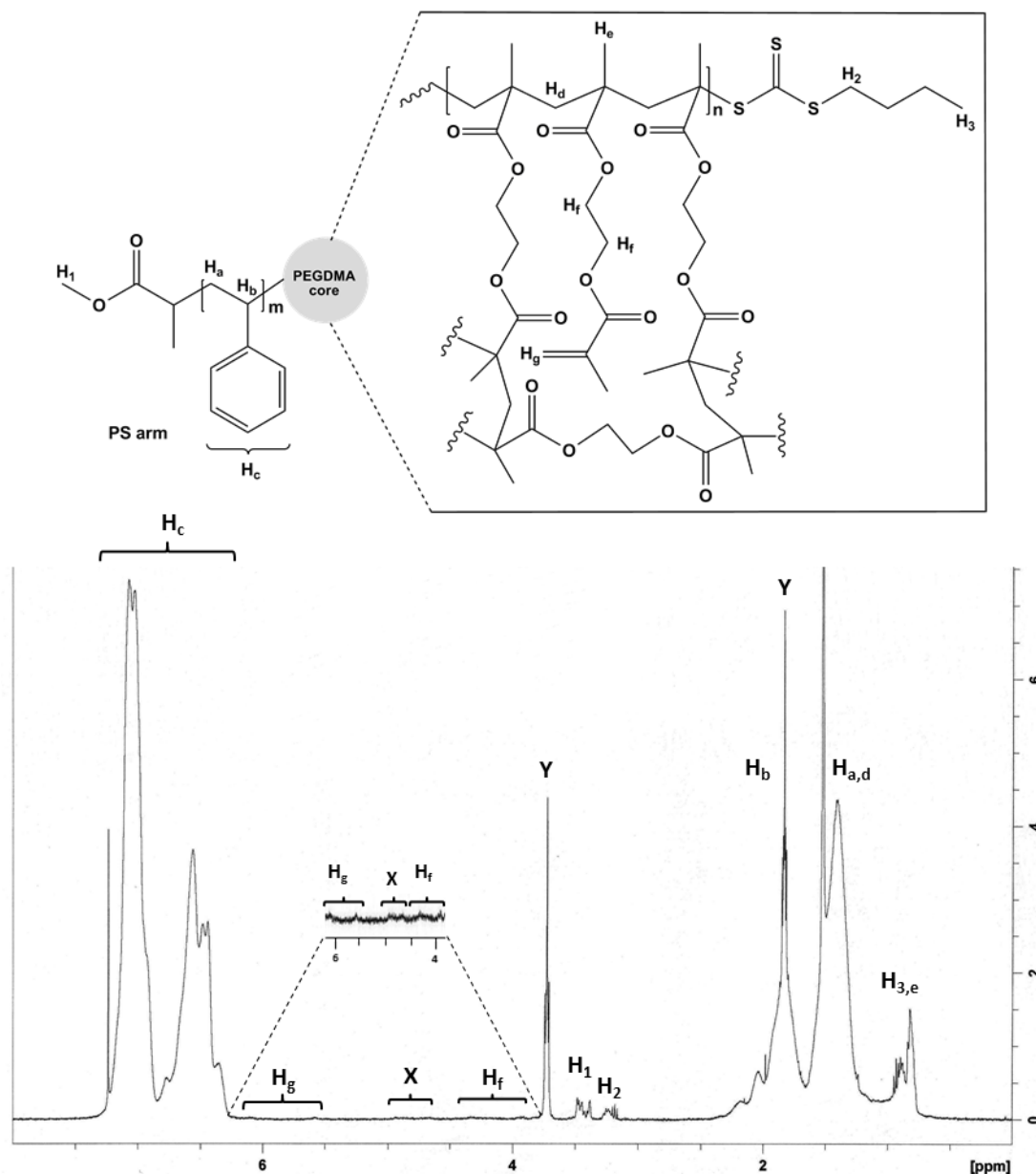


**Figure 3.10.**  $^1\text{H}$  NMR spectrum of a typical arm-first CCS polymer (CCS-R6) prepared via RAFT. (X is attributed to the methine proton peak of styrene adjacent to the trithiocarbonate (Peak  $\text{H}_a$ , Figure 3.3) whereas Y denotes a contaminant peak from THF).

#### 3.4.1.8 Preparation of Arm-First CCS Polymers via RAFT

As previously reported, the amount of crosslinker has a significant effect on the formation of CCS polymers.<sup>28, 201, 219</sup> Thus, it is important to determine the appropriate molar ratio of EGDMA PEGDMA crosslinker to the PS arm. Following the polymerisation procedure in §3.2.4.1, several parameters were varied to prepare the CCS polymers, as shown in the experimental data tabulated in Table 3.5.

**Table 3.5.** Experimental data for preparation of arm-first CCS polymers via RAFT.<sup>a</sup>

Polymer	Reaction time (h)	[PS arm] (mM)			[EGDMA]: [PS arm]	[AIBN] (mM)	Product
		Code <sup>b</sup>	$M_n$ (kDa)	mM			
CCS-R1	3, 6, 12, 24, 48	PS-R1	5.8	5.0	5:1	0	PS arm only
CCS-R2	24	PS-R3	10.8	5.0	5:1	0.01	PS arm only
CCS-R3	16	PS-R9	4.3	18.0	15:1	0.01	Gelation
CCS-R4	4	PS-R10	6.7	10.0	15:1	0.10	Soft gel
CCS-R5	6	PS-R10	6.7	10.0	15:1	0	CCS and PS arm <sup>c</sup>
CCS-R6	6	PS-R13	5.0	13.0	15:1	0	CCS and PS arm <sup>c</sup>

<sup>a</sup> Polymerisation solvent = THF, temperature = 60°C.

<sup>b</sup> Taken from Table 3.1, 3.3 and 3.4.

<sup>c</sup> CCS yield (from GPC) = 2%.

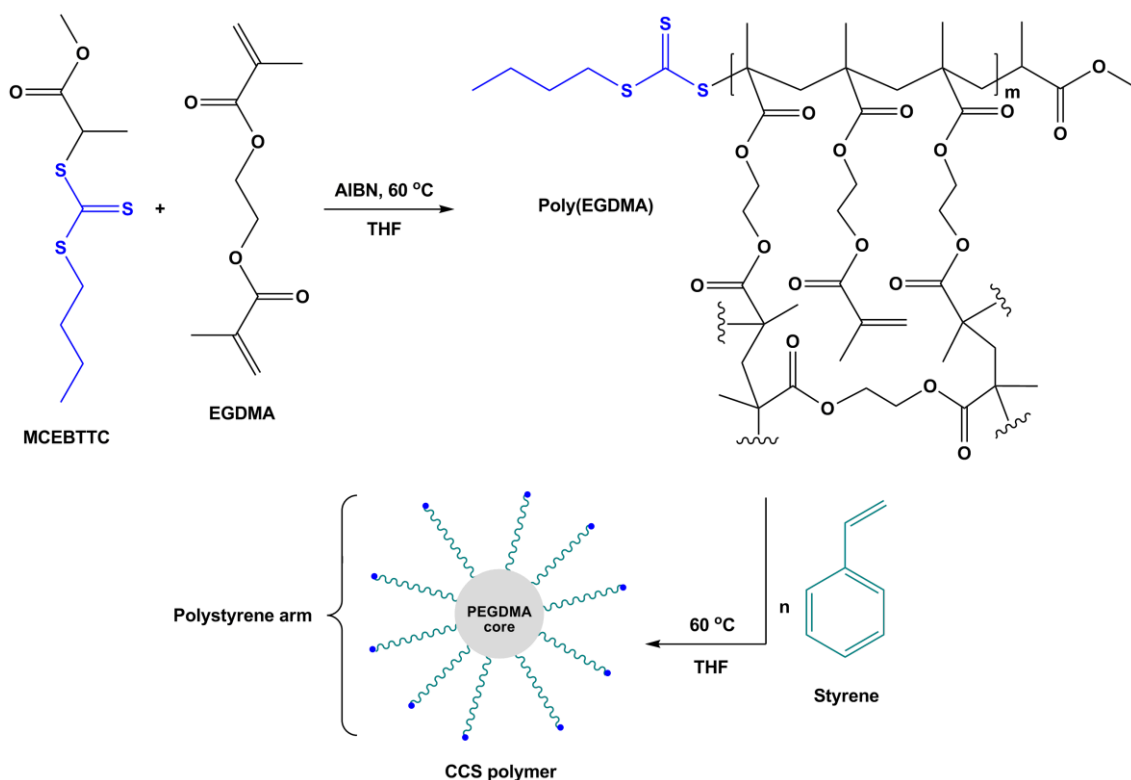
As can be seen in Table 3.5, initial experiment involved conducting the polymerisation of EGDMA using PS arm with  $M_n$  of 5.8 kDa ([PS-R1] = 5.0 mM) at [EGDMA]:[PS arm] of 5:1 for 48 h. GPC analysis results of the aliquots taken at 3, 6, 12, 24 and 48 h intervals showed only one peak at about the same retention time as that of the PS arm precursor. This indicates that no crosslinking reaction occurs between the arm and the crosslinker to form a CCS polymer using this formulation. When the experiment was repeated at the same concentration, but using a higher MW of PS (PS-R3,  $M_n$  = 10.8 kDa in the presence of AIBN ([PS arm]:[AIBN] = 1:0.1), similar result was observed after 24 hr, where no evidence of higher MW peak could be seen in the GPC curve of the product. Another formulation was then prepared at higher concentration (18 mM) of PS arm (PS-R9) and higher ratio of EGDMA to PS arm ([EGDMA]:[PS arm] = 15:1 in the presence of a small amount of AIBN ([PS arm]:[AIBN] = 1:0.1). After polymerising for about 16 h, gelation occurred (CCS-R3). The experiment was then repeated at the same ratio of EGDMA to PS arm ([EGDMA]:[PS arm] = 15:1) but using lower

concentration of arm in the presence ( $[\text{PS arm}]:[\text{AIBN}] = 1:0.2$ ) and absence of AIBN, respectively. After about 4 h of polymerisation, soft gel was formed in the former (CCS-R4) whereas the latter resulted in a viscous mixture (CCS-R5) after 6 h. The yield of CCS-R5 determined by GPC was approximately 2%. Similar result was obtained when the experiment was repeated in the absence of AIBN using a higher concentration of PS arm (PSR10,  $[\text{PS arm}] = 13 \text{ mM}$ ). The polymer (CCS-R6) contained a mixture of CCS polymers (2%) and the residual unreacted PS arm, as evidenced in the FTIR and NMR spectra of the polymer (Figure 3.19 and 3.10, respectively).

The above results showed that CCS polymers could be prepared via the arm-first method using MCEBTTC as the RAFT agent. It was found that greater ratio of EGDMA to PS arm as well as higher PS arm concentration were necessary for a successful preparation of CCS polymer. However, conducting the polymerisation at high concentration of PS arm for a long time should be avoided as it resulted in macroscopic gelation (CCS-R3). Comparing between CCS-R5 and CCS-R6, the polymerisation rate was faster in the presence of AIBN.

#### **3.4.2 Core-first CCS Polymers via RAFT**

The core-first CCS polymer was prepared by employing a two-pot approach, where the PEGDMA core with trithiocarbonate functionality on the surface was firstly synthesised and isolated, before being subjected to further photopolymerisation in the presence of styrene to form the CCS polymer by growing PS arms from the active core surface as shown in Scheme 3.2.



**Scheme 3.2.** Synthetic route of CCS polymers via the core-first RAFT polymerisation.

#### 3.4.2.1 Preparation of PEGDMA Core Precursor

The PEGDMA core was synthesised following the procedure described in §3.2.3.1 using THF as the polymerisation solvent. In the first attempt, the core was prepared by conducting polymerisation of EGDMA at [EGDMA]:[RAFT]:[AIBN] ratio of 100:1:0.1 in THF (5 vol %) for 6 h at 60 °C, which resulted in gelation (PE-R1). The next polymerisation was carried out using a lower molar ratio of EGDMA to RAFT, i.e. 25:1 while maintaining the same ratio of RAFT to AIBN (1:0.1) in THF (6 vol %) for 3 h, which resulted in viscous reaction mixture (PE-R2). Another experiment was then conducted by reducing the [EGDMA]:[RAFT] to 5:1 yet maintaining the same ratio of RAFT to AIBN (1:0.1) in THF (4 vol %). Similar to PE-R2, a viscous reaction mixture was formed after 3 h. The reaction mixture was then stirred in methanol to precipitate out the polymer (PE-R3). Since the PEGDMA core was not dispersible in any NMR solvent, FTIR was used to confirm the structure of the core and a typical FTIR spectrum of a PEGDMA core (PE-R3) is shown in Figure 3.11.

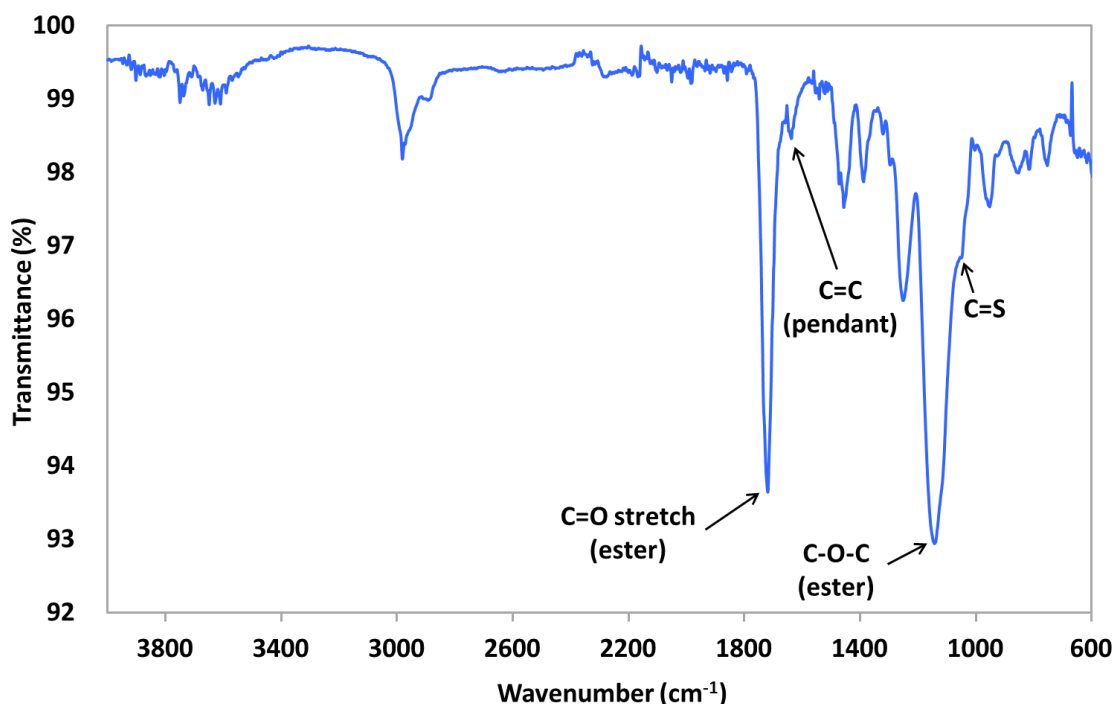


**Figure 3.11.** FTIR spectrum of a PEGDMA core synthesised using MCEBTTC RAFT agent.

As shown in Figure 3.11, the strong peak at  $1719\text{ cm}^{-1}$  and the broad peak at  $1143\text{ cm}^{-1}$  are assigned to the carbonyl (C=O) and ester (C-O-C) stretching vibration of EGDMA respectively. The weak peak at  $1638\text{ cm}^{-1}$  is attributed to the pendant unreacted C=C double bond in the microsphere, which indicates the incomplete conversion of pendant double bonds in EGDMA. The characteristic peak of the TTC end group can be observed at  $1049\text{ cm}^{-1}$  (C=S). The result showed that the MCEBTTC RAFT agent was successfully incorporated into the resulting PEGDMA microsphere.

#### 3.4.2.2 Core-First CCS Polymers

The core-first CCS polymer was prepared using the synthesised PEGDMA core in THF following the procedure in §3.2.3.2. The core-first CCS polymer was prepared using the PEGDMA core (PE-R3) synthesised beforehand following the procedure in §3.2.5.2. This was done by preparing a mixture of PEGDMA core (50 mg) and styrene (8.7 mmol) in THF (styrene:THF = 1:3 v/v) followed by polymerisation for about 24 h at  $60\text{ }^{\circ}\text{C}$ . Unlike its core precursor, the CCS polymer was dispersible in the NMR solvent, thus was subjected to NMR and FTIR analyses for structural confirmation. The difference in

dispersibility of the CCS polymer compared to its core precursor was attributed to the presence of PS arms around the central core of the former, which were not present in the latter.

A typical FTIR spectrum of the CCS polymer (CCS-R7) is shown in Figure 3.12(B) and compared with its core precursor Figure 3.12(A). In the spectrum of CCS polymer (Figure 3.12(B)), the strong peaks at 1602, 1493 and 1452  $\text{cm}^{-1}$  are assigned to the C-C stretching of the aromatic rings, whilst the peaks at 756 and 697  $\text{cm}^{-1}$  are characteristic of the aromatic C-H out-of-plane bending modes of the polystyrene arms. These peaks were not present in the spectrum of the core precursor (Figure 3.12(A)), thus confirming the successful growth of PS arm around the core. The carbonyl C=O stretching vibration of EGDMA in the core can be seen at 1735  $\text{cm}^{-1}$ . The weaker intensity is possibly due to the fact that it is surrounded by the very long PS arms, which reduces its intensity. The characteristic peak of the trithiocarboante group can be observed at 1071  $\text{cm}^{-1}$  (-C=S).

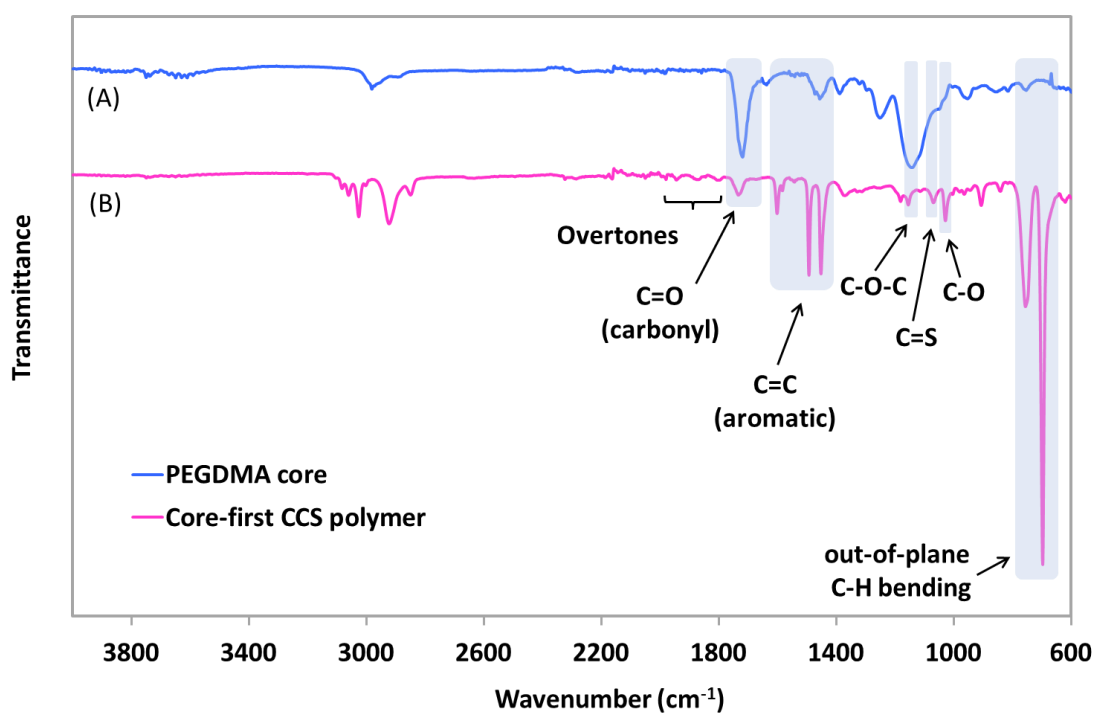


**Figure 3.12.** FTIR spectra of (A) a core-first CCS polymer via RAFT and (B) the corresponding PEGDMA core precursor

Figure 3.13 shows a typical  $^1\text{H}$  NMR spectrum of a core-first CCS polymer (CCS-R7) prepared via RAFT. As shown in Figure 3.13, the peaks observed between 4.2 - 4.5 ppm ( $\text{H}_c$ ) were assigned to the protons of EGDMA units. The low intensity of these peaks suggested the presence of either high crosslinking density of core or long PS arm chain length. In addition, the peak at about 1.0 ppm attributed to the methyl backbone proton of EGDMA ( $\text{H}_b$ ) could not be clearly seen, which supports the aforementioned hypothesis. The two peaks observed at 5.5 and 6.2 ppm ( $\text{H}_d$ ) were attributed to the pendant double bond of the PEGDMA core, suggesting the incomplete crosslinking of the core. Characteristic signals for phenyl protons can be seen between 6.3 – 7.6 ppm ( $\text{H}_g$ ), confirming the presence of PS arms connected to the PEGDMA core. The presence of peaks between 4.9 – 5.2 ppm (X), attributed to the methine proton of styrene unit adjacent to the trithiocarbonate (Figure 3.3, §3.4.1.2), strongly supports the successful incorporation of PS arm around the core precursor.

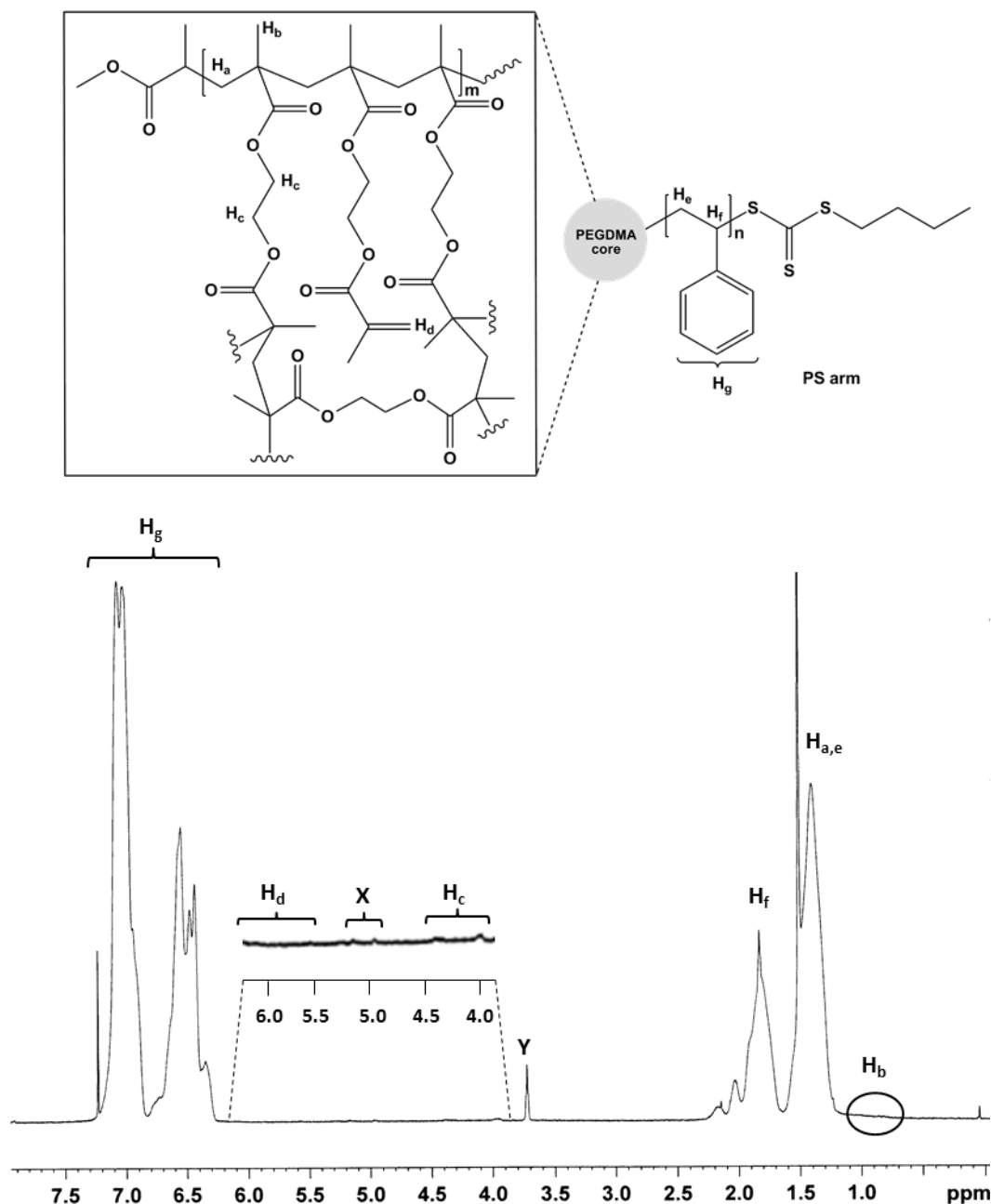


**Figure 3.13.**  $^1\text{H}$  NMR spectrum of a typical core-first CCS polymer prepared via RAFT. (Y denotes a contaminant peak from THF).

Apart from FTIR and NMR, the CCS polymer (CCS-R7) was also subjected to GPC and DLS analyses to determine the MW and hydrodynamic size of the CCS polymer. The GPC and DLS intensity distribution curves are shown in Figure 3.14 and 3.15, respectively. From Figure 3.14, it can be seen that only one peak was observed, which was attributed to the CCS polymer, having  $M_n$  value of 61.9 kDa with quite a broad polydispersity (PDI = 4.5). On the other hand, the intensity particle size distribution of

the CCS polymer obtained from DLS (Figure 3.15) showed a bimodal distribution. As can be seen in the figure, the DLS result showed that the CCS polymer exhibited average hydrodynamic diameters of  $26 \pm 1$  nm and  $184 \pm 18$  nm, suggesting that the CCS polymer was polydispersed.

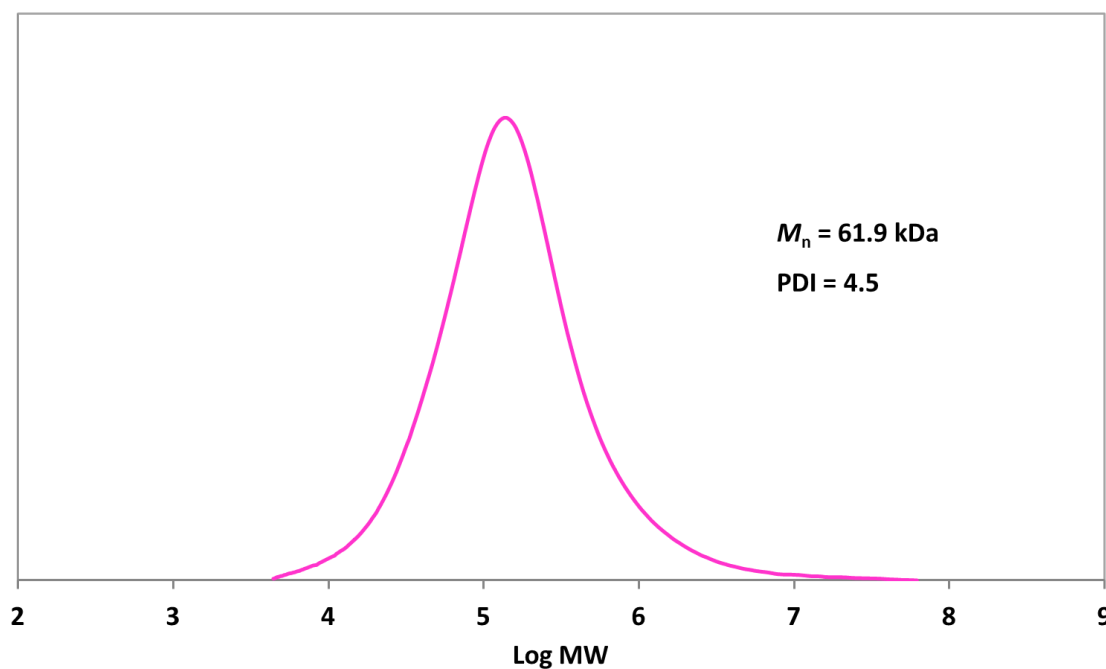


**Figure 3.14.** GPC curve of a core-first CCS polymer prepared via RAFT.

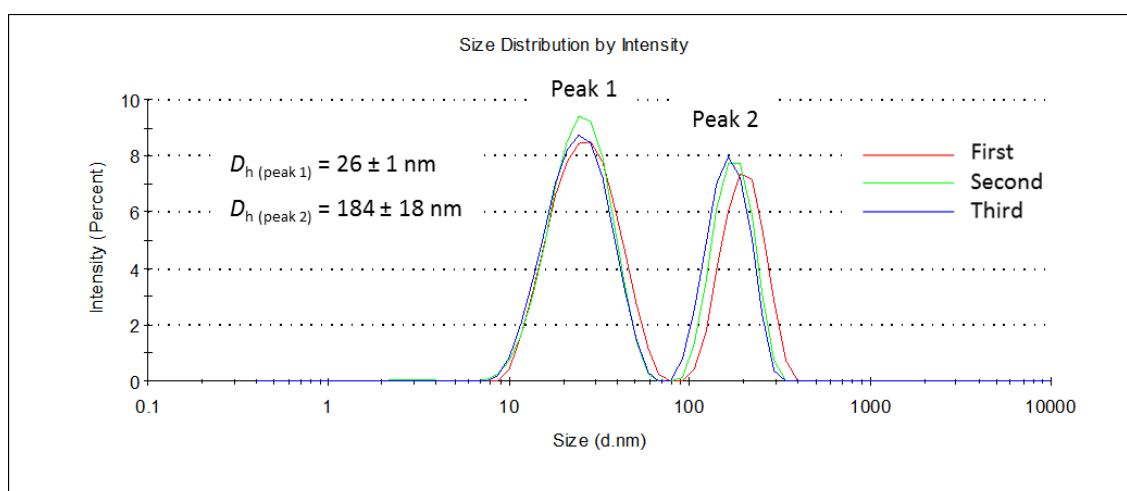


**Figure 3.15.** DLS intensity particle size distribution of a core-first CCS polymer prepared via RAFT.

The above results showed that the CCS polymers were successfully formed via the core-first RAFT polymerisation method. Since no AIBN was added in the polymerisation mixture, thus the PS should have grown from the trithiocarbonate functionality on the surface of the core precursor. Although require further optimisation, it was much easier to prepare the CCS polymer via the core-first method using the MCEBTTC RAFT agent.

### 3.4.3 Comparison between RAFT and Iniferter Polymerisation

A comparison between selected PS arms obtained via iniferter and RAFT, respectively, is displayed in Table 3.6. After 24 hr of polymerisation, the highest monomer conversion for the polymerisation of styrene using iniferter was 47%. This was achieved when St to BDDC molar ratio of 155 was used, producing PS arm with  $M_n$  value of 33.2 kDa. On the other hand, RAFT polymerisation of styrene achieved its highest monomer conversion (i.e. 36%) at St to RAFT agent molar ratio of 300 in the presence of 10% AIBN with respect to RAFT. This value was about 25% lower than that of the iniferter polymerisation, and the resultant PS arm exhibited  $M_n$  value of 10.8 kDa (about 3-fold lower than that of the iniferter. It can also be observed that the highest MW PS arm ( $M_n = 37.2$  kDa) was produced when St to BDDC mole ratio of 390 was used during the polymerisation of styrene via iniferter. As for RAFT polymerisation, the highest MW PS arm was formed at St to RAFT agent molar ratio of 600, resulted in PS arm having  $M_n$  value of 20.5 kDa. This value was about 2-fold smaller than that of the iniferter. Both the percent monomer conversion and MW of the PS arm of polymers prepared via iniferter were higher than those prepared via RAFT. The result indicates that RAFT polymerisation of styrene occurred at a much lower rate than the iniferter polymerisation. On the other hand, the PS arms prepared via RAFT exhibited much narrower MW distribution ( $PDI < 2$ ) compared to those of iniferter.

**Table 3.6.** Comparison between RAFT and Iniferter Polymerisation of Styrene.

PS arm	[St]:[BDDC] or [RAFT]	Conversion <sup>b</sup> (%)	$M_n^c$ (kDa)	$M_w^c$ (kDa)	$M_p^c$ (kDa)	PDI <sup>d</sup>
PS-I7	155:1	47	33.2	251	63.5	7.58
PS-I8	390:1	39	37.3	268	76.9	7.20
PS-R3	300:1	36	10.8	15.6	12.6	1.44
PS-R9	600:1	32	20.5	33.5	25.6	1.63

<sup>a</sup> Polymerisation conditions: reaction time = 24 h; iniferter: bulk at room temperature; RAFT: 80 °C in DMSO; [RAFT]:[AIBN] = 1:0.1).

<sup>b</sup> Monomer conversion (%) was calculated based on the gravimetric method.

<sup>c</sup> Number average molecular weight ( $M_n$ ), weight average molecular weight ( $M_w$ ) and peak molecular weight ( $M_p$ ) obtained by GPC.

<sup>d</sup> Polydispersity index (PDI) =  $M_w/M_n$ .

Comparing the results of arm-first CCS polymerisation via RAFT to those of iniferter, it can be concluded that the formation of CCS polymer via the latter was more successful compared to the former. Although low polydispersity PS arm could be obtained via RAFT, it was much more difficult to prepare CCS polymer in good yield compared to that of the iniferter. Further optimisation was necessary for its successful preparation.

On the other hand, it was much easier to prepare the core-first CCS polymers via both the iniferter and RAFT compared to that of the arm-first CCS polymers.

### 3.5 Conclusion

The synthesis of CCS polymers was investigated using MCEBTTC as the RAFT agent via the arm-first and the core-first method in two-pot, which afforded CCS polymers with trithiocarbonate end groups confined at the core and the periphery of the CCS polymers, respectively. The preparation of CCS polymers via the arm-first method using BDDC iniferter was more successful compared to using the RAFT agent.

Although a good yield of arm-first CCS polymers could be obtained, we found that this arm-first method has a drawback whereby quite a high proportion of unincorporated arm precursors were present in the final products and requires extra purification steps in order to obtain CCS polymers with high purity. Our attempts to isolate the CCS

polymers from the unincorporated arm precursors were unsuccessful. Apart from that, the core of the CCS polymers could not be directly characterised since non-cleavable arm was used in the preparation of the polymers. The characterisation of the core is very important in MIP applications as it is where the imprinting sites were created during the preparation of CCS MIP. In addition, the arm-first CCS polymers were found to be polydisperse in both size and shape, thus may not yield good selectivity or specificity when applied in imprinting.

These problems could be overcome by preparing CCS polymers via the core-first method. The core could be directly characterised before attaching arms to obtain the CCS polymers. In addition, the resultant CCS polymers were able to be separated from any residual unreacted cores due to the difference in the dispersibility of the two polymers in solvents such as THF. Our results showed that both the iniferter and RAFT methods were successful in synthesising the core-first CCS polymers. Although requiring further optimisation, the core-first method proved to be an easier method to use in the synthesis of CCS polymer compared to the arm-first method and thus was applied in the synthesis of our CCS MIP. Optimisation of the MIP microsphere to be further used as the core precursor and CCS MIP synthesis will be presented in Chapters 4 and 5, respectively.

## Chapter 4

### Reactive MIP Microspheres

#### 4.1 Introduction

The preparation of core crosslinked star (CCS) polymers via the iniferter and RAFT techniques was discussed in the previous chapters (Chapters 2 and 3 respectively). These CCS polymers were prepared primarily by the arm-first method with some preliminary investigation of the core-first method. The iniferter technique proved to be more successful in the preparation of arm-first CCS polymers compared to RAFT. Nevertheless, the arm-first method has its own drawback, whereby the residual unreacted linear arm precursors remain in the product. On the other hand, CCS polymers synthesised via the core-first method were more easily separated (as they are more readily dispersed) from any residual unreacted core precursors. Thus, the core-first method was chosen as the method to prepare core crosslinked star molecular imprinted polymers (CCS MIPs). One of the advantages of the core-first CCS polymer in the field of molecular imprinting is that characterisation of the MIP core is possible, which is not the case for the arm-first CCS polymers, unless, for instance, a degradable arm such as poly( $\epsilon$ -caprolactone) (PCL) is employed.<sup>24, 220, 221</sup> Thus, the focus of this chapter is the preparation and characterisation of MIP microspheres, which will then be used as MIP core precursors in the preparation of CCS-MIPs discussed in the next chapter (Chapter 5).

Molecular imprinted polymers are polymers formed in the presence of the molecule of interest – the target, which is used as a template. After polymerisation, the template is

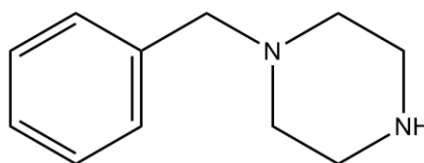
extracted, leaving behind cavities in the polymer complementary to the shape, size or functional groups of the original template. In this way, a molecular memory, capable of selectively rebinding the target molecule is introduced into the polymer. Traditionally, MIPs have been synthesised by bulk polymerisation and are monolithic, and thus require grinding prior to use, which results in irregular shapes and destruction of some binding cavities.<sup>144, 222</sup> The irregularly shaped MIPs are not ideal for most applications such as liquid chromatography,<sup>223</sup> capillary electrochromatography<sup>147</sup> and drug delivery.<sup>224</sup> To avoid the detrimental grinding process, several formats such as monoliths prepared *in situ*,<sup>166, 225</sup> nanofibers,<sup>226, 227</sup> thin-films,<sup>228, 229</sup> microspheres<sup>230, 231</sup> and grafting of an imprinted layer on the surface of pre-formed particles such as silica,<sup>156, 232</sup> have been reported.

MIP microspheres have been prepared using several polymerisation techniques such as precipitation polymerisation,<sup>231, 233, 234</sup> suspension polymerisation,<sup>235</sup> emulsion polymerisation,<sup>235</sup> swelling polymerisation<sup>236</sup> as well as imprinted core-shell nanoparticles.<sup>164</sup> Preparation of MIP microspheres by the precipitation polymerisation method appears very promising not only due to its easy operation, which does not require the use of surfactant or steric stabiliser, but also in yielding spherical particles with a narrow size distribution of excellent reproducibility.<sup>231, 237</sup>

Generally, MIP microspheres have been prepared using traditional free radical polymerisation (FRP). FRP has the inherent drawback of difficulty in controlling the chain propagation and termination, which normally results in heterogeneous polymer networks<sup>87, 238</sup> and more importantly, precludes the creation of other architectures such as CCS polymers. This drawback has been circumvented by using reversible-deactivation radical polymerisation (RDRP) methods such as ATRP, RAFT and iniferter. The use of RDRP techniques in precipitation polymerisation allows the one-pot synthesis of reactive polymer microspheres with surface bound reactive groups,<sup>239, 240</sup> which is highly useful for controlled surface modification by RDRP re-initiation for the synthesis of advanced architecture such as CCS polymers.

The benefit of using RDRP in the creation of imprinted polymer microspheres has already been demonstrated.<sup>157, 161, 165, 241, 242</sup> Zhang and coworkers have reported the combined use of controlled radical and precipitation polymerisation to achieve improved binding and structural characteristics in imprinted polymer particles. Using a precipitation polymerisation method, RDRP techniques such as ATRP,<sup>242</sup> RAFT<sup>165</sup> and iniferter<sup>161</sup> mediated polymerisation were employed to create the MIP microspheres. Using these methods, MIP microspheres with successful molecular imprinting capacity for the 2,4-dichlorophenoxyacetic acid template, fast template binding kinetics and an appreciable selectivity over structurally related compounds were produced.

For this study, benzylpiperazine (BZP, Figure 4.1), a drug that has been abused and used as ‘party pills’ and subsequently banned in a few countries including Australia<sup>243, 244</sup> was chosen as a template. Various techniques have been reported for the identification and quantification of BZP such as LC-MS,<sup>245, 246</sup> LC-MS/MS,<sup>247</sup> GC-MS,<sup>248</sup> capillary electrophoresis,<sup>249</sup> HPLC-fluorescence<sup>250</sup> and chemiluminescence,<sup>251</sup> whilst only less approaches focused on the in-field detection. Due to the increasing reported cases on BZP abuse,<sup>252, 253</sup> it is therefore desirable to have a rapid, accurate and specific in-field tests for BZP. The ease of preparation and low cost of MIPs make them attractive as recognition elements for sensing applications<sup>254, 255</sup> and has the potential for the in-field detection.<sup>256</sup> BZP MIPs were first studied by our group employing traditional bulk polymerisation.<sup>257</sup> The current study builds on this work by employing the combined approach of controlled radical and precipitation polymerisation to prepare the imprinted polymers, rather than bulk polymerisation.



[1]

**Figure 4.1.** Structure of benzylpiperazine.

## 4.2 Experimental

### 4.2.1 Materials

Benzylpiperazine (97%) [1] (BZP, Figure 4.1) was obtained from Fluka, (1R,2S)-(-)-ephedrine [2] (EPH, Figure 4.2) and 1-phenylpiperazine [3] (PHP, Figure 4.2) were obtained from Sigma-Aldrich and used as received. Ethylene glycol dimethacrylate [4] (EGDMA, Figure 4.2) and methacrylic acid [5] (MAA, Figure 4.2) were obtained from Sigma-Aldrich ( $\geq 98\%$  purity) and were passed through a column of activated basic alumina (Aldrich, Brockmann I, standard grade,  $\sim 150$  mesh, 5.8 nm) to remove radical inhibitors. Azobisisobutyronitrile (AIBN) (Dupont) was recrystallized twice from acetone prior to use. Benzyl *N,N*-diethyldithiocarbamate [6] (BDDC, Figure 4.2) and methyl 2-(butylthiocarbonothioylthio) propanoate [7] (MCEBTTC, Figure 4.2) were synthesised using the procedures previously described in Chapter 2 (§2.2.2) and Chapter 3 (§3.2.2), respectively. Deuterated chloroform ( $\text{CDCl}_3$ , 99.6 atom %) was obtained from Aldrich. HPLC grade tetrahydrofuran (THF) and acetonitrile were obtained from Scharlau and Merck, respectively. Dimethyl sulfoxide (DMSO) was obtained from Sigma-Aldrich. Bulk grade methanol was distilled prior to use. All water was purified by reverse osmosis prior to use.

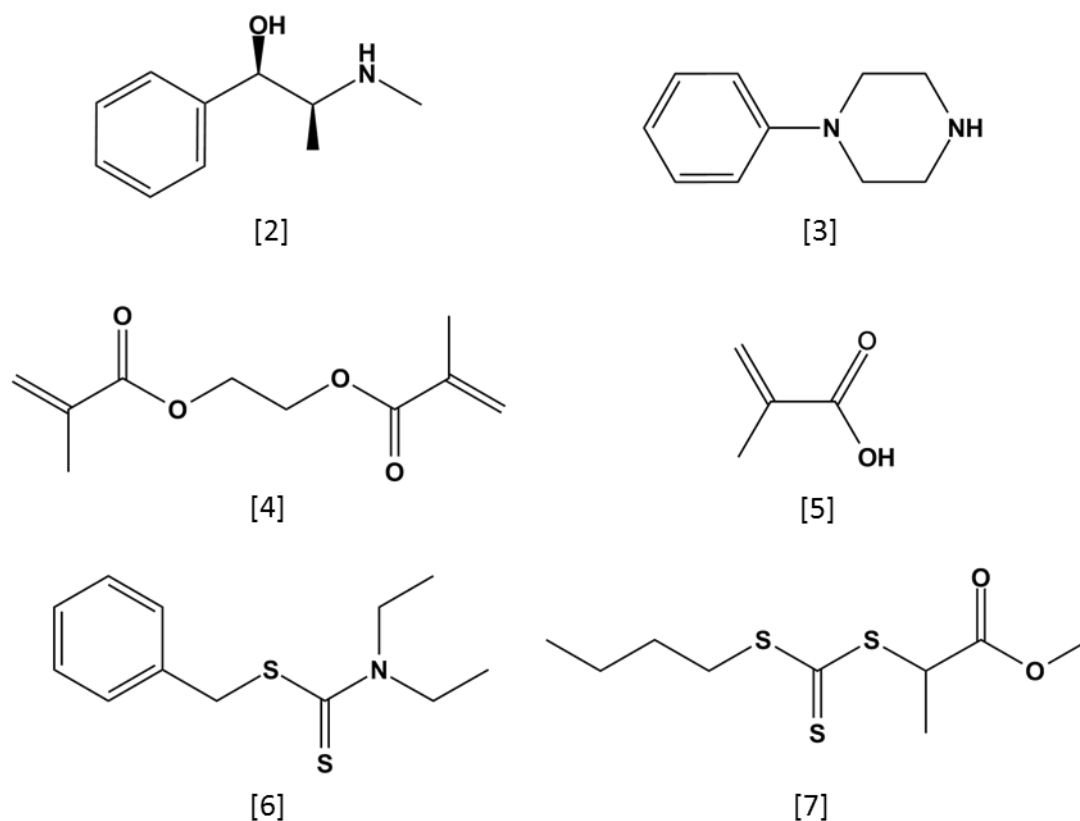


**Figure 4.2.** Structures of (1R,2S)-(-)-ephedrine [2], 1-phenylpiperazine [3], ethylene glycol dimethacrylate [4], methacrylic acid [5], benzyl *N,N*-diethyldithiocarbamate [6] and methyl 2-(butylthiocarbonothioylthio) propanoate [7].

## 4.2.2 Synthesis of MIP Microspheres

### 4.2.2.1 Iniferter Method

The MIP microspheres were prepared using benzylpiperazine, BZP as the template molecule, methacrylic acid, MAA as the functional monomer and benzyl *N,N*-diethyldithiocarbamate, BDDC as the iniferter. Molar ratios of 1:1:5 (template:functional monomer:crosslinker) were used for all formulations. These ratio was chosen based on previous studies as described in §4.3.1.1 and §4.3.1.2. A typical iniferter polymerisation procedure was as follows: the template molecule (BZP, 2.12 mmol; 374 mg), functional monomer (MAA, 2.12 mmol; 0.180 mL), crosslinker (EGDMA, 10.6 mmol; 2.10 mL) and iniferter (BDDC, 0.636 mmol; 152 mg) were mixed in a round bottom flask, dissolved in the porogen (acetonitrile, 100 mL) and left to

equilibrate for 2 hrs. The mixture was then purged with nitrogen for 30 min and placed under UV irradiation from a 450W medium pressure mercury vapour, quartz *UV lamp* (Ace glass, No. 7825-34) at room temperature to polymerise for the desired time. The solution was then transferred into a large beaker and the solvent was left to evaporate. Methanol was then added to the remaining precipitate in the beaker while stirring, followed by washing in THF then methanol. Finally, the precipitate was collected by vacuum filtration and dried at room temperature. The yield of the MIP microspheres was determined gravimetrically. As a reference, non-imprinted polymer (NIP) microspheres, for control experiments were also prepared following the same procedure except that no BZP template was added during the polymerisation.

Three different sets of BZP imprinted polymers and their corresponding NIPs were synthesised by varying the amount of BDDC iniferter (i.e. 5, 10 and 20 mol % with respect to the total monomers) in the polymerisation mixture.

#### 4.2.2.2 RAFT Method

The MIP microspheres were prepared using BZP as the template molecule, MAA as the functional monomer as well as methyl 2-(butylthiocarbonothioylthio) propanoate, MCEBTTC and AIBN as the RAFT agent and initiator respectively. Molar ratios of 1:1:5 (template:functional monomer:crosslinker) were used for all formulations. Initial experiment conducted using similar total monomer concentration as that of iniferter method (2 vol %) resulted in a very low yield of RAFT microspheres. Therefore, the total monomer concentration was doubled (4 vol %) in the preparation of microspheres via RAFT, while maintaining the same template:functional monomer:crosslinker molar ratio. A typical RAFT polymerisation formulation is as follows: the template molecule (BZP, 4.24 mmol; 748 mg), functional monomer (MAA, 4.24 mmol; 0.360 mL), cross-linker (EGDMA, 21.2 mmol; 4.00 mL), RAFT agent (MCEBTTC [7], 1.27 mmol; 321 mg) and initiator (AIBN, 1.27  $\mu$ mol; 2.09 mg) were mixed in a round bottom flask, dissolved in the porogen (acetonitrile, 100 mL) and left to equilibrate for 2 hrs. The mixture was then purged with nitrogen for 30 min and

placed in an oil bath at 60 °C to undergo polymerisation for the desired time. The solution was then transferred into a large beaker and the solvent was left to evaporate. Methanol was then added to the remaining precipitate in the beaker while stirring, followed by washing in THF then methanol. Finally, the precipitate was collected by vacuum filtration and dried at room temperature. The yield of the MIP microspheres was determined gravimetrically. The NIP microspheres (control) were prepared following the same procedure except in the absence of the BZP template molecule.

Similarly, three different sets of BZP imprinted polymers and their corresponding NIPs were synthesised by varying the amount of RAFT agent (i.e. 5, 10 and 20 mol % with respect to the total monomers) in the polymerisation mixture.

#### **4.2.3 Template extraction**

BZP template removal was carried out by Soxhlet extraction using a mixture of 10% acetic acid in methanol for 24 hours, followed by 100% methanol for another 24 hrs. The polymers were then dried overnight under vacuum. HPLC was used to assess the removal of the template in the washing solutions. The washed MIP microspheres were also checked to be free of BZP by equilibrating 10 mg of the polymers in 1 mL of acetonitrile for several hours and performing HPLC analysis to detect any bleeding of BZP into the solution.

#### **4.2.4 Batch Rebinding Studies**

Batch rebinding experiments were carried out using a known molarity of BZP stock solution in acetonitrile or THF. A known mass (5 – 10 mg) of polymer was left in contact with a fixed volume (1 mL) of a known concentration of BZP stock solution on a rotary mixer. After the required time, the solution was centrifuged and filtered using a 0.45 µm membrane filter into a 1.5 mL vial for BZP quantification by HPLC.

The HPLC analysis was performed using a Shimadzu HPLC instrument equipped with an Econosphere™ C18, 5µm column (Grace), LC-20 AD pump, an SPD-20A UV detector and SIL-20A/20AC injector operated with SIL-20A autosampler. A solution of 50% acetonitrile and 50% buffer (25 mM KH<sub>2</sub>PO<sub>4</sub>; 30 mM KCl; 7 mM TEA; adjusted to pH 3 with H<sub>3</sub>PO<sub>4</sub>) was used as the mobile phase. A 10 µL injection volume was used with a run time of 4 min at a flow rate of 2 mL/min and detection wavelength of 205 nm. A calibration curve was generated every time a batch of samples was analysed using seven BZP solutions in the range of 0.05 to 1.0 mM. An example of the BZP calibration curve is shown in Figure 4.3. The data were collected and analysed using Shimadzu LCsolution software.

The amount of bound BZP ( $S_B$ ) was calculated by subtracting the free BZP concentration ( $C_f$ )<sup>67</sup> from the total amount of BZP ( $C_t$ ) initially present in the polymer solution. All experiments were conducted in triplicate and the mean values are reported. Binding affinities of the MIPs and NIPs were thus calculated according to equation 4.1:

$$S_B = \frac{(C_t - C_f)}{Z} \quad (4.1)$$

where  $S_B$  is the amount of BZP bound, and  $Z$  is either the mass of polymer (g) in the solution or the surface area (m<sup>2</sup> per g polymer).

Specific binding was determined from the difference between the binding affinity of MIP and NIP, as shown in equation 4.2:

$$\Delta S_B = S_{B(MIP)} - S_{B(NIP)} \quad (4.2)$$

where  $S_{B(MIP)}$  and  $S_{B(NIP)}$  are the binding affinity of BZP on the imprinted and non-imprinted microspheres, respectively.

The imprinting factor (IF), which is defined as the ratio of amount of substrate bound by the MIP to that bound by the corresponding NIP was also used to determine the specific recognition characteristic of the microspheres, as shown in equation 4.3:

$$IF = \frac{S_{B(MIP)}}{S_{B(NIP)}} \quad (4.3)$$

NIPs were used to quantify the level of non-specific binding and because the IF value takes into account the non-specific binding, the value can be said to represent the binding linked solely to the imprinting effect.<sup>258</sup> Hence the greater the IF value, the more influential the imprinting procedure is on analyte binding.

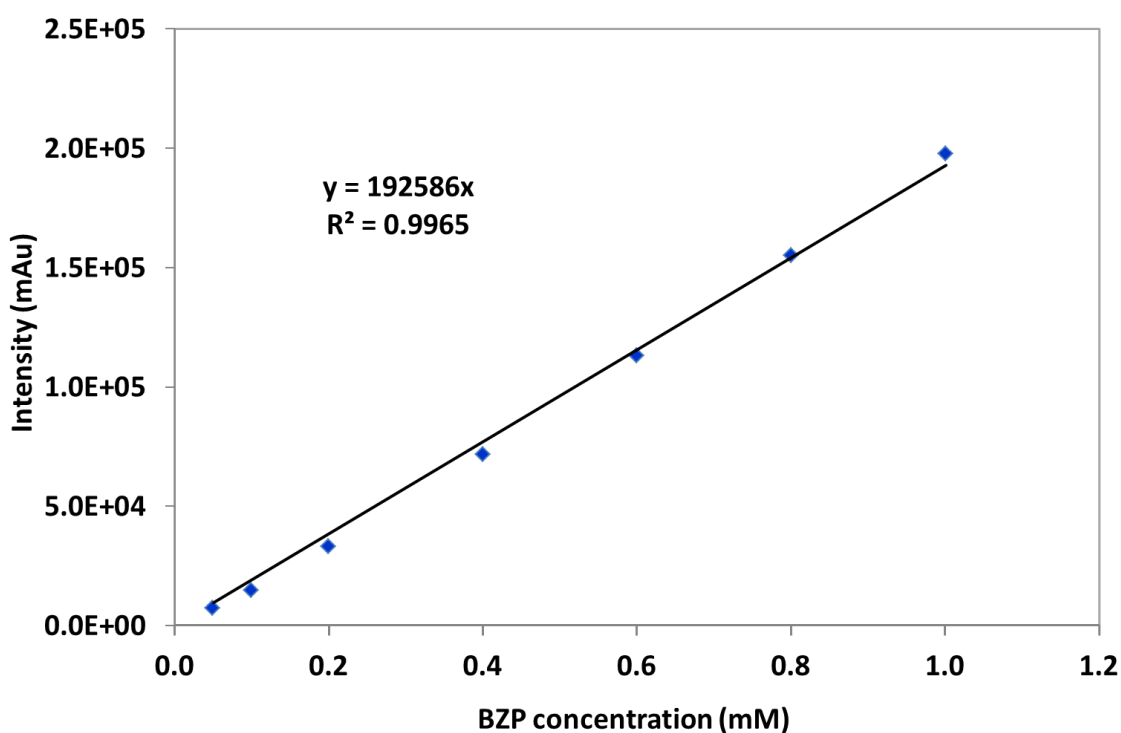


**Figure 4.3.** Calibration curve used for the determination of concentration of BZP.

#### 4.2.4.1 Optimum Binding Time

Kinetic experiments were performed to evaluate the optimum binding time within the range 1 – 8 hr. Following the procedure in §4.2.4, the rebinding experiment was

carried out on MIPs and their respective NIPs for 1, 2, 4 and 8 hr. The mass of polymer used was either 5 or 10 mg and the BZP concentration was fixed at 1.0 mM. The experiments were conducted in both acetonitrile and THF. The experiments were conducted in triplicate and the mean values are reported.

#### 4.2.4.2 Binding Isotherms

The binding isotherm studies were carried out to better understand the sorption interaction mechanism between the template and the MIP surface. Following the procedure in §4.2.4, a constant volume of solution (1 mL) of varying BZP concentration (0.1 – 6.0 mM) was added to the required mass of polymer and mixed on a rotary mixer for 2 hours to allow for equilibrium sorption to be achieved. The mass of polymer was adjusted so that the percentage of BZP depleted from the solution was at an acceptable level of template binding in order to keep the error to a minimum. The binding isotherm was then plotted as either the concentration of BZP bound per mass or per surface area of polymer ( $S_B$ ) versus the equilibrium concentration of free BZP <sup>67</sup> remaining in the solution. The relative binding ability of the MIP and its corresponding NIP can then be assessed by comparing their respective isotherms.

Each equilibrium adsorption isotherm was analysed using both the Langmuir and Scatchard isotherm models to determine binding parameters such as the number of binding site ( $N$ ), and the equilibrium binding constant ( $K$ ). Equations 4.4 and 4.5 show the linearised forms of the Langmuir and Scatchard isotherms, respectively:

$$\frac{C_f}{S_B} = \frac{1}{NK} + \frac{C_f}{N} \quad (4.4)$$

$$\frac{S_B}{C_f} = NK - KS_B \quad (4.5)$$

For the Langmuir model, the value of  $N$  and  $K$  can be determined by plotting  $C_f/S_B$  vs  $C_f$  where  $N$  can be obtained from the inverse of the slope of any linear region and  $K$  can then be obtained from the intercept. Plotting  $S_B/C_f$  vs  $S_B$  should give a straight line in

the Scatchard plot, where  $NK$  is the y-intercept and  $-K$  is the slope. Equation 4.6 was then used to calculate the equilibrium dissociation constant ( $K_d$ ):<sup>259</sup>

$$K_d = \frac{1}{K} \quad (4.6)$$

#### 4.2.5 Selectivity Studies

In the selectivity experiments, due to their closely related structures to BZP, two types of drugs, namely Ephedrine [2] (EPH, Figure 4.2) and 1-Phenylpiperazine [3] (PHP, Figure 4.2) were chosen as the reference substrates to investigate the selectivity of the BZP imprinted microspheres to the BZP template. Two sets of experiments i.e. non-competitive adsorption experiments (also known as a cross-reactivity study) and competitive adsorption experiments were carried out on the best performing MIP microsphere, based on the highest imprinting factor. Competitive adsorption studies were conducted to determine the selectivity of the BZP imprinted polymer towards the BZP template in the presence of other analytes and these were conducted in binary and tertiary competitive environments.

The procedure for the non-competitive adsorption experiment was as follows: 1.0 mL of BZP, EPH or PHP at a concentration of 3.00 mM in acetonitrile was added to 1.5-mL Eppendorf tubes containing 5 and 6 mg of MIP and NIP microspheres, respectively. After being shaken for 2 hours at room temperature, the mixture was centrifuged and filtered. The final equilibrium concentration of the analyte in the filtrate was analysed by HPLC. Calibration curves were generated using BZP, EPH and PHP solutions in the range of 0.2 to 3.5 mM, as shown in Figure 4.4(A), (B) and (C), respectively.

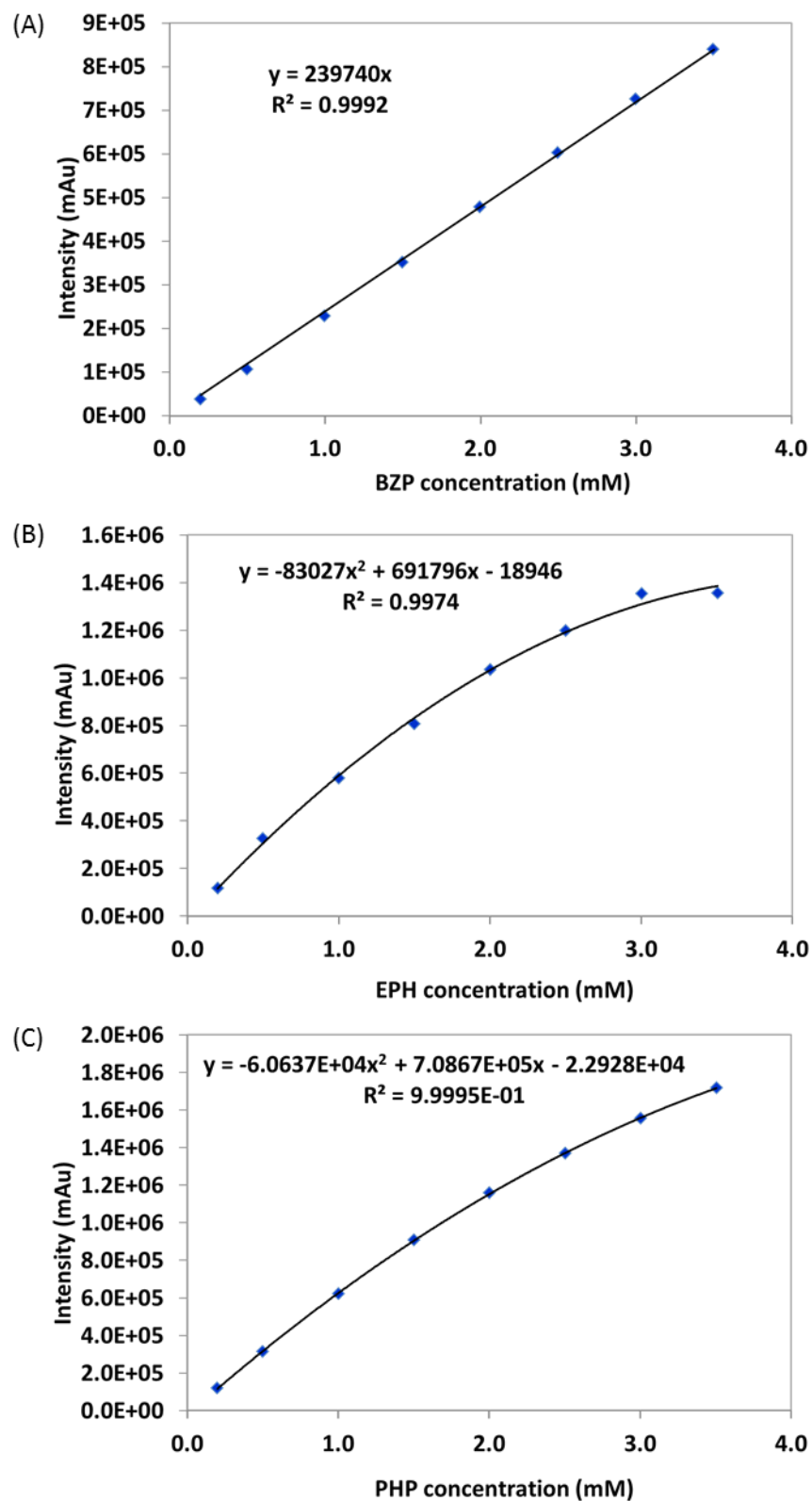


**Figure 4.4.** Calibration curves used for the determination of concentration of (A) BZP, (B) EPH and (C) PHP analytes.

The non-competitive binding experiment (single-analyte binding assay) was used to assess the ability of the MIP microspheres to discriminate between BZP and other structurally related drugs.<sup>260</sup> This binding selectivity of the imprinted microspheres towards different substrates is expressed as a specific selectivity factor (*SSF*) and can be defined as the ratio of specific binding of the two different substrates as shown in Equation 4.7:

$$SSF = \frac{\Delta S_{B(\text{template})}}{\Delta S_{B(\text{analogue})}} \quad (4.7)$$

where  $\Delta S_{B(\text{template})}$  and  $\Delta S_{B(\text{analogue})}$  are the specific binding of BZP template and the analogue, respectively. The above equation was also used for the competitive binding studies.

For the competitive binary-analyte assay, a 1.0 mL mixture of BZP and EPH, or BZP and PHP (each with a concentration of 3.00 mM) in acetonitrile was added to 1.5-mL Eppendorf tubes containing 5 and 6 mg of MIP and NIP microspheres, respectively. After being shaken for 2 hour at room temperature, the samples were centrifuged and filtered. The final equilibrium concentration of each analyte in the filtrate were analysed by HPLC. The tertiary-analyte assay was conducted following the above procedure, but using a 1.0 mL mixture of BZP, EPH and PHP (each with a concentration of 3.00 mM in acetonitrile). All experiments were performed in triplicate and overlapping HPLC peaks of BZP and PHP were deconvoluted using the Excel<sup>TM</sup> solver function using the same procedure used for the overlapping GPC curve (see §2.3.3) to determine the individual peak heights. The deconvolution of overlapped peaks by means of the non-linear least-squares method has already been reported.<sup>180, 181, 261</sup> For example, among the several approaches of peak resolution that Nikitas *et al.* have investigated, Solver was found to perform the best.<sup>181</sup> An example of the deconvoluted HPLC curve of the competitive binary-analyte assay (Table 4.9) is shown in Figure 4.5. The best fit between the measured HPLC curve and the fitted HPLC curve (sum of the deconvoluted curves) was obtained using the Solver function by minimising the sum of the squares of the differences between the measured and the fitted HPLC curves

( $\Sigma\Delta^2$ ). The concentration of each analyte was then determined from the height of individual deconvoluted peaks (G1 and G2) using the calibration curves in Figure 4.4(A) and (C), respectively.

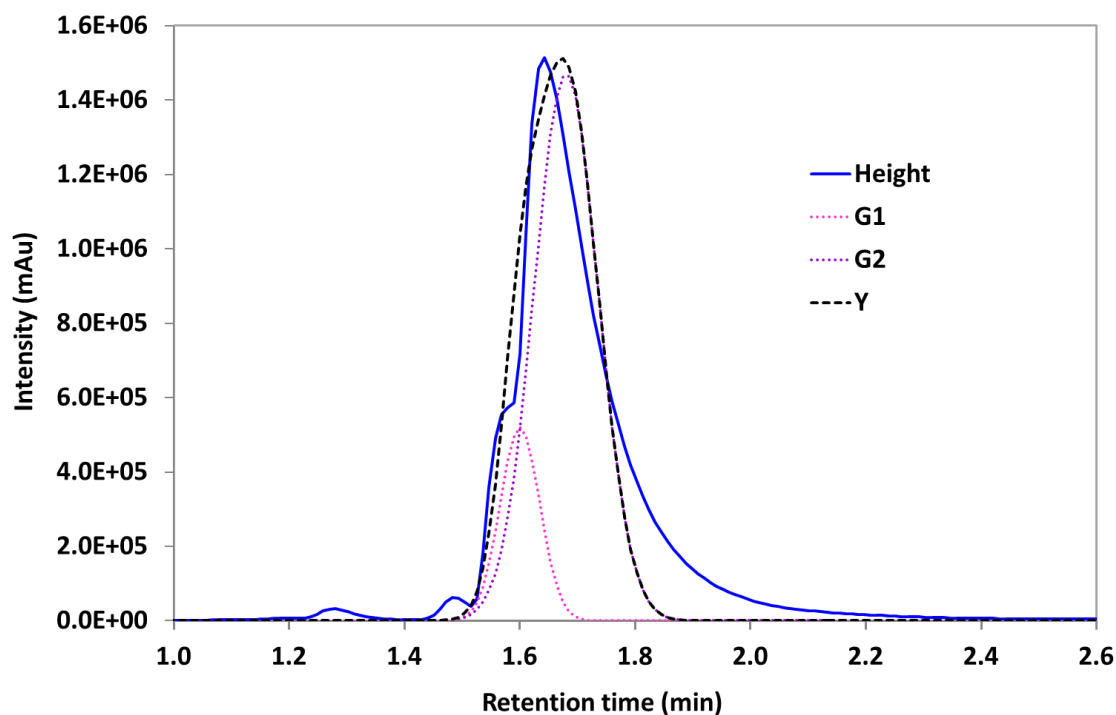


**Figure 4.5.** Deconvolution of a HPLC curve (MIP-5%BDDC, Table 4.9) carried out using the Solver function in Microsoft Excel 2010. G1 and G2 represent BZP and PHP respectively. The solid blue (height) and the black dashed (Y) lines are the measured and fitted HPLC curves, respectively.

#### 4.2.6 Surface Area and Porosity

MIP and NIP microspheres were subjected to surface area and porosity measurements using Brunauer-Emmet-Teller (BET) and Barret-Joyner-Halenda (BJH) analysis, respectively. Measurements were performed on a Micromimetics ASAP 3030 surface area and porosity analyser using a 5-point surface area analysis. Approximately 100 mg of polymer sample was analysed using  $N_2$  as the adsorption gas. The specific surface area of the polymers was then calculated according to the following BET isotherm equation (Equation 4.8):

$$\frac{p}{V(p_0 - p)} = \frac{1}{V_m c} + \frac{(c-1)}{V_m c} \cdot \frac{p}{p_0} \quad (4.8)$$

where  $V$  = volume of adsorbed gas,  $V_m$  = monolayer adsorbed volume of gas,  $p$  = equilibrium vapour pressure,  $p_0$  = saturation vapour pressure and  $c$  is the BET constant, which is expressed as follows (Equation 4.9):

$$c \approx \exp[(\Delta H_{\text{liq}} - \Delta H_1)/RT] \quad (4.9)$$

where  $\Delta H_{\text{liq}}$  refers to second and further layers adsorbed and  $\Delta H_1$  refers to monolayer adsorption, whilst  $R$  and  $T$  equal to the ideal gas constant and absolute temperature respectively.

According to equation 4.8, a plot of  $p/(V(p_0-p))$  versus  $p/p_0$  gives a straight line, usually in the approximate relative pressure range 0.05 to 0.3. The  $V_m$  and  $c$  were calculated from the slope and intercept according to the following equations (Equations 4.10 and 4.11, respectively):

$$V_m = \frac{1}{\text{slope} + \text{intercept}} \quad (4.10)$$

$$c = 1 + \frac{\text{slope}}{\text{intercept}} \quad (4.11)$$

Finally, the surface area was calculated according to Equation 4.12 as follows:

$$A = \frac{V_m N_A A_m}{m} \quad (4.12)$$

where  $A$  = specific surface area,  $N_A$  = Avogadro's number,  $A_m$  = area per molecule for adsorbed nitrogen and  $m$  = mass of the adsorbent in grams.

## 4.2.7 Other Characterisation Methods

DLS analyses were carried out following the same procedures outlined in Chapter 2 (§2.3). The SEM images of the NIP-10%BDDC and NIP-20%BDDC (Figure 4.9(E and F)) were generated using Zeiss Sigma VP FE-SEM while the SEM images of the rest of the microspheres were generated using a Philips XL30 SEM and Oxford ISIS EDS (1997) software. Surface micrographs were taken at various magnifications ranging from 15000 – 30000X.

### 4.2.7.1 FTIR

FTIR spectra of the solid and liquid samples were recorded on Perkin Elmer Spectrum One FTIR spectrometer controlled by *Spectrum v5.3.1* software and Perkin Elmer Spectrum Two controlled by *Spectrum 10™* software, respectively.

The crosslinking density of the microspheres was estimated by determining the extent of C=C conversion of the crosslinker (EGDMA). This was carried out by determining the ratio of absorbance peak attributed to the stretching vibration of the pendant C=C double bond ( $1639\text{ cm}^{-1}$ ) to that of the carbonyl (C=O,  $1727\text{ cm}^{-1}$ ) from the FTIR spectrum of the polymer (Figure 4.6(B)) and comparing them with that of the starting monomers (Figure 4.6(A)). The carbonyl band is related to both EGDMA and MAA since they both contain a C=O bond, whereas the pendant C=C double bond belongs to EGDMA only. The final EGDMA:MAA ratio in the crosslinked polymer is assumed to be the same as the initial ratio used during polymerisation i.e. 5:1, due to the nearly similar reactivity of EGDMA and MAA towards the iniferter radicals.<sup>262</sup> Hence, no peak normalisation was carried out to account for the peak contribution by the MAA carbonyl. The extent of C=C bond conversion of the EGDMA, DC (%), which is equivalent to the degree of crosslinking, was calculated according to following equation (Equation 4.13):<sup>263</sup>

$$\text{DC (\%)} = 100 \times \left[ 1 - \frac{(A_{\text{C=C}}/A_{\text{C=O}})_{\text{polymer}}}{(A_{\text{C=C}}/A_{\text{C=O}})_{\text{monomer}}} \right] \quad (4.13)$$

where DC(%) represents the extent of C=C bond conversion of the EGDMA whereas  $A_{(C=C)}$  and  $A_{(C=O)}$  are the FTIR absorbance values of C=C and C=O, respectively. A higher DC value indicates greater degree of crosslinking. The results are presented in Tables 4.3 and 4.6.

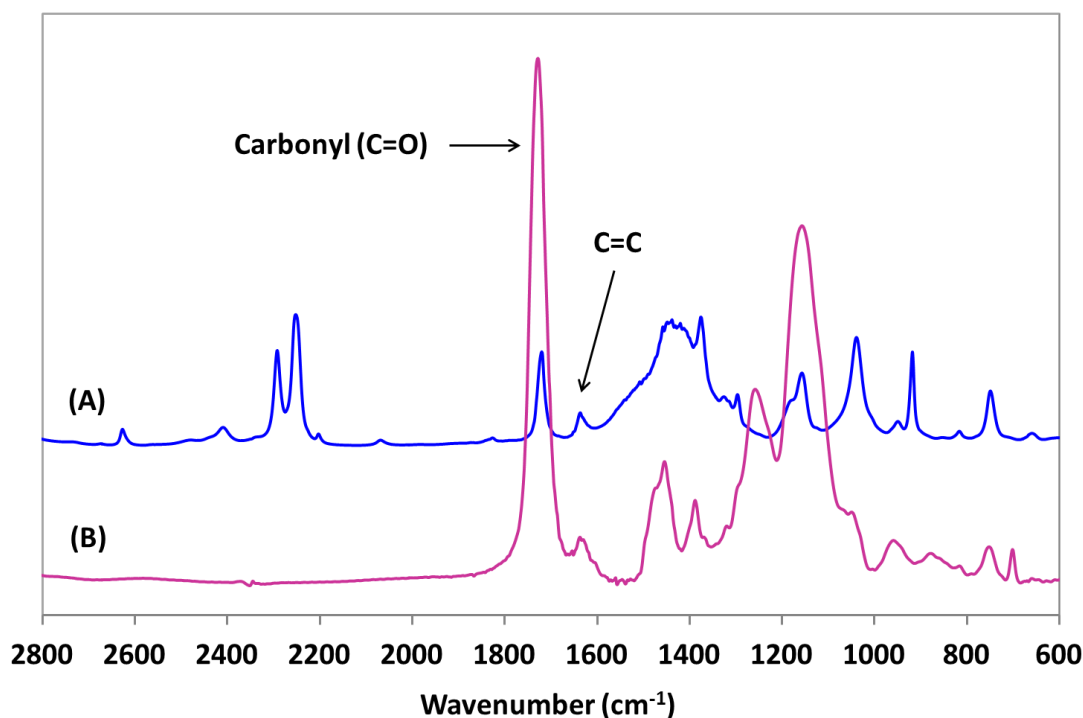


**Figure 4.6.** Comparison of FTIR absorbance spectra of (A) the monomers (EGDMA:MAA = 5:1) and (B) the MIP microsphere (MIP-20%BDDC).

## 4.3 Results and Discussion

### 4.3.1 MIP Design and Synthesis

There are a large number of factors involved in the MIP protocol that would affect the final performance of the prepared polymers such as amount and type of functional monomer, crosslinker, template, porogen, initiator, the method of initiation (thermal or photochemical initiation), temperature and also the intensity of the UV light.<sup>264, 265</sup> The molecular recognition properties of these tailor-made polymers would therefore be greatly enhanced by optimal selection of these factors.<sup>266</sup>

#### 4.3.1.1 Choice of Functional Monomer

The formation of the complex between the template and a functional monomer in the pre-polymerisation mixture is a key step for the preparation of a MIP that is selective for the template. In the non-covalent imprinting approach, hydrogen bonding and ionic interactions have been shown to be primarily responsible for the selective binding that occurs.<sup>267</sup> The stronger the interaction, the more stable the complexes formed. In the previous work carried out by Wright on the synthesis of bulk MIPs for BZP, both non-covalent and covalent imprinting techniques were developed.<sup>257</sup> A combination of molecular modelling and NMR spectroscopy was applied at the beginning of the study and used as a tool to identify functional monomers that could form non-covalent interactions with BZP. Several functional monomers such as itaconic acid (IA), acrylic acid (AA) and methacrylic acid (MAA) were investigated, and MAA was found to give the most favourable interaction with BZP. The binding results also showed that it gave the highest performing MIP (IF >2.0).<sup>257</sup> In the same study, it was also observed that among the template-functional monomer ratios (T:M) tested that included 1:1, 1:3, and the most commonly used 1:4, it was the 1:1 that gave the greatest binding discrimination between the MIP and NIP, i.e. IF > 2. Based on this previous study, a BZP:MAA ratio of 1:1 was used here to prepare the MIP microspheres.

MAA is commonly used as a functional monomer in non-covalent molecular imprinting and has been reported to have a strong interaction with basic templates due to proton transfer and hydrogen bonding.<sup>268</sup> Since BZP is a weak base ( $pK_a = 9.59$ ),<sup>249</sup> MAA is predicted to form a strong interaction with BZP, either via ionic interaction and/or hydrogen bonds, between its carboxyl group and the -NH group of BZP. Figure 4.7 shows the computer generated image of a 1:1 BZP:MAA complex showing that one monomer unit of MAA is capable of forming moderate to strong hydrogen bonds with BZP in two positions, i.e. between the carbonyl group of MAA with the -NH group of BZP (2.29 Å) as well as between the acidic hydrogen of MAA and the -NH group of BZP (1.72 Å), respectively.

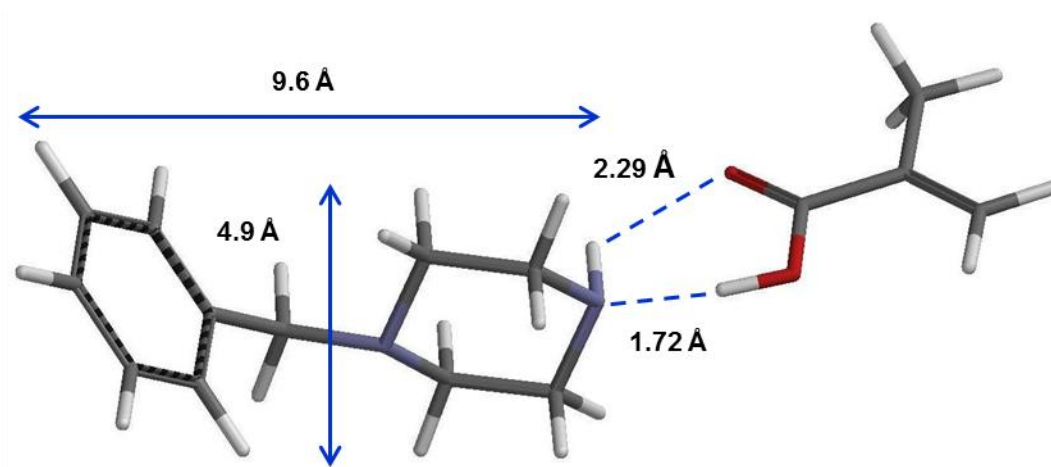


**Figure 4.7.** Molecular modelling image obtained using the molecular simulation software, Spartan '04 (Wavefunction, Inc. USA) of BZP:MAA 1:1 for the geometry optimised T:M cluster using gas phase AM1 force field at the semi-empirical level. Estimated molecular size of BZP: diameter = 4.9 Å, length = 9.6 Å. Distance between the >C=O of MAA and –NH of BZP is 2.29 Å; between –COOH of MAA and –NH of BZP is 1.72 Å.

FTIR analysis was carried out to investigate the interaction between MAA and BZP by comparing the spectra of a mixture of MAA and BZP with those of the individual compounds as shown in Figure 4.8. As can be seen in Figure 4.8(A), the bands at 1691, 1429 and 1297  $\text{cm}^{-1}$  are assigned to the carbonyl (C=O) stretching, O-H bending and C-O stretching vibration of pure MAA, respectively. The carbonyl stretching vibration shows a reduction in intensity when forming a complex with BZP (Figure 4.8(C)) while the O-H bending vibration has disappeared. The appearance of bands at 736 and 698  $\text{cm}^{-1}$  (Figure 4.8(C)) are attributed to the benzyl group of BZP. The band at 913  $\text{cm}^{-1}$  observed in the spectrum of pure BZP (Figure 4.8(B)) has disappeared when MAA-BZP complex is formed (Figure 4.8(C)). New bands observed at 1545 and 1404  $\text{cm}^{-1}$  are attributed to the asymmetric and symmetric stretching vibration of  $\text{COO}^{-269-272}$  of MAA, respectively. The band observed at 1050  $\text{cm}^{-1}$  is attributed to the C-N stretching<sup>273</sup> of BZP that has become broader compared to that in pure BZP (Figure 4.8(B)), probably due to the formation of hydrogen bond with the carbonyl group of MAA (see Figure 4.7), whilst the band at 834  $\text{cm}^{-1}$  is attributed to the C-N bending<sup>273</sup> of the BZP. The result indicates that MAA interacts with the basic BZP template possibly via ionic interaction and hydrogen bonding.

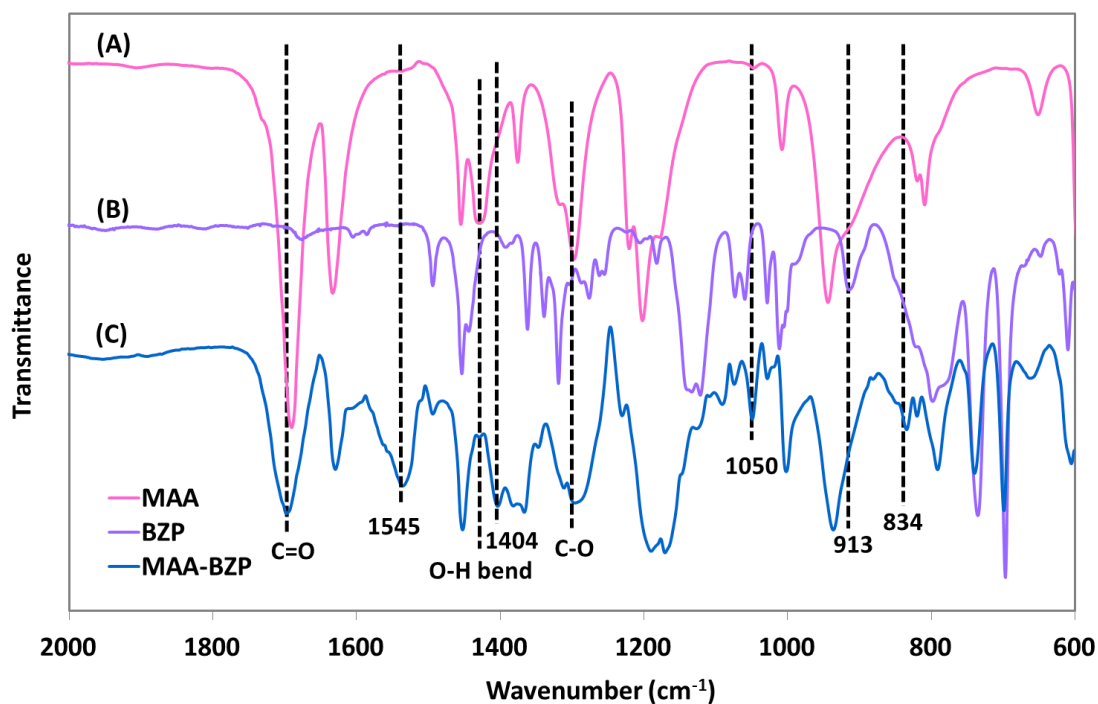


**Figure 4.8.** FTIR spectra of (A) MAA, (B) BZP and (C) MAA-BZP complex. The peaks at 1545 and 1404  $\text{cm}^{-1}$  are attributed to the asymmetric and symmetric stretching vibration of  $\text{COO}^-$  of MAA, respectively.

#### 4.3.1.2 Choice of Crosslinker

It has been found that the binding capacity of the polymers increases with the degree of crosslinking.<sup>274</sup> Although a specific quantity is needed to produce a rigid polymer, the crosslinker can also form a non-specific interaction with the template during the pre-polymerisation and rebinding. Therefore, the choice of crosslinker is also important to obtain good imprinting sites. Based on the previous results obtained by Wright, EGDMA was chosen as the crosslinker due to its minimal interactions with BZP compared to other crosslinkers that were studied such as divinylbenzene (DVB) and trimethylolpropane trimethacrylate (TRIM).<sup>257</sup> In addition, Wright also observed that the use of EGDMA produced the best performing BZP imprinted polymer ( $\text{IF} > 6$ ) when combined with MAA as the functional monomer at [BZP]:[MAA] ratio of 1:1 in chloroform, while still maintaining good performance ( $\text{IF} = 2$  to 3) at [BZP]:[MAA] ratio of 1:1 in acetonitrile. As for the optimum amount of crosslinker in the MIP, depending

on the functional monomer employed, previous studies have shown that an optimum crosslinker percentage was in the range of 50% to 80%.<sup>275</sup>

#### **4.3.1.3 Choice of Porogenic Solvent**

Apart from bringing all of the polymerisation components i.e. template, functional monomer(s), crosslinker and initiator into one phase, the solvent has an additional function where it is responsible for creating the pores in the polymer. For this reason, it is commonly referred to as the “porogen”. It has been reported that a solvent with strong affinity for the template molecule and for the monomer hindered the formation of interactions such as hydrogen bonds and electrostatic interactions between the template and the monomer.<sup>276, 277</sup> Therefore, the selection of solvent for the polymerisation is an important factor in designing a molecular imprinting system for a given target molecule. In a non-covalent imprinting polymerisation, the solvent with the potential to maximise the likelihood of template-functional monomer complex formation should be chosen. Thus non- to moderately polar and aprotic solvents, such as toluene, dichloromethane, chloroform and acetonitrile are suitable porogen choices because they do not disrupt the interactions between the template and the monomer.<sup>276</sup> Our MIPs were prepared in acetonitrile, which is a polar aprotic solvent because of its ability to dissolve BZP. In addition, acetonitrile has been found to give spherical monodisperse particles in precipitation polymerisation which should ideally result in a more homogeneous binding site distribution.<sup>142, 231, 278-282</sup>

### **4.3.2 Molecular imprinted Polymers by the Iniferter Method**

#### **4.3.2.1 Synthesis and Physical Characterisation**

The iniferter method using BDDC has already been discussed for the synthesis of CCS polymers in Chapter 2. BDDC is again used here for the synthesis of MIP microspheres selective for BZP using the non-covalent imprinting approach. The polymerisation was carried out under UV irradiation at room temperature (§4.2.2.1) and template removal was performed using Soxhlet extraction (§4.2.2.3).

BDDC has been used to synthesise linear polymers such as polystyrene and polyisoprene as well as the surface photo-grafted copolymerisation of monomers such as St and MAA.<sup>77, 84, 191</sup> While BDDC has also been used for the preparation of functionally imprinted composite materials by modification of a porous silica support<sup>283</sup> and in the preparation of highly crosslinked polymer microspheres,<sup>161</sup> the effect of the concentration of BDDC iniferter on the binding performance of MIPs using precipitation methods has not been reported. Therefore, it is of interest to investigate this effect on the binding performance of BZP imprinted polymers. Using a 1:1 mol ratio of the template BZP to MAA, MIP microspheres containing 5 mol % of BDDC (MIP-5%BDDC) with respect to the total amount of EGDMA and MAA monomers were prepared, followed by 10 mol % (MIP-10 %BDDC) and 20 mol % of BDDC (MIP-20%BDDC). The corresponding NIP microspheres were prepared using identical formulations but in the absence of the BZP template. In precipitation polymerisation, a large volume of solvent is typically used for the preparation of microspheres. The monomer concentration should be kept low ( $\leq 5$  vol %) in order to prevent coagulation, and hence produce monodisperse particles.<sup>284, 285</sup> In this work, 2 vol % of total monomer (EGDMA and MAA) was used to prepare the BZP imprinted polymers.

Figure 4.9 shows the SEM images of the polymers obtained by the iniferter method. As can be seen from the images (Figure 4.9 (A-C)), all the MIP microspheres are spherical with smooth surfaces and are monodisperse. This result is in agreement with previous studies, which found that spherical microspheres with narrow size distribution are formed when a crosslinking polymerisation is started from a dilute (usually  $\leq 5$  vol %), homogeneous monomer solution.<sup>161, 223, 234, 279</sup> It is common for microspheres to be formed in dilute solution under good solvency conditions since the intramolecular reactions are favoured due to radical chain ends having a higher local concentration of pendant reactive groups from their own chain compared to those from other macromolecules.<sup>286</sup> In precipitation polymerisation, it was proposed that these particles were formed in two stages: nucleation and growth.<sup>287</sup> Nucleation was postulated to start by aggregation of soluble oligomers to form swollen microgels, which subsequently desolvate to form the particle nuclei. The nuclei continued to

grow by capturing the newly formed oligomers from the solution with the aid of the residual carbon-carbon double bonds on the surface of the microsphere.<sup>287</sup>

The SEM results also show that the presence of the template has a major effect on the size of the imprinted microspheres, resulting in a much bigger size for the MIPs compared to the NIP counterpart, as can be clearly seen by comparing the SEM images of MIP-5%BDDC and NIP-5%BDDC (Figure 4.9(A) and (D), respectively). The template molecules may act as more efficient nucleation points for the formation of molecular clusters during the polymerisation.<sup>288</sup> It is possible that complexation with BZP increased the local concentration of monomer in the vicinity of the template, which resulted in a faster polymerisation rate for the imprinted system compared to that of the non-imprinted system.<sup>237</sup> The solubility of the growing polymer chains might also be affected in the presence of the template, by forming the template-polymer complexes, thereby promoting the nucleation and growth process of the crosslinked particles.<sup>161</sup>

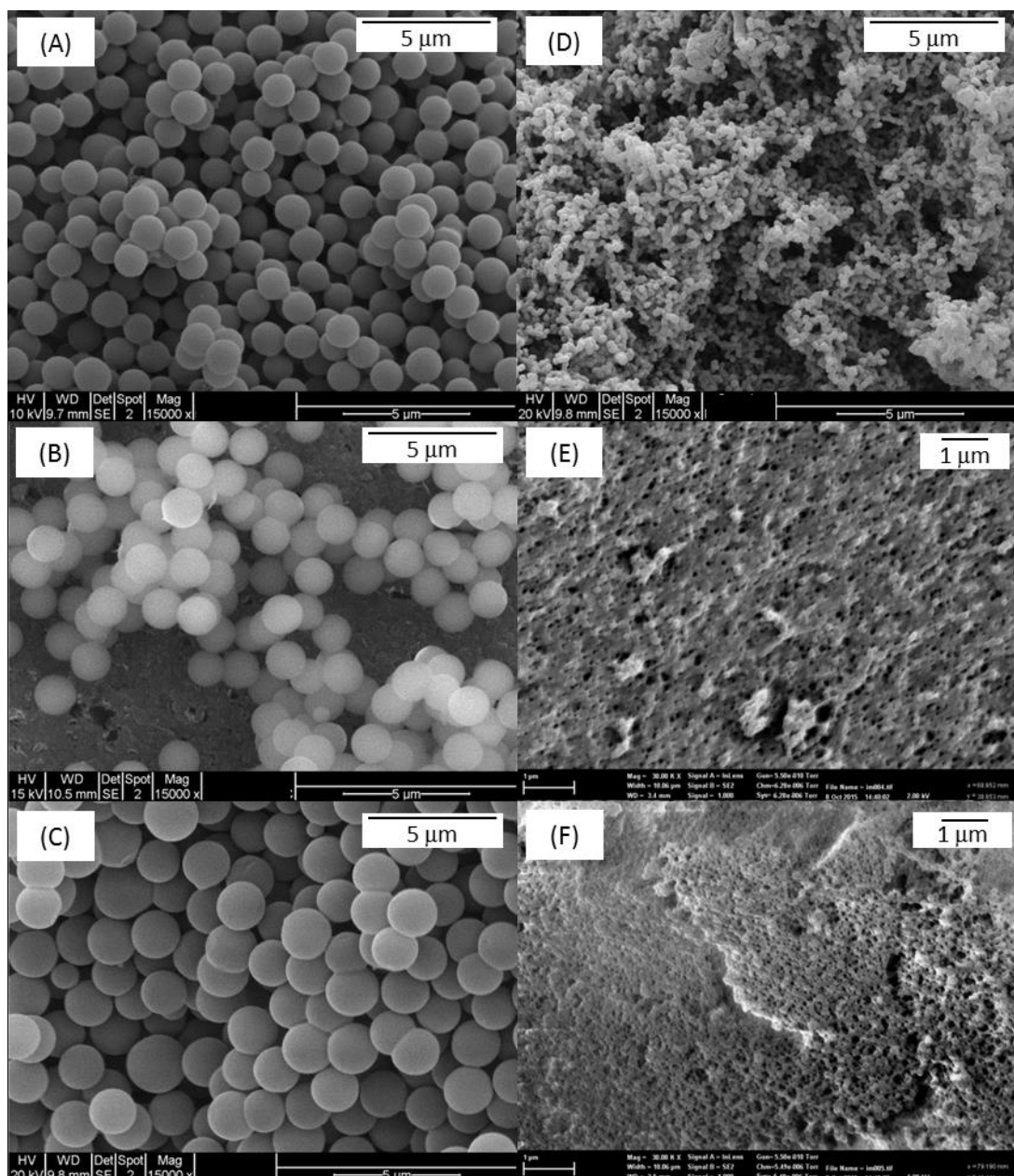


**Figure 4.9.** SEM images of spherical MIP microspheres prepared using (A) 5 mol %, (B) 10 mol % and (C) 20 mol % BDDC and their corresponding NIP microspheres (D), (E) and (F) respectively. Images A – D were recorded at 15000X magnification (using Philips XL30 SEM, whilst E – F were recorded at 30000X magnification (using Zeiss Sigma VP FE-SEM).

The influence of template on particle size has been reported to depend on the nature of the template.<sup>142, 231, 237, 289</sup> For instance, uniform propranolol imprinted nanoparticles have been obtained by precipitation polymerisation using MAA and TRIM as the functional monomer and crosslinker respectively, however, the equivalent non-imprinted particles (*ca.* 220 nm) were found to be bigger than the size of the

propranolol imprinted nanoparticles (*ca.* 140 nm).<sup>237</sup> Using the same polymerisation recipe and protocol, but employing testosterone<sup>237</sup> and atrazine<sup>289</sup> as templates, the MIP particles formed were larger than the NIP counterparts. These results demonstrate that in precipitation polymerisation, the apparent polymerisation rate and the size of the crosslinked particles were affected by the addition of template and are template-dependant.

The particle size of the MIP and NIP microspheres was obtained from their SEM images and the results are tabulated in Table 4.1. DLS was also used to determine the hydrodynamic size ( $D_h$ ) as well as particle size distribution of the NIPs. Repeated DLS measurements showed narrow, unimodal distribution of NIP particles, with no evidence of aggregates and the averages of the three repeat measurements are tabulated in Table 4.1. On the other hand, sedimentation of the MIP dispersions precluded accurate determination of their hydrodynamic size by DLS.

From Table 4.1, it can be observed that the SEM particle size of the MIP microspheres increases as the amount of BDDC increases. Similarly, the hydrodynamic size of the control (NIPs) also increases with increasing amount of BDDC iniferter. However, different trend is observed for the SEM particle size of the NIPs, where NIP-10%BDDC and NIP-20%BDDC were comparable in size but slightly smaller than that of the NIP-5%BDDC. It can also be noted that the diameter of NIP-5%BDDC particles measured from SEM was about 2-fold bigger than its hydrodynamic diameter. This is attributed to sampling errors while measuring the diameter since the boundaries of the bigger sized particles were more readily identified compared to those of the smaller ones. For both the MIP and NIP microspheres, the polymerisation rates were also found to increase with increasing amount of iniferter as indicated by the increased yield. These results are in good agreement with the results obtained by Yang *et al.* in the preparation of poly(MMA-co-DVB) microspheres by precipitation polymerisation<sup>290</sup> and the studies conducted by Li *et al.* using the iniferter-induced “living” radical precipitation polymerisation.<sup>161</sup> In precipitation polymerisation, the nucleus formation is attributed to the crosslinked polymer molecules having a chain length larger than

the critical limit of solubility in the medium. By increasing the amount of iniferter, a greater number of poly(EGDMA-co-MAA) oligomers with a lower molecular weight are generated. Lower molecular weight oligomers are more soluble, thus a smaller amount of oligomer precipitated, resulting in fewer primary particles during the nucleation step. The adsorption of the monomer or oligomeric species on the particle surface of the lower number of primary particles resulted in the reported larger particle size. In our case, this result is more pronounced for the MIP microspheres, which were formed in the presence of the template which is attributed to the creation of more efficient nucleation points for the formation of molecular clusters during the polymerisation process.

**Table 4.1.** Physical characteristics of the BZP-imprinted polymer microspheres and the NIP prepared by precipitation polymerisation using BDDC iniferter.

Microspheres	Yield (%)	SEM average diameter (nm)	$D_h$ (DLS) <sup>a</sup> (nm)	BET specific surface area <sup>b</sup> (m <sup>2</sup> /g)
MIP-5%BDDC	36	1290 ± 70	N/A	6.0 ± 0.1
NIP-5%BDDC	26	180 ± 20	90 ± 2	67 ± 13
MIP-10%BDDC	49	1490 ± 70	N/A	9.9 ± 0.3
NIP-10%BDDC	61	130 ± 19	190 ± 3	60 ± 1
MIP20%BDDC	58	1810 ± 100	N/A	7.6 ± 0.1
NIP-20%BDDC	82	132 ± 16	200 ± 16	56 ± 1

<sup>a</sup> Measured in THF at 20°C.

<sup>b</sup> Determined by nitrogen adsorption porosimetry.

<sup>c</sup> NA – not available (all the MIP dispersions in THF were unstable against sedimentation).

Specific surface area and pore volume were reported to have a strong influence on the efficiency of template adsorption,<sup>291</sup> thus these parameters are worth investigating, especially considering the fact that there is a large difference in size between the MIP and NIP microspheres. Therefore, the microspheres were sent for pore size distribution and BET specific surface area (SSA) analysis by nitrogen adsorption porosimetry. The BET specific surface areas of MIP and NIP microspheres are tabulated

in Table 4.1. As an example, the pore size distributions of the MIP-5%BDDC and NIP-5%BDDC are shown in Figure 4.10.

From Table 4.1, it can be seen that the MIP microspheres exhibited small measured specific surface areas ( $< 10.0 \text{ m}^2/\text{g}$ ), which is consistent with the previous results obtained for microspheres prepared via precipitation in pure acetonitrile.<sup>284, 292</sup> The BET specific surface areas of the MIP-10%BDDC and -20%BDDC were higher (about 1.6- and 1.3-fold higher, respectively) than that of the MIP-5%BDDC microsphere. On the other hand, the BET specific surface areas of the NIPs decreased with increasing amount of iniferter, which resulted in the NIP-20%BDDC to exhibit the smallest specific area ( $56 \pm 1 \text{ m}^2/\text{g}$ ). It can also be noticed that the specific surface area of the NIP-5%BDDC is an order of magnitude higher, as expected based on the smaller particle size of the NIP compared to the corresponding MIP ( $67 \pm 13 \text{ m}^2/\text{g}$  and  $6.0 \pm 0.1 \text{ m}^2/\text{g}$ , respectively).

Figure 4.10 shows that both the MIP and NIP display a large size distribution. Typically, pore size has been separated into three size categories: micropores ( $< 2\text{nm}$ ), mesopores (2-50 nm) and macropores ( $> 50 \text{ nm}$ ).<sup>264</sup> The NIP-5%BDDC is more porous than the corresponding MIP, having mesoporous particles with average pore widths of 2.0, 3.0 and 9.3 nm. On the other hand, most of the pores in MIP-5%BDDC are in the mesoporous region ( $> 10 \text{ nm}$  pore width), with average pore width of 11.7 nm and a very low number of pores in the microporous region, having average pore width of 1.5 nm. The binding sites located in the mesopores and macropores are expected to be easily accessible compared to those in micropores due to the slow diffusion in the latter. Considering the small size of BZP molecule (about 0.5 nm and 1.0 nm in diameter and length respectively), a small number of BZP molecules would have access to the sites located in the micropores of MIP with the majority of them having easier access to the sites in the mesopores. The binding sites in the NIP on the other hand would be much more accessible to the BZP molecules due to its larger amount of mesopores. Similar to that of the NIP-5%BDDC, the NIP-10%BDDC and -20%BDDC are more porous than their MIP counterparts (their pore size distributions are not shown),

having a large portion of mesopores ( $> 3$  nm pore width) and a small portion of micropores with average pore width of 0.6 and 1.2 nm for the former and 0.6 nm for the latter. On the other hand, most of the pores in their MIP counterparts are mostly in the micropore region ( $< 3$  nm pore width) with average pore width of 0.4 and 0.9 nm for the MIP-10%BDDC and 1.2 nm for the MIP-20%BDDC. The difference in morphologies of MIP and NIP microspheres in terms of particle size, specific surface area and pore diameter demonstrated that the presence of template in the precipitation polymerisation significantly influence the polymer morphology. The influence of particle size and/or porosity of the MIP and NIP microspheres on their binding performance will be discussed later in §4.3.2.2.

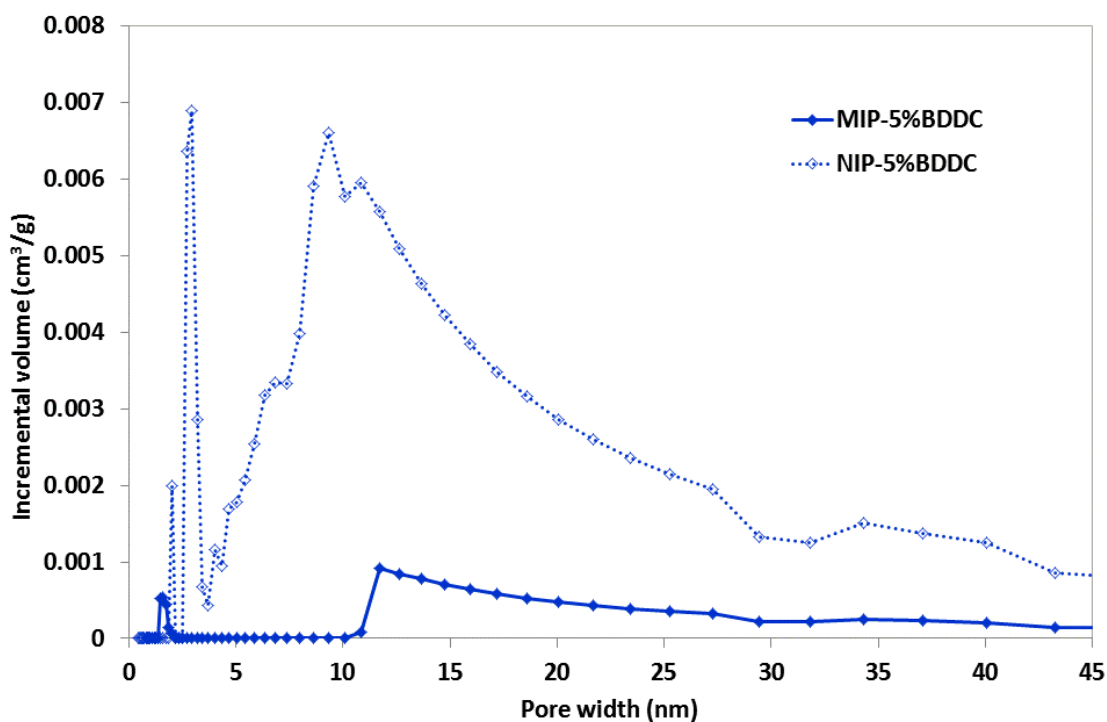


**Figure 4.10.** Incremental pore volume versus pore width plots for MIP-5%BDDC and NIP-5%BDDC.

#### 4.3.2.2 Binding Performance

The performance of the MIPs and their corresponding NIPs were investigated by batch rebinding studies. Batch binding experiments were conducted in acetonitrile (the porogen used during the preparation of the microspheres) and THF. THF was also used

as a rebinding solvent because the binding performance of the microspheres will later be compared with the corresponding CCS polymers, where the PS arms are soluble in THF (Chapter 5). The binding affinity, specific binding and imprinting factor values were calculated according to Equations 4.1, 4.2 and 4.3, respectively (§4.2.4).

The majority of the existing literature reports the binding affinity values normalised with respect to the sample mass, although the particle size of the MIPs and NIPs which reflects the surface area, was very different.<sup>161, 165</sup> In the bulk polymerisation, the monolithic polymers can be subjected to a grinding process to generate small particles followed by sieving into the desired size ranges, thus producing MIP and NIP particles of comparable size. Therefore, it is acceptable to express the binding with respect to the mass. As for microspheres, although MIP and NIP particles of almost similar size have been reported,<sup>293, 294</sup> most of the MIP and NIP microspheres obtained have different sizes depending on the nature of the templates used.<sup>161, 165</sup> For example, the diameter of the propanol-imprinted polymer microspheres was reported to be smaller than the non-imprinted polymers, whereas the testosterone-imprinted particles were larger than the non-imprinted particles, prepared using the same polymerisation conditions.<sup>237</sup> Due to a marked difference in size between our prepared MIP microspheres and their NIP counterparts as seen in Figure 4.8, the template binding capacity was expressed as both the amount bound per mass ( $\mu\text{mol per g sample}$ ) as well as per surface area ( $\mu\text{mol per m}^2 \text{ sample}$ ).

#### 4.3.2.2.1 Optimum Binding Time

To determine the optimum contact time for binding, batch rebinding studies were carried out on the MIP-5%BDDC microspheres using acetonitrile and THF as rebinding solvents. The concentration of the BZP solution was kept constant (1.00 mM) and the contact time was varied from 1 to 8 hrs. These contact times were chosen based on previous results by Wright, where the equilibrium for the synthesised BZP imprinted polymers was established between 1 to 8 hours.<sup>257</sup> The control (NIP microspheres) was also subjected to the same tests and the results are shown in Figure 4.11.

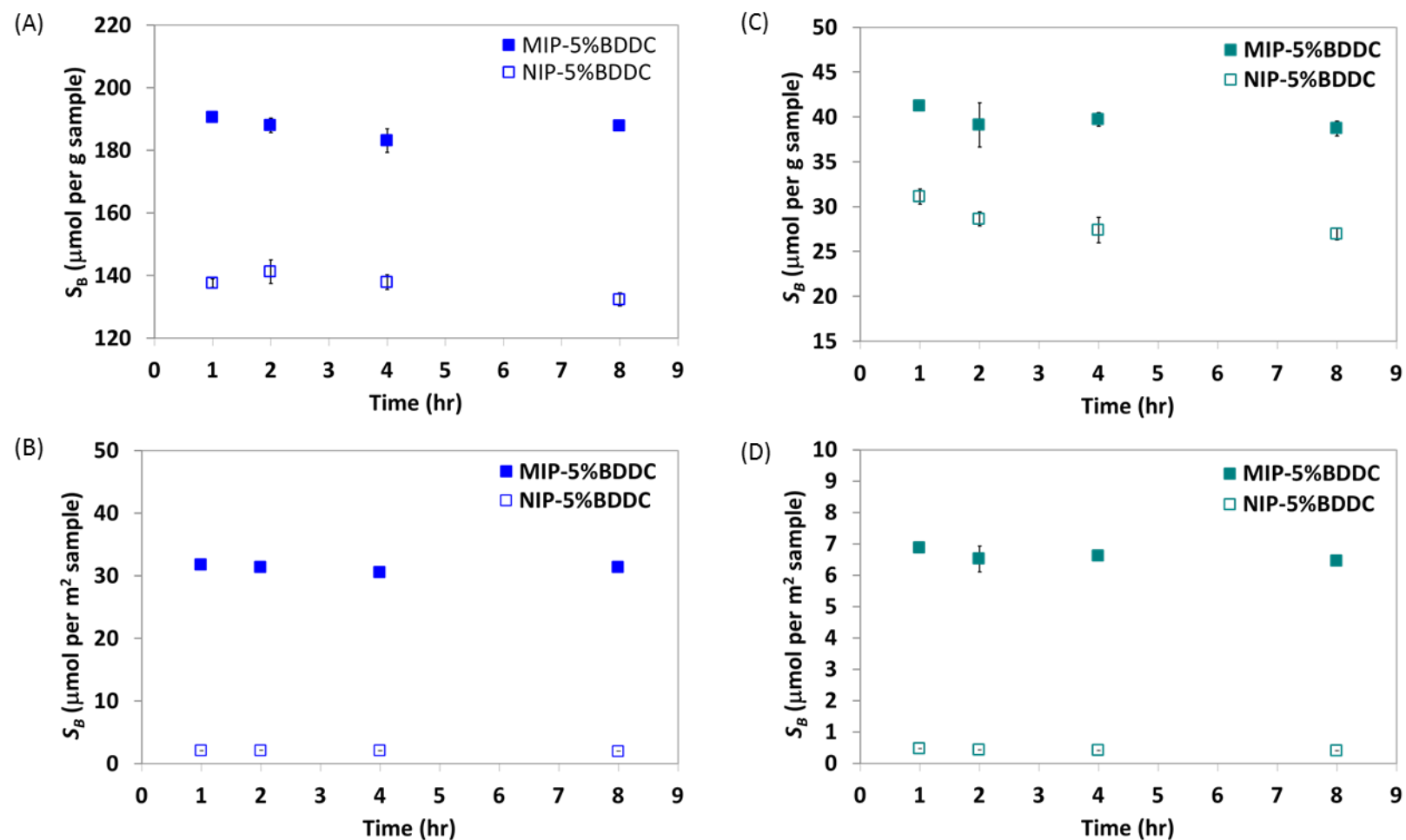


**Figure 4.11.** Time rebinding results for the MIP and NIP prepared using 5%BDDC in acetonitrile normalised with respect to (A) mass and (B) surface area as well as in THF normalised with respect to (C) mass and (D) surface area.

From Figure 4.11, it can be observed that the MIP-5%BDDC exhibited higher BZP binding affinity than the corresponding NIP when rebinding was carried out in both acetonitrile and THF, indicating that there were specific binding sites for BZP and that the imprinting process was successful. When the rebinding was carried out in acetonitrile, equilibrium was achieved in about 2 hours, which indicates that the binding processes occur quite rapidly.

#### 4.3.2.2 Binding Isotherm Studies

The binding characteristics of MIP-5%BDDC and its control (NIP-5%BDDC) were subjected to further investigation via a study of their binding isotherms. A more quantitative analysis can be made by comparing the binding parameters such as the number of binding sites ( $N$ ) and equilibrium dissociation constant ( $K_d$ ) which can be determined from the respective isotherms using either Equations 4.4 or 4.5 as well as Equation 4.6.

Figure 4.12 shows the binding isotherms of MIP microspheres prepared using 5% BDDC and the corresponding control (NIP). In Figure 4.12(A), the amount of BZP bound ( $\mu\text{mol}$ ) was normalised with respect to the mass (g) of the polymer and plotted against the free BZP concentration (mM). As mentioned in §4.3.2.2, due to the difference in size of the MIP and NIP microspheres, the binding capacity was also normalised with respect to the surface area ( $\text{m}^2$ ) of the polymer using the BET surface area given in Table 4.1 and plotted against the free BZP concentration as shown in Figure 4.12(B).

As can be seen in Figure 4.12(A), the binding affinity of both the imprinted polymer (MIP-5%BDDC) and the non-imprinted polymer (NIP-5%BDDC) increased with the increasing concentration of BZP in the solution, up to a certain limit where a plateau is reached. This happens because the template uptake has reached the saturation value, beyond which no further adsorption can take place.<sup>295, 296</sup> These values allow for the calculation of surface binding capacity. It can also be observed that the MIP exhibited higher affinity for BZP template than the NIP. Since the NIP has a surface area an order

of magnitude larger when compared to the MIP microsphere, the difference in the binding capacity between them on this scale is actually larger, as evidenced in Figure 4.12(B). Considering that the NIP has a higher surface area and more pores in the mesoporous region compared to the MIP (Figure 4.9), but yet bound less BZP compared to that of the MIP, it can be concluded that the better binding capacity of the MIP is most likely to be the result of cavity-based binding of BZP rather than the non-specific binding occurring for the NIP. The interaction between the functional groups and the template in NIPs is much weaker because the functional groups are expected to be randomly distributed and are isolated from each other in the polymerised network, resulting in reduced BZP adsorption.

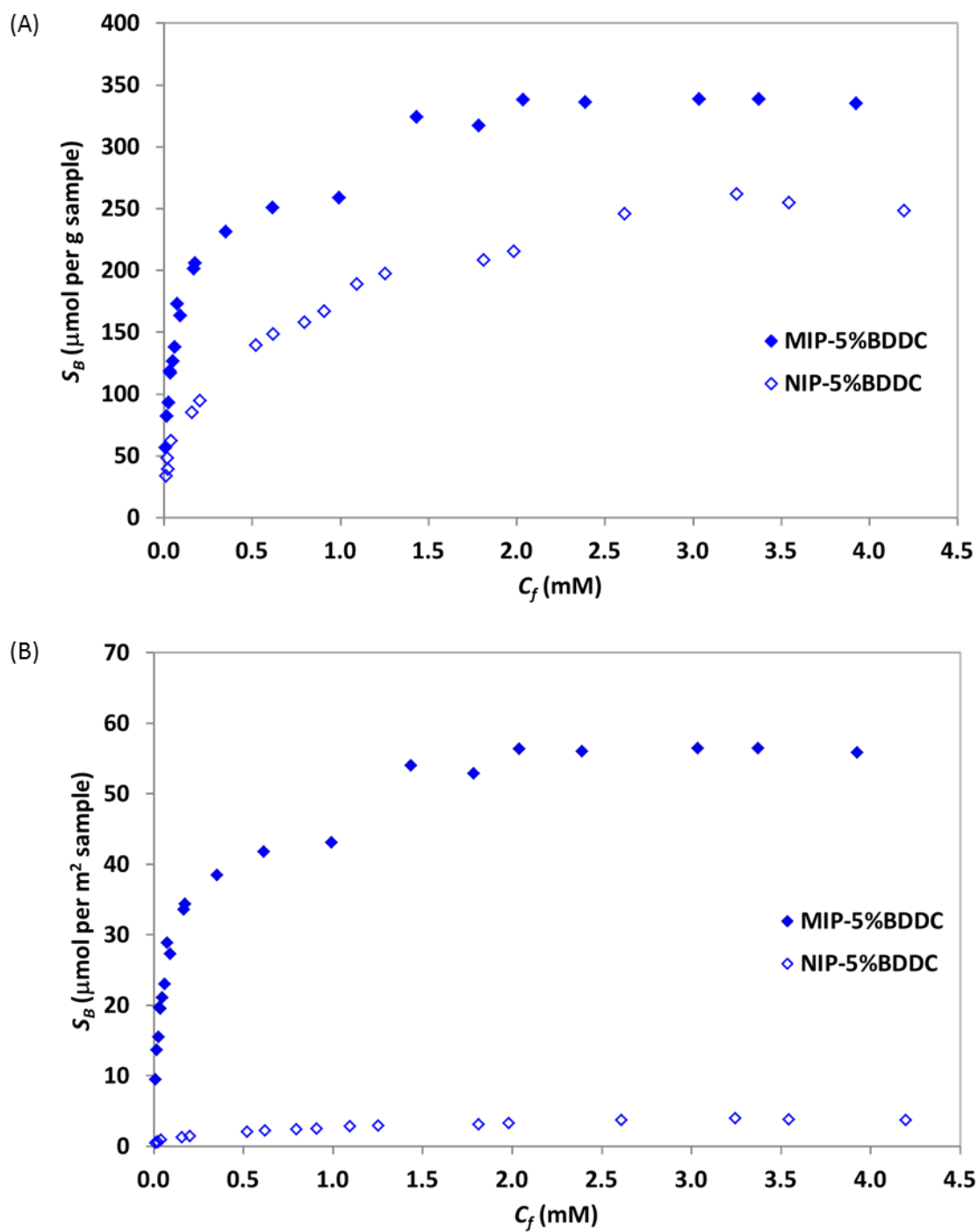


**Figure 4.12.** Binding isotherms for BZP imprinted polymers prepared using 5% BDDC and the control (NIP) carried out in acetonitrile normalised with respect to (A) mass and (B) surface area.

From the equilibrium binding isotherms (Figure 4.12), the maximum number of binding sites ( $N$ ) was determined by averaging the binding capacity values after a plateau was reached and the results are tabulated in Table 4.2. As can be seen in the table, the  $N$  values for MIP-5%BDDC normalised with respect to the mass and surface area were found to be 388  $\mu\text{mol/g}$  and 56  $\mu\text{mol/m}^2$ , respectively. These values are about 1.3 and 15-fold higher than those of the NIP counterpart (253  $\mu\text{mol/g}$  and 3.8  $\mu\text{mol/m}^2$ , respectively), indicating the presence of specific binding sites in the MIP.

**Table 4.2.** Equilibrium dissociation constant ( $K_d$ ) and maximum number of binding sites ( $N$ ) estimated from the binding isotherm (Figure 4.12), and derived from the Langmuir (Figure 4.13) and Scatchard (Figure 4.14) plots for the MIP and NIP prepared using 5% BDDC in acetonitrile.

Model	Polymer	$K_d$ (mM)		$N$ ( $\mu\text{mol/g}$ )		$N$ ( $\mu\text{mol/m}^2$ )	
		1 <sup>a</sup>	2 <sup>b</sup>	1 <sup>a</sup>	2 <sup>b</sup>	1 <sup>a</sup>	2 <sup>b</sup>
Binding isotherm	MIP-5%BDDC	N/A		338		56	
	NIP-5%BDDC	N/A		253		3.8	
Langmuir (Equation 4.4)	MIP-5%BDDC	0.111		346		58	
	NIP-5%BDDC	0.340		269		4.1	
Scatchard (Equation 4.5)	MIP-5%BDDC	0.041	0.268	249	369	42	62
	NIP-5%BDDC	0.029	0.498	106	280	1.6	4.2

<sup>a</sup> High affinity site.

<sup>b</sup> Low affinity site.

In this work, the binding isotherms have been subjected to linear transformation methods using Langmuir and Scatchard regressions according to Equations 4.4 and 4.5, respectively, to calculate  $N$  and  $K_d$ . These equations are well-known for their wide application in the field of molecular imprinting.<sup>288, 297-300</sup> The Langmuir is the simplest and more frequently used model in adsorption studies.<sup>295</sup> The Langmuir isotherm model is based on three assumptions: (1) all surface binding sites are equivalent and can accommodate one adsorbed template molecule, (2) the ability to bind at a given site for a template does not rely on the occupation of neighbouring sites and (3) adsorption cannot proceed beyond monolayer coverage.<sup>299</sup> It has been reported that

the Langmuir isotherm accounts very well for adsorption data acquired at low and moderate concentrations, but not at high concentrations.<sup>301</sup> This is because at higher concentrations, the activity coefficients of the analytes in solution are found to be concentration dependent and thus, deviations from the Langmuir model are observed.

Figure 4.13(A) shows the Langmuir plots for the MIP-5%BDDC and the corresponding NIP from the binding isotherm in Figure 4.12(A). The Langmuir isotherm was obtained by plotting  $C_f / S_B$  vs  $C_f$ , where the slope and the intercept can be used to calculate the maximum number of binding site ( $N$ ) and equilibrium binding constant ( $K$ ), respectively (§4.2.4). The correlation coefficient ( $R^2$ ) values are also included in the figure. A relatively high value of  $R^2$  indicates that the adsorption is successfully described by a particular model. The equilibrium dissociation constant ( $K_d$ ), was then calculated according to Eq. 4.6 and the resulting values are tabulated in Table 4.2. The smaller the  $K_d$  value, the greater the affinity of the polymer for the analyte. In Figure 4.13(A), the binding affinities are reported as amount of BZP bound per mass of the polymers. Taking into account the large difference in size of the MIP microspheres and the control, the Langmuir isotherm was also replotted as binding affinity per surface area of the polymer against the free analyte concentration, as shown in Figure 4.13(B). The  $N$  and  $K_d$  values were again calculated and the results are tabulated in Table 4.2.

As shown in Figure 4.13, it can be observed that good linearity was obtained for both the MIP-5%BDDC and NIP-5%BDDC ( $R^2 = 0.9971$  and  $0.9827$ , respectively) indicating that the Langmuir isotherms are a good fit of the experimental data. The  $N$  values calculated from the Langmuir isotherm plots (Figure 4.13(A)) showed that MIP-5%BDDC possessed about 30% higher maximum number of binding sites when normalised with respect to the mass of the polymer compared to that of the NIP (Table 4.2). The difference in the maximum number of binding sites was even greater when the  $N$  value was normalised with respect to the surface area of the polymer (Figure 4.13(B)), where the  $N$  value of the MIP was about 15-fold higher than that of the NIP. This was not surprising considering that the MIP contains both the specific and non-specific binding sites. Comparing the equilibrium dissociation constant of the

polymers, the MIP possessed a  $K_d$  value 3 times lower than that of the NIP ( $K_d = 0.111$  and  $0.340$  mM, respectively). The lower  $K_d$  value of the MIP means that it has higher affinity towards the BZP template compared to the NIP, which confirms the presence of specific binding sites for BZP in the MIP.

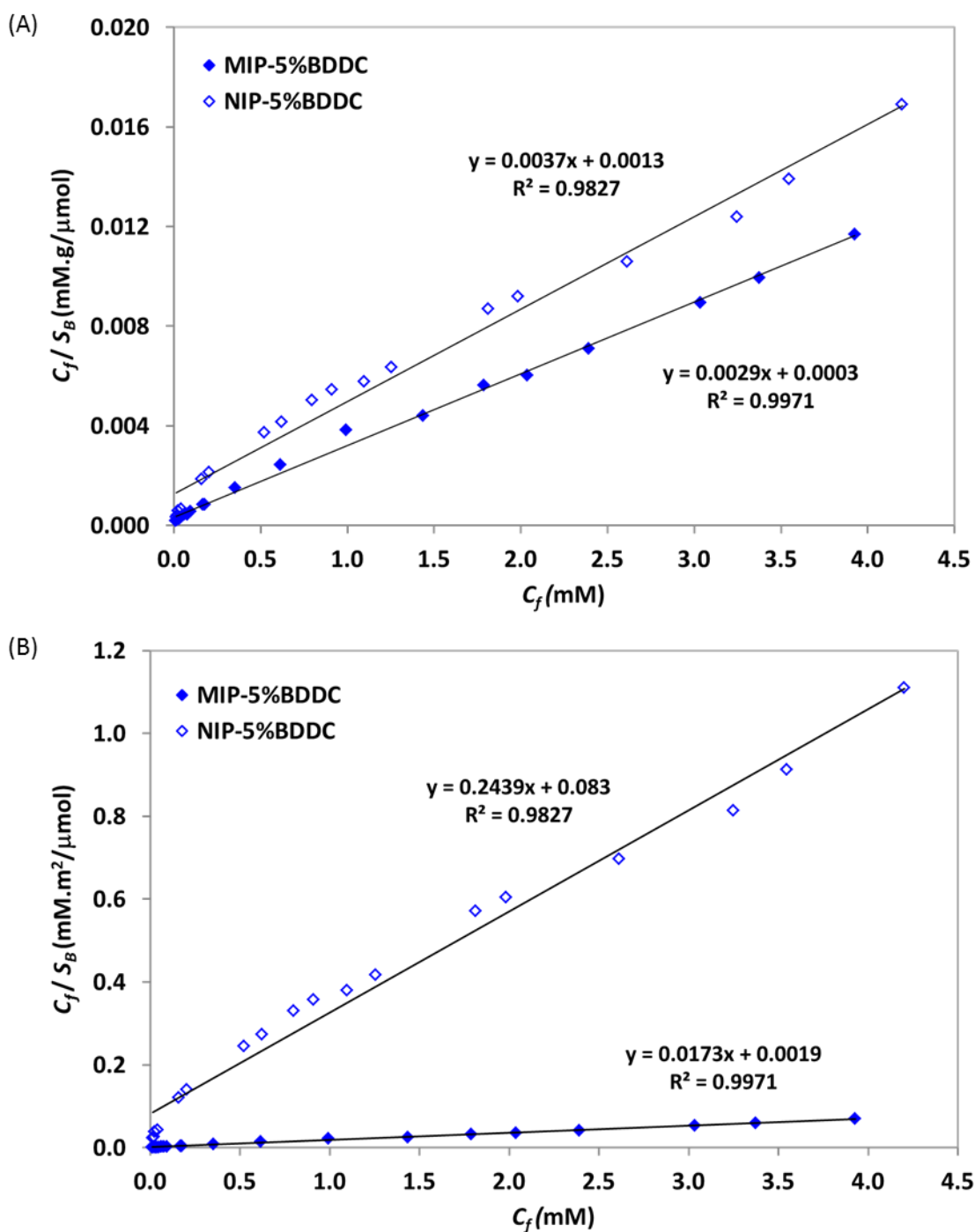


**Figure 4.13.** Langmuir plots for BZP imprinted polymers prepared using 5% BDDC and the control (NIP) normalised with respect to (A) mass and (B) surface area.

In a homogeneous system that contains only one type of binding site, the Scatchard plot, which is obtained by plotting  $S_B/C_f$  vs  $S_B$  should give a straight line where  $NK$  is the y-intercept and  $-K$  is the slope (Equation 4.5). The values of  $N$  and  $K_d$  can then be calculated from the slope and y-intercept. In many cases, the surface of the adsorbent is not homogeneous and different types of binding sites are present. If this is the case, a curve rather than a straight line is observed in the Scatchard plot, as evidenced in Figure 4.14. This curvature has been cited as evidence for binding site heterogeneity.<sup>295, 302</sup> Scatchard analysis can be used to accommodate this heterogeneity by modelling the curve as two separate straight lines. This limiting slopes method, also known as Bi-Langmuir, has been extensively used in the study of MIPs.<sup>288, 301, 302</sup> This method yields two separate sets of binding parameters for two types of sites in which the steeper lines characterise the high affinity sites whereas the gentle slope line characterises the low affinity sites, as usually observed for MIPs prepared using the noncovalent approach.<sup>161, 275, 303, 304</sup> Employing the limiting slopes method to the Scatchard plots in Figure 4.14 resulted in two sets of maximum binding sites ( $N$ ) and equilibrium dissociation constants ( $K_d$ ) and the values are also tabulated in Table 4.2.

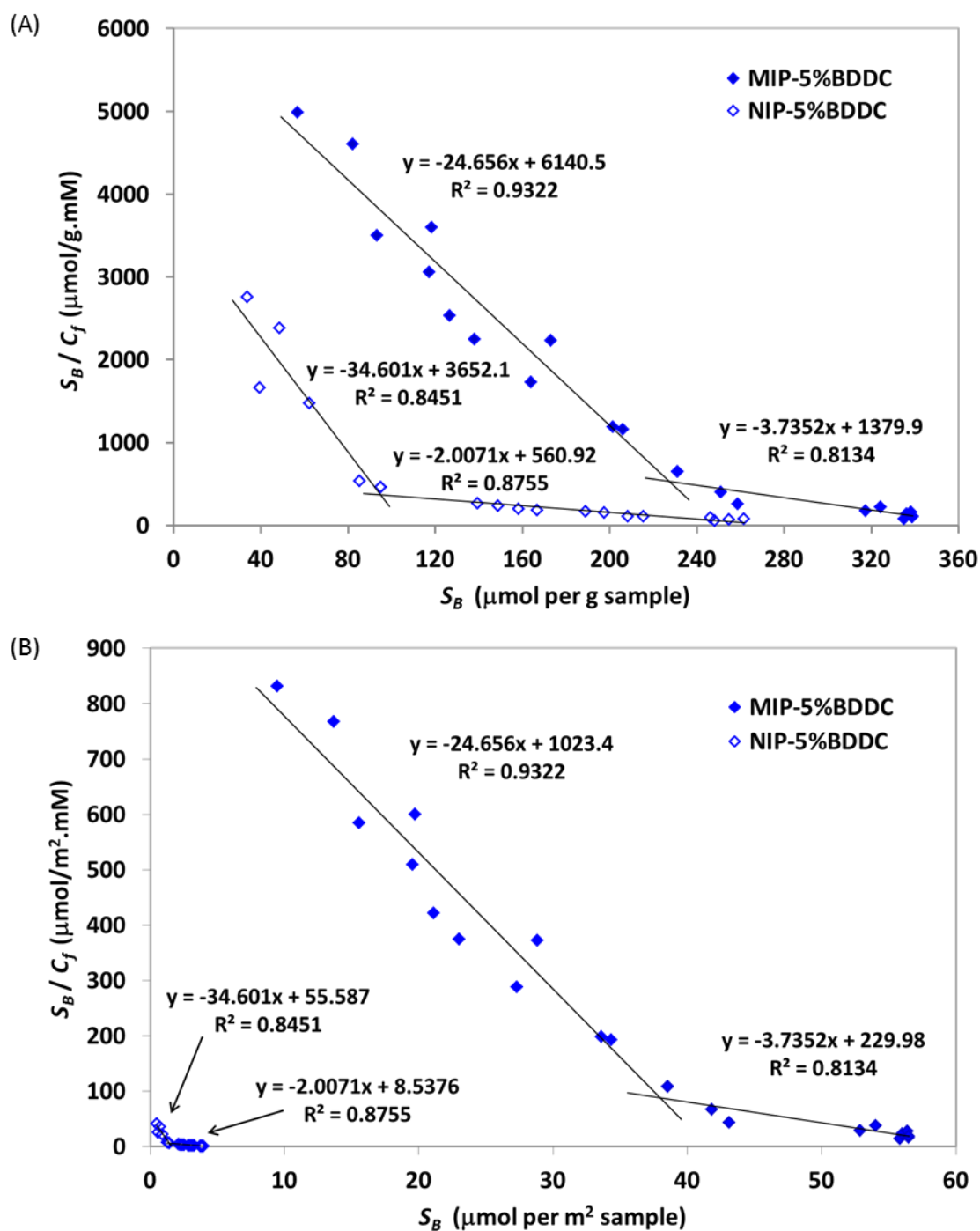


**Figure 4.14.** Scatchard plots for BZP imprinted polymers prepared using 5% BDDC and the control (NIP) normalised with respect to (A) mass and (B) surface area.

The Scatchard plots (Figure 4.14) give two sets of  $N$  and  $K_d$  values (Table 4.2) for both the MIP and NIP, which indicates that two types of binding sites are present (i.e. low and high affinity sites) in both microspheres. From Table 4.2, it can be seen that MIP-5%BDDC contained about 1.5-fold higher number of low affinity sites compared to the

high affinity sites. This is in agreement with the previous studies on MIP binding sites which proved that MIPs typically contain a high number of non-selective binding sites in comparison to the needed high affinity sites.<sup>305</sup> It can also be observed that the number of both the high and low affinity sites of the MIP was higher compared to that of the NIP. The  $N$  values of the high affinity sites of the MIP normalised with respect to the sample mass and surface area (249  $\mu\text{mol/g}$  and 42  $\mu\text{mol/m}^2$ , respectively) are about 2.5-fold and 20-fold higher than those of the NIP (106  $\mu\text{mol/g}$  and 1.6  $\mu\text{mol/m}^2$ , respectively.) As for the low affinity sites, the MIP exhibited about 1.5-fold and 15-fold higher number of low affinity sites (compared to that of the NIP when normalised with respect to the sample mass and surface area, respectively. The ratio of the  $N$  value of the high affinity to the low affinity sites of the MIP is about 2-fold higher than that of the NIP (0.7 and 0.4, respectively), indicating the presence of an imprinting effect. Compared to the Langmuir plots, the correlation coefficients of both the MIP and NIP for the Scatchard plots are much lower indicating a poorer fit for the latter compared to the former.

As can be seen in Table 4.2, the  $K_d$  value of the low affinity sites for the MIP obtained from the Scatchard isotherm is about 45% lower than that of the corresponding NIP (0.268 and 0.498 mM, respectively). This means that the former has a stronger affinity towards the BZP template at these low affinity sites compared to the latter. The imprinting binding sites in the MIP can be partial or within the bulk, which are associated with the low and high affinity binding sites, respectively, as shown in Figure 4.14. The partial imprinting sites in the MIP are more accessible to the BZP template, thus could be responsible for its stronger affinity for the template molecules at these sites. However, a contradictory result was obtained for the high affinity sites, where the  $K_d$  value is about 30% lower for the NIP compared to that of the MIP (0.029 and 0.041 mM, respectively), which indicates that the NIP has stronger affinity towards the BZP template at these high affinity sites. This could be attributed to the difference in the pore size distribution of the polymers (Figure 4.7), where the NIP contains quite a large fraction of pores in the lower range of the mesoporous region (2 – 10 nm pore width), as opposed to the MIP where none of the pores were in that size range,

although a small fraction of pores existed in the micropore region (1.5 - 2 nm pore width). Considering the small size of the BZP template molecule (0.5 x 1.0 nm, Figure 4.4) the presence of a higher fraction of pores in the mesoporous region allows easy access for the template, and thus resulted in the higher binding affinity of the NIP for BZP compared to the MIP in the high affinity sites. However, despite the stronger affinity shown by the NIP towards BZP at the high affinity sites, only a small portion of BZP was bound compared to the MIP in these high affinity binding sites. Furthermore, this stronger affinity of NIP towards BZP occurred at very low concentrations of BZP, which indicates superficial binding.

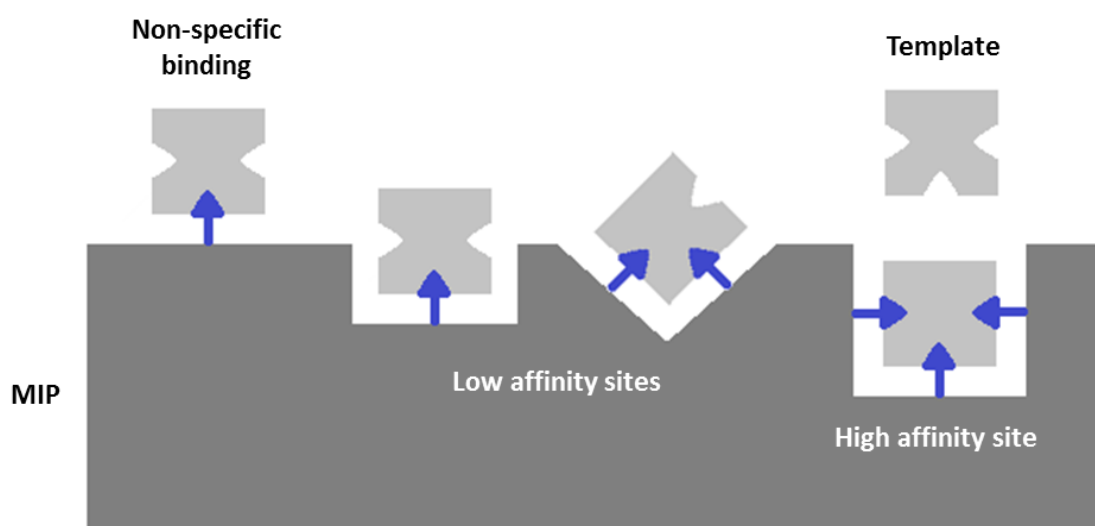


**Figure 4.15.** Types of binding sites in the MIP microspheres.

#### 4.3.2.2.3 Effect of Iniferter Concentration

To study the effect of iniferter concentration on the binding performance of BZP imprinted polymers, batch rebinding experiments were also carried out on MIP-10%BDDC and MIP-20%BDDC as well as their corresponding NIPs at 2 hr contact time. Both acetonitrile and THF were used as the rebinding solvents and the results are compared with those of the MIP-5%BDDC and its NIP counterpart as shown in Table 4.3.

**Table 4.3.** BZP binding affinity ( $S_B$ ), specific binding ( $\Delta S_B$ ) and imprinting factor (IF) values of microspheres prepared using 5%, 10% and 20% BDDC after 2 hr of contact time in acetonitrile and THF.

Polymers	DC (%) <sup>a</sup>	Acetonitrile						THF					
		Mass			Surface Area			Mass			Surface Area		
		$S_B^b$ ( $\mu\text{mol per g sample}$ )	$\Delta S_B$	IF	$S_B^c$ ( $\mu\text{mol per m}^2 \text{ sample}$ )	$\Delta S_B$	IF	$S_B^b$ ( $\mu\text{mol per g sample}$ )	$\Delta S_B$	IF	$S_B^c$ ( $\mu\text{mol per m}^2 \text{ sample}$ )	$\Delta S_B$	IF
MIP-5%BDDC	60	$188 \pm 2$	$47 \pm 4$	1.3	$31.3 \pm 0.3$	$29 \pm 0.3$	15	$39 \pm 2$	$10 \pm 2$	1.3	$6.5 \pm 0.4$	$6.1 \pm 0.4$	15
NIP-5%BDDC	48	$141 \pm 4$			$2.1 \pm 0.1$			$29 \pm 1$			$0.43 \pm 0.01$		
MIP-10%BDDC	60	$190 \pm 2$	$48 \pm 3$	1.3	$19.2 \pm 0.2$	$17 \pm 0.2$	8.1	$31 \pm 1$	$5 \pm 1$	1.2	$3.1 \pm 0.1$	$2.7 \pm 0.1$	7.2
NIP-10%BDDC	53	$142 \pm 2$			$2.4 \pm 0.1$			$26 \pm 1$			$0.43 \pm 0.02$		
MIP-20%BDDC	68	$194 \pm 3$	$1 \pm 4$	1.0	$25.5 \pm 0.4$	$22 \pm 0.4$	7.4	$31 \pm 1$	$-5 \pm 1$	0.9	$4.1 \pm 0.1$	$3.5 \pm 0.1$	6.3
NIP-20%BDDC	67	$193 \pm 3$			$3.4 \pm 0.1$			$36 \pm 1$			$0.65 \pm 0.01$		

<sup>a</sup> Extent of C=C bond conversion of the EGDMA, DC (%), calculated according to the following equation (Equation 4.1) :

$$\text{DC (\%)} = 100 \times \left[ 1 - \frac{(A_{C=C}/A_{C=O})_{\text{polymer}}}{(A_{C=C}/A_{C=O})_{\text{monomer}}} \right]$$

where DC (%) represents the extent of C=C bond conversion of the EGDMA whereas  $A_{(C=C)}$  and  $A_{(C=O)}$  are the FTIR absorbance values of C=C and C=O, respectively. This value is used to estimate the degree of crosslinking of the polymer in order to investigate the relationship between crosslinking density and the binding performance of the polymer.

<sup>b</sup> Actual experimental result.

<sup>c</sup> Calculated using the experimental BET specific surface areas of the polymers.

From Table 4.3, when the binding affinity was normalised with respect to the mass of the polymer, it can be seen that all the MIPs exhibited comparable BZP binding capacity in acetonitrile. As for the NIPs, in contrast to the NIP-5% and -10%BDDC, which exhibited similar amount of BZP bound, the NIP-20%BDDC showed a much higher BZP binding capacity (about 35% higher), which was as high as its MIP counterpart. As a result, the specific binding was comparable for the MIP-5% and -10%BDDC ( $\Delta S_B \approx 50 \mu\text{mol per g sample}$ ), resulting in similar IF values (IF = 1.3). On the other hand, no difference in binding capacity is observed between the MIP-20%BDDC and its NIP counterpart, resulting in an IF of 1.0.

The binding affinity normalised with respect to the surface area should give a more useful comparison considering the big difference in the particle size of the MIP and NIP microspheres. As shown in Table 4.3, the BZP binding affinity of the NIP microspheres increased with increasing amount of BDDC iniferter when rebinding was carried out in acetonitrile. However, a different trend is observed for the MIP microspheres, whereby both MIP-10%BDDC and MIP-20%BDDC exhibited lower binding affinity (about 40% and 20% lower) compared to that of the MIP-5%BDDC. This has resulted in the highest specific binding for ( $\Delta S_B = 29 \pm 0.3 \mu\text{mol per m}^2 \text{ sample}$ ), whilst the lowest specific binding was exhibited by the MIP-10%BDDC ( $\Delta S_B = 17 \pm 0.2 \mu\text{mol per m}^2 \text{ sample}$ ). However, a slightly different trend is observed in the imprinting factor value. As can be seen from Table 4.3, MIP-5%BDDC exhibited the highest IF value (IF = 15). Although the binding affinity value of MIP-20%BDDC was about 30% higher than that of the MIP-10%BDDC ( $25.5 \pm 0.4$  and  $19.2 \pm 0.2 \mu\text{mol per m}^2 \text{ sample}$ , respectively), the NIP counterpart of the former bound even higher amount of BZP (about 40% higher) compared to that of the latter ( $3.4 \pm 0.1$  and  $2.4 \pm 0.1 \mu\text{mol per m}^2 \text{ sample}$ , respectively). As a result, both MIP-10% and -20%BDDC exhibited comparable IF values (IF  $\approx$  8). It can be concluded that among the formulations, MIP-5%BDDC exhibited the highest specific binding as well as the highest imprinting factor normalised with respect to the surface area.

When rebinding was carried out in THF, almost the same trend as in acetonitrile was observed for the NIP, where the highest binding affinity normalised with respect to the mass was exhibited by NIP-20%BDDC (Table 4.3). However, the NIP-10%BDDC exhibited slightly lower binding affinity (about 10% lower) than that of the NIP-5%BDDC. In contrast, the MIP-5%BDDC exhibited the highest binding affinity compared to those of the MIP-10 and 20%-BDDC, which exhibited similar binding affinity. As a result, MIP-5%BDDC exhibited the highest specific binding, followed by MIP-10%BDDC ( $\Delta S_B = 10 \pm 2$  and  $5 \pm 1$   $\mu\text{mol per g polymer}$ , respectively) whereas MIP-20%BDDC exhibited negative specific binding ( $\Delta S_B = -5 \pm 1$   $\mu\text{mol per g polymer}$ ) since its NIP counterpart bound a higher amount of BZP compared to the MIP-20%BDDC. This in turn resulted in comparable IF values for the MIP-5%BDDC and MIP-10%BDDC whilst the MIP-20%BDDC exhibited the lowest IF value. On the other hand, the binding affinity normalised with respect to the surface area in THF showed almost a similar trend as that in acetonitrile (Table 4.3). From Table 4.3, it can be observed that the MIP-10%BDDC and MIP-20%BDDC exhibited lower binding affinity (about 55% and 35% lower, respectively) compared to that of the MIP-5%BDDC. As for the NIP microspheres, the highest specific binding was exhibited by the NIP-20%BDDC ( $0.65 \pm 0.01$   $\mu\text{mol per m}^2$  sample) whereas the NIP-5%BDDC and NIP-10%BDDC bound similar amount of BZP ( $0.43 \pm 0.01$   $\mu\text{mol per m}^2$  sample). As a result, the MIP-5%BDDC exhibited the greatest specific binding whilst the lowest specific binding was exhibited by the MIP-10%BDDC ( $6.1 \pm 0.4$  and  $2.7 \pm 0.1$   $\mu\text{mol per m}^2$  sample, respectively). The same trend as that in acetonitrile was also observed for the IF values of the polymers in THF. The highest IF value (IF = 15.0) was also exhibited by the MIP-5%BDDC whilst the IF values of MIP-10% and -20%BDDC are almost similar (IF  $\approx$  7). Not only that, these values were comparable to the IF values obtained when the rebinding was carried out in acetonitrile. The result indicates that MIP-5%BDDC showed better selectivity towards the BZP template compared to MIP-10% and -20%BDDC.

The difference in the binding affinity of the polymers could be attributed to the different in the degree of crosslinking of the MIP and NIP microspheres prepared using different amount of initiator. As mentioned previously, the nucleus formation in

precipitation polymerisation is attributed to the crosslinked polymer having a chain length larger than the critical limit of solubility in the reaction medium. Increasing the amount of iniferter resulted in the formation of higher number oligomer radicals with shorter chain lengths (low molecular weight). As these short oligomers are more soluble in the continuous phase, only a lower amount of lightly crosslinked oligomers are formed during the nucleation step. These primary particles continue to grow by adsorption of new oligomers and monomers onto the particle surface to form the final microspheres with bigger final diameters. Hence, microspheres prepared using 20% BDDC are expected to consist of a higher number of shorter linear chains between the crosslinked networks than the microspheres prepared using 5 and 10% BDDC. This will affect the crosslinking density of the polymers, which might in turn influence their binding properties. To investigate the relation between crosslinking density of the microsphere network and the binding performance, these properties are compared between the MIPs and their NIP counterparts.

As shown in Table 4.3, the degree of crosslinking of the NIP microspheres was found to increase with increasing amount of iniferter. The reason for this could be attributed to the faster rates of initiation and polymerisation as the iniferter concentration is increased, which resulted in higher maximum double bond conversion.<sup>306</sup> It is interesting to note that the binding affinity of the NIPs was somewhat enhanced in the presence of higher crosslinking density, despite the lower surface area of the polymers (Table 4.1). This could be attributed to the presence of larger amount of pendant non-crosslinked EGDMA in the lower crosslinked NIP, which are most probably distributed at the surface of the microsphere and hindered the BZP template from approaching MAA. However, a slightly different trend was observed for the MIPs, indicating a different behaviour in the presence of the template. From Table 4.3, it can be observed that the MIP-20%BDDC exhibited a higher degree of crosslinking (about 13% higher) compared to that of the MIP-5%BDDC and MIP-10%BDDC, which exhibited similar degree of crosslinking (DC = 68 and 60%, respectively). This indicates that both the MIP-5%BDDC and MIP-10%BDDC were less crosslinked and thus were more flexible than MIP-20%BDDC. It is interesting to note that the MIP-5%BDDC exhibited greater

specific binding with respect to the surface area in acetonitrile than the MIP-10%BDDC (about 40% higher), albeit having similar crosslinking density, whilst the MIP-20%BDDC, which was more crosslinked than both the MIP-5%BDDC and -10%BDDC, exhibited lower specific binding than that of the MIP-5%BDDC (about 25% lower) but higher specific binding (about 30% higher) compared to that of the MIP-10%BDDC. It can also be noticed that both the MIP-10%BDDC and -20%BDDC exhibited almost similar IF values despite the different in their degree of crosslinking. The result suggests that carrying the polymerisation reaction in the presence of the BZP template somehow resulted in a slightly different behaviour compared to when no template was added. Higher crosslinking density was found to enhance the binding performance of the NIPs, whereas no specific trend was observed for the MIPs.

#### 4.3.2.2.4 Effect of solvent

To investigate the effect of rebinding solvent on the binding performance of the polymers, the binding parameters of MIP-5%BDDC and its NIP counterpart from Table 4.3 are compared, as shown in Figure 4.16.

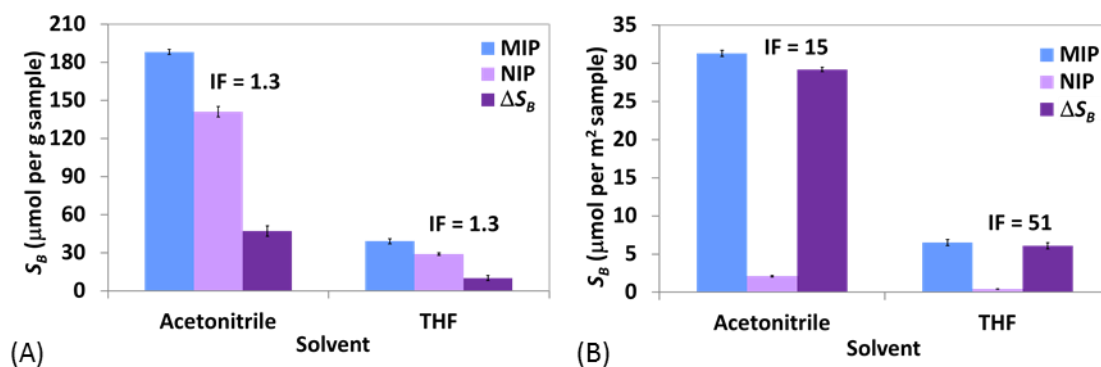


**Figure 4.16.** Comparison between the binding capacity of MIP microspheres prepared via iniferter in acetonitrile and THF normalised with respect to (A) mass and (B) surface area.

From Table 4.3 and Figure 4.16, it can be seen that the amount of BZP bound normalised with respect to either the mass or surface area of the polymers for both the MIP microsphere and the control (NIP) was about 5-fold higher in acetonitrile

compared to that in THF. This difference in the binding capacity values of both polymers in different rebinding solvents indicates a strong solvent effect. It can be observed that the IF values of the MIP in both solvents are much higher (about 11-fold higher) when the binding capacity was normalised with respect to the surface area compared to the mass. From Table 4.3, it can also be seen that although comparable IF values were observed in both solvents, the specific binding of the MIP was found to be about 5-fold higher in acetonitrile compared to that in THF. The result showed that better discrimination between the MIP and NIP was achieved when rebinding was carried out in acetonitrile, which was the solvent used during imprinting compared to that in THF. This result is in agreement with the general observations that MIPs offer the highest selectivity when samples are dispersed in the solvent used during the MIP preparation (porogen).<sup>139, 275, 307-309</sup>

The existing literature suggests several reasons for this behaviour. Firstly, the polarity of the solvent has been reported to have an influence in the binding properties of the MIPs.<sup>297, 298, 310</sup> A higher polarity solvent competes more efficiently with the template for binding of the functional groups of the recognition sites in the polymer and therefore weakens the specific interaction. When the predominant rebinding interaction between the template and the MIP was hydrogen bonding, it was found that the lower the polarity of the solvent, the higher the selectivity and affinity of the MIP.<sup>310, 311</sup> The MIP contains specific cavities created by imprinting as well as nonspecific binding sites, which was attributed to the functional groups on the polymer backbone. During rebinding, a highly polar solvent which has the tendency to form hydrogen bonds can compete for the hydrogen binding sites on the template molecules as well as both the specific and nonspecific binding sites of the polymers, thus weakening the interaction between the template and the binding sites.<sup>138, 312</sup> Interestingly, although acetonitrile is more polar than THF, the binding affinity of the polymers is higher in the former. This shows that an increased solvent polarity does not necessarily lead to a decrease in recognition, as observed by some researchers.<sup>313,</sup>

314

It was reported that the nature of the solvent employed during the rebinding step can influence the relative swelling of the polymer.<sup>308</sup> Depending on the type of solvent used in rebinding, an increase in size (diameter) was observed during the rebinding of MIP particles prepared by bulk polymerisation.<sup>315</sup> The effect of solvent identity on the recognition properties of molecular imprinted polymers was studied by Turner *et al.* and the result suggested that the polymer may undergo conformational modifications affected by the changes in solvent, which led to disruption of binding due to changes in the size and shape of the template-complementary binding pockets.<sup>275, 315</sup> Swelling can affect the shape and distance between functional groups of the recognition sites in the polymer, thus causing the MIP to lose its specificity. This is, however, not true in our case, since the binding capacity in different solvents was altered in not only the MIP but the NIP as well.

Another possible reason is that THF has a stronger hydrogen bond capacity than acetonitrile and can interact by forming hydrogen bonds with the amine and carboxylic acid of BZP and MAA, respectively.<sup>316, 317</sup> Therefore, it may more strongly interfere with the binding interaction between the BZP template and MAA functional monomer in the polymer, which leads to a decrease in the amount of BZP bound by the polymers. Previous study has proven the existence of the correlation between the hydrogen bonding capacity of the solvent and the polymer selectivity,<sup>317</sup> which could very well explain the reduction in the binding capacity when using THF as the rebinding solvent. Among the above possible reasons, it is more likely that the better hydrogen bonding capability of THF is one of the factors that may contribute to the lower binding capacities of both the MIP and NIP in that solvent compared to those in acetonitrile. In addition, conducting the rebinding studies in the same solvent as the porogen used during polymerisation might account for the higher binding capacity of the polymers in acetonitrile by providing a microenvironment that would mimic the interactions existing prior to and during the polymerisation.<sup>314</sup>

### 4.3.3 Molecular imprinted Polymers by RAFT

The RAFT method using MCEBTTC has already been discussed in Chapter 3. In this work, MCEBTTC is again used as the RAFT agent for the synthesis of BZP MIP microspheres using the non-covalent imprinting approach. The polymerisation was carried out thermally at 60 °C (§4.2.2.2) and template removal was performed using a similar procedure of Soxhlet extraction as used with the BDDC MIPs (§4.2.3).

#### 4.3.3.1 Synthesis and Physical Characterisation

While MCEBTTC RAFT agent has been used to synthesise linear polymers such as poly(*N*-isopropylacrylamide) (PNIPAM) for the preparation of polymer nanoparticles (PNPs) via miniemulsion polymerisation by the group of Monteiro,<sup>318, 319</sup> MIP microspheres prepared using MCEBTTC has not been reported. In this work, three different formulations of MIP microspheres were prepared by varying the amount of RAFT agent (MCEBTTC) with respect to the total amount of EGDMA and MAA monomers. Maintaining the same mole ratios of RAFT agent to monomers as in the iniferter polymerisation, the MIP microspheres were prepared using 5 mol %, 10 mol % and 20 mol % RAFT with respect to EGDMA and MAA monomers at 1:1 BZP:MAA mol ratio in acetonitrile. 1% of AIBN was also added to the polymerisation mixture to generate the initiating radicals. The corresponding NIP microspheres were prepared using the same formulations but in the absence of BZP template.

The SEM images of all the MIP microspheres prepared using the MCEBTTC RAFT agent and their corresponding NIPs are shown in Figure 4.17. The average particle diameter and the hydrodynamic size of the polymers were determined by SEM and DLS, respectively and the results are tabulated in Table 4.4.

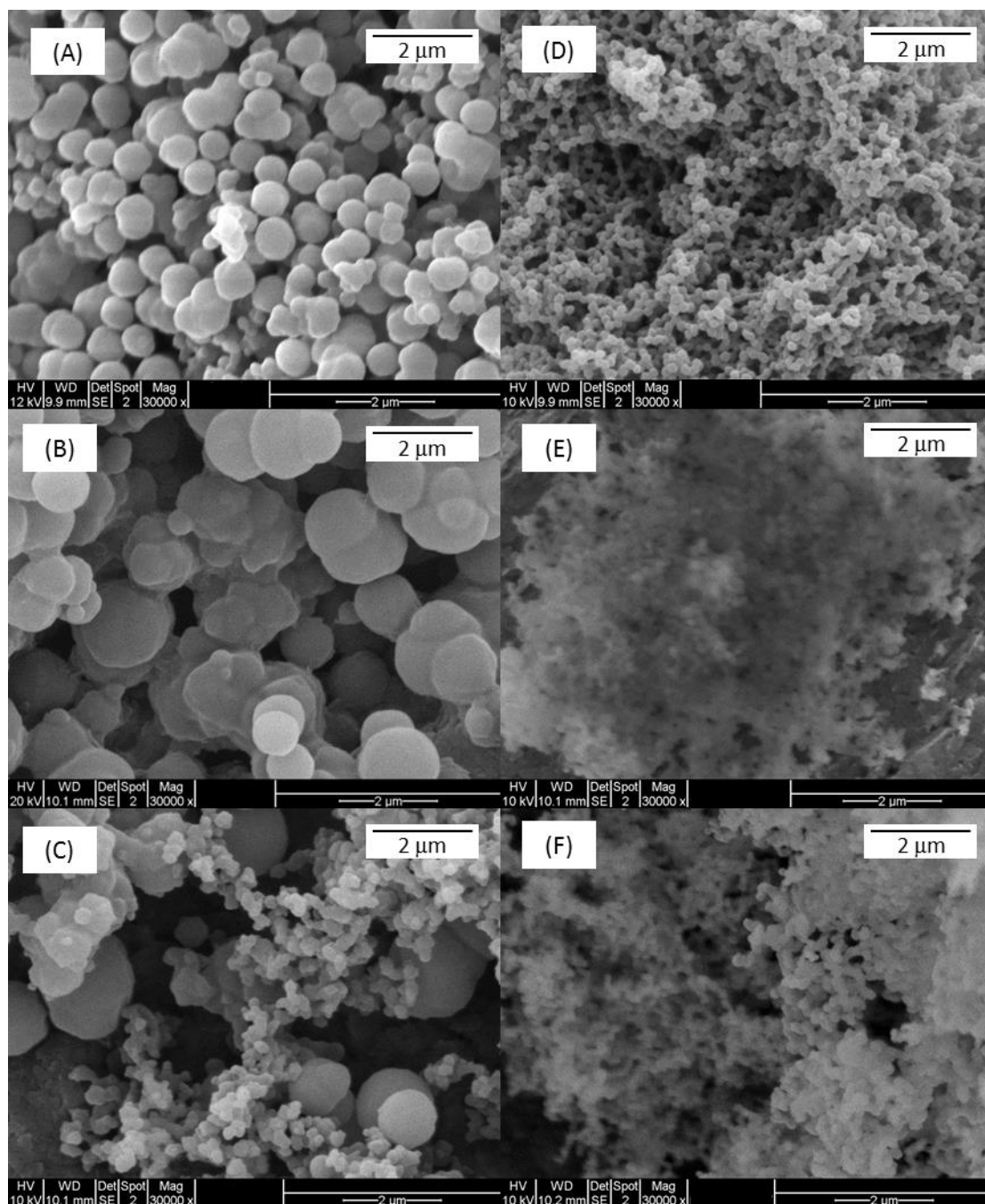


**Figure 4.17.** SEM images of MIP microspheres prepared using various amount of MCEBTTc RAFT agent i.e. (A) 5 mol %, (B) 10 mol % and (C) 20 mol % and their corresponding NIP microspheres (D), (E) and (F), respectively. All the images were recorded at 30000X magnification.

**Table 4.4.** Physical characteristics of the BZP-imprinted polymer microspheres and the corresponding NIPs prepared by precipitation polymerisation using RAFT agent.

Microspheres	Yield (%)	SEM average diameter (nm)	$D_h$ (DLS) (nm) <sup>a</sup>	BET specific surface area <sup>b</sup> (m <sup>2</sup> /g)	Estimated surface area of average particle <sup>c</sup> (m <sup>2</sup> x 10 <sup>-13</sup> )	Estimated specific surface area (m <sup>2</sup> /g)
MIP-5% RAFT	25	290 ± 50 740 ± 70	N/A	9.0 ± 0.1	2.6 ± 0.9 17 ± 3	N/A
NIP-5% RAFT	58	160 ± 20	140 ± 20	226 ± 2	0.6 ± 0.9	N/A
MIP-10% RAFT	27	510 ± 70 1000 ± 120 1570 ± 150	N/A	N/A	8 ± 2 31 ± 8 77 ± 15	11 ± 5 <sup>d</sup>
NIP-10% RAFT	77	150 ± 20	165 ± 30	N/A	0.9 ± 0.3	226 ± 2 <sup>e</sup>
MIP-20% RAFT	44	350 ± 60 650 ± 90 1910 ± 260	N/A	N/A	3.8 ± 1.3 13 ± 4 115 ± 31	23 ± 13 <sup>d</sup>
NIP-20% RAFT	90	160 ± 20	120 ± 10	N/A	0.45 ± 0.07	226 ± 2 <sup>e</sup>

<sup>a</sup> Measured in THF at 20°C.

<sup>b</sup> Determined by nitrogen adsorption porosimetry.

<sup>c</sup> Calculated using the formula of a sphere =  $4\pi r^2$ , where  $r$  is the radius of the sphere.

<sup>d</sup> Estimated from  $a$  as well as BET surface area and mean value of estimated surface area of average particle of MIP-5%RAFT ( $b$  and  $c$  respectively) assuming the same density, porosity and PSD as the MIP-5%RAFT. Only the smallest value of estimated surface area of average particle was considered since the majority of the particles were of this size.

<sup>e</sup> Estimated to be the same as the specific surface area of NIP-5%RAFT ( $b$ ) based on their comparable  $D_h$  values ( $a$ ) and assuming that they have the same density, porosity and PSD.

NA – not available (all the MIP dispersions in THF were unstable against sedimentation).

As shown by the SEM images in Figure 4.17, the NIP microspheres consist of globular particles of about equal sizes, regardless of the concentration of RAFT agent used during the polymerisation. This result is in contrast to the results obtained by other researchers, where the particle size of microspheres prepared via precipitation polymerisation was found to increase with increasing concentration of initiator or

iniferter.<sup>161, 290, 320</sup> The reason for this could be attributed to the concentration of AIBN initiator used in the formulations. Since the ratio of RAFT agent to AIBN was fixed at 1:0.01, therefore when the concentration of RAFT agent was increased, the concentration of AIBN was also increased to maintain the same RAFT agent to AIBN ratio. The effect of increasing the amount of AIBN might have compensated the effect of increasing the concentration of the RAFT agent, resulting in an almost similar size of NIP microspheres.

On the other hand, the MIP microspheres obtained using different concentrations of RAFT are irregular and consist of particles with a broad size distribution, which is consistent with the polydisperse MIP microspheres obtained by Pan and coworkers via RAFT precipitation polymerisation, albeit their spherical shape.<sup>165</sup> For the MIP-5%RAFT, two different sizes of particles of equal amount and quite globular shape are formed. Increasing the amount of RAFT agent resulted in higher polydispersity as particles of much bigger size with a less circular shape are formed, in conjunction with the smaller sized particles. The difference in size, shape and uniformity between the MIP and NIP microspheres clearly shows that the template played a major role on the final particle size of the MIPs. The presence of the BZP template clearly influenced the formation and growth of the particle nuclei in the solution. As can be seen in Table 4.4, both the MIP and NIP microspheres showed a similar trend when it comes to the rate of polymerisation, where the yield of both MIP and NIP microspheres increases with increasing amount of RAFT agent. This result is in agreement with the results of previous studies,<sup>290, 320, 321</sup> where an increase in the monomer conversion was reported at higher concentration of initiator in precipitation polymerisation. In our case, the increase in both the RAFT agent as well as the AIBN initiator could have caused the acceleration in the polymerization rates.

Similar to the microspheres prepared via BDDC, the microspheres prepared using RAFT were sent for pore size distribution and BET specific surface area analysis by nitrogen adsorption porosimetry. However, only the BET specific surface and pore size distribution of the MIP-5%RAFT and its corresponding NIP microsphere could be

obtained because the MIP-10%RAFT and MIP-20%RAFT as well as their NIP counterpart samples were not able to be sufficiently degassed to enable this measurement. The BET specific surface and pore size distribution of the MIP-5%RAFT and NIP-5%RAFT are tabulated in Table 4.4 and shown in Figure 4.18, respectively. The BET specific surface area of MIP-5%RAFT was used to estimate the specific surface area of the MIP-10%RAFT and MIP-20%RAFT. This was done by first estimating the surface area of an average particle of the MIPs and NIPs from their SEM average diameter and hydrodynamic diameter respectively. The specific surface area of the polymer (e.g. MIP-10%RAFT) was then estimated by dividing the BET specific surface area of the MIP-5%RAFT with the ratio of the surface area of average particle of the former to the mean surface area of average particle of the latter. Only the smallest SEM average diameter was taken into account when performing the calculation since the majority of particles were of this size. On the other hand, specific surface areas of NIP-10%RAFT and NIP-20%RAFT were assumed to be similar to the measured specific surface area of NIP-5%RAFT due to their almost comparable hydrodynamic diameters. The calculation of specific surface area was carried out assuming that the 10 and 20% RAFT MIPs and NIPs have the same density, porosity and particle size distribution as the 5% RAFT MIP and NIP respectively.

From Table 4.4, it can be seen that the MIP-5%RAFT exhibited a small measured specific surface area ( $9 \text{ m}^2/\text{g}$ ), which is in agreement with the previous results obtained for microspheres prepared via precipitation in pure acetonitrile.<sup>284, 292</sup> It can also be observed that the specific surface area of the NIP-5%RAFT ( $226 \text{ m}^2/\text{g}$ ) is about 25-fold higher than that of the MIP-5%RAFT, which is expected based on the smaller particle size of the NIP compared to the MIP. The estimated specific surface areas of MIP-10% and -20%RAFT microspheres were about 1.5- and 3-fold higher than the BET specific surface area of MIP-5%RAFT, respectively, indicating that the specific surface area of the MIPs increases with increasing amount of RAFT agent. The NIPs on the other hand, were estimated to exhibit similar specific surface area based on their comparable hydrodynamic diameter values.

From Figure 4.18, it can be observed that NIP-5%RAFT is more porous than MIP-5%RAFT, having pores in the micropore as well as mesopore regions, with average pore widths of 0.6, 1.2, 3.2, 5 and 11.7 nm. On the other hand, the MIP-5%RAFT contains pores in the mesopore region only, with average pore widths of 5 and 13.7 nm. This means that the BZP molecules having 0.5 nm and 1.0 nm in diameter and length, respectively, would have greater access to the more porous NIP, which contains both the micropores and mesopores in larger proportion compared to the MIP. Note that no comparison can be made between the porosity of the MIP and NIP microspheres prepared using 10% and 20% BDDC, respectively, since the pore size distribution of the samples could not be obtained.

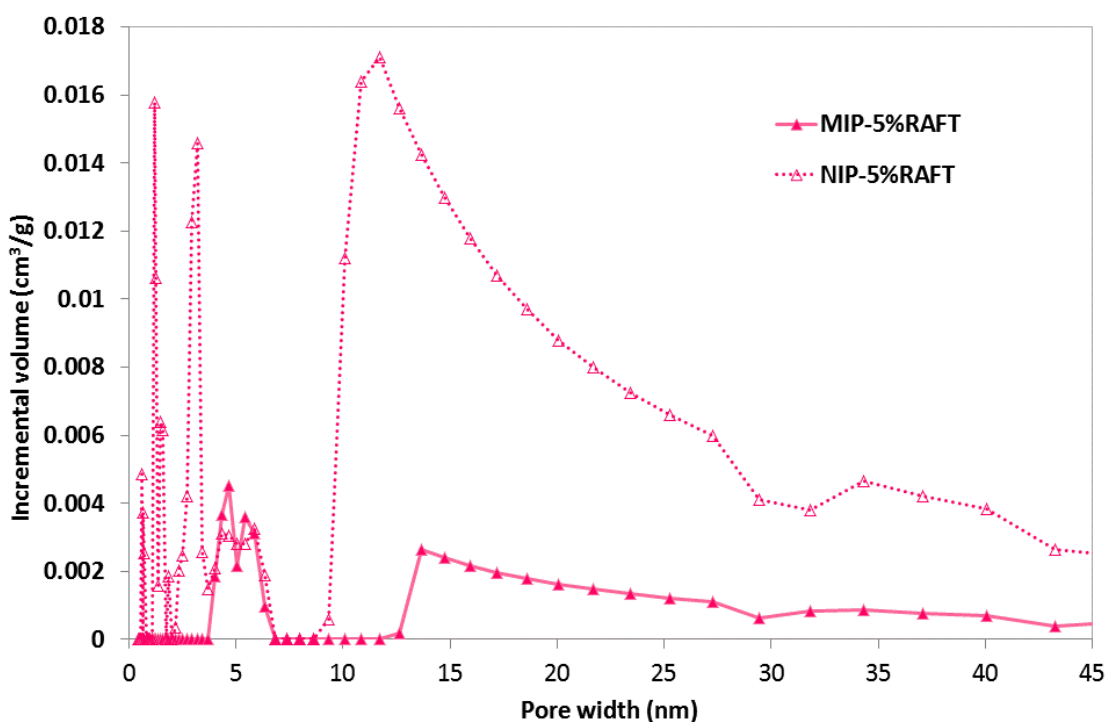


**Figure 4.18.** Incremental pore volume versus pore width plots for MIP-5%RAFT and NIP-5%RAFT.

#### 4.3.3.2 Binding Performance

The performance of the MIPs and their corresponding NIPs prepared via RAFT precipitation polymerisation were investigated by batch rebinding studies, conducted in two type of solvents i.e. acetonitrile and THF. BZP quantification was then carried

out by HPLC analysis, followed by calculation of the binding affinity, specific binding and the imprinting factor of the polymers using Equations 4.1, 4.2 and 4.3, respectively (§4.2.4).

#### 4.3.3.2.1 Optimum Binding Time

To determine the optimum contact time, batch rebinding studies were carried out on the MIP microspheres prepared using 5%RAFT in acetonitrile and THF. The concentration of the BZP solution was kept constant (1.00 mM) and the contact time was varied from 1 to 8 hrs. The controls (NIPs) were also subjected to the same tests. Figure 4.19 shows the amount of BZP bound normalised with respect to the mass ( $\mu\text{mol per g sample}$ ) and surface area ( $\mu\text{mol per m}^2 \text{ sample}$ ) of the polymers versus contact time when acetonitrile (A and B) and THF (C and D) were used as the rebinding solvents.

From Figure 4.19, it can be observed that the MIP-5%RAFT exhibited higher BZP binding affinity than the corresponding NIP when rebinding was carried out in both acetonitrile and THF, which indicates the existence of specific binding sites for BZP and hence successful imprinting. When the rebinding was carried out in acetonitrile, maximum binding affinity was achieved in about 2 hours, which indicates that the binding processes occur quite rapidly. The slightly higher BZP binding affinity observed at 1 h compared to the rest of the binding times (Figure 4.18(A) and (C)) was attributed to the very fast occurrence of non-selective binding, before achieving a stable state after 2 h. This behaviour has been observed in the binding profile carried out at low, non-saturating template concentration,<sup>322</sup> which is similar to our case.

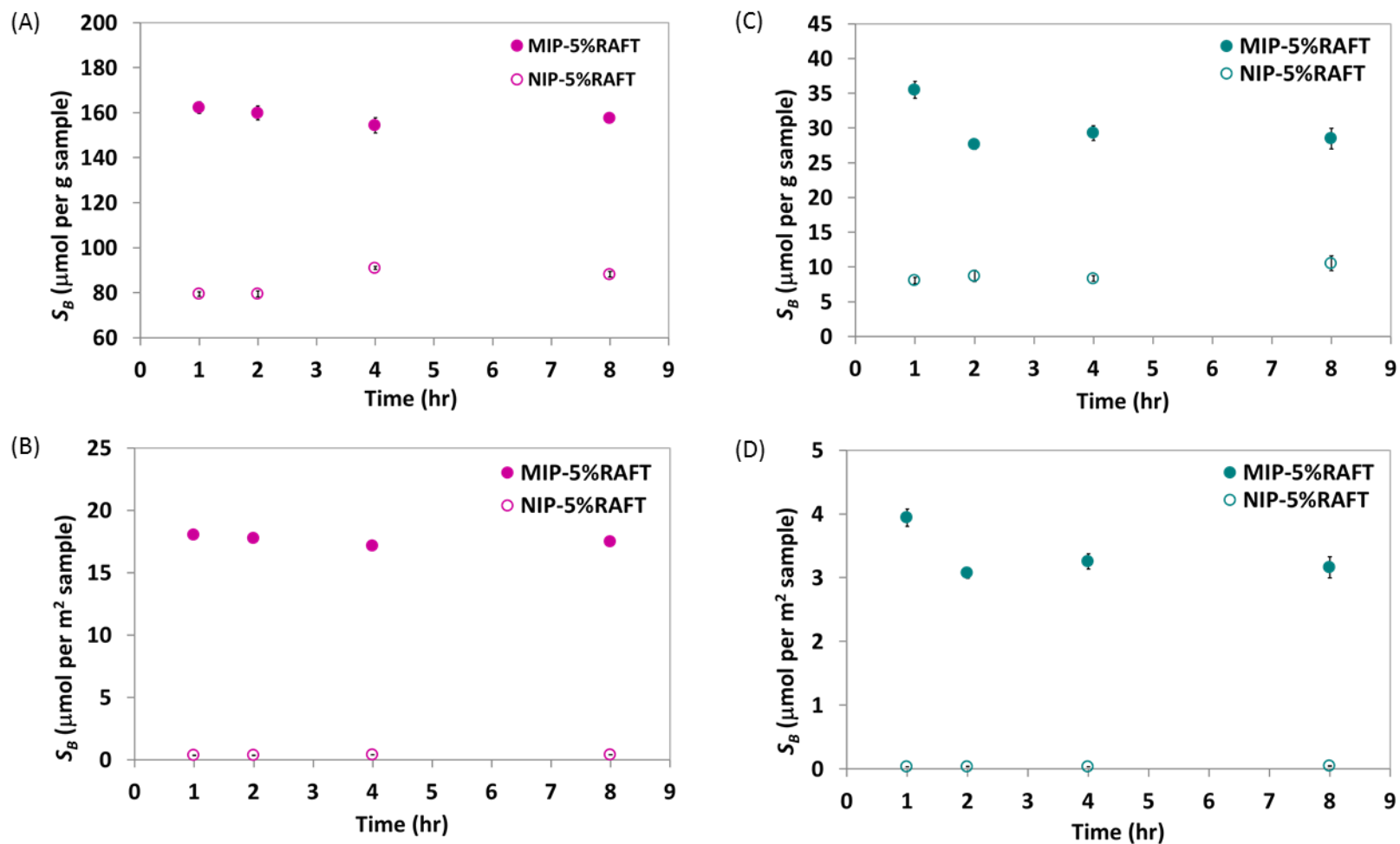


**Figure 4.19.** Time rebinding results for MIP and NIP prepared using 5%RAFT in acetonitrile normalised with respect to (A) mass and (B) surface area as well as in THF normalised with respect to (C) mass and (D) surface area.

#### 4.3.3.2 Binding Isotherm Studies

The MIP-5%RAFT and its NIP counterpart (NIP-5%RAFT) were then subjected to further investigation of their binding isotherms. Figure 4.20(A) shows the binding isotherm of MIP microspheres prepared using 5% RAFT and the corresponding control (NIP) normalised with respect to the mass of the polymers. Due to the difference in size between the MIP and NIP, the binding capacities were also normalised with respect to the surface area of the polymers using the BET surface areas given in Table 4.5 and the binding isotherm is shown in Figure 4.20(B).

As can be seen from the binding isotherms (Figure 4.20), the amount of BZP bound increased as the amount of free BZP concentration increased for both MIP and NIP microspheres and finally reaching a plateau upon saturation.<sup>295, 296</sup> It can also be observed that the MIP-5%RAFT exhibited higher affinity for BZP template than the NIP-5%RAFT, indicating successful imprinting process. The maximum number of binding sites ( $N$ ) was estimated by taking the average of binding capacity values after the plateau was reached and the results are tabulated in Table 4.5. From the table, it can be observed that the MIP exhibited about 2-fold higher  $N$  value compared to that of the NIP (271  $\mu\text{mol/g}$  and 142  $\mu\text{mol/g}$ , respectively). Since the NIP microspheres have a much larger surface area (about 25-fold higher) compared to the MIP microspheres, the difference in the binding capacity between them on this scale is actually larger, as evidenced in Figure 4.19(B). The  $N$  value of the MIP normalised with respect to the sample surface area is about 45-fold higher in magnitude than that of the NIP (Table 4.5). Considering that the NIP has higher surface area and more pores in the mesopore region as well as having pores in the micropore region compared to the MIP which has no pores in that region (Figure 4.18), the former is expected to bind a greater amount of BZP (diameter = 0.5 x 1.0 nm, Figure 4.7). However, since the experimental result showed that NIP bound much less BZP compared to the MIP, the better binding capacity of the MIP is most likely to be the result of cavity-based binding of BZP rather than the non-specific binding occurring for the NIP.

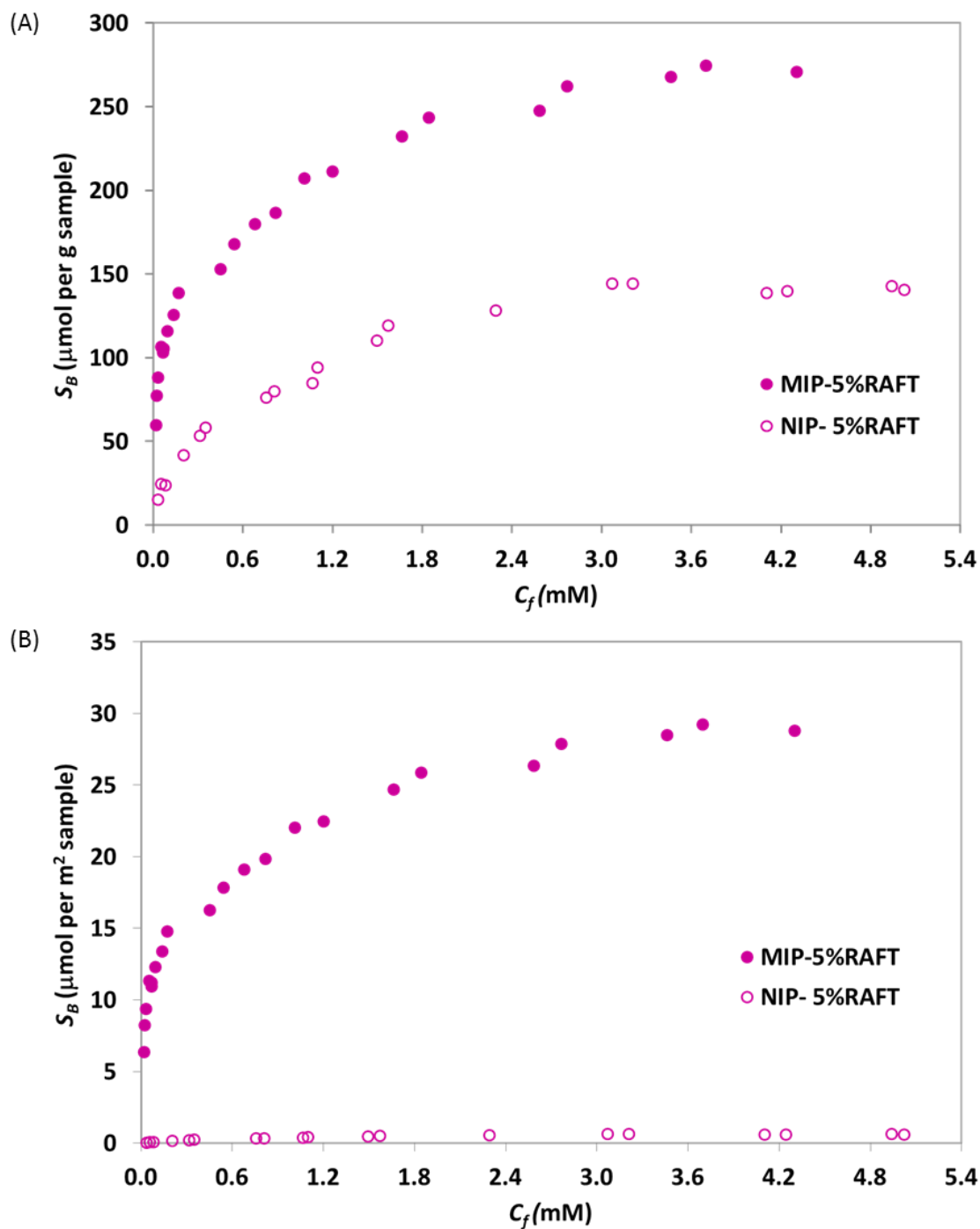


**Figure 4.20.** Binding isotherms for BZP imprinted polymers prepared using 5% RAFT carried out in acetonitrile normalised with respect to (A) mass and (B) surface area.

Figure 4.21 shows the Langmuir plots for the MIP microspheres prepared using 5% RAFT and its NIP counterpart. The  $N$  and  $K_d$  values were calculated from the binding isotherms according to Equation 4.4 and the results are tabulated in Table 4.5. From the table, it can be observed that the MIP-5%RAFT possessed about 2-fold higher

maximum number of binding site compared to that of the NIP ( $N = 279$  and  $160 \mu\text{mol/g}$  respectively). However, when the binding capacity was normalised with respect to the specific surface area of the polymers, it can be seen that the MIP exhibited even much higher  $N$  value (about 50-fold higher) than that of the NIP ( $29$  and  $0.6 \mu\text{mol/m}^2$  respectively). Comparing the equilibrium dissociation constant of the polymers, the MIP possessed about 65% lower  $K_d$  value than that of the NIP ( $0.214$  and  $0.598 \text{ mM}$  respectively). The lower  $K_d$  value means that the MIP prepared via RAFT has higher affinity towards the BZP template compared to the corresponding NIP, which confirms the creation of specific binding sites for BZP. It can also be observed that good linearity was obtained for both the MIP-5%RAFT and NIP-5%RAFT ( $R^2 = 0.9898$  and  $0.9916$  respectively), which indicates that the Langmuir isotherms of the polymers are a good fit to the experimental data.

**Table 4.5.** Equilibrium dissociation constant ( $K_d$ ) and number of binding site ( $N$ ) extracted from the binding isotherm (Figure 4.20), and derived from the Langmuir (Figure 4.21) and Scatchard (Figure 4.22) plots for the MIP and NIP prepared using 5% RAFT in acetonitrile.

Model	Polymer	$K_d$ (mM)		$N$ ( $\mu\text{mol/g}$ )		$N$ ( $\mu\text{mol/m}^2$ )	
		1 <sup>a</sup>	2 <sup>b</sup>	1 <sup>a</sup>	2 <sup>b</sup>	1 <sup>a</sup>	2 <sup>b</sup>
Binding isotherm	MIP-5%RAFT	N/A		271		29	
	NIP-5%RAFT	N/A		142		0.6	
Langmuir (Equation 4.4)	MIP-5%RAFT	0.214		279		30	
	NIP-5%RAFT	0.598		160		0.7	
Scatchard (Equation 4.5)	MIP-5%RAFT	0.033	0.458	162	301	17	32
	NIP-5%RAFT	0.209	1.06	96	183	0.4	0.8

<sup>a</sup> High affinity site.

<sup>b</sup> Low affinity site.

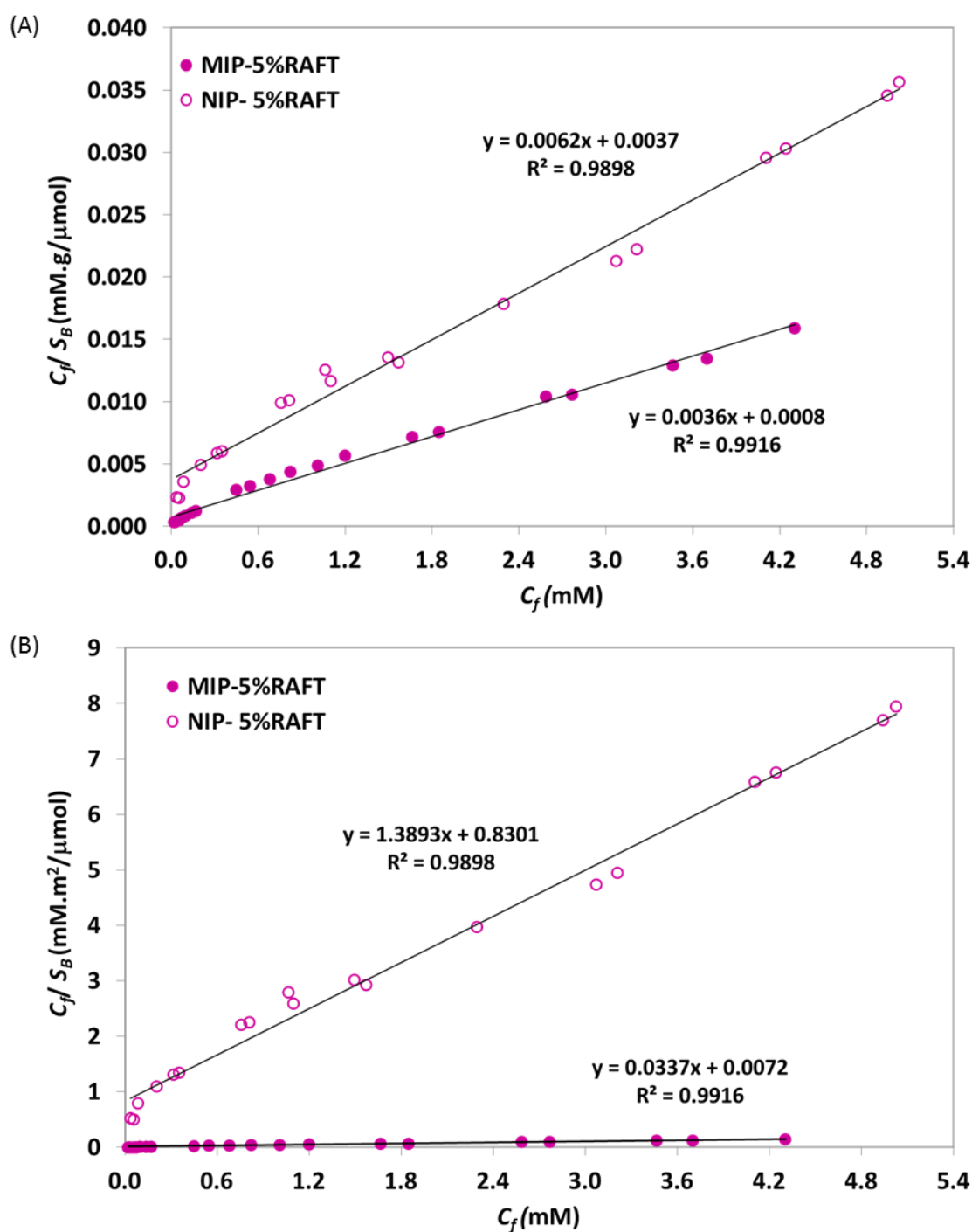


**Figure 4.21.** Langmuir plots for BZP imprinted polymers prepared using 5% RAFT and the control (NIP) normalised with respect to (A) mass and (B) surface area.

The Scatchard plots for the MIP microsphere prepared using 5% RAFT and its corresponding NIP (control) where the binding capacities were normalised with respect to the mass and surface area of the polymers are shown in Figure 4.22(A) and (B), respectively. The values of  $N$  and  $K_d$  were calculated from the slopes and  $y$ -

intercepts according to equation 4.5 and the results are tabulated in Table 4.5. As can be observed from the plots, two sets of  $N$  and  $K_d$  values for both the MIP and NIP microspheres were obtained, indicating the presence of both low and high affinity binding sites in the two polymers. From Table 4.5, it can be seen that the MIP exhibited about 2-fold higher number of low binding sites compared to the high binding sites, which is consistent with the previous studies that showed that MIPs typically contain higher proportion of the former than the latter.<sup>305</sup>

From Table 4.5, it can also be observed that generally the MIP exhibited a higher number of binding sites ( $N$ ) than the corresponding NIP. The  $N$  values of the high affinity sites of the MIP, which are mainly responsible for the specific binding of the MIP, were about 1.5- and 40-fold higher than those of the NIP with respect to the sample mass and surface area, respectively. Nevertheless, the ratio of the  $N$  value of the low affinity to the high affinity sites of the MIP is similar to that of the NIP ( $N_{\text{low affinity}}/N_{\text{high affinity}} \approx 2$ ). This may be because the NIP-5%RAFT contains a higher number of pores in the lower range of the mesopore region (2 – 7 nm pore width) compared to the corresponding MIP, as well as having additional pores in the micropore region (0.4 – 2 nm pore width). Considering the small size of the BZP template molecule (0.5 x 1.0 nm, Figure 4.7), the presence of these pores allows easy access of the template to the high affinity sites of the NIP, which unlike in the MIP, is due to the partial occupation of cavities or pores by the template.

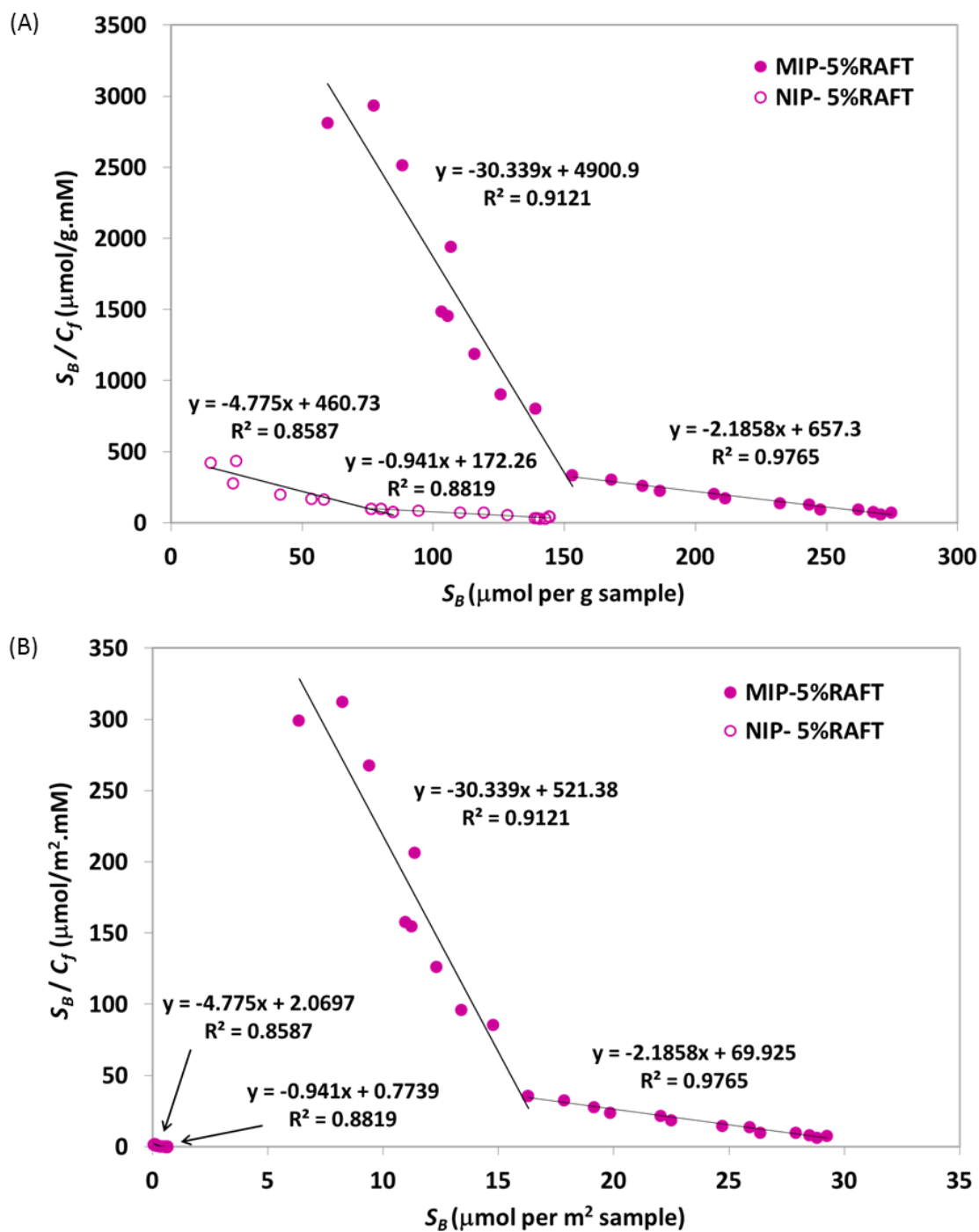


**Figure 4.22.** Scatchard plots for BZP imprinted polymers prepared using 5% RAFT and the corresponding NIP normalised with respect to (A) mass and (B) surface area.

As can be seen in Table 4.5, the  $K_d$  value of the high affinity sites for the NIP obtained from the Scatchard isotherm was about 6-fold higher than that of the MIP, which indicates that the latter has stronger affinity towards the BZP template at the high affinity sites compared to the former. Similarly, the  $K_d$  value of the low affinity sites for

the NIP is about 2-fold higher than that of the corresponding MIP, indicating stronger BZP binding in the latter, which could be attributed to the more accessible partial imprinting sites (see Figure 4.15). Nevertheless, the  $K_d$  value of the low affinity sites of the MIP was much higher than that of the high affinity sites (about 14-fold higher), which indicates weaker BZP binding in the former and is most likely due to non-specific surface binding. Compared to the Langmuir plots, the correlation coefficients of both the MIP and NIP for the Scatchard plots are much lower indicating a poorer fit for the latter compared to the former.

#### 4.3.3.2.3 Effect of RAFT Agent Concentration

The effect of RAFT agent concentration on the binding performance of the prepared BZP imprinted polymers was investigated by performing batch rebinding experiments on the MIP-10%RAFT and MIP-20%RAFT along with their NIP counterparts. The experiments were carried out using both acetonitrile and THF as the rebinding solvents at 2 hr contact time. The results were then compared with those of MIP-5%RAFT and shown in Table 4.6.

As can be seen in Table 4.6, regardless of the amount of RAFT agent used, the BZP binding affinity normalised with respect to the mass of all the MIP microspheres were almost similar in acetonitrile. As for the NIP microspheres, the NIP-10%RAFT exhibited the highest binding affinity, followed by the NIP-20% and -5%BDDC respectively. As a result, the MIP-5%RAFT exhibited the highest specific binding ( $\Delta S_B \approx 80 \mu\text{mol per g sample}$ ), whilst those of the MIP-10% and -20%BDDC were comparable.

**Table 4.6.** BZP binding affinity ( $S_B$ ), specific binding ( $\Delta S_B$ ) and imprinting factor (IF) values of microspheres prepared using 5%, 10% and 20% RAFT agent, after 2 hr of contact time in acetonitrile and THF.

Polymers	DC (%) <sup>a</sup>	Acetonitrile						THF					
		Mass			Surface Area			Mass			Surface Area		
		$S_B^b$ ( $\mu\text{mol per g sample}$ )	$\Delta S_B$	IF	$S_B^c$ ( $\mu\text{mol per m}^2 \text{ sample}$ )	$\Delta S_B$	IF	$S_B^b$ ( $\mu\text{mol per g sample}$ )	$\Delta S_B$	IF	$S_B^c$ ( $\mu\text{mol per m}^2 \text{ sample}$ )	$\Delta S_B$	IF
MIP-5%RAFT	53	$160 \pm 3$	$81 \pm 3$	2.0	$17.8 \pm 0.3$	$17.4 \pm 0.3$	51	$28 \pm 1$	$19 \pm 1$	3.1	$3.1 \pm 0.1$	$3.1 \pm 0.1$	78
NIP-5%RAFT	33	$79 \pm 1$			$0.35 \pm 0.01$			$9 \pm 1$					
MIP-10%RAFT	47	$165 \pm 2$	$74 \pm 3$	1.8	$15.0 \pm 0.1$	$14.6 \pm 0.1$	37	$37 \pm 1$	$21 \pm 1$	2.3	$3.4 \pm 0.1$	$3.3 \pm 0.1$	48
NIP-10%RAFT	25	$91 \pm 1$			$0.40 \pm 0.01$			$16 \pm 1$					
MIP-20%RAFT	48	$153 \pm 5$	$68 \pm 6$	1.8	$6.7 \pm 0.2$	$6.3 \pm 0.2$	18	$34 \pm 1$	$19 \pm 1$	2.3	$1.5 \pm 0.01$	$1.4 \pm 0.01$	22
NIP-20%RAFT	67	$85 \pm 3$			$0.38 \pm 0.01$			$15 \pm 1$					

<sup>a</sup> Extent of C=C bond conversion of the EGDMA, DC (%), calculated according to the following equation (Equation 4.1) :

$$\text{DC (\%)} = 100 \times \left[ 1 - \frac{(A_{C=C}/A_{C=O})_{\text{polymer}}}{(A_{C=C}/A_{C=O})_{\text{monomer}}} \right]$$

where DC (%) represents the extent of C=C bond conversion of the EGDMA whereas  $A_{(C=C)}$  and  $A_{(C=O)}$  are the FTIR absorbance values of C=C and C=O, respectively. This value is used to estimate the degree of crosslinking of the polymer in order to investigate the relationship between crosslinking density and the binding performance of the polymer.

<sup>b</sup> Actual experimental result.

<sup>c</sup> Calculated using the experimental BET specific surface area of 5% RAFT polymers; the BET specific surface areas of polymers prepared using 10% and 20% RAFT were estimated from that of the 5% RAFT polymers.

Considering the difference in morphology and particle size of the microspheres, a more useful comparison can be obtained from the data of binding affinity normalised with respect to the sample surface area. From Table 4.6, it can be observed that in general, the BZP binding affinity normalised with respect to the surface area of the MIP microspheres in acetonitrile decreases with increasing amount of RAFT agent. On the other hand, the NIP-5%RAFT exhibited the lowest binding affinity whereas those of the NIP-10% and -20%RAFT are comparable. As a result, the MIP-5%RAFT exhibited the highest specific binding (about 1.2- and 2.8-fold higher than those of the MIP-10% and -20%RAFT, respectively) as well as the highest IF value (about 1.4- and 2.8-fold higher than those of the MIP-10% and -20%RAFT, respectively).

Quite a different result was obtained when the rebinding was carried out in THF compared to that in acetonitrile, where the MIP-5%RAFT exhibited the lowest binding affinity normalised with respect to the mass of polymer (about 20% lower) whilst comparable binding affinity values were exhibited by the MIP-10% and -20%RAFT. Similarly, the lowest binding affinity was exhibited by the NIP-5%RAFT (about 40% lower) whilst the NIP-10% and -20%BDDC exhibited comparable binding affinity values. As a result, all the MIP microspheres exhibited almost similar specific binding values ( $\Delta S_B \approx 20 \mu\text{mol per g sample}$ ). On the other hand, the MIP-5%RAFT exhibited the highest IF value (about 1.5-fold higher) compared to the other two formulations, which exhibited similar IF values.

A different trend was obtained for the MIP, when the binding affinity in THF was normalised with respect to the surface area. The MIP-20%RAFT exhibited the lowest binding affinity (about 50% lower), whilst the MIP-5% and -10%RAFT exhibited comparable binding affinity values. On the other hand, a similar trend was observed for the NIP, where the NIP-5%RAFT exhibited the lowest binding affinity (about 40% lower) than the NIP-10% and -20%BDDC, since the surface areas of the NIPs are estimated to be about the same. As a result, the MIP-20%RAFT exhibited the lowest specific binding affinity value whereas comparable specific binding affinity values were exhibited by the MIP-5% and -10%RAFT. Despite the comparable specific binding

values of the MIP-5% and -10%RAFT, the highest IF value was exhibited by the former due to the much lower binding affinity of its NIP counterpart compared to the latter. This result is consistent with the result obtained in acetonitrile, where the IF value seemed to increase with decreasing amount of RAFT agent, which indicates that the MIP-5%RAFT showed better selectivity towards the BZP template compared to the MIP-10% and -20%RAFT.

The difference in the binding affinity of the polymers could be attributed to the different in the degree of crosslinking of the MIP and NIP microspheres, when prepared using different amount of RAFT agent. The different crosslinking density of the microsphere network might affect the porosity of the polymers, which might in turn influence the mass transfer of the template to the cavities. In order to investigate the relation between crosslinking density of the microsphere network and the binding performance, these properties are compared between the MIP-5%RAFT and its NIP counterpart.

From Table 4.6, it can be observed that there was no specific trend in the degree of crosslinking of the NIP microspheres with increasing RAFT concentration. The NIP-20%RAFT exhibited the highest degree of crosslinking whilst the lowest degree of crosslinking was exhibited by the NIP-10%BDDC (DC = 67 and 33%, respectively). This result is inconsistent with the result obtained for the NIP microspheres prepared using iniferter, where the degree of crosslinking was found to increase with increasing iniferter concentration. Comparing the binding affinity of the NIPs normalised with respect to the mass of the polymer in acetonitrile, the highest binding affinity was exhibited by the NIP-10%BDDC ( $S_B \approx 90 \mu\text{mol per g sample}$ ), which exhibited the lowest degree of crosslinking (DC = 25%) whereas the lowest binding affinity was exhibited by the MIP-5%RAFT ( $S_B \approx 80 \mu\text{mol per g sample}$ ), whose degree of crosslinking (DC = 33%) was in between those of the MIP-10% and -20%RAFT. Comparing the binding affinity of the NIPs normalised with respect to the surface area of the polymer in acetonitrile, the lowest binding affinity was exhibited by the NIP-5%RAFT ( $S_B \approx 0.35 \pm 0.01 \mu\text{mol per m}^2 \text{ sample}$ ), whereas both the NIP-20%RAFT and

the NIP-10%RAFT exhibited comparable binding affinity ( $S_B \approx 0.40 \pm 0.01 \mu\text{mol per m}^2$  sample). The results showed that the binding affinity of the NIPs was not affected by their crosslinking density.

A different trend was observed for the MIPs (Table 4.6), where the highest degree of crosslinking was exhibited by the MIP-5%RAFT (DC = 53%), whereas those of the MIP-10%RAFT and -20%RAFT were comparable (DC  $\approx$  48%), which indicates that the MIP-5%RAFT was more crosslinked than both the MIP-10%RAFT and -20%RAFT. Comparing the binding affinity of the MIPs normalised with respect to the mass of the polymer in acetonitrile, the MIP-10%BDDC exhibited the highest binding affinity ( $S_B \approx 165 \mu\text{mol per g sample}$ ) whereas the lowest binding affinity was exhibited by the MIP-20%RAFT ( $S_B \approx 153 \mu\text{mol per g sample}$ ), albeit having similar degree of crosslinking (DC  $\approx$  48%). Comparing the binding affinity of the MIPs normalised with respect to the surface area of the polymer in acetonitrile, the highest binding affinity was exhibited by the MIP-5%RAFT ( $S_B \approx 18 \mu\text{mol per m}^2$  sample), which exhibited the highest degree of crosslinking (DC = 53%) whereas the MIP-20%RAFT exhibited the lowest binding affinity ( $S_B \approx 7 \mu\text{mol per m}^2$  sample, despite having the same crosslinking density as that of the MIP-10%RAFT (DC  $\approx$  48%). The results showed that the binding affinity of the MIPs was also not affected by their crosslinking density.

The effect of solvents on the swelling behaviour of the MIPs was not investigated since dispersions of the MIPs in both acetonitrile and THF were unstable against sedimentation.

#### 4.3.3.2.4 Effect of Solvent

In order to investigate the effect of rebinding solvent on the binding performance of the MIP microsphere prepared via RAFT, the binding parameters of MIP-5%RAFT and the corresponding NIP from Table 4.6 was compared, as shown in Figure 4.23.

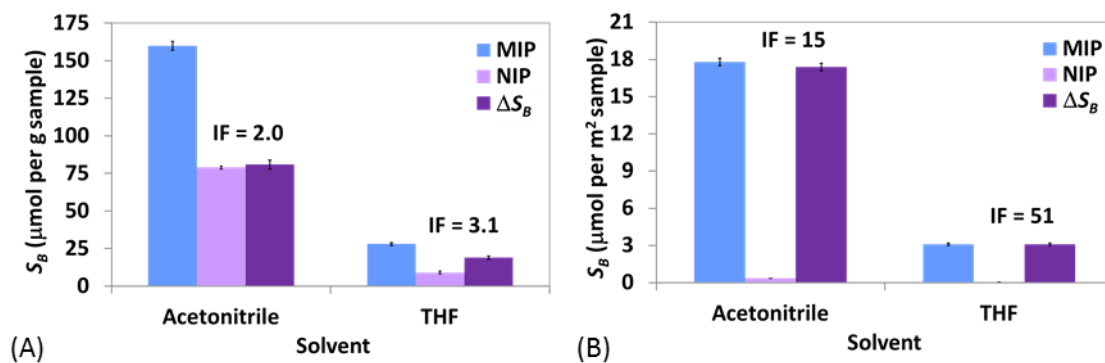


**Figure 4.23.** Comparison between the binding capacity of MIP microspheres prepared via RAFT in acetonitrile and THF normalised with respect to (A) mass and (B) surface area.

From Table 4.6, it can be seen that, the BZP binding affinities of both the MIP and the corresponding NIP (control) microspheres were much higher (about 6- and 9-fold higher, respectively) when the rebinding was carried out in acetonitrile compared to those in THF. This is consistent with the result obtained for the MIP and NIP microspheres prepared using the iniferter (§4.3.2.2.3), which could be attributed to the different hydrogen bonding ability of THF compared to that of acetonitrile.<sup>316, 317</sup> The weaker hydrogen bonding capacity of acetonitrile compared to THF limits its ability to compete for the hydrogen bonding sites on the template or the binding sites. In addition, conducting the binding experiment in acetonitrile, which is the porogen used during polymerisation provides a microenvironment that mimics the interactions existing prior to and during the polymerisation,<sup>314</sup> thus resulted in higher binding affinity of the polymers. From the table, it can also be observed that the IF values were about 50% higher in THF compared to those in acetonitrile. On the contrary, the specific binding values of the MIP were much higher in the latter than the former (about 4- and 6-fold higher when the binding capacity was normalised with respect to the sample mass and surface area respectively). The results showed that using acetonitrile as the rebinding solvent led to higher binding affinity and better discrimination between the MIP and the NIP microspheres as shown by the large difference in their binding affinity values compared to when the rebinding was carried out in THF, which is consistent with the results obtained by the MIP and NIP microspheres prepared using 5% BDDC.

#### 4.3.4 Comparison between Microspheres Prepared via Iniferter and RAFT

This section deals with the comparison of binding performance between the MIP microspheres prepared via the iniferter and RAFT methods using 5 mol % of BDDC and MCEBTTC, respectively. These polymers were chosen as they are the best performing MIP microspheres, i.e. exhibiting the highest specific binding and imprinting factors, among all of the formulations in their series.

The difference in concentration of total monomer used during the polymerisation reaction via iniferter and RAFT (2 vol % and 4 vol %, respectively, §4.2.2) could have affected the morphology of the resulting microspheres, thus resulted in different particle sizes and surface areas. The particle size of the polymer microspheres has been reported to increase with increasing monomer concentration<sup>161, 240, 321, 323-325</sup> whereas the specific surface area of the microspheres was found to slightly decreased with increasing monomer concentration.<sup>323</sup> In our case, this is true for the NIP microspheres, where the hydrodynamic diameter of the NIP-5%RAFT, which was prepared using higher concentration of monomers, was bigger than that of the NIP-5%BDDC (Table 4.7). The BET specific surface area of the former, however, was much higher than that of the latter. On the other hand, the SEM particle size of MIP-5%RAFT, which was prepared using higher concentration of monomer, was smaller than the MIP-5%BDDC, whereas its BET specific surface area was about 30% higher than that of the latter. Apart from monomer concentration, other factors such as polymerisation temperature<sup>326</sup> and method of initiation (thermal versus UV)<sup>327</sup> might have contributed to this difference in morphologies. For example, thermal initiation has been reported to give rise to smaller beads compared to that of UV initiation<sup>327</sup> whereas BET surface area has been reported to increase with increasing temperature.<sup>328</sup>

As can be observed from the binding kinetic experiments (Figures 4.11 and 4.19), the MIP and NIP microspheres prepared via both iniferter and RAFT reached their binding equilibrium after about 2 h, demonstrating quite fast binding processes. The binding

affinities of the MIPs prepared via both methods were higher when the rebinding was carried out in acetonitrile compared to those in THF (Tables 4.3 and 4.6), thus the binding data from the former was used for comparison purposes. The binding parameters such as binding affinity, specific binding as well as IF of the MIPs prepared via iniferter and RAFT are then compared, as shown in Figure 4.24.

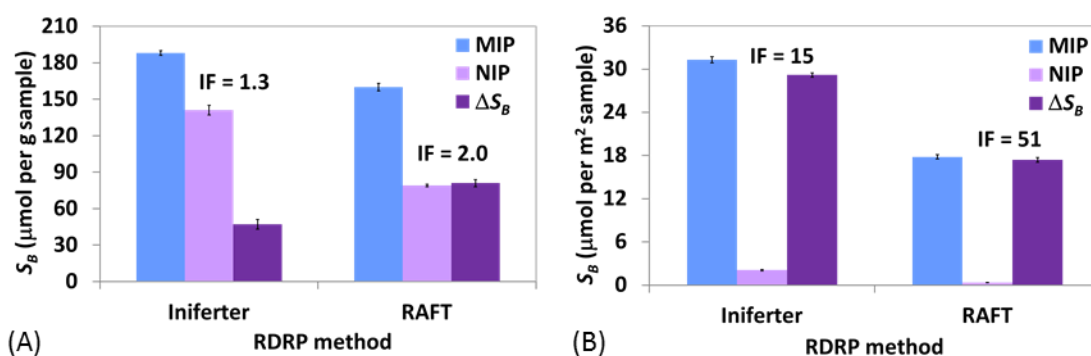


**Figure 4.24.** Comparison between the binding capacity of MIP microspheres prepared via iniferter and RAFT normalised with respect to (A) mass and (B) surface area.

As can be seen from Figure 4.24, the binding affinities of the MIPs prepared via both the iniferter and RAFT were higher than their NIP counterparts, indicating the creation of specific binding sites in both polymers and thus the successful imprinting processes via both methods. From Figure 4.24(A), it can also be observed that the BZP binding affinity of the MIP microsphere prepared via iniferter normalised with respect to the mass of the polymer was higher (about 20% higher) than that of RAFT. However, the level of non-specific binding in the former was also higher than the latter (about 80% higher) resulting in lower specific binding and IF values of MIP microsphere prepared via iniferter. As the polymers exhibited different particle sizes, which translated to different surface area values (Table 4.7), binding capacity normalised with respect to the surface area of the polymers gives a more meaningful comparison (Figure 4.24(B)).

From Figure 4.24(B), it can be observed that the BZP binding affinity normalised with respect to the surface area of the MIP microsphere prepared via iniferter was much higher (about 75% higher) than that of RAFT. However, the level of non-specific binding in the former was also higher (about 6-fold higher), which resulted in the lower

IF value of the former compared to the latter (IF = 15 and 51, respectively). Moreover having a higher level of non-specific binding, the total specific binding in the MIP microsphere prepared via iniferter was actually about 70% higher than that of the RAFT.

**Table 4.7.** Physical characteristics of the BZP-imprinted polymer microspheres and the corresponding NIPs prepared by precipitation polymerisation using BDDC iniferter and MCEBTTC RAFT agent (extracted from Tables 4.1, 4.3, 4.4 and 4.6).

Parameters	Iniferter		RAFT	
	MIP	NIP	MIP	NIP
Diameter <sup>a</sup> (nm)	1290 ± 70	180 ± 20 90 ± 2 <sup>b</sup>	290 ± 50 740 ± 70	160 ± 20 140 ± 20 <sup>b</sup>
BET specific surface area (m <sup>2</sup> /g) <sup>c</sup>	6.0 ± 0.1	67 ± 13	9.0 ± 0.1	226 ± 2
DC (%) <sup>d</sup>	60	48	53	33

<sup>a</sup> Average diameter measured by SEM.

<sup>b</sup> Hydrodynamic diameter measured by DLS in THF at 20°C.

<sup>c</sup> Determined by nitrogen adsorption porosimetry.

<sup>d</sup> Extent of C=C bond conversion of the EGDMA, DC (%), calculated according to the following equation (Equation 4.1) :

$$DC (\%) = 100 \times \left[ 1 - \frac{\left( \frac{A_{C=C}}{A_{C=O}} \right)_{\text{polymer}}}{\left( \frac{A_{C=C}}{A_{C=O}} \right)_{\text{monomer}}} \right]$$

To get further insight on the binding characteristics of the MIPs prepared via different synthetic approaches i.e. iniferter and RAFT, Langmuir and Scatchard isotherm models were used for further analysis. Binding parameters normalised with respect to the surface area such as maximum number of binding site ( $N$ ) and equilibrium binding constant ( $K_d$ ) values were obtained from their respective Langmuir (Figures 4.13(B) and 4.21(B), respectively) and Scatchard plots (4.14(B) and 4.22(B), respectively) and the results (extracted from Tables 4.2 and 4.5) are compared in Table 4.8. The Scatchard plots of the MIPs prepared via iniferter and RAFT were nonlinear indicating that the binding sites in both MIPs are heterogeneous with respect to their affinity for BZP.

**Table 4.8.** Comparison between the binding dissociation constant ( $K_d$ ) and maximum binding capacity ( $N$ ) normalised with respect to the surface area of the microspheres prepared via iniferter and RAFT.

Model	Polymer	Iniferter				RAFT			
		$K_d$ (mM)		$N$ ( $\mu\text{mol}/\text{m}^2$ )		$K_d$ (mM)		$N$ ( $\mu\text{mol}/\text{m}^2$ )	
		1 <sup>a</sup>	2 <sup>b</sup>	1 <sup>a</sup>	2 <sup>b</sup>	1 <sup>a</sup>	2 <sup>b</sup>	1 <sup>a</sup>	2 <sup>b</sup>
Binding isotherm	MIP	N/A		56		N/A		29	
	NIP	N/A		3.8		N/A		0.6	
Langmuir (Equation 4.4)	MIP	0.111		58		0.214		30	
	NIP	0.340		4.1		0.598		0.7	
Scatchard (Equation 4.5)	MIP	0.041	0.268	42	62	0.033	0.458	17	32
	NIP	0.029	0.498	1.6	4.2	0.209	1.06	0.4	0.8

<sup>a</sup> High affinity site.

<sup>b</sup> Low affinity site.

N/A - not available.

From Table 4.8, it can be seen that the maximum number of binding sites ( $N$ ) normalised with respect to surface area of the MIP microsphere prepared via iniferter obtained from all the isotherm models were higher than those of the MIP prepared via RAFT. The  $N$  values of the MIP prepared via iniferter estimated from both the binding isotherm and Langmuir plot were about 90% higher than those prepared by RAFT. Apart from that, the MIP microspheres prepared via iniferter showed significantly higher number of high affinity binding sites (about 2.5-fold higher) than the MIP prepared via RAFT. This could be attributed to the different conditions employed during their preparation such as method of initiation and polymerisation temperature. The iniferter polymerisation was carried out under UV irradiation at room temperature whereas RAFT polymerisation was conducted thermally at 60 °C. Higher reaction temperature was expected to cause a decrease in the number of strongly binding cavities by reducing the stable configuration of the template-functional monomer complex.<sup>314, 329-331</sup>

From Table 4.8, it can also be observed that the  $K_d$  value of the MIP prepared via iniferter calculated from the Langmuir plot was about 50% lower than that of the MIP prepared via RAFT. Lower  $K_d$  values mean higher binding association constant ( $K_a$ ), suggesting the presence of higher specific binding in the iniferter system. On the contrary, the  $K_d$  value of the high affinity sites of the MIP prepared via iniferter was about 25% higher than that of the RAFT, suggesting the stronger affinity of the latter towards BZP compared to the former. The difference in the binding affinity between the MIP microspheres prepared via iniferter and RAFT could be attributed to the difference in the crosslinking density of the microspheres. From Table 4.8, it can be noticed that the MIP microspheres prepared via RAFT was less crosslinked than the MIP microspheres prepared via iniferter (DC = 53 and 60, respectively). Moreover, the specific surface area of the MIP prepared via RAFT was higher than that of the iniferter ( $9.0 \pm 0.1 \text{ m}^2/\text{g}$  and  $6.0 \pm 0.1 \text{ m}^2/\text{g}$ , respectively, Table 4.7). In addition, the MIP prepared via RAFT exhibited quite a high proportion of pores in the low mesopore region (3.5 – 7.0 nm, Figure 4.18) relative to the MIP prepared via iniferter (Figure 4.10), which contains only a small proportion of pore in the micropore region (1.5 – 2.0 nm), whilst the rest of the pores are distributed in the mesopore region (between 10 – 30 nm). The lower crosslinking density and larger specific surface area (about 1.5-fold higher), combined with the greater porosity of the polymer prepared via RAFT could have enhanced the mass transfer of the BZP template (0.5 x 1.0 nm, Figure 4.7) to the high binding sites, thus resulting in lower  $K_d$  value compares to that of the iniferter. However, despite the stronger affinity of the MIP prepared via RAFT compared to that of the iniferter, the latter exhibited higher maximum number of binding sites (about 2.5-fold higher), resulting in higher specific binding value compared to that of the former (Figure 4.24). As a comparison, the  $K_d$  value of the high affinity sites of the BZP imprinted MIP prepared via traditional bulk method in chloroform using the same 1:1 ratio of MAA:BZP was reported to be 0.255 mM.<sup>257</sup> This value is about 6- and 8-fold higher than those of our MIPs, which were prepared via iniferter and RAFT respectively. The results showed that both the MIP prepared via iniferter and RAFT showed improved binding affinity normalised with respect to the surface area compared to the MIP prepared via the traditional bulk polymerisation.

### 4.3.5 Selectivity Studies

Based on the binding isotherm experiment results, although MIP-5%RAFT showed stronger high binding site affinity and higher imprinting factor values than the MIP-5%BDDC, the latter exhibited higher binding capacity and better specific template binding compared to the former. In addition, preliminary experiments conducted to prepare star MIP from these two microspheres showed that using the MIP prepared via iniferter as the core precursor was more successful than using the MIP prepared via RAFT. This could be attributed to the more uniform size of the former compared to the latter, which led to better controlled polymerisation. Due to these factors, MIP-5%BDDC was selected for further analysis to investigate the binding selectivity of the MIP. Two sets of experiments were conducted to investigate the selectivity of the MIP-5%BDDC microsphere towards the BZP template. Non-competitive and competitive adsorption experiments were carried out on MIP-5%BDDC and its NIP counterpart following the procedure in §4.2.5 using (1R,2S)-(-)-ephedrine (EPH, [2], Figure 4.2) and 1-phenylpiperazine (PHP, [3], Figure 4.2) as the reference substrates.

The binding affinities of the BZP imprinted polymer and the corresponding NIP for different analytes were calculated according to Equation 4.1. Since the MIP and its NIP counterpart differ greatly in diameter and thus surface area, the binding capacity obtained was also normalised with respect to the polymer surface area. The values of specific binding ( $\Delta S_B$ ), imprinting factor (IF) and the specific selectivity factor (SSF) of the analytes on the MIP microspheres were calculated according to Equations 4.2, 4.3 and 4.7, respectively. A template with a large specific binding and an analogue with a small specific binding will result in a large specific selectivity factor value, which indicates good selectivity.

### 4.3.6 Non-competitive and Competitive Binding Experiment

The non-competitive binding experiment (also known as a single-analyte assay or cross-reactivity study) was carried out on the MIP-5%BDDC and the corresponding NIP to assess the ability of the MIP microsphere to discriminate between BZP and other

structurally related drugs. The experiments were performed in 1.0 mL of acetonitrile solution containing either BZP, EPH or PHP at a concentration of 3.00 mM. The binding affinity, specific binding imprinting factor and specific selectivity factor values normalised with respect to the mass and surface area of the polymers are tabulated in Tables 4.9 and 4.10 respectively, and compared in Figure 4.25(A) and (B) respectively.

To determine the selectivity of the BZP imprinted polymer towards the BZP template in the presence of another analytes, competitive binding studies were conducted in binary and tertiary competitive environments. The binding parameters normalised with respect to the mass and surface area of the polymers are then tabulated in Tables 4.9 and 4.10 respectively, and are shown in Figure 4.25 (C, E, G) and Figure 4.25(D, F, H) respectively. As mentioned in the experimental procedure (§4.2.5), the HPLC peaks associated with PHP and BZP overlapped, therefore Excel solver was used to deconvolute the peaks, as shown in Figure 4.5 (§4.2.5).

**Table 4.9.** Binding affinity ( $S_B$ ), specific binding  $\Delta S_B$ , imprinting factor (IF) and standardised specific selectivity factor (SSF) values normalised with respect to mass in a single-analyte, binary-analyte and tertiary-analyte binding assays of BZP imprinted polymer prepared via iniferter.<sup>a</sup>

System	Polymer	BZP			EPH				PHP			
		$S_B^d$ ( $\mu\text{mol per g sample}$ )	$\Delta S_B$	IF	$S_B^d$ ( $\mu\text{mol per g sample}$ )	$\Delta S_B$	IF	SSF <sup>e</sup>	$S_B^d$ ( $\mu\text{mol per g sample}$ )	$\Delta S_B$	IF	SSF <sup>e</sup>
Single-analyte assay	MIP	281 $\pm$ 6	69 $\pm$ 8	1.3	340 $\pm$ 7	85 $\pm$ 9	1.3	0.81	255 $\pm$ 1	99 $\pm$ 1	1.6	0.70
	NIP	212 $\pm$ 6			255 $\pm$ 5				156 $\pm$ 1			
Binary-analyte assay <sup>b</sup>	MIP	198 $\pm$ 4	60 $\pm$ 10	1.4	200 $\pm$ 3	27 $\pm$ 9	1.2	2.22				
	NIP	138 $\pm$ 9			173 $\pm$ 9							
Binary-analyte assay <sup>c</sup>	MIP	171 $\pm$ 5	68 $\pm$ 7	1.7					46 $\pm$ 2	6 $\pm$ 5	1.2	11.3
	NIP	103 $\pm$ 5							40 $\pm$ 5			
Tertiary-analyte assay	MIP	194 $\pm$ 3	45 $\pm$ 5	1.3	185 $\pm$ 4	21 $\pm$ 4	1.1	2.14	37 $\pm$ 3	18 $\pm$ 4	1.9	2.50
	NIP	149 $\pm$ 4			164 $\pm$ 1				19 $\pm$ 2			

<sup>a</sup> Binding time: 2 hr; initial concentration of each substrates: 3.0 mM; solvent: acetonitrile; volume of solvent: 1.0 mL.

<sup>b</sup> Contains a mixture of BZP and EPH.

<sup>c</sup> Contains a mixture of BZP and PHP.

<sup>d</sup> Actual experimental result.

<sup>e</sup> Standardised specific selectivity factor (SSF), calculated according to the following equation (Equation 4.7):

$$SSF = \frac{\Delta S_{B(\text{template})}}{\Delta S_{B(\text{analogue})}}$$

**Table 4.10.** Binding affinity ( $S_B$ ), specific binding  $\Delta S_B$ , imprinting factor (IF) and standardised specific selectivity factor (SSF) values normalised with respect to surface area in a single-analyte, binary-analyte and tertiary-analyte binding assays of BZP imprinted polymer prepared via iniferter.<sup>a</sup>

System	Polymer	BZP			EPH				PHP			
		$S_B^d$ ( $\mu\text{mol per m}^2$ sample)	$\Delta S_B$	IF	$S_B^d$ ( $\mu\text{mol per m}^2$ sample)	$\Delta S_B$	IF	SSF <sup>e</sup>	$S_B^d$ ( $\mu\text{mol per m}^2$ sample)	$\Delta S_B$	IF	SSF <sup>e</sup>
Single-analyte assay	MIP	$47 \pm 1$	$44 \pm 1$	14.7	$57 \pm 0.2$	$53 \pm 0.2$	14.6	0.83	$42 \pm 0.2$	$40 \pm 0.2$	17.5	1.10
	NIP	$3.2 \pm 0.1$			$3.9 \pm 0.1$	0.2			$2.4 \pm 0.01$	0.2		
Binary-analyte assay <sup>b</sup>	MIP	$33.1 \pm 0.7$	$31 \pm 0.7$	15.8	$33.4 \pm 0.5$	$31 \pm 0.5$	12.8	1.00				
	NIP	$2.1 \pm 0.1$			$2.6 \pm 0.1$	0.5						
Binary-analyte assay <sup>c</sup>	MIP	$29 \pm 1$	$27 \pm 1$	18.1					$7.7 \pm 0.4$	$7.1 \pm 0.4$	12.8	3.80
	NIP	$1.6 \pm 0.1$							$0.6 \pm 0.1$	0.4		
Tertiary-analyte assay	MIP	$32 \pm 0.5$	$30 \pm 0.5$	13.9	$31 \pm 0.6$	$29 \pm 0.6$	12.4	1.03	$6.1 \pm 0.4$	$5.8 \pm 0.4$	20.3	5.17
	NIP	$2.3 \pm 0.1$			$2.5 \pm 0.02$	0.6			$0.3 \pm 0.03$	0.4		

<sup>a</sup> Binding time: 2 hr; initial concentration of substrates: 3.0 mM; solvent: acetonitrile; volume of solvent: 1.0 mL.

<sup>b</sup> Contains a mixture of BZP and EPH.

<sup>c</sup> Contains a mixture of BZP and PHP.

<sup>d</sup> Calculated using the BET surface area.

<sup>e</sup> Standardised specific selectivity factor (SSF), calculated according to the following equation (Equation 4.7):

$$SSF = \frac{\Delta S_{B(\text{template})}}{\Delta S_{B(\text{analogue})}}$$

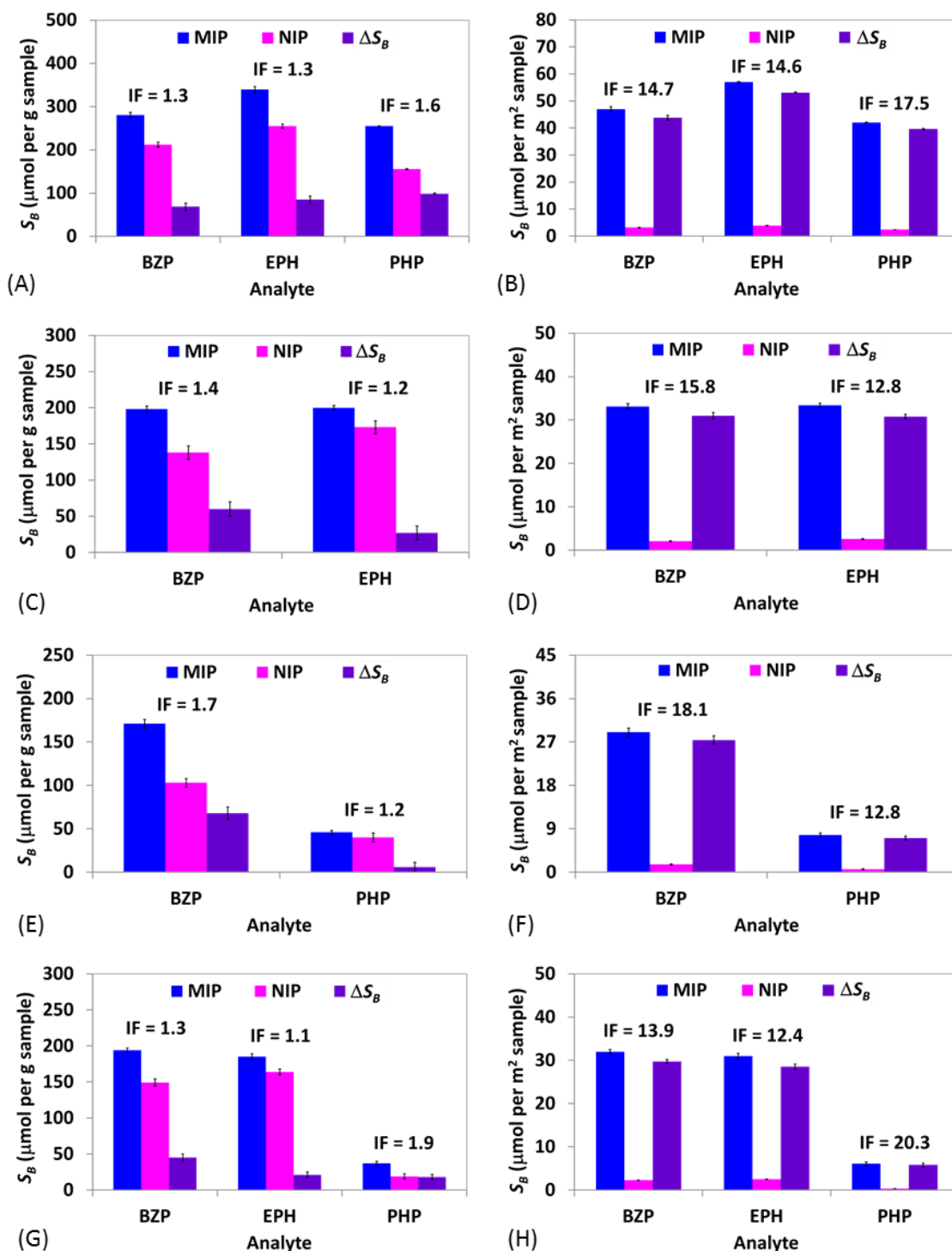


**Figure 4.25.** Single-analyte (A and B), binary-analyte (C - F) and tertiary-analyte (G and H) binding assays of BZP imprinted polymer with BZP, EPH and PHP normalised with respect to mass (A, C, E and G) and surface area (B, D, F and H).

As can be seen from Figure 4.25(A) and Table 4.9 for the non-competitive (single-analyte) binding, the BZP imprinted MIP exhibited higher binding affinity normalised

with respect to the mass of the polymer towards the BZP template and its analogues (EPH and PHP) compared to its NIP counterpart, which resulted in IF values greater than 1.0 for all analytes. It can also be observed that both the BZP imprinted MIP and its NIP counterpart exhibited about 20% higher binding affinity towards EPH compared to BZP. Although this has resulted in similar imprinting factor to that of BZP (IF = 1.3), greater specific binding towards EPH (about 23% higher) was observed, resulting in lower SSF value (SSF < 1.0). Higher IF values towards EPH and BZP (IF > 12 and IF > 15 respectively) were exhibited by the MIP when the binding affinity was normalised with respect to the surface area of the polymer, as can be seen in Figure 4.25(B) and Table 4.10. Although the MIP exhibited higher IF value towards BZP, greater specific binding towards EPH (about 20% higher) was observed, resulting in lower SSF value (SSF < 1.0). The lower SSF value indicates that the MIP recognized and bound a higher number of EPH molecules compared to BZP. The reason for this could be attributed to the presence of an extra functional group (hydroxyl) in the EPH structure (Figure 4.2[2]), in addition to the amine group which is also present in BZP. The extra hydroxyl group of EPH enhanced the interaction between EPH and MAA by forming strong hydrogen bond with the acidic hydrogen of MAA (1.62 Å, Figure 4.26(A)). In addition, the hydrogen bond distance between the –NH group of EPH and the carbonyl group of MAA (1.97 Å, Figure 4.26(A)) is shorter than that of BZP and MAA (2.29 Å, Figure 4.7) whilst the size of EPH is slightly smaller than that of BZP (191.3 Å<sup>3</sup> and 204.6 Å<sup>3</sup>, respectively).<sup>257</sup> Therefore, EPH is expected to have greater excess to the binding site functionality, which can be observed from the higher binding capacity and specific binding of the MIP for EPH.

On the other hand, both the MIP and NIP microspheres exhibited lower binding affinity towards PHP compared to the BZP template (Figure 4.25(A)). As can be seen in Table 4.9, the amount of PHP bound normalised with respect to the mass of the polymers by the MIP and NIP, respectively, were about 10% and 25% less compared to those of BZP, which leads to greater specific binding (50% higher) and slightly higher IF value of the former, thus resulting in SSF value lower than 1.0. However, although a higher IF value was also observed for PHP compared to BZP when the binding affinity was

normalised with respect to the surface area (Figure 4.25(B)), the specific binding of the former was about 10% lower than the latter, thus resulting in a higher SSF value ( $SSF > 1.0$ ). The higher SSF value indicates that the MIP recognized and bound less PHP compared to BZP. The reason for this could be postulated to the slightly different structure of PHP to BZP (Figure 4.26(B) and 4.7, respectively). Although PHP has smaller volume ( $186.0 \text{ \AA}^3$ ) compared to that of BZP ( $204.6 \text{ \AA}^3$ ),<sup>257</sup> the hydrogen bond distance between the secondary amine of PHP and the carboxylic acid of MAA ( $1.71 \text{ \AA}$ , Figure 4.26(B)) is about the same as that between BZP and MAA ( $1.72 \text{ \AA}$ , Figure 4.7), whilst the hydrogen bond H-bond distance between the  $-\text{NH}$  group of PHP and the carbonyl group of MAA ( $2.48 \text{ \AA}$ , Figure 4.26(B)) is longer than that of BZP ( $2.29 \text{ \AA}$ , Figure 4.7). This means that PHP could form weaker hydrogen bonding with MAA compared to BZP. Another possible reason is that PHP has a single carbon linker between the two cyclic structures (Figure 4.26(B)) and therefore is less able to conform to the binding site morphology to set up appropriate binding interactions within the binding site due to its much more rigid molecule compared to BZP, which would likely to be more adept at this since it has two carbon linker between the two cyclic structures (Figure 4.7).

Different trends are observed when the rebinding was carried out in the presence of two analytes (binary-analyte assay), as can be seen in Figure 4.25(B - E). The presence of EPH has resulted in the decreased in the BZP binding affinity of the MIP normalised with respect to the mass (Figure 4.25(C)), compared to that in a single-analyte assay (Figure 4.25(A)), resulting in almost similar amount of binding for EPH and BZP. However, from Table 4.9, it can be seen that the EPH binding affinity of the NIP was also higher (about 25% higher) compared to BZP, resulting in slightly lower IF value and much lower specific binding, and hence higher SSF value ( $SSF \approx 2.0$ ). On the contrary, when the binding affinity was normalised with respect to the surface area (Figure 4.25(D) and Table 4.10), almost similar binding affinities were observed by the MIP towards BZP and EPH as well as the NIP towards both analytes, resulting in slightly higher IF value of BZP compared to EPH but similar amount of specific binding ( $SSF =$

1.0). This result indicates that the MIP exhibited similar selectivity towards BZP and EPH in a competitive binding assay.

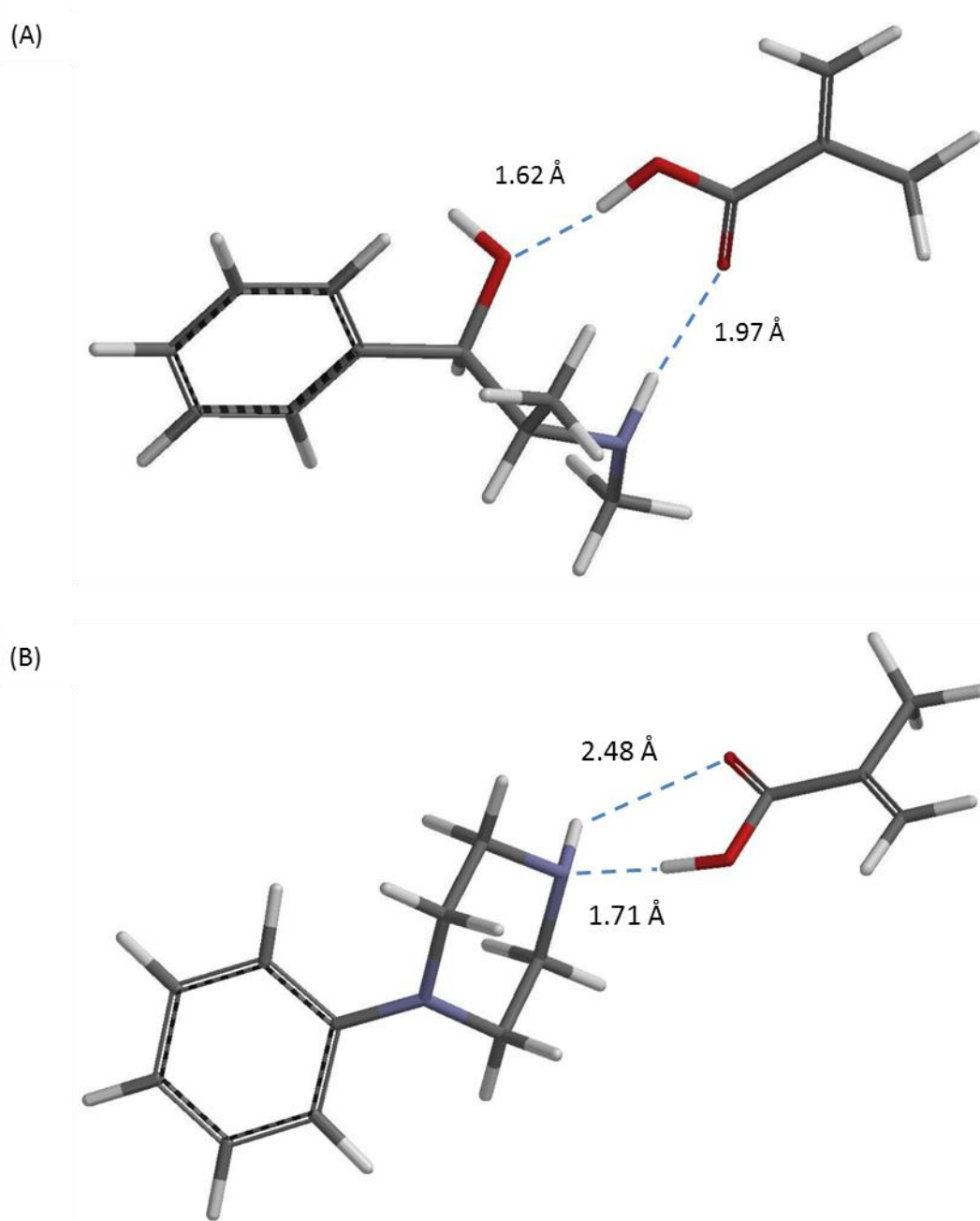


**Figure 4.26.** Computer generated molecular modelling images of (A) EPH:MAA 1:1 and (B) PHP:MAA 1:1 for the geometry optimised T:M clusters.

When the rebinding was carried out in the presence of both BZP and PHP (Figure 4.25(E) and Table 4.9), the binding affinities normalised with respect to the mass of the polymer of the BZP imprinted polymer and the non-imprinted polymer towards BZP have been reduced to about 40% and 50% respectively, compared to that in a single-analyte assay (Figure 4.52(A) and Table 4.9). However, these values are much higher than the binding affinities exhibited towards PHP (about 4-fold and 2.5-fold higher for the MIP and NIP respectively), resulting in much higher IF value and specific binding of BZP, and hence also higher SSF value ( $SSF \approx 11$ ). A similar trend was observed when the binding affinity was normalised with respect to the surface area (Figure 4.25(F) and Table 4.10). Much higher binding affinities were observed for both the MIP and the NIP towards BZP compared to PHP, resulting in much higher IF value and specific binding of the former compared to the latter, and hence also higher SSF value ( $SSF = 3.8$ ). This result indicates that the MIP exhibited much better selectivity (about 3.5-fold higher) towards BZP over PHP in the competitive binding assay, compared to that in the non-competitive binding assay ( $SSF = 3.8$  and  $1.1$ , respectively). This could be attributed to the creation of specific cavities designed for the BZP template in the MIP, which resulted in better selectivity of the MIP towards BZP over PHP in the presence of both analytes.

The competitive binding study conducted in a tertiary-analyte binding assay showed that the MIP exhibited higher binding affinities normalised with respect to the mass of the polymer towards all the analytes compared to those of the NIP, as can be observed in Figure 4.25(G) and Table 4.9. The presence of both EPH and PHP has caused a decrease in the binding affinity of the MIP towards BZP to about 70% of its binding affinity in the absence of any other analytes. Nevertheless, this value was still higher than those of the EPH and PHP (about 5% and 5-fold higher, respectively). The NIP, however, bound a higher amount of EPH (about 10% higher) compared to BZP, resulting in a higher IF value towards BZP and greater specific binding (about 2-fold higher), and hence also higher SSF value ( $SSF \approx 2$ ). On the other hand, the binding capacity of the NIP towards BZP was about 8-fold higher than PHP, resulting in higher

IF value towards PHP. However, the specific binding of BZP was higher compared to PHP, which resulted in higher SSF value (SSF = 2.5).

A contrary result was obtained, when the binding capacity was normalised with respect to the surface area (Figure 4.25(H) and Table 4.10), where almost similar binding capacities were observed by the MIP towards BZP and EPH as well as the NIP towards both analyte, resulting in a slightly higher IF value of BZP compared to EPH but similar amount of specific binding (SSF = 1.03). The MIP and the NIP bound about 5-fold and 8-fold respectively, higher amount of BZP compared to PHP, resulting in much higher IF value and specific binding of the former compared to the latter, and hence also higher SSF value (SSF  $\approx$  5). These results are consistent with the results obtained in the binary-analyte assay, which indicates that the MIP exhibited similar selectivity towards BZP and EPH, and better selectivity towards BZP over PHP in a competitive binding assay.

#### **4.4 Summary**

BZP imprinted polymers have been prepared via both iniferter and RAFT precipitation polymerisations using different concentration of iniferter or RAFT agent (i.e. 5, 10 and 20 mol %). Among the three formulations, MIP prepared using 5% of iniferter or RAFT gave the best binding performance in their series. Comparing the physical characteristics between the MIP-5%BDDC and MIP-5%RAFT microspheres, the former was more spherical and monodisperse, whilst the latter was less spherical and polydisperse. Despite the higher specific surface area and greater porosity of the MIP-5%RAFT compared to those of the MIP-5%BDDC, the latter exhibited higher binding capacity and greater specific binding compared to the former.

Due to the better binding performance of MIP-5%BDDC and the relatively easier preparation of CCS polymer when the microspheres prepared via iniferter was used as the core precursor compared to that of RAFT, the former was selected for further studies to determine the specificity of the BZP prepared polymer. Two drugs having

closely related structures to the BZP were selected as the analytes. In the non-competitive binding, it was found that the MIP-5%BDDC exhibited better selectivity towards EPH over BZP, but showed comparable selectivity towards both analytes in the competitive binding environments, which could be attributed to the smaller size and stronger hydrogen bonding ability of EPH compared to BZP. On the other hand, MIP-5%BDDC exhibited better selectivity towards BZP over PHP in both the non-competitive and competitive binding environments, indicating greater recognition properties for the template molecules. The MIP-5%BDDC formulation was used in a pilot study in Chapter 5 to prepare the core precursor for the synthesis of CCS MIPs followed by batch binding analysis to assess their binding performance.

## Chapter 5

### Core Crosslinked Star Molecular imprinted Polymers

#### 5.1 Introduction

Relatively little attention has been given to the preparation of star polymers in molecular imprinting. Several methods such as UV irradiation<sup>122</sup>, RAFT,<sup>172</sup> as well as a combination of RAFT and ring-closing metathesis,<sup>173, 332</sup> have been employed to prepare molecular imprinted star polymers but core crosslinked star (CCS) MIPs prepared via RDRP have not been extensively investigated. Prior literature appears to be only limited to a conference paper by Nakayama and his co-workers, who reported the synthesis of CCS MIP for L-phenylalanine (L-PA) via the arm-first method using BDDC iniferter.<sup>174, 175</sup> The ability of the CCS MIP as a carrier for L-PA has been estimated by bulk liquid membrane method using U-shaped glass tube. It was found that the star MIP retained 1.6 mM of L-PA during the 120 h operation of the liquid membrane experiment whereas zero concentration of L-PA was detected for the CCS NIP. This transport loading of the L-PA imprinted CCS polymer was lower compared to that of the non CCS MIP (i.e. conventional crosslinked MIP) prepared by Laio and his co-workers<sup>333</sup> using D-PA as the template, where about 4.0 mM of DPA was transported after 72 h, whilst the NIP did not transport D-PA at an appreciable rate.

By taking advantage of the iniferter technique and in combination with precipitation polymerisation, MIP microspheres with surface bound active groups can be prepared and used as the core precursor in the formation of CCS MIP by growing arms around

the imprinted core. Compared to other available forms, molecular imprinted polymer in the form of a core crosslinked star has the advantage of being processable and additionally, has the potential to be deployed as a thin MIP film. In this approach, imprinting occurs at the crosslinked core while solubility is provided by the arms, as shown in Scheme 5.1 (§5.2.2). The dispersible CCS MIP is expected to have good prospects for sensing applications because the material can be readily formulated into a thin film coating supported on a solid substrate while the MIP component can impart enhanced and selective recognition.

Herein, this chapter describes the preparation of core crosslinked star molecular imprinted polymers (CCS MIP) via the core-first iniferter method. CCS polymers were previously synthesised using BDDC iniferter and discussed in great detail in Chapter 2. In that chapter, the focus was on the synthesis of CCS polymers via the arm-first method, i.e. synthesising the active linear arms and using them as the precursor for the formation of CCS polymers. Synthesis of CCS polymer via the core-first approach was also investigated and compared with that of the arm-first approach. Although the degree of polymerisation (DP) of the arms can be well-controlled since they are synthesised independently, the arm-first approach was complicated by the need to separate the unreacted arm precursor from the CCS MIP during the purification step. In addition, it was difficult to characterise the core because the arms were not cleavable. Characterisation of the core is very important since it is the location of the template cavities and template rebinding should take place near the surface of the core. Due to the above reasons, the focus was shifted to the preparation of CCS MIPs via the core-first method. The first step in the synthesis of a CCS MIP is the preparation of the core, thus MIP microspheres were prepared from various formulations, characterised and discussed in great detail in Chapter 4. The best performing MIP microspheres from Chapter 4 have been chosen to be further used as the core for the preparation of the CCS MIP presented in this chapter.

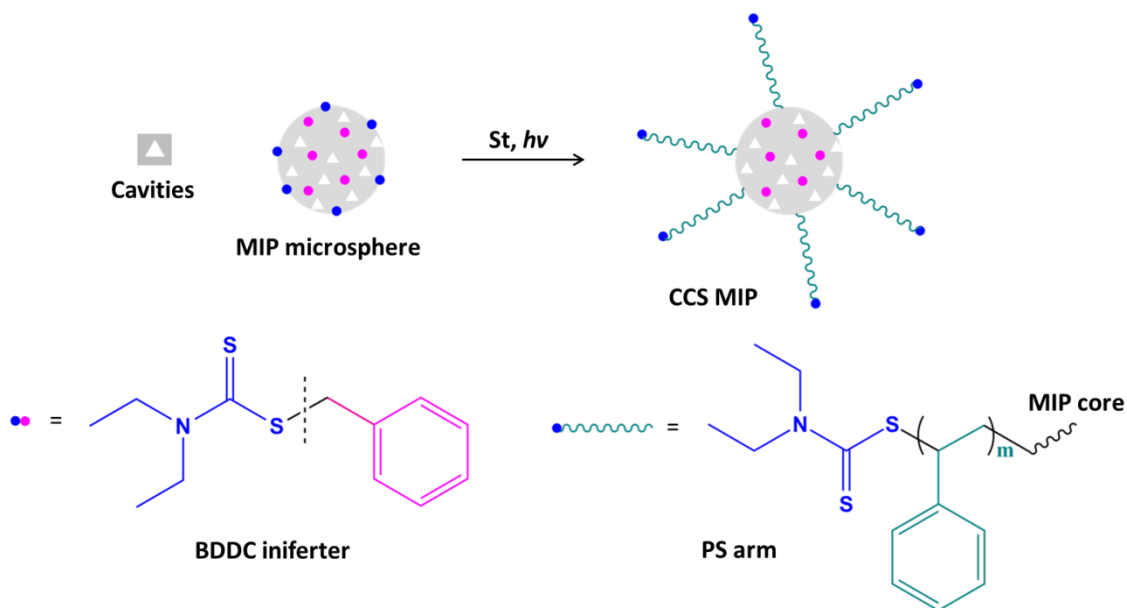
## 5.2 Experimental

### 5.2.1 Materials

Potassium dihydrogen phosphate ( $\text{KH}_2\text{PO}_4$ ), potassium chloride (KCl), phosphoric acid ( $\text{H}_3\text{PO}_4$ ) and triethylamine were obtained from Sigma-Aldrich. Ethylene glycol dimethacrylate (EGDMA), methacrylic acid (MAA) and styrene (St) was obtained from Sigma-Aldrich ( $\geq 98\%$  purity), and passed through a column of activated basic alumina (Aldrich, Brockmann I, standard grade,  $\sim 150$  mesh, 5.8 nm) to remove radical inhibitors. Benzyl *N,N*-diethyldithiocarbamate (BDDC) was synthesised following the procedure described in §2.2.2. Benzylpiperazine (97%) was obtained from Fluka and used as received. Deuterated chloroform ( $\text{CDCl}_3$ , 99.6 atom %) for NMR analysis was obtained from Aldrich. HPLC grade tetrahydrofuran (THF) and acetonitrile were obtained from Scharlau and Merck respectively. Bulk grade methanol was distilled prior to use. All water was purified by reverse osmosis prior to use.

### 5.2.2 CCS MIP Synthesis

The CCS MIPs were synthesised by reacting the MIP microspheres and styrene monomer via the reactive iniferter group on the surface of the former (Scheme 5.1).



**Scheme 5.1.** Synthesis of core-first CCS MIP by iniferter-mediated precipitation polymerisation.

The MIP microspheres (MIP-5%BDDC-B2) were prepared using the same formulation as MIP-5%BDDC (Chapter 4), following the procedure in §4.2.2. The corresponding NIP microspheres (NIP-5%BDDC-B2) were also prepared following the same procedure except that no BZP template was added in the polymerisation process. The MIP microspheres were then subjected to Soxhlet extraction to remove the BZP template, following the procedure in §4.2.3. The NIP microspheres were subjected to an identical Soxhlet extraction in case this processing had any secondary effect on the microspheres. The MIP and NIP microspheres were used as core precursors in the preparation of CCS MIP and CCS NIP, respectively, and thus are also referred to as the MIP and NIP cores.

A typical polymerisation procedure for the synthesis of the CCS MIP is as follows: 200 mg of the MIP core (MIP-5%BDDC-B2) and styrene monomer (5.6 mmol) were mixed in THF (8.0 mL) in a test tube. The mixture was then purged with nitrogen for 30 mins and photopolymerised using the set-up described in §2.2.5 at room temperature for 48 hours. The turbid polymerisation mixture was then added dropwise to a large amount

of methanol to precipitate any soluble products and separate them from any unreacted monomer. The precipitate was collected by centrifugation and subjected to further purification and fractionation, as shown in Figure 5.1(A). Firstly, the precipitate was redispersed in THF while stirring. The mixture was centrifuged (Thermoline Scientific) at 6000 rpm for about 15 min, after which the sediment was separated from the supernatant, washed with methanol, labelled as CCS MIP-F1 and kept for future use. The supernatant was then added dropwise to methanol to form another fraction of precipitate. The mixture was again centrifuged for about 15 min and the precipitate, labelled as CCS MIP-F2 was collected. Both precipitates were dried overnight under vacuum and the yields were determined gravimetrically. The CCS NIP was prepared following the same procedure as the CCS MIP with a slight modification in the purification steps, as shown in Fig. 5.1(B).

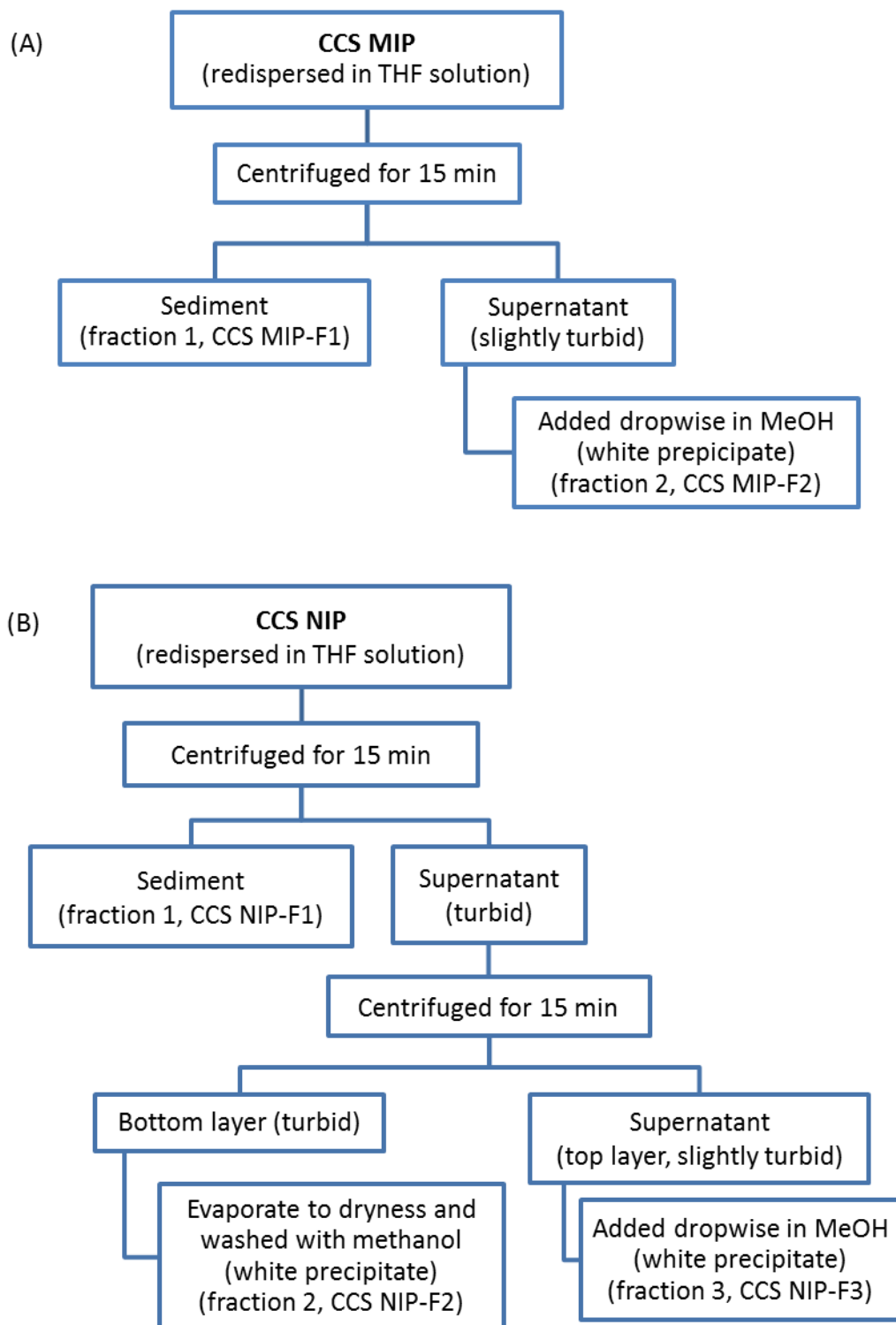


**Figure 5.1.** Purification steps of (A) CCS MIP and (B) CCS NIP.

### 5.2.3 Characterisation of CCS MIP

The CCS MIP and the corresponding NIP samples were subjected to a range of characterisations such as NMR, SEM and DLS to determine their composition, morphology, particle size and particle size distribution following the procedures outlined in §2.3.

#### 5.2.3.1 FTIR

FTIR spectra of both the solid and liquid samples were recorded on Perkin Elmer Spectrum Two, controlled by Spectrum 10™ software at 4 cm<sup>-1</sup> resolution in the range of 4000 – 400 cm<sup>-1</sup>. In order to investigate the possible relation between the crosslinking density of the polymers and their binding performance, the degree of crosslinking of the microspheres and the CCS polymers was determined according to the procedure in §4.2.7.1.

### 5.2.4 CCS MIP Composition by FTIR Analysis

Given that the template binding by the CCS MIP is expected to be primarily confined to the core, it is important to determine the mass fraction of the core in each of the CCS MIP samples in order to facilitate the calculation of meaningful template binding data. The mass fraction of the core relative to that of the PS arms was determined from FTIR analysis against standard mixtures of EGDMA/MAA and St. Note that it was necessary to assume the same mole ratio of EGDMA to MAA in the polymer as the monomer feed ratio (i.e. EGDMA:MAA = 4:1). To obtain a calibration curve, a mixture of EGDMA and MAA monomers in a fixed mole ratio of 4 to 1 were prepared and added to different amounts of styrene monomer so that the weight percent of the EGDMA/MAA mixture varied between 5 to 95% with respect to the total weight. The FTIR absorbance spectra of these mixtures were obtained and the absorbance peak height ratios of EGDMA/MAA (as uniquely defined by the carbonyl absorbance at 1727 cm<sup>-1</sup>) to the St (out-of-plane C-H bending absorbance mode of the aromatic ring at 697 cm<sup>-1</sup>)

were calculated. An example of the FTIR absorbance spectrum of a mixture containing 5% St is shown in Figure 5.2(A) and compared with those of the CCS MIP and its core precursor (Figure 5.3(C) and (B) respectively).

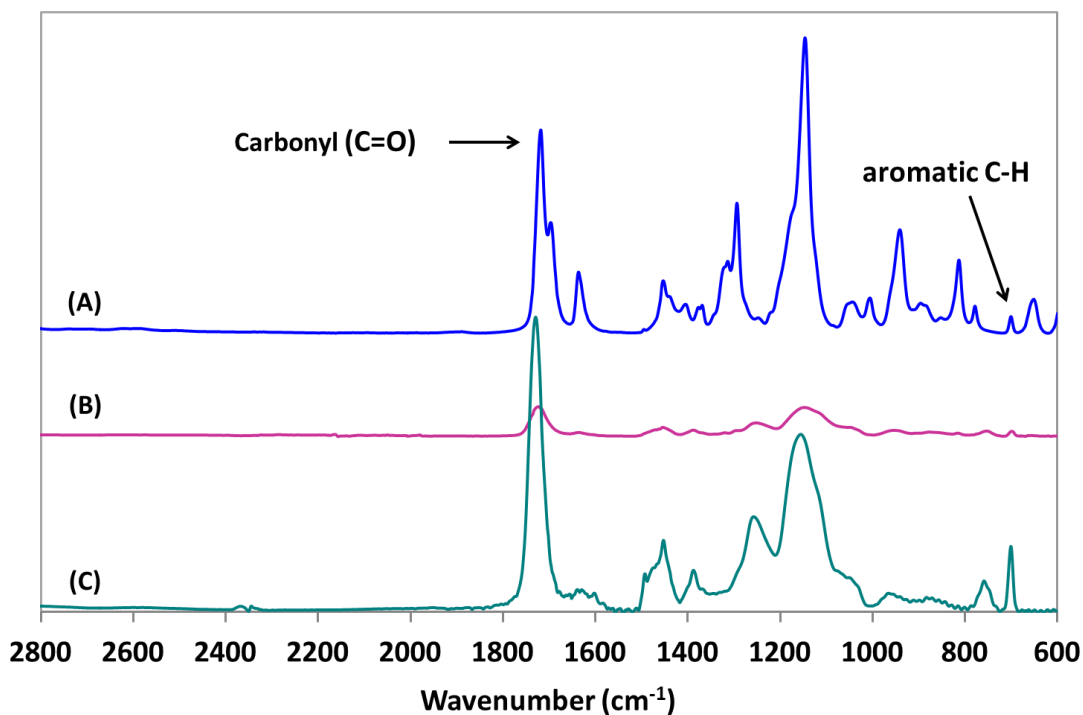


**Figure 5.2.** Comparison of FTIR absorbance spectra of the (A) calibration mixture (5% w/w styrene), (B) core precursor (MIP-5%BDDC-B2) and (C) CCS MIP (CCS MIP-F1).

Calibration curves were then plotted as the (C=O/aromatic C-H) absorbance peak ratio versus the EGDMA/MAA mixture mass fraction with respect to the total weight. Subsequently, the ratio of (C=O/aromatic C-H) in the CCS polymer was calculated from its FTIR spectrum (Figure 5.2(C)) and the corresponding mass fraction of EGDMA/MAA mixture with respect to the total mass was estimated from the calibration curve. This value was then taken as the mass fraction of the polymer core with respect to the total mass of the CCS MIP. Since the absorbance mode at 699 cm<sup>-1</sup> was also present in the core precursor (Figure 5.2(B)), which was attributed to the absorbance of the benzyl group of the iniferter, this absorbance was normalised against that of the core precursor before calculating the (C=O/aromatic C-H) ratio. The calibration curve in Figure 5.3(A) was used to estimate the core mass fraction for samples having values of

C=O/aromatic C-H ratio less than 2, whereas for samples that exhibit ratios greater than that, their core mass fraction was estimated using the calibration curve in Figure 5.3(B) instead.

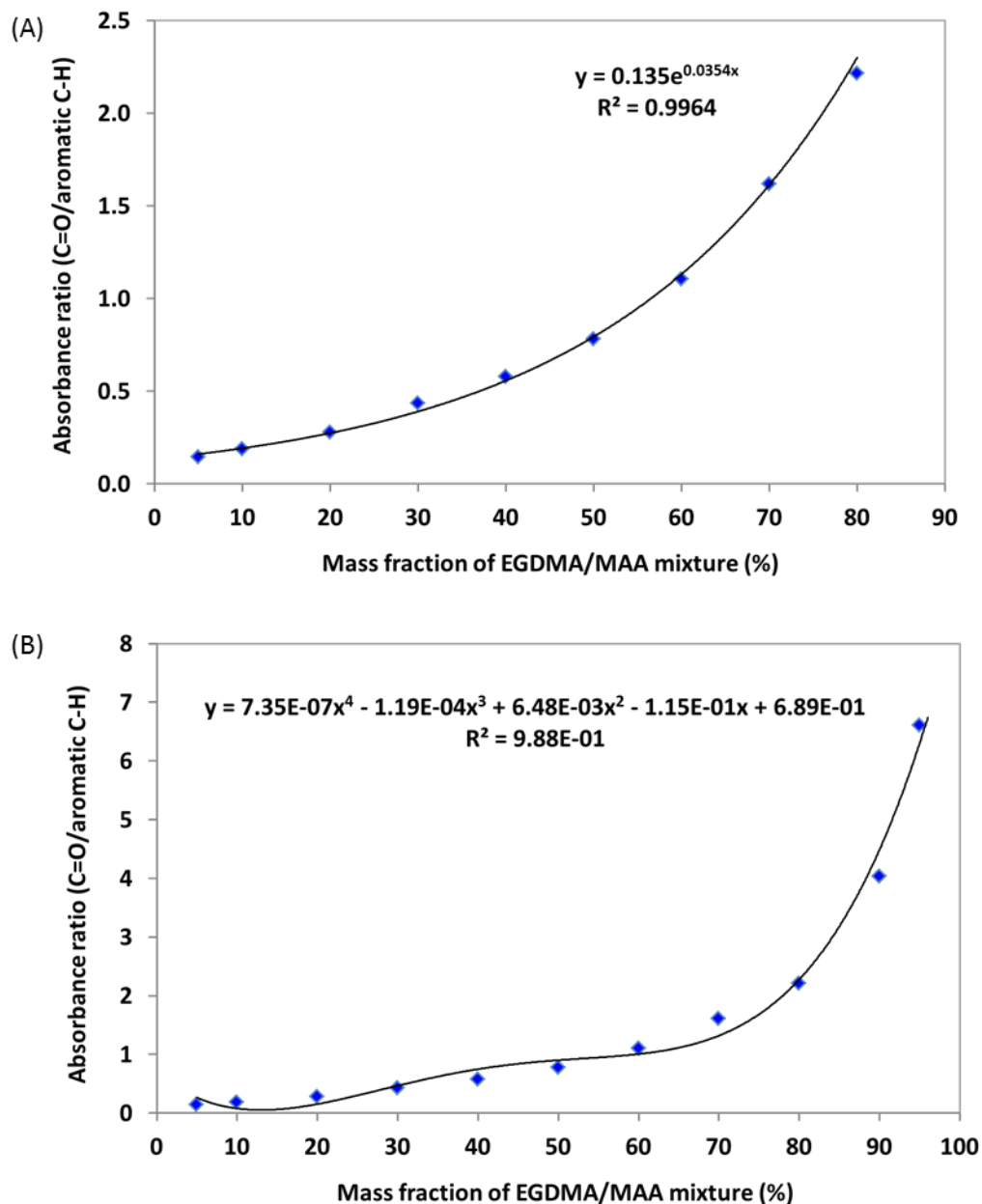


**Figure 5.3.** The calibration curves used for the estimation of the mass fraction of the MAA and EGDMA constituent of the core in the CCS polymer with styrene arms. The y-axis indicates the (C=O/aromatic C-H) absorbance ratio of a mixture of EGDMA, MAA and styrene whilst the x-axis is the mass fraction of the EGDMA/MAA mixture with respect to the total mass. (A) used for calibration for C=O/aromatic C-H ratios less than 2, and (B) used for C=O/aromatic C-H ratios greater than 2.

### 5.2.5 Determination of $M_n$ of PS Arm by $^1\text{H}$ NMR

The number-average molecular weight ( $M_n$ ) of the PS arm attached to the core of the CCS polymers was determined from their  $^1\text{H}$  NMR spectra.<sup>334, 335</sup> The integrated peak intensity ratio of the styrene aromatic protons of the main chain to the BDDC iniferter moiety gives the degree of polymerisation (DP) and hence the  $M_n$  of the PS arm.

### 5.2.6 Batch Rebinding Studies

Batch rebinding experiments were carried out using a known molarity of BZP stock solution in both acetonitrile and THF, following the procedure in §4.2.4. The experiments were conducted in duplicate and the mean values are reported. The amount of BZP bound,  $S_B$  was calculated according to Equation 4.1 (see §4.2.4) except that only the mass of the core (not the entire polymer) was considered since the binding is assumed to occur only at the core as concluded in §5.3.2 from Figure 5.10, and expressed as  $\mu\text{mol}$  of substrate bound per g of polymer core ( $\mu\text{mol g}^{-1}$ ). The mass of the core was calculated as outlined in §5.2.4.

## 5.3 Results and Discussion

### 5.3.1 Preparation and Characterisation of CCS MIPs and NIPs

#### 5.3.1.1 Preparation of CCS MIPs/NIPs

BZP imprinted microspheres with reactive functional groups have been prepared by precipitation polymerisation using both BDDC iniferter and RAFT agent (MCABTTC) approaches (§4.2.2). These reactive functional groups could be further polymerised by growing PS arms anchored at the core to yield BZP imprinted core crosslinked star polymers. Comparison of the results of the binding studies between the MIP microsphere obtained via iniferter and RAFT (§4.3.4) showed that the former exhibited better BZP binding performance in terms of higher BZP binding capacity and specific binding values when prepared using 5% BDDC compared to those prepared by RAFT.

The synthesis of MIP microspheres was carried out in acetonitrile because it was able to dissolve all the polymerisation ingredients. In addition, it was also reported to give monodisperse spherical particles,<sup>142, 231, 279</sup> which was consistent with the results of our MIP microspheres prepared via iniferter (see §4.3.2.1). However, since polystyrene is not soluble in acetonitrile, the preparation of CCS MIP was carried out in THF, which is a good solvent for PS. Thus the presence of PS arms anchored to the MIP core is anticipated to result in a dispersible CCS MIP in THF.

During the purification and fractionation process of CCS MIP and NIP illustrated in Figure 5.1(A) and (B), respectively, several fractions of CCS polymers were obtained. For the CCS MIP, two fractions were obtained: one fraction was not dispersed in THF and formed sediment when left overnight (CCS MIP-F1) while the other fraction was dispersible in THF resulting in a slightly turbid solution (CCS MIP-F2). For the CCS NIP, three fractions were obtained: a fraction that was not dispersed in THF and formed sediment when left overnight (CCS NIP-F1), a fraction that was dispersed in THF, but was colloidally stable, resulting in a turbid solution (CCS NIP-F2) and finally a fraction that was dispersed in THF, forming a slightly turbid solution (CCS NIP-F3). The isolation of multiple polymer fractions per formulation suggests that photopolymerisation of styrene at the surface of iniferter-bound MIP and NIP core precursors resulted in CCS polymers with variable chain length or chain distribution as indicated by the different degrees of dispersibility in THF. Detailed characterisation of each CCS MIP and NIP fraction is presented in the succeeding sections.

### 5.3.1.2 Particle Size Analysis by SEM and DLS

The SEM images of MIP-5%BDDC-B2 (MIP core precursor), CCS MIP-F1 and CCS MIP-F2 are shown in Figure 5.4(A - C) and the average particle diameter of the MIPs determined from the SEM are tabulated in Table 5.1. As can be seen in Figure 5.4(A), the MIP core microspheres (MIP-5%BDDC-B2) are monodisperse spherical particles, having SEM average particle size of  $1180 \pm 130$  nm (Table 5.1), which is consistent with

the particle size of the MIP-5%BDDC prepared in Chapter 4 (§4.3.2) indicating the batch reproducibility of the polymerisation. In addition, a very low fraction of small-sized particles could also be observed in the spectrum of the MIP core precursor. The SEM images of CCS MIP-F1 and CCS MIP-F2 showed similar monodisperse spherical particles as those of the MIP core precursor.

The SEM images of NIP-5%BDDC-B2 (NIP core precursor), CCS NIP-F1, CCS NIP-F2 and CCS NIP-F3 are shown in Figure 5.4(D - G). The hydrodynamic diameters of the CCS NIP fractions and their NIP core precursor were determined by DLS and the results are tabulated in Table 5.1. As can be seen in Figure 5.4(D), discrete particles could not be observed in the SEM image of the NIP core precursor (NIP-5%BDDC-B2), unlike that of the NIP-5%BDDC (Figure 4.9, §4.3.2.1), despite being prepared by the same procedure. The reason was postulated to be as a result of poor sample preparation rather than the property of the polymer. This is supported by the hydrodynamic diameter of the NIP-5%BDDC-B2, which showed evidence of monodisperse particles of about 132 nm. From Table 5.1, it can be observed that the  $D_h$  values of the CCS NIPs were essentially equal within error, ranging from 122 – 139 nm. It can also be noticed that the hydrodynamic size of the NIP core precursor (NIP-5%BDDC-B2) was much smaller than the SEM particle size of its MIP counterpart ( $132 \pm 2$  and  $1180 \pm 130$  nm, respectively), which was attributed to the effect of the presence of the template during the polymerisation (see §4.3.2.1).

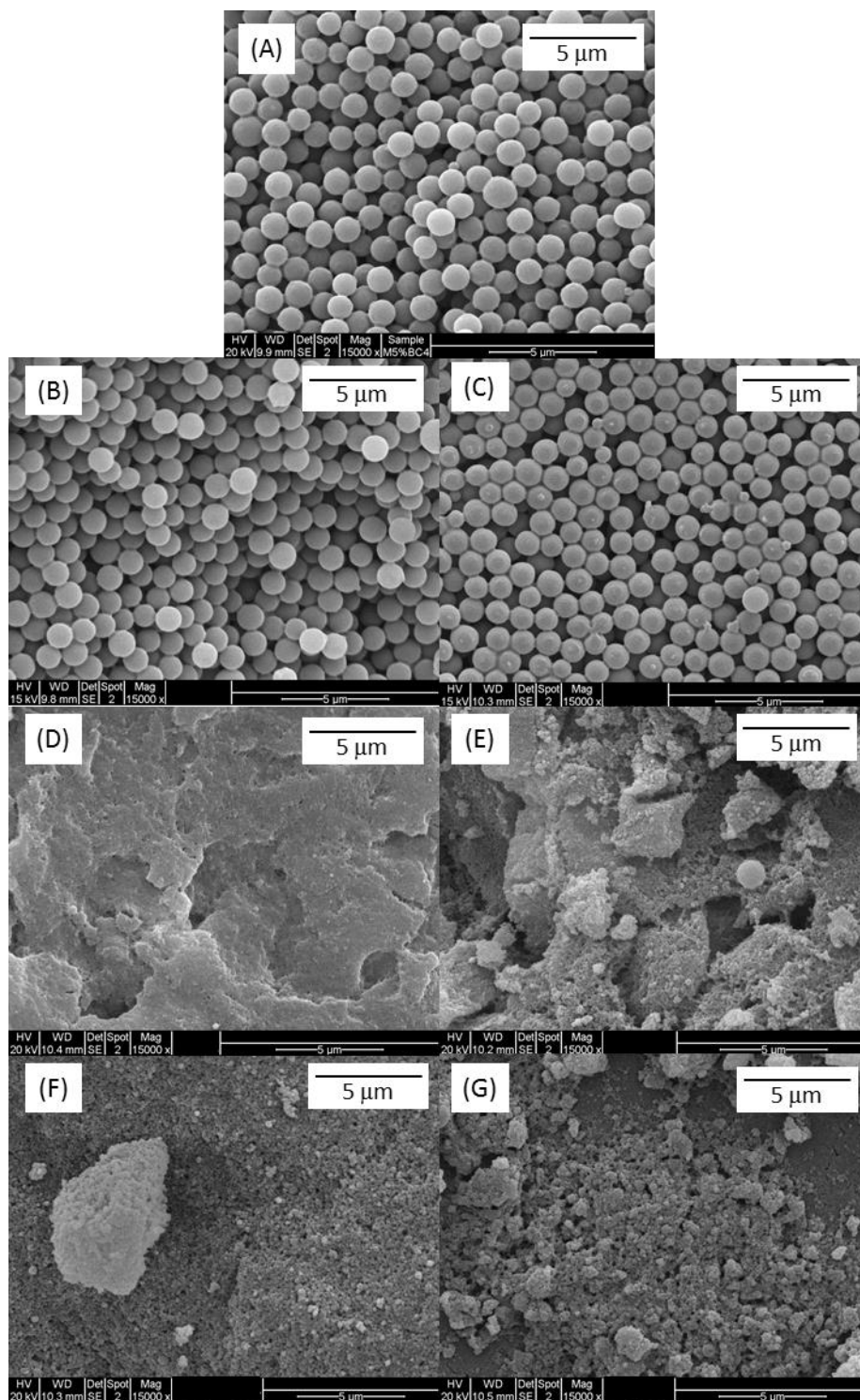


**Figure 5.4.** SEM images of (A) MIP-5%BDDC-B2, (B) CCS MIP-F1, (C) CCS MIP-F2, (D) NIP-5%BDDC-B2, (E) CCS NIP-F1, (F) CCS NIP-F2 and (G) CCS NIP-F3. The images were recorded at 15000X magnifications.

**Table 5.1.** Physical characteristics of CCS imprinted and non-imprinted polymers versus the core microspheres.

Polymer	Yield (%)	SEM average diameter (nm)	$D_h$ (nm) <sup>a</sup>	Core weight (%) <sup>b</sup>	DC (%) <sup>c</sup>	$M_{n,PS}$ (kDa) <sup>d</sup>
MIP-5%BDDC-B2	N/A	1180 ± 130	N/A	N/A	61	N/A
CCS MIP-F1	77	1130 ± 80	N/A	92	77	N/A
CCS MIP-F2	23	1120 ± 90	N/A	22	65	2.8
NIP-5%BDDC-B2	N/A	N/A	132 ± 2	N/A	62	N/A
CCS NIP-F1	55	N/A	135 ± 6	83	76	N/A
CCS NIP-F2	16	N/A	122 ± 2	57	73	0.8
CCS NIP-F3	29	N/A	139 ± 1	44	71	1.8

<sup>a</sup> Hydrodynamic diameter of filtered sample of polymers (using a 450 nm membrane filter) obtained by DLS.

<sup>b</sup> Core weight percent (%) of CCS polymers calculated from FTIR data (Figure 5.5).

<sup>c</sup> Extent of C=C bond conversion of the EGDMA, DC (%), calculated according to the following equation (Equation 4.1) :

$$DC (\%) = 100 \times \left[ 1 - \frac{(A_{C=C}/A_{C=O})_{polymer}}{(A_{C=C}/A_{C=O})_{monomer}} \right]$$

<sup>d</sup>  $M_n$  of PS arm calculated from <sup>1</sup>H NMR data (Figures 5.6 – 5.8).

N/A – not available

### 5.3.1.3 FTIR Analysis

Structural confirmation of the CCS polymers was performed using FTIR spectroscopy. To confirm the difference in the structure of the CCS MIP fractions compared to their core precursor, the absorbance FTIR spectra of the former and the latter are compared, as shown in Figure 5.5(A). As can be seen in the spectrum of the MIP core precursor (MIP-5%BDDC-B2), the strong absorption peak at 1729 cm<sup>-1</sup> is assigned to the carbonyl (C=O) stretching vibration of both the EGDMA and MAA units in the core whilst the absorption peak at 754 and 699 cm<sup>-1</sup> are attributed to the aromatic ring out of plane C-H bending vibration of benzyl group of BDDC. All three peaks can also be observed in the FTIR spectra of both the CCS MIP fractions. Compared with that of

MIP-5%BDDC-B2, the emergence of new peaks at 3061, 3026, 1601, 1493 and 1451  $\text{cm}^{-1}$  in the FTIR spectrum of CCS MIP-F2 are assigned to the characteristic peaks of styrene.<sup>336</sup> Although these peaks are also observed in the spectrum of CCS MIP-F1, they are less intense compared to those of the CCS MIP-F2, which indicates greater surface density of PS arm of the latter, probably due to its longer PS arm compared to the former.<sup>337</sup> This might explain the different behaviour of the CCS MIPs when dispersed in THF, whereby the CCS MIP-F2 was more dispersible in THF compared to the CCS MIP-F1. The strong absorption band at 699  $\text{cm}^{-1}$  in the spectra of both the CCS MIP-F1 and CCS MIP-F2 is attributed to the out-of-plane CH bending of the mono-substituted benzene ring of the PS arm, which overlapped with that of the benzyl group of BDDC. It can be clearly observed that the intensity of the out-of-plane C-H bending absorbance of the aromatic ring at 699  $\text{cm}^{-1}$  in the spectra of the CCS MIP fractions has increased significantly compared to that of their core precursor, which confirms the incorporation of PS arms around the core microsphere.

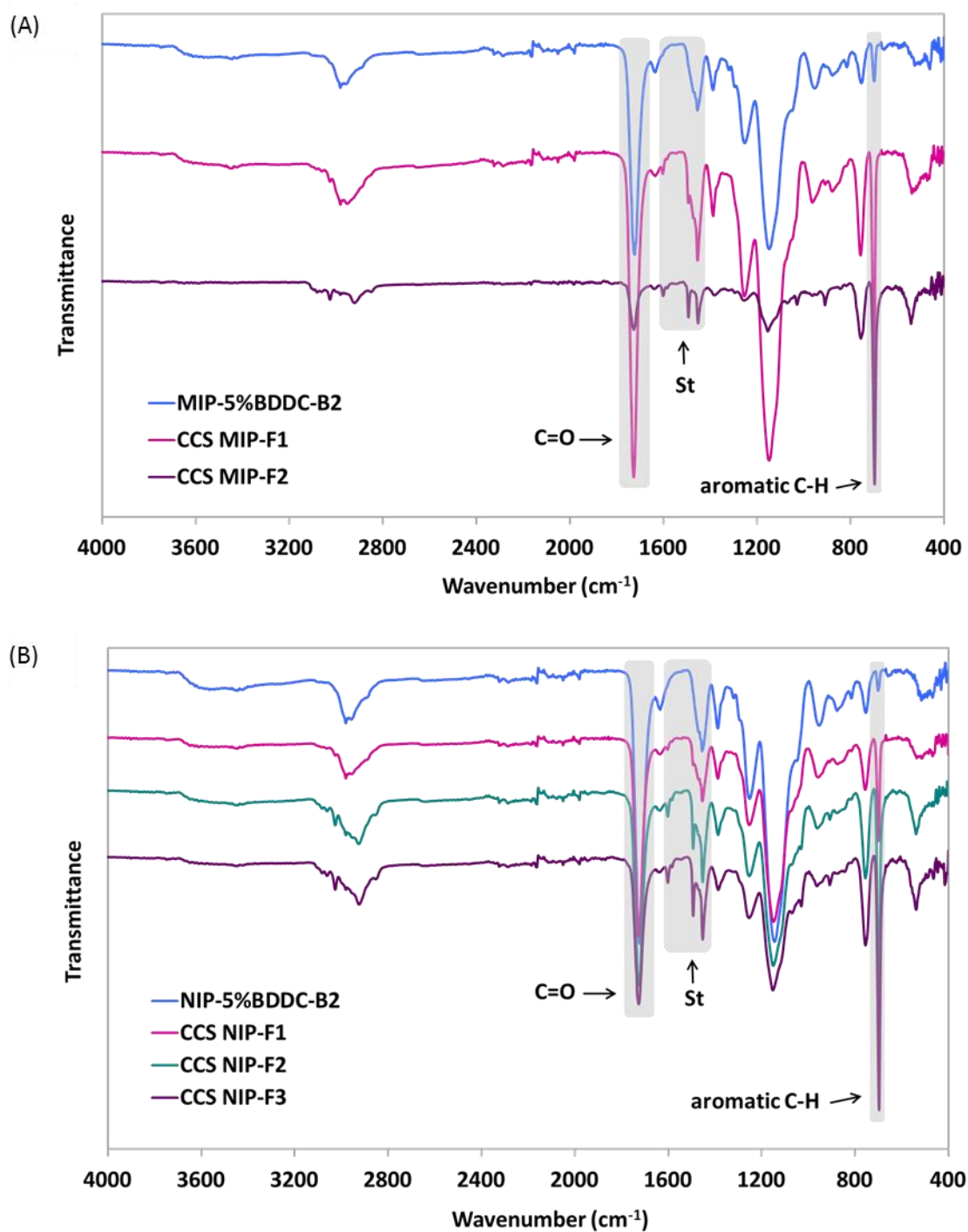


**Figure 5.5.** FTIR spectra of (A) CCS MIP and (B) CCS NIP fractions compared to their corresponding core precursors.

The FTIR spectra of the CCS NIP fractions are also compared with their core precursor as shown in Figure 5.5(B). Similar to the results obtained with the CCS MIP fractions, the spectra of the CCS NIP fractions also showed the characteristic peaks of styrene at 3061, 3026, 1601, 1493 and 1451  $\text{cm}^{-1}$ , which were not present in the spectrum of their core precursor (NIP-5%BDDC-B2). It can also be observed that intensity of the out-of-plane C-H bending absorbance of the aromatic ring at 699  $\text{cm}^{-1}$  in the spectra of the CCS NIP fractions has increased significantly compared to that of their core precursor, confirming the incorporation of PS arms around the NIP core microsphere.

The ratios of the carbonyl (C=O) absorbance mode at 1729  $\text{cm}^{-1}$  to the normalised C-H bending absorbance of the aromatic ring at 699  $\text{cm}^{-1}$  of the CCS MIP and NIP fractions were determined. The calibration curves in Figure 5.3 were then used to estimate the corresponding weight percent of EGDMA/MAA with respect to the total mass of the mixture. This value is taken as the mass fraction of the core with respect to the total weight of the CCS polymer and the results are tabulated in Table 5.1.

As can be seen from Table 5.1, the weight percent of the core of CCS MIP-F1 with respect to the total mass of the polymer was about 4-fold higher than that of the CCS MIP-F2 (92% and 22%, respectively) which indicates that the latter contains a higher PS arm content relative to the core. It can also be seen that CCS NIP-F1 exhibit the highest core weight percent, followed by CCS NIP-F2 and CCS NIP-F3 (83, 57 and 60%, respectively). This indicates that CCS NIP-F1 contained the lowest PS arm content by weight relative to the core, whilst that of CCS NIP-F3 was the highest.

In order to determine the effect of further polymerisation to the crosslinking density of the MIP and NIP core precursors and its possible relation with the binding performance, the degree of crosslinking of the polymers was determined from the FTIR spectra of the CCS MIP and NIP fractions, following the procedure in §4.2.7.1. These values are then compared with those of their core precursors as tabulated in Table 5.1.

From the table, it can be observed that the degree of crosslinking of both CCS MIP-F1 and CCS MIP-F2 was higher (about 26% and 7% higher, respectively) to that of the core precursor. This indicates that both the CCS MIP fractions were more crosslinked than the core precursor. As for the NIP, all the CCS NIP fractions exhibited higher degree of crosslinking (between 15 – 23 % higher) compared to that of the NIP core precursor. This indicates that during the polymerisation reaction to prepare the CCS MIP and NIP polymers, further intra crosslinking also occurs within the core of the CCS polymers, thus resulted in higher crosslinking density compared to the respective core precursors.

#### 5.3.1.4 <sup>1</sup>H NMR Analysis.

Only the <sup>1</sup>H NMR spectra of CCS MIP-F2, CCS NIP-F2 and CCS NIP-F3 were recorded (Figures 5.6, 5.7 and 5.8 respectively) using deuterated chloroform since the rest of the polymers were not dispersible in this NMR solvent. As shown in the <sup>1</sup>H NMR spectrum of CCS MIP-F2 in Figure 5.6, the peak at about 0.8 – 0.9 ppm (H<sub>b</sub>) is assigned to the –CH<sub>3</sub> of EGDMA and MAA whilst the peak between 3.9 – 4.0 ppm (H<sub>2</sub>) is attributed to the methylene protons of diethyl dithiocarbamate (DDC) at the periphery of the CCS polymer. The broad peak at about 4.1-4.4 ppm (H<sub>c</sub>) corresponds to four protons of EGDMA (-CH<sub>2</sub>CH<sub>2</sub>O). The very low intensity assigned to these protons in the spectrum illustrates the very low mobility of EGDMA in solution due to the highly crosslinked network. The peaks at 5.6 and 6.1 ppm (H<sub>d</sub>) are assigned to the pendant carbon-carbon double bonds of EGDMA present in the core due to incomplete crosslinking. The peaks between 1.2 – 1.6 ppm (H<sub>a</sub>) are attributed to the backbone methylene of PS as well as PEGDMA and PMAA in the core. Finally, the peaks between 1.6 – 2.2 ppm (H<sub>e</sub>) are assigned to the backbone methine protons of PS whilst the peaks at 6.3 – 7.3 ppm (H<sub>f</sub>) are attributed to the aromatic protons of styrene, which overlapped with the aromatic protons of benzyl group of the iniferter (H<sub>1</sub>). The presence of these peaks confirms the attachment of the PS arms around the core resulting in a core crosslinked star MIP.

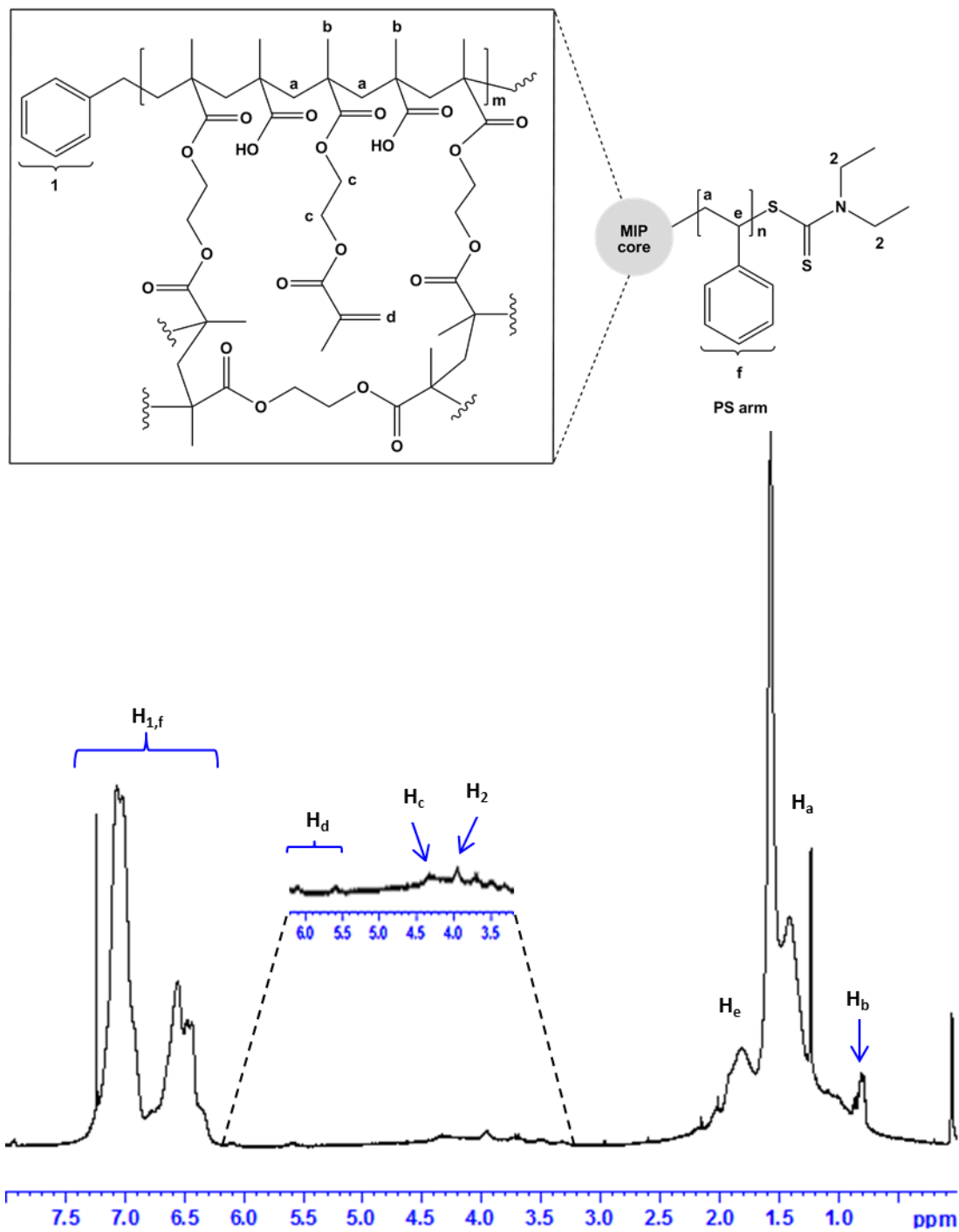


**Figure 5.6.**  $^1\text{H}$  NMR spectrum of CCS MIP-F2.

As can be seen in the  $^1\text{H}$  NMR spectra of CCS NIP-F2 and CCS NIP-F3, Figures 5.7 and 5.8, respectively, both the CCS NIP fractions contained similar peaks as those of the

CCS MIP-F1. However, the peaks attributed to the pendant double bonds of EGDMA (between 4.1 - 4.4 ppm) were not clearly visible compared to that of the CCS MIP. This could be due to the slightly lower mobility of the PEGDMA core of CCS NIP fractions in solution compared to that of the CCS MIP fraction, as can be seen from their lower percentage of pendant C=C double bond relative to carbonyl (C=O) estimated from their FTIR spectra (Table 5.1. The presence of peaks between 5.5 – 6.0 ppm (X) attributed to the vinyl protons of styrene monomer were probably due to the incomplete removal of the unreacted monomers during the purification process. The intensity ratio between the peak attributed to the methylene protons of diethyl dithiocarbamate, -DDC ( $H_2$ ) and the aromatic proton peaks ( $H_f$ ) was used to estimate the number average molecular weight ( $M_n$ ) of the PS arms attached to the core of the CCS polymers and the results are tabulated in Table 5.1. As shown in the table, the estimated PS arm length of CCS NIP-F3 was about twice of that of the CCS NIP-F2 ( $M_n = 1.8$  and  $0.8$  kDa, respectively). It can also be seen that the  $M_n$  of the PS arm segment anchored to the core of the CCS MIP-F2 was about  $2.8$  kDa. This value was about  $1.5$  and  $3.5$ -fold longer than those of the CCS NIP-F2 and CCS NIP-F3, respectively. Comparing the NMR spectra of the CCS NIP fractions to the NMR spectrum of CCS polymer prepared via the core-first iniferter (Figure 2.20, §2.4.2.2), the peaks attributed to the methylene protons of DDC were not visible in the latter and thus calculation of the  $M_n$  of the PS arm was not possible. This could be due to the difference in the length of the PS arms of CCS polymer and CCS NIP, where the former could have contained longer styrene units relative to the DDC end group compared to the latter.

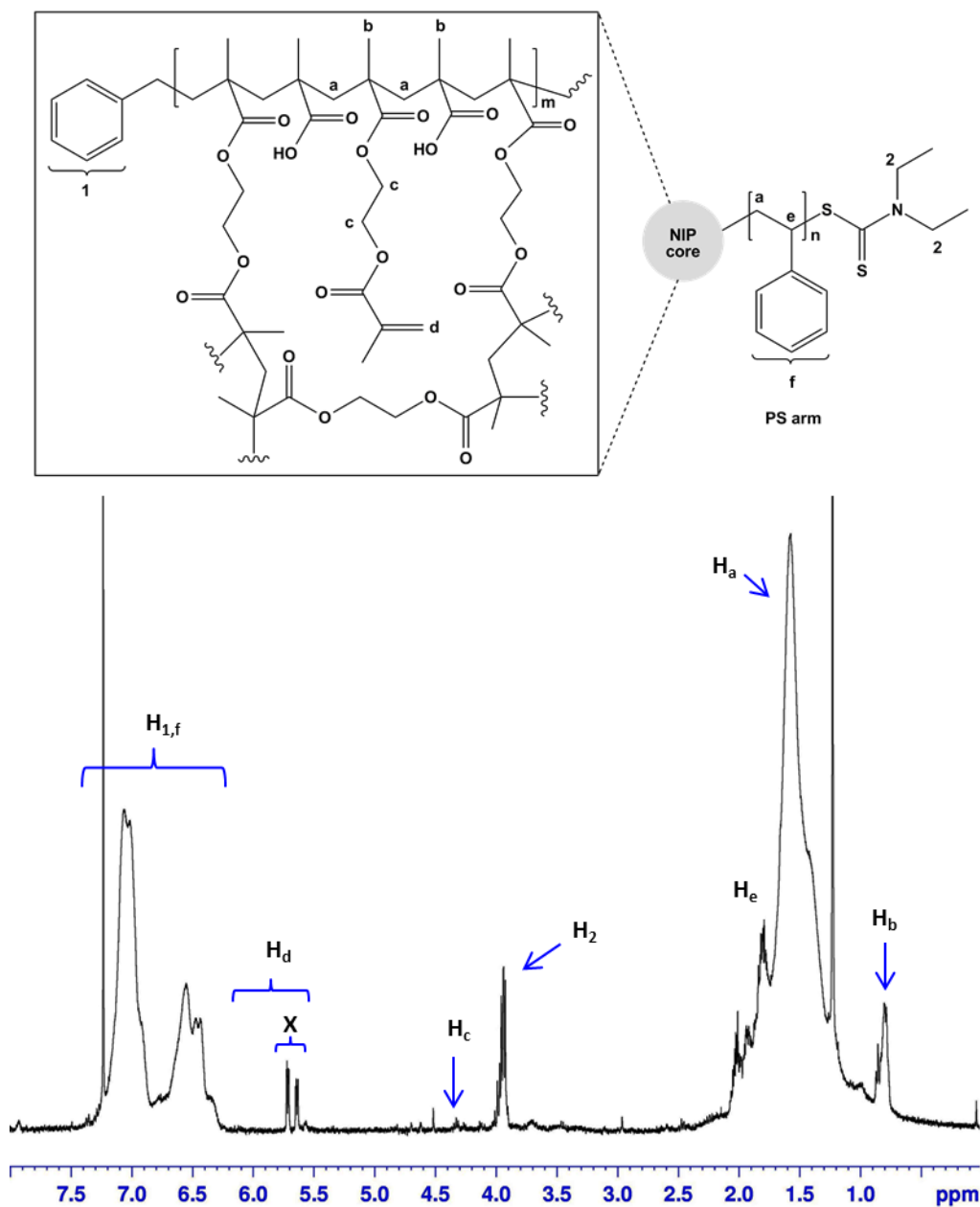


Figure 5.7.  $^1\text{H}$  NMR spectra of CCS NIP-F2.

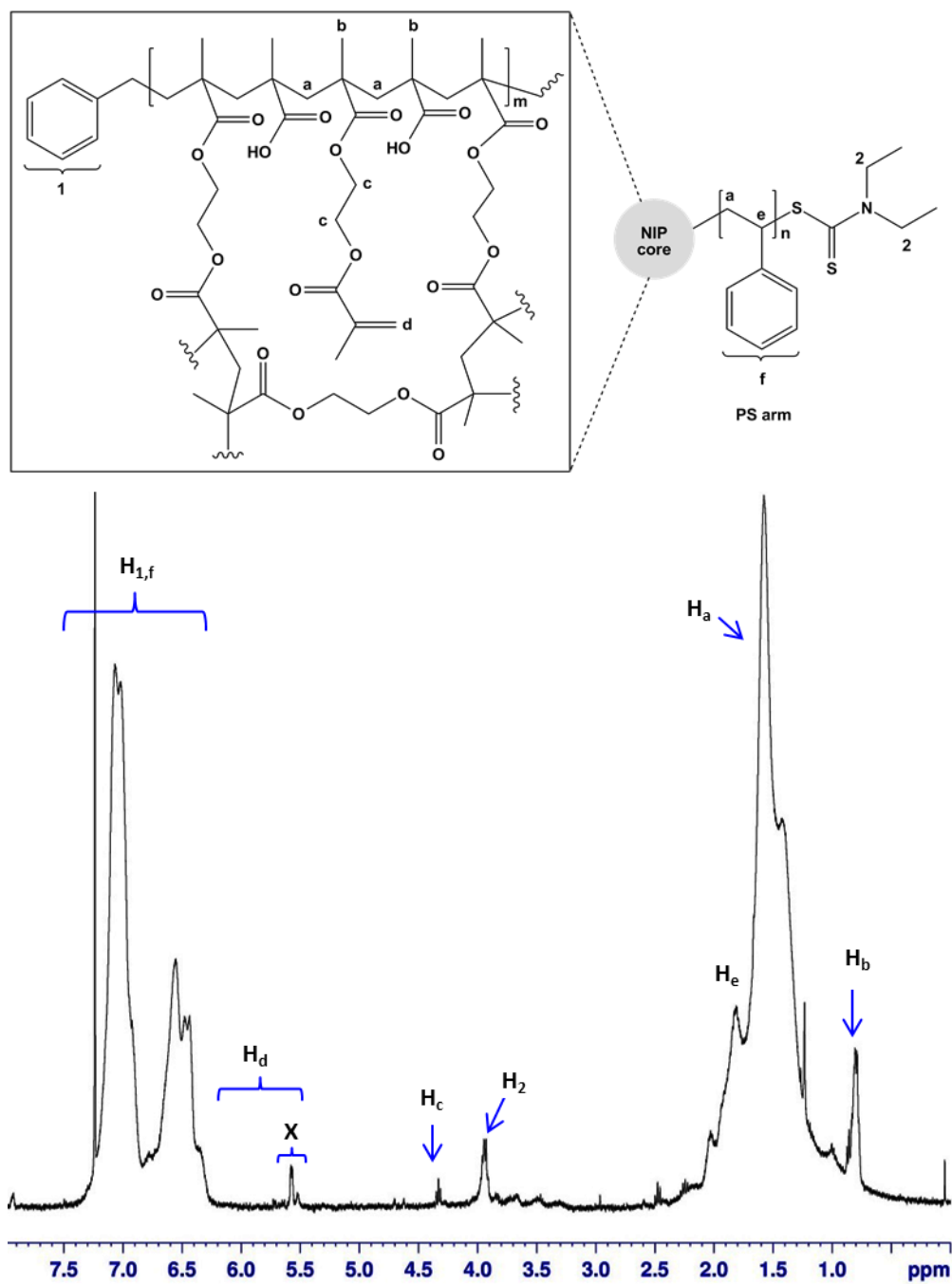


Figure 5.8.  $^1\text{H}$  NMR spectrum of CCS NIP-F3.

### 5.3.1.5 Structural Analysis

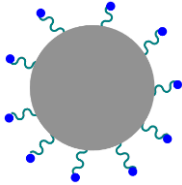
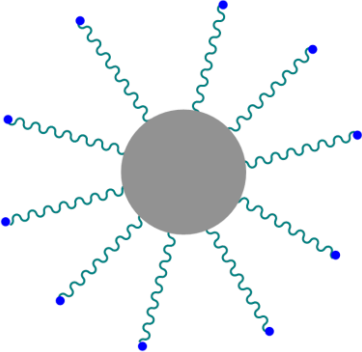
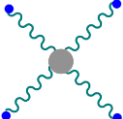
The preparation of CCS MIPs and their corresponding CCS NIPs has resulted in the formation of several fractions of CCS polymers. A combination of NMR, FTIR, SEM, TEM and DLS was used to investigate the structure, morphology and particle size of the resultant polymers.

The equivalent SEM average particle diameters of the CCS MIP-F1 and the core MIP precursor are in contrast to the evidence of the presence of styrene by NMR and FTIR which led us to conclude that short PS arms have grown from the core microsphere. Moreover in view of the non-dispersibility of the CCS MIP-F1 in THF and in addition to the low mass fraction of PS arm relative to the polymer core, it was confirmed that the length of the PS arm around the large core particles was too short to facilitate dispersion in THF, which is the good solvent for the PS arm (see schematic, Table 5.2). A similar result was obtained for the CCS MIP-F2, where its SEM average particle diameter was comparable to that of the MIP core precursor, however, it was found to contain quite a large mass fraction of PS arm relative to the polymer core. Compared to CCS MIP-F1, the dispersibility of CCS MIP-F2 in THF could be attributed to the presence of longer PS arm length around the core particles, as estimated by NMR ( $M_n = 2.8$  kDa) (see schematic, Table 5.2).

All the CCS NIP fractions exhibited similar particle diameters to the core NIP precursor, yet they showed different behaviour when suspended in THF. In view of the non-dispersibility of CCS NIP-F1 in THF and in addition to the smaller mass fraction of PS arm relative to the polymer core compared to the rest of the CCS NIP fractions, it is postulated that CCS NIP-F1 consisted of short-chain PS arms. In contrast, both CCS NIP-F2 and CCS NIP-F3 were dispersible in THF, but with a slight difference in turbidity; CCS NIP-F2 formed a slightly turbid solution whereas CCS NIP-F3 solution was more transparent. Both polymers contained almost similar mass fraction of PS arm relative to the polymer core, yet the length of PS arm around the core of CCS NIP-F3 was found

to be almost twice of that of the CCS NIP-F2. From these observations, it can be hypothesised that CCS NIP-F3 contains lower arm number but longer arm length compared to that of the CCS NIP-F2 (see proposed structure, Table 5.2), which might account for the difference in the turbidity of their THF solutions.

**Table 5.2.** Proposed dominant structures within the CCS MIP and NIP fractions.

Polymer	Proposed structure
MIP-5%BDDC-B2	
CCS MIP-F1	
CCS MIP-F2	
NIP-5%BDDC-B2	
CCS NIP-F1	
CCS NIP-F2	
CCS NIP-F3	

### 5.3.2 Batch rebinding studies

From the previous discussion, it can be concluded that photopolymerisation of styrene in the presence of iniferter-bound polymer core resulted in formation of several fractions of CCS polymers. In order to investigate the effect of the presence of PS arms attached to the core precursor on the BZP binding performance, batch rebinding studies were carried out on all of the CCS MIP and NIP fractions as well as their corresponding core precursors. The rebinding experiments were performed for 2 hours in 4.0 mM BZP using both acetonitrile and THF, which are the bad and the good solvents for the PS arms, respectively. The results of the rebinding studies of all polymer samples are then compared as shown in Figure 5.9 and Table 5.3. The amount of BZP bound obtained from HPLC analysis was calculated according to equation 4.1 (§4.2.4) and corrected against the actual mass of the core estimated from FTIR analysis, as discussed in §5.3.1.3 (see Table 5.1).

**Table 5.3.** Binding affinities of the CCS MIP and NIP fractions compared to their corresponding core precursors.

Polymer	$S_B$ ( $\mu\text{mol per g core}$ )	
	Acetonitrile	THF
<b>MIP-5%BDDC-B2</b>	$278 \pm 1.1$	$71 \pm 0.6$
<b>CCS MIP-F1</b>	$230 \pm 0.6$	$40 \pm 1.9$
<b>CCS MIP-F2</b>	$192 \pm 0.4$	$59 \pm 4.3$
<b>NIP-5%BDDC-B2</b>	$204 \pm 0.3$	$50 \pm 0.4$
<b>CCS NIP-F1</b>	$212 \pm 0.1$	$41 \pm 0.5$
<b>CCS NIP-F2</b>	$183 \pm 1.8$	$6 \pm 0.3$
<b>CCS NIP-F3</b>	$331 \pm 1.3$	$51 \pm 2.0$

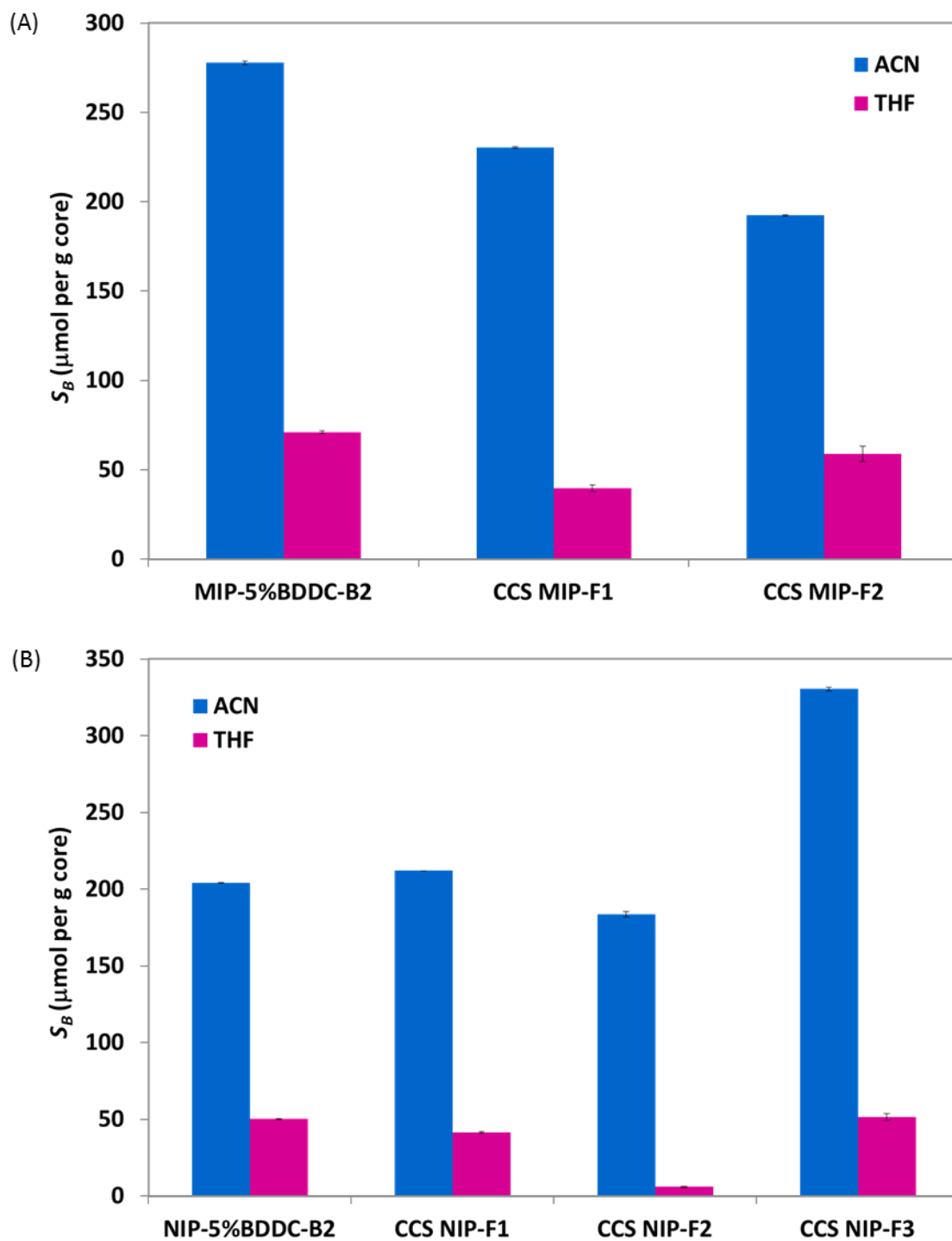


**Figure 5.9.** The BZP binding affinity of the (A) CCS MIP and (B) NIP fractions compared with their corresponding core precursors in acetonitrile and THF.

As can be seen from Figure 5.9 and Table 5.3, the BZP binding affinities of all of the polymers were higher when rebinding was carried out in acetonitrile compared to that in THF, which is consistent with the results obtained in Chapter 4 (§4.3.2.2.4 and 4.3.3.2.4). This was attributed to the higher hydrogen bonding capability of THF compared to acetonitrile, which caused a disruption between the interaction of the template with the functional monomer (MAA) of the polymer core, as already discussed in Chapter 4. Apart from that, conducting the rebinding studies in the same solvent as the porogen used during the preparation of the core precursor might account for the higher binding affinity of the polymers in acetonitrile by providing a microenvironment that would mimic the interactions existing prior to and during the polymerisation.<sup>314</sup>

All of the CCS NIP fractions, except for the CCS NIP-F2 exhibited higher BZP binding affinity compared to that of the NIP core precursor when rebinding was carried out in acetonitrile (Table 5.3). Considering that the particle sizes of all of the CCS NIP fractions were almost similar to the NIP core precursor, the presence of PS arms that are attached to the CCS NIP cores might be expected to have contributed to the difference in the binding affinity of the polymers in acetonitrile, the bad solvent for the PS arm. No correlation can be seen between the binding affinities of the CCS NIP fractions with the degree of polymerisation of the PS arm in acetonitrile, where the arms were expected to be in a collapsed state. However, a contradictory result was obtained when the rebinding was carried out in THF, the good solvent for the PS arm. In THF, the non-dispersible CCS NIP (CCS NIP-F1), which contains a very small fraction of PS arms relative to the polymer core (according to the FTIR analysis in §5.3.1.3, Figure 5.5(B)) exhibited about 18% reduction in binding affinity compared to that of the NIP core precursor. This suggests that the presence of PS arms did have a slight effect on the binding performance of CCS NIP-F1. Comparing the binding affinities of the dispersible fractions of the CCS NIP with that of their core precursor, CCS NIP-F2 exhibited a significantly lower binding affinity (about 88% lower) compared to that of

the core precursor whereas similar binding affinity was exhibited by CCS NIP-F3. Thus, CCS NIP-F3, which contained fewer but longer arms (see proposed structure, Table 5.2) bound higher amount of BZP compared to the CCS NIP-F2, which contained more but shorter arms (see proposed structure, Table 5.2). A few possible reasons were postulated for this behaviour. The first one was attributed to the easier mass transfer of the BZP molecules to the core of CCS NIP-F3 due to the more extended arms compared to that of CCS NIP-F2. In another words, the presence of these longer arms did not hinder the movement of BZP molecules from the solution to the core, where the MAA functional groups were located. The other possible reason was the interaction that might occur between the BZP molecules and the styrene units in the PS arms itself. Since the arms of CCS NIP-F3 were longer than that of the CCS NIP-F2, it was possible that the apparent higher binding affinity of the former compared to the latter was contributed by the higher interaction between the BZP molecules and the PS arms rather than with the MAA at the core. The third possible reason was that as CCS NIP-F2 contained more PS arms than the CCS NIP-F3, its surface density of the PS arms was greater. The high surface density of PS arms of the former might be shielding the core, thus reducing the amount of BZP bound to its core compared to the latter.

In order to investigate which of the above hypotheses was more likely to occur, computer generated modelling was carried out using the molecular simulation software, Spartan '04 (Wavefunction, Inc. USA) using gas phase AM1 force field at the semi-empirical level to estimate possible interactions that could occur between styrene monomer and the BZP template. Two, four and eight styrene monomer units in the chain were modelled to study the effect of number of styrene in the chain to the geometry optimised images of the styrene: BZP template, as shown in Fig. 5.10.

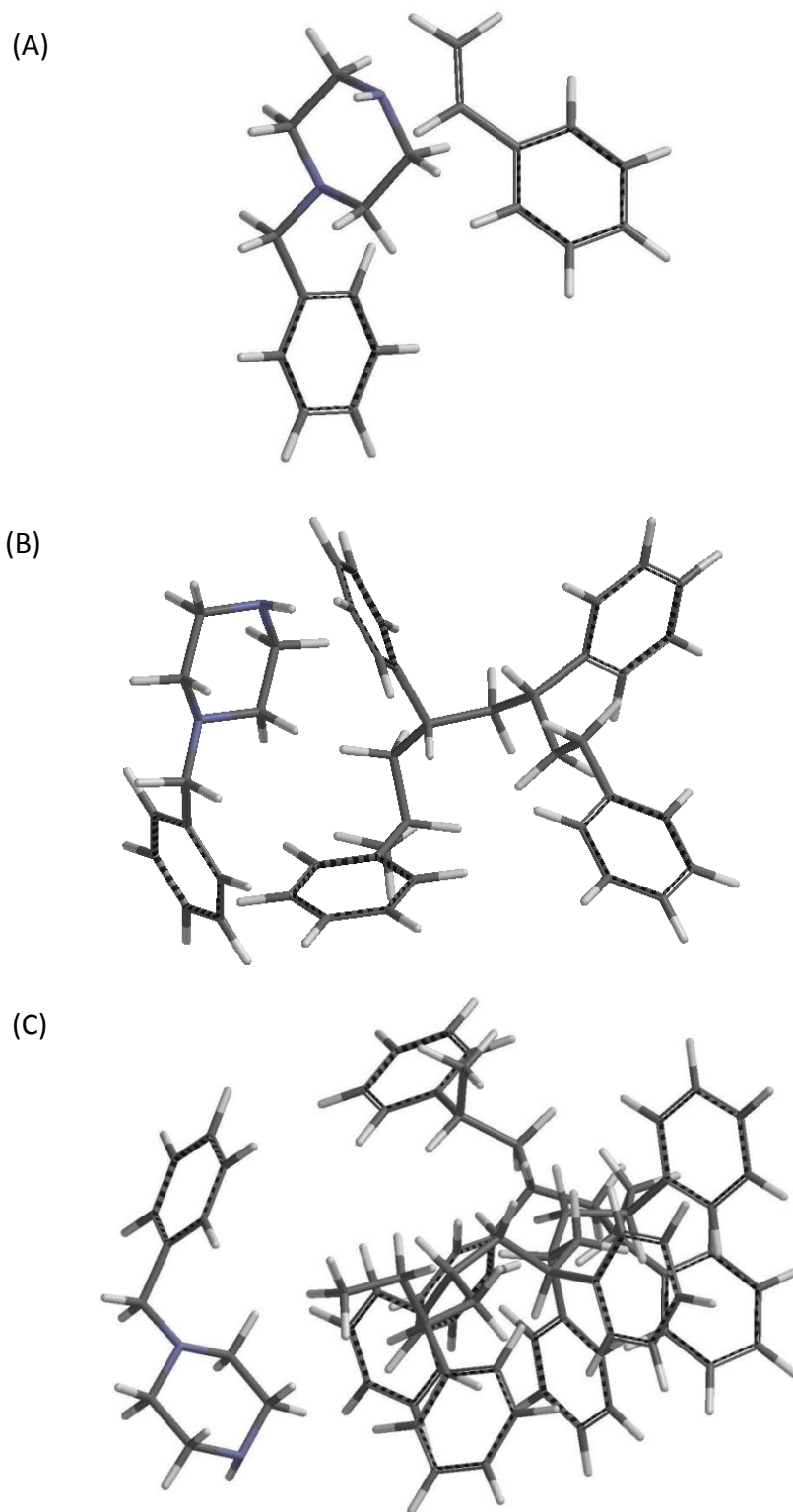


**Figure 5.10.** Computer generated molecular modelling images of BZP and (A) 2, (B) 4 and (C) 8 units of styrene for the geometry optimised BZP:St clusters.

As can be seen from Figure 5.10, all of the styrene chain models exhibited a certain degree of interaction with BZP. It can also be observed that the presence of a higher number of styrene units in the chain provides more interaction points with the BZP template, which is consistent with the result obtained by Wright where the degree of interaction increased with increasing number of styrene monomer unit.<sup>257257</sup> However, the strength of this interaction seemed to be weaker with increasing styrene units as demonstrated by the increase in the distance between the BZP molecule and styrene. It is also interesting to note that the interaction was not restricted to the locations where possible binding would occur. Since no functional group was present in the system capable of hydrogen bond association, the interaction was postulated to consist of weak non-covalent interactions such as van der Waals forces.

The computer generated molecular modelling image (Figure 5.10) could be used to explain the higher binding affinity at the core of CCS NIP-F3 compared to that of the CCS NIP-F2 when rebinding was carried out in acetonitrile as some of the BZP template could be trapped in the collapsed PS arm chains. This possible physical entrapment may have resulted in the reduced amount of BZP left in solution, which in turn caused the binding affinity of the former to be higher than the latter. In THF, the PS arms attached to the CCS NIP core were expected to be in an expanded state. The lower binding affinity of CCS NIP-F2 compared to that of CCS NIP-F3 could be attributed to the different degree of polymerisation (that is, arm length) of the polymers. The longer PS arms of CCS NIP-F3 could be in a fully extended state, thus allowing the BZP template to reach the core whereas the shorter arms of CCS NIP-F2 which are not fully extended in THF could have hindered the BZP template from reaching the core. The CCS NIP-F2 on the other hand, contained shorter but more PS arms compared to the CCS NIP-F3, thus exhibited higher surface density of the arms, which might shield the core, resulting in lower amount of BZP bound of the former compared to the latter. This shows that the arm length could be optimised for enhanced processability and binding performance of the CCS polymers.

As can be seen in Figure 5.9(A) and Table 5.3, CCS MIP fractions showed a slightly different trend in the binding affinity compared to that of the CCS NIP fractions. CCS MIP-F1, which was about the same size as the MIP core precursor bound about 17% less BZP compared to that of the MIP core precursor (MIP-5%BDDC-B2) when rebinding was carried out in acetonitrile. The decrease in binding affinity of the former compared to that of the latter was even greater (about 44% lower) when rebinding was carried out in THF, which is the good solvent for the arm. This result demonstrates that the presence of PS arms around the core might account for the lower binding affinity of CCS MIP-F1 compared to that of the MIP core in both solvents. In acetonitrile, the collapsed PS arms could hinder the approach of the BZP template to the core, where the imprinting sites were located, thus reducing the amount of specific binding. In THF, further decrease in the binding affinity of the polymer could be attributed to the contribution caused by the interaction between the extended PS arms and the BZP template, thus reducing the total binding at the core.

Similar to the result obtained for CCS MIP-F1, CCS MIP-F2 exhibited lower BZP binding affinity compared to that of the MIP core precursor when rebinding was carried out in both acetonitrile and THF (31% and 17% lower, respectively). It can also be noted that the amount of BZP bound of CCS MIP-F2 was lower in acetonitrile but higher in THF compared to that of CCS MIP-F1. Considering that the SEM average diameter of CCS MIP-F2 was comparable to that of CCS MIP-F1, but contained higher styrene mass fraction relative to the core. The slightly higher binding affinity of CCS MIP-F2 compared to that of CCS MIP-F1 in THF could be attributed to the fully extended PS arms in the good solvent, which allows more BZP to approach the core, hence increasing the contribution of specific binding. The opposite effect occurred in acetonitrile, where the collapsed PS arms, which covered the surface of the core, resulting in greater surface densities of the PS arms, were concluded to hinder the approach of the BZP template to the binding sites.

The result showed that binding affinities of the CCS MIPs and NIPs having different arm lengths and surface density of arms differ, depending on the type of solvents used during the rebinding studies. In acetonitrile, which was the bad solvent for the arm, having long arms was detrimental to the CCS MIP since the collapsed arms caused an increased in the surface density of the arms, thus reduced the mass transfer of the BZP molecules to the imprinted sites within the core. On the other hand, having long arms was beneficial when the CSS MIP was dispersed in the good solvent, THF. The arms when in the extended state, improved the dispersibility of the CCS MIP, yet did not hinder the mass transfer of BZP molecules to the core. As for the CCS NIP fractions, although having long arms were advantageous since the nonspecific binding was reduced, if the arms were too long, the BZP molecules could be trapped in the collapsed PS arm chains, thus contributed to the increase in the non-specific binding. Having more arms was not necessarily good either because the greater surface density of the arms might shield the core, thus reducing the amount of BZP bound. Therefore, an optimum balance between the arm lengths, number of arms and the size of the core is necessary in order to improve the polymer dispersibility without jeopardising the binding performance.

Despite enhancing the dispersibility of the MIP, it is difficult to assess the binding performance of the CCS MIPs using the conventional comparison with the NIP (see §4.2.4) due to the presence of different number of arm and/or arm length around the MIP core and its NIP counterpart. Nevertheless, the arms have the potential to promote binding if carefully selected. It seemed that PS was not the best arm to use as it could form interactions with the functional monomer and/or the template. Other arms could be tested to find a suitable arm that can improve the binding capacity of the MIP.

## 5.4 Conclusion

CCS MIP and NIP have been prepared using the MIP and NIP microspheres synthesised using 5% BDDC iniferter, as the core precursors respectively. Starting from the same core precursor, several fractions of CCS MIP and NIP were obtained, which differ in their degree of dispersibility in THF, the good solvent for the arm. The effect of template (as already discussed in Chapter 4) could be observed from the large difference in particle diameter between the MIP and NIP core precursors, where the latter was much smaller compared to the former. This difference in sizes and perhaps in the number of initiating sites in the core precursors will affect the growth of arms around the core of the polymers, making the assessment of binding performance complex. Preliminary studies showed that dispersibility improved with increasing arm length, although it did not necessarily contribute to better binding performance. The result also indicates that the CCS polymers could be used as stimuli responsive polymers<sup>338</sup> since they respond differently when dispersed in different solvents. The CCS polymers could bind the BZP when dispersed in acetonitrile, and then release the drug when the solvent is switched to THF. The result showed that CCS polymer could provide a path to dispersible and processable MIP. To the best of our knowledge, this is the first report on the core-first CCS MIPs prepared via RDRP.

## Chapter 6

### Summary and Recommendations

#### 6.1 Summary of Results

Synthesis of core crosslinked star (CCS) polymers via RDRP has been investigated and then applied to molecular imprinting. Molecular imprinted CCS polymers have potential as delivery systems in solution and, by virtue of their improved processability, may be used to produce thin films with recognition capability for sensing applications. Both methods i.e. arm-first and core-first were employed during the synthesis of CCS polymers via iniferter and RAFT in order to find the best possible method to prepare the CCS MIPs. In the arm-first method, linear PS arms with reactivatable chain-end initiating sites were synthesized using either BDDC iniferter or MCEBTTC RAFT agent before undergoing a crosslinking reaction with EGDMA to afford CCS polymer with the initiating sites confined at the core. On the other hand, the core-first method involves the polymerisation of EGDMA crosslinker in the presence of BDDC iniferter/MCEBTTC RAFT agent to generate a multifunctional crosslinked core before addition of styrene monomer to grow the arms from the active core surface. By using this method, in contrast to the arm-first method, the initiating sites are preserved at the periphery of the CCS polymer.

In the preparation of CCS polymers via the arm-first method, PS arms with DDC end groups of various arm lengths were synthesised using BDDC iniferter by varying the

parameters such as the polymerisation time and monomer to iniferter ratio. CCS polymers of various molecular weight and particle size were then successfully prepared by subsequent crosslinking of the PS arms with EGDMA as the crosslinker. It was found that higher molecular weight and bigger particle size of CCS polymers were formed by increasing the polymerisation time, concentration of the PS arm, molar ratio of EGDMA to PS arm and PS arm length.

On the other hand, the preparation of arm-first CCS polymers via RAFT was not as straightforward as that of the iniferter. Although PS arms of different lengths with low polydispersity could be prepared by varying parameters such as monomer to RAFT agent and RAFT agent to initiator mol ratios, careful selection of EGDMA and PS arm concentration as well as molar ratio of EGDMA to PS arm was necessary for the successful formation of CCS polymers via RAFT. Formation of CCS polymers in good yield could be achieved at higher ratio of EGDMA to PS arm and PS arm concentration. However, conducting the polymerisation at high concentration of PS arm for a long time should be avoided as it resulted in macroscopic gelation.

Polymerisation of styrene via iniferter was found to result in faster polymerisation than RAFT, which was demonstrated by the much higher MW and higher yield of the PS arms obtained via the former. On the other hand, PS arms prepared via RAFT exhibited much lower polydispersities compared to the iniferter, suggesting better control of polymerisation by RAFT.

One of the advantages of the arm-first method in the preparation of CCS polymers is that the length of the arms could be well-controlled since they were synthesised independently. However, the final product is accompanied by the residual unreacted linear arm precursors, which require extra purification step to obtain CCS polymers of high purity.

For the preparation of the core precursor for the core-first CCS polymers, it was necessary to maintain lower ratio of crosslinker to iniferter/RAFT agents and conduct the polymerisation of EGDMA in high dilution in order to prevent macroscopic gelation. Varying the polymerisation time during the polymerisation of styrene monomer in the presence of the core precursors resulted in CCS polymers with different arm lengths. Although requires further optimisation, core-first CCS polymers was successfully synthesised via both the iniferter and RAFT and requires a much simpler purification step compared to the arm-first method. Moreover, characterisation of the core was possible when the CCS polymers were prepared via the core-first method, which is crucial when applied to molecular imprinting.

Hence, the CCS MIPs were prepared via the core-first method starting with the preparation of the MIP microspheric core precursor. Using BZP as the model template, the MIP microspheres were prepared via a combination of iniferter/RAFT and precipitation polymerisation. The BZP imprinted polymers have been prepared using three different concentration of iniferter/RAFT agent (i.e. 5, 10 and 20 mol % with respect to the total monomer). The large difference in size between the MIPs and their NIP counterparts, which translated to a large difference in the specific surface area of the microspheres, has implications on the assessment of binding efficiency generally normalised against NIPs with respect to mass. To take into account the difference in surface area between the MIPs and their respective NIPs, the binding efficiency of the MIPs was also expressed with respect to the specific surface area. The MIP microspheres prepared using 5% of iniferter/RAFT agent exhibited the best binding performance in their series. Comparing the binding performance between the MIP-5%BDDC and MIP-5%RAFT, the former exhibited higher binding capacity and greater specific binding, despite its lower specific surface area and reduced porosity compared to those of the latter. On the other hand, the IF value of the MIP-5%RAFT was about 3.5-fold higher than that of the MIP-5%BDDC due to the higher level of non-specific binding to the latter.

Due to the better binding performance of MIP-5%BDDC and the relatively easier preparation of CCS polymer when the microspheres prepared via iniferter was used as the core precursor compared to that of RAFT, the former was selected for further studies to determine the specificity of the BZP prepared polymer. Two drugs, EPH and PHP, having closely related structures to the BZP were selected as the analytes. In the non-competitive binding, it was found that the MIP-5%BDDC exhibited better selectivity towards EPH over BZP, but showed comparable selectivity towards both analytes in the competitive binding environments, which could be attributed to the smaller size and stronger hydrogen bonding ability of EPH compared to BZP. On the other hand, MIP-5%BDDC exhibited better selectivity towards BZP over PHP in both the non-competitive and competitive binding environments, indicating greater recognition properties for the BZP template molecules, which was attributed to the creation of specific cavities designed for the BZP template in the MIP.

A pilot study carried out to synthesise CCS MIPs using the MIP microsphere prepared using 5%BDDC as the core precursor has resulted in different fractions of CCS MIPs, which exhibited different degree of dispersibility in the THF, the good solvent for the PS arm. Dispersibility of the CCS MIPs improved with increasing arm length, although it did not necessarily contribute to better binding performance. In both acetonitrile and THF, which were a bad and good solvent for the arm, respectively, the presence of PS arms around the imprinted core resulted in a decrease in binding capacity of the CCS MIPs compared to that of the core precursor. However, contrary to the binding results obtained in acetonitrile where binding capacity seemed to decrease with increasing arm length, greater binding affinity was exhibited by the CCS MIP with longer arms than those with shorter arms in THF. Greater binding affinity of the MIP having longer arms was attributed to the easier access of the BZP when the arms are were fully extended in THF, whereas in acetonitrile, the greater surface density of the arms when in collapsed state shielded the core and thus causing less BZP to reach the binding sites.

## 6.2 Recommendations for Future Work

The high degree of crosslinking in MIPs is necessary in order to maintain the conformation of the three-dimensional binding sites obtained through the molecular imprinting process, and thus the ability of the polymer to specifically and selectively recognize its target molecule. However, the insolubility of these crosslinked polymers limits the applicability of MIPs by imposing tedious or difficult processes for their inclusion in organic electronic devices. Although the PS arms enhanced the dispersibility of the CCS MIPs, it should be noted, however, that the presence of arms around the imprinted core might inadvertently cause a reduced selectivity of the MIP by preventing template accessibility to the imprinted sites when the arms are not in a fully extended state. In addition, possible interaction between the arms and the target analyte (template) could also lead to a reduction in template binding at the binding sites on the core. Therefore, a careful CCS MIP synthetic design is necessary in order for the growing arms to have a positive effect on the binding performance.

One of the possible ways to improve the binding performance of the CCS MIPs is by optimising the lengths of the arms so that the dispersibility of the CCS MIPs could be enhanced, which could improve their processability as thin films but at the same time, still exhibit high binding capacity. Apart from that, the binding capacity could be improved by changing the nature of the arm, for example by using other neutral monomer apart from styrene such as methyl methacrylate. Ideally, the monomer should not form ionic interaction or hydrogen bond with the functional group or the template molecule but can actually promote binding of template. The core size could also be optimised to enhance template binding capacities of the CCS MIPs. Bigger size of MIP microspheres allows the creation of more binding cavities and able to accommodate more arms, yet at the same time resulted in reduced surface area. However, having more arms could hinder the mass transfer of template to the binding sites. Thus, it is very important to optimise the size of the core for maximum binding capacity. In this study, BZP, a designer drug, was used as the model template. The

study could be extended to other illicit drugs, such as morphine and cocaine. Utilizing the iniferter-induced RDRP in combination with precipitation polymerisation, a thin film of MIP could be grafted onto the surface of silica seed particles, which could then undergo surface modification to form the CCS polymer.

In the binding assessment, the binding efficiency of the MIPs are generally normalised against the respective NIPs with respect to the mass of the polymers. Taking into account the variability in particle sizes between MIPs and NIPs, it is strongly suggested that future study includes the binding efficiency of the MIPs expressed with respect to the specific surface area. Despite enhancing the dispersibility of the MIP by incorporating arms, it is difficult to assess the binding performance of the CCS MIP using the conventional comparison with the NIP due to the presence of different number of arm and/or arm length around the MIP core and its NIP counterpart. The binding evaluation of the CCS MIP could be performed by comparing the binding capacity of the CCS MIP against its core precursor, whereby ideal binding is obtained when binding capacity of the former over the latter equals one.

Finally, we have demonstrated that the processability of MIP microspheres could be readily introduced by attaching linear polymeric arms via iniferter technique. Future work involving the application of the CCS MIPs in thin film format for potential application in electronic devices is highly recommended.

## References

1. Hadjichristidis, N.; Iatrou, H.; Pitsikalis, M.; Mays, J. *Progress in Polymer Science* **2006**, *31*, (12), 1068-1132.
2. Hadjichristidis, N.; Pitsikalis, M.; Pispas, S.; Iatrou, H. *Chem. Rev* **2001**, *101*, (12), 3747-3792.
3. Qiao, J. *Australian Journal of Chemistry* **2007**, *60*, (10).
4. Helms, B.; Guillaudeu, S. J.; Xie, Y.; McMurdo, M.; Hawker, C. J.; Fréchet, J. M. J. *Angewandte Chemie International Edition* **2005**, *44*, (39), 6384-6387.
5. Lupitskyy, R.; Roiter, Y.; Tsitsilianis, C.; Minko, S. *Langmuir* **2005**, *21*, (19), 8591-8593.
6. Blencowe, A.; Tan, J. F.; Goh, T. K.; Qiao, G. G. *Polymer* **2009**, *50*, (1), 5-32.
7. Gao, H.; Matyjaszewski, K. *Progress in Polymer Science* **2009**, *34*, (4), 317-350.
8. Sugii, R.; Hitaka, Y.; Yokoyama, A.; Yokozawa, T. *Macromolecules* **2005**, *38*, (13), 5526-5531.
9. Hirao, A.; Kawasaki, K.; Higashihara, T. *Science and Technology of Advanced Materials* **2004**, *5*, (4), 469-477.
10. Lee, J. S.; Quirk, R. P.; Foster, M. D.; Wollyung, K. M.; Wesdemiotis, C. *Macromolecules* **2004**, *37*, (17), 6385-6394.
11. Colombani, D. *Progress in Polymer Science* **1997**, *22*, (8), 1649-1720.
12. Patten, T.; Matyjaszewski, K. *Advanced Materials* **1999**, *10*, (12), 901-915.
13. Jenkins, A. D.; Jones, R. G.; Moad, G. *Pure & Applied Chemistry* **2010**, *82*, (2), 483-491.
14. Shipp, D. A.; Wang, J. L.; Matyjaszewski, K. *Macromolecules* **1998**, *31*, (23), 8005-8008.
15. Pyun, J.; Matyjaszewski, K. *Chem. Mater* **2001**, *13*, (10), 3436-3448.
16. Gao, H.; Ohno, S.; Matyjaszewski, K. *Journal of the American Chemical Society* **2006**, *128*, (47), 15111-15113.
17. Liu, J.; Tao, L.; Xu, J.; Jia, Z.; Boyer, C.; Davis, T. P. *Polymer* **2009**, *50*, (19), 4455-4463.
18. Gao, H.; Matyjaszewski, K. *Macromolecular Symposia* **2010**, 291-292, (1), 12-16.
19. Zilliox JG, R. P., Parrod J. *Journal of Polymer Science, Polymer Symposia* **1968**, *22*, 12.
20. Simms, J. A.; Spinelli, H. J. *JCT, Journal of coatings technology* **1987**, *59*, (752), 125-131.
21. Xia, J.; Zhang, X.; Matyjaszewski, K. *Macromolecules* **1999**, *32*, 4482-4484.
22. Baek, K.; Kamigaito, M.; Sawamoto, M. *Macromolecules* **2002**, *35*, (5), 1493-1498.
23. Baek, K.; Kamigaito, M.; Sawamoto, M. *Macromolecules* **2001**, *34*, (22), 7629-7635.
24. Wiltshire, J. T.; Qiao, G. G. *Macromolecules* **2006**, *39*, (26), 9018-9027.
25. Goh, T. K.; Coventry, K. D.; Blencowe, A.; Qiao, G. G. *Polymer* **2008**, *49*, (23), 5095-5104.
26. Qiu, L.; Wang, Y.; Lin, Q.; Zhou, X. *Asia-Pacific Journal of Chemical Engineering* **2009**, *4*, (5), 678-682.
27. Tsoukatos, T.; Pispas, S.; Hadjichristidis, N. *Journal of Polymer Science Part A: Polymer Chemistry* **2001**, *39*, (2), 320-325.
28. Ferreira, J.; Syrett, J.; Whittaker, M.; Haddleton, D.; Davis, T. P.; Boyer, C. *Polymer Chemistry* **2011**, *2*, (8), 1671-1677.
29. Lacroix-Desmazes, P.; Severac, R.; Boutevin, B. *Macromolecules* **2005**, *38*, (15), 6299-6309.
30. Wayland, B. B.; Peng, C.-H.; Fu, X.; Lu, Z.; Fryd, M. *Macromolecules* **2006**, *39*, (24), 8219-8222.

31. Matyjaszewski, K., General Concepts and History of Living Radical Polymerization. In *Handbook of Radical Polymerization*, Davis, K. M. a. T. P., Ed. John Wiley & Sons, Inc.: 2002; pp 361-405.
32. Braunecker, W. A.; Itami, Y.; Matyjaszewski, K. *Macromolecules* **2005**, 38, (23), 9402-9404.
33. Otsu, T. *Journal of Polymer Science Part A: Polymer Chemistry* **2000**, 38, (12), 2121-2136.
34. Hadjichristidis, N. *Journal of Polymer Science-A-Polymer Chemistry Edition* **1999**, 37, (7), 857-872.
35. Wei, X.; Moad, G.; Muir, B. W.; Rizzardo, E.; Rosselgong, J.; Yang, W.; Thang, S. H. *Macromolecular Rapid Communications* **2014**, 35, (8), 840-845.
36. Du, J.; Chen, Y. *Macromolecules* **2004**, 37, (10), 3588-3594.
37. Ohno, S.; Gao, H.; Cusick, B.; Kowalewski, T.; Matyjaszewski, K. *Macromolecular chemistry and physics* **2009**, 210, (6), 421-430.
38. Baek, K. Y.; Kamigaito, M.; Sawamoto, M. *Journal of Polymer Science Part a-Polymer Chemistry* **2002**, 40, (14), 2245-2255.
39. Zheng, G.; Pan, C. *Polymer* **2005**, 46, (8), 2802-2810.
40. Ito, K. *Progress in Polymer Science* **1998**, 23, (4), 581-620.
41. Gao, H.; Matyjaszewski, K. *Macromolecules* **2007**, 40, (3), 399-401.
42. Gao, H.; Matyjaszewski, K. *Macromolecules* **2008**, 41, (12), 4250-4257.
43. Audouin, F.; Knoop, R. J. I.; Huang, J.; Heise, A. *Journal of Polymer Science Part A: Polymer Chemistry* **2010**, 48, (20), 4602-4610.
44. Cao, X.; Zhang, C.; Wu, S.; An, Z. *Polymer Chemistry* **2014**.
45. Hadjichristidis, N.; Pitsikalis, M.; Iatrou, H.; Pispas, S. *Macromolecular rapid communications* **2003**, 24, (17), 979-1013.
46. Muehlebach, A.; Rime, F. *Journal of Polymer Science Part A: Polymer Chemistry* **2003**, 41, (21), 3425-3439.
47. Ishizu, K.; Sunahara, K. *POLYMER-LONDON-* **1995**, 36, 4155-4155.
48. Gao, H. F.; Matyjaszewski, K. *Chemistry-a European Journal* **2009**, 15, (25), 6107-6111.
49. Gao, H.; Matyjaszewski, K. *Macromolecules* **2008**, 41, (4), 1118-1125.
50. Stenzel-Rosenbaum, M.; Davis, T.; Chen, V.; Fane, A. *Journal of Polymer Science Part A: Polymer Chemistry* **2001**, 39, (16), 2777-2783.
51. Matyjaszewski, K. *Polymer International* **2003**, 52, (10), 1559-1565.
52. Bernard, J.; Favier, A.; Zhang, L.; Nilasaroya, A.; Davis, T. P.; Barner-Kowollik, C.; Stenzel, M. H. *Macromolecules* **2005**, 38, (13), 5475-5484.
53. Moad, G.; Rizzardo, E.; Thang, S. H. *Australian Journal of Chemistry* **2005**, 58, (6), 379-410.
54. Taton, D.; Gnanou, Y.; Matmour, R.; Angot, S.; Hou, S.; Francis, R.; Lepoittevin, B.; Moinard, D.; Babin, J. *Polymer International* **2006**, 55, (10), 1138-1145.
55. Polanowski, P.; Jeszka, J. K.; Matyjaszewski, K. *Polymer* **2014**, 55, (10), 2552-2561.
56. Otsu, T.; Yoshida, M. *Die Makromolekulare Chemie, Rapid Communications* **1982**, 3, (2), 127-132.
57. Moad, G.; Rizzardo, E.; Thang, S. H. *Accounts of Chemical Research* **2008**, 41, (9), 1133-1142.
58. di Lena, F.; Matyjaszewski, K. *Progress in Polymer Science* **2010**, 35, (8), 959-1021.
59. Shipp, D. A. *Polymer Reviews* **2011**, 51, (2), 99-103.
60. Goto, A.; Fukuda, T. *Progress in Polymer Science* **2004**, 29, (4), 329-385.
61. Matyjaszewski, K.; Tsarevsky, N. V. *Nat Chem* **2009**, 1, (4), 276-288.

62. Gao, H.; Matyjaszewski, K. *Macromolecules* **2006**, 39, (9), 3154-3160.
63. Zhang, X.; Xia, J.; Matyjaszewski, K. *Macromolecules* **2000**, 33, (7), 2340-2345.
64. Gao, H.; Min, K.; Matyjaszewski, K. *Macromolecules* **2007**, 40, (22), 7763-7770.
65. Matyjaszewski, K.; Miller, P.; Fossum, E.; Nakagawa, Y. *Applied Organometallic Chemistry* **1998**, 12, (10-11), 667-673.
66. Matyjaszewski, K.; Miller, P. J.; Pyun, J.; Kickelbick, G.; Diamanti, S. *Macromolecules* **1999**, 32, (20), 6526-6535.
67. Huang, C.; Lee, H.; Kuo, S.; Xu, H.; Chang, F. *Polymer* **2004**, 45, (7), 2261-2269.
68. Heise, A.; Diamanti, S.; Hedrick, J.; Frank, C.; Miller, R. *Macromolecules* **2001**, 34, (11), 3798-3801.
69. Angot, S.; Murthy, K.; Taton, D.; Gnanou, Y. *Macromolecules* **1998**, 31, (21), 7218-7225.
70. Matyjaszewski, K.; Xia, J. *Chem. Rev* **2001**, 101, (9), 2921-2990.
71. Kamigaito, M.; Ando, T.; Sawamoto, M. *Chem. Rev* **2001**, 101, (12), 3689-3746.
72. Zhang, H.; Abeln, C.; Fijten, M.; Schubert, U. *Polymers* **2006**, 2006, 008.
73. Shen, Y.; Tang, H.; Ding, S. *Progress in Polymer Science* **2004**, 29, (10), 1053-1078.
74. Otsu, T.; Yoshida, M. *Macromol Rapid Commun* **1982**, 3, 127-132.
75. Kuriyama, A.; Otsu, T. *Polymer Journal* **1984**, 16, (6), 511-514.
76. Otsu, T.; Matsumoto, A., Controlled synthesis of polymers using the iniferter technique: Developments in living radical polymerization. In *Microencapsulation - Microgels - Iniferters*, Springer Berlin / Heidelberg: 1998; Vol. 136, pp 75-137.
77. Otsu, T.; Yoshida, M.; Kuriyama, A. *Polymer Bulletin* **1982**, 7, (1), 45-50.
78. Otsu, T.; Matsunaga, T.; Kuriyama, A.; Yoshioka, M. *European Polymer Journal* **1989**, 25, (7-8), 643-650.
79. Lalevee, J.; Blanchard, N.; El-Roz, M.; Allonas, X.; Fouassier, J. P. *Macromolecules (Washington, DC, U. S.) FIELD Full Journal Title:Macromolecules (Washington, DC, United States)* **2008**, 41, (7), 2347-2352.
80. Kuchanov, S. I. *Journal of Polymer Science Part A: Polymer Chemistry* **1994**, 32, (8), 1557-1568.
81. Otsu, T.; Yoshida, M.; Tazaki, T. *Die Makromolekulare Chemie, Rapid Communications* **1982**, 3, (2), 133-140.
82. Nakayama, Y.; Miyamura, M.; Hirano, Y.; Goto, K.; Matsuda, T. *Biomaterials* **1999**, 20, (10), 963-970.
83. Kwon, I.; Matsuda, T. *Biomaterials* **2006**, 27, (7), 986-995.
84. Nakayama, Y.; Matsuda, T. *Macromolecules* **1996**, 29, (27), 8622-8630.
85. Nakayama, Y.; Matsuda, T. *Langmuir* **1999**, 15, (17), 5560-5566.
86. Ishizu, K.; Ohta, Y.; Kawachi, S. *Macromolecules* **2002**, 35, (9), 3781-3784.
87. Kannurpatti, A. R.; Anderson, K. J.; Anseth, J. W.; Bowman, C. N. *Journal of Polymer Science Part B: Polymer Physics* **1997**, 35, (14), 2297-2307.
88. Ishizu, K.; Katsuhara, H.; Itoya, K. *Journal of Polymer Science Part A: Polymer Chemistry* **2006**, 44, (10), 3321-3327.
89. Ishizu, K.; Ochi, K. *Macromolecules* **2006**, 39, (9), 3238-3244.
90. Joung, Y. K.; Choi, J. H.; Bae, J. W.; Park, K. D. *Acta Biomaterialia* **2008**, 4, (4), 960-966.
91. Tsuji, S.; Kawaguchi, H. *Langmuir* **2004**, 20, (6), 2449-2455.
92. Mijangos, I.; Guerreiro, A.; Piletska, E.; Whitcombe, M. J.; Karim, K.; Chianella, I.; Piletsky, S. *Journal of separation science* **2009**, 32, (19), 3340-3346.
93. Doi, T.; Matsumoto, A.; Otsu, T. *Journal of Polymer Science Part A: Polymer Chemistry* **1994**, 32, (15), 2911-2918.

94. Otsu, T.; Matsunaga, T.; Doi, T.; Matsumoto, A. *European Polymer Journal* **1995**, *31*, (1), 67-78.
95. Dyer, D. J., Photoinitiated synthesis of grafted polymers. In *Surface-Initiated Polymerization I*, Springer-Verlag Berlin: Berlin, 2006; Vol. 197, pp 47-65.
96. Chiefari, J.; Chong, Y.; Ercole, F.; Krstina, J.; Jeffery, J.; Le, T.; Mayadunne, R.; Meijs, G.; Moad, C.; Moad, G. *Macromolecules* **1998**, *31*, (16), 5559-5562.
97. Chiefari, J.; Mayadunne, R. T. A.; Moad, C. L.; Moad, G.; Rizzardo, E.; Postma, A.; Skidmore, M. A.; Thang, S. H. *Macromolecules* **2003**, *36*, (7), 2273-2283.
98. Chong, Y. K.; Krstina, J.; Le, T. P. T.; Moad, G.; Postma, A.; Rizzardo, E.; Thang, S. H. *Macromolecules* **2003**, *36*, (7), 2256-2272.
99. Moad, G.; Rizzardo, E.; Thang, S. *ChemInform* **2007**, *38*, (8).
100. Mayadunne, R. T. A.; Rizzardo, E.; Chiefari, J.; Chong, Y. K.; Moad, G.; Thang, S. H. *Macromolecules* **1999**, *32*, (21), 6977-6980.
101. Moad, G.; Chiefari, J.; Krstina, J.; Mayadunne, R. T. A.; Postma, A.; Rizzardo, E.; Thang, S. H. *Polymer International* **2000**, *49*, (9), 993-1001.
102. Matyjaszewski, K.; Davis, T. P., *Handbook of radical polymerization*. Wiley Online Library: 2002.
103. Moad, G.; Chong, Y. K.; Postma, A.; Rizzardo, E.; Thang, S. H. *Polymer* **2005**, *46*, (19), 8458-8468.
104. Chong, Y.; Krstina, J.; Le, T.; Moad, G.; Postma, A.; Rizzardo, E.; Thang, S. *Macromolecules* **2003**, *36*, (7), 2256-2272.
105. Gregory, A.; Stenzel, M. H. *Progress in Polymer Science* **2012**, *37*, (1), 38-105.
106. Moad, G.; Mayadunne, R. T. A.; Rizzardo, E.; Skidmore, M.; Thang, S. H. In *Synthesis of novel architectures by radical polymerization with reversible addition fragmentation chain transfer (RAFT polymerization)*, 2003; John Wiley & Sons: 2003; pp 1-12.
107. Lord, H. T.; Quinn, J. F.; Angus, S. D.; Whittaker, M. R.; Stenzel, M. H.; Davis, T. P. *Journal of Materials Chemistry* **2003**, *13*, (11), 2819-2824.
108. Zhang, L.; Chen, Y. *Polymer* **2006**, *47*, (15), 5259-5266.
109. Gaborieau, M.; Gilbert, R. G.; Gray-Weale, A.; Hernandez, J. M.; Castignolles, P. *Macromolecular Theory and Simulations* **2007**, *16*, (1), 13-28.
110. Barner, L.; Davis, T. P.; Stenzel, M. H.; Barner-Kowollik, C. *Macromolecular rapid communications* **2007**, *28*, (5), 539-559.
111. Wang, K.; Peng, H.; Thurecht, K. J.; Puttick, S.; Whittaker, A. K. *Polymer Chemistry* **2014**, *5*, (5), 1760-1771.
112. Favier, A.; Charreyre, M. *Macromolecular rapid communications* **2006**, *27*, (9), 653-692.
113. Barner-Kowollik, C.; Davis, T.; Heuts, J.; Stenzel, M.; Vana, P.; Whittaker, M. *Journal of Polymer Science Part A Polymer Chemistry* **2003**, *41*, (3), 365-407.
114. Perrier, S.; Takolpuckdee, P. *Journal of Polymer Science Part A: Polymer Chemistry* **2005**, *43*, (22), 5347-5393.
115. Chong, Y. K.; Le, T. P. T.; Moad, G.; Rizzardo, E.; Thang, S. H. *Macromolecules* **1999**, *32*, (6), 2071-2074.
116. Monteiro, M. J.; Hodgson, M.; De Brouwer, H. *Journal of Polymer Science Part a-Polymer Chemistry* **2000**, *38*, (21), 3864-3874.
117. Chen, Q.; Xu, Y.; Cao, X.; Qin, L.; An, Z. *Polymer Chemistry* **2014**, *5*, (1), 175-185.
118. Quinn, J.; Davis, T.; Rizzardo, E. *Chemical Communications* **2001**, 2001, (11), 1044-1045.

119. Sumerlin, B. S.; Donovan, M. S.; Mitsukami, Y.; Lowe, A. B.; McCormick, C. L. *Macromolecules* **2001**, 34, (19), 6561-6564.
120. Lu, L.; Zhang, H.; Yang, N.; Cai, Y. *Macromolecules* **2006**, 39, (11), 3770-3776.
121. Quinn, J.; Barner, L.; Rizzardo, E.; Davis, T. *Journal of Polymer Science Part A: Polymer Chemistry* **2001**, 40, (1), 19-25.
122. Oral, E.; Peppas, N. A. *Journal of Biomedical Materials Research Part A* **2004**, 68A, (3), 439-447.
123. Peppas, N. A.; Keys, K. B.; Torres-Lugo, M.; Lowman, A. M. *Journal of Controlled Release* **1999**, 62, (1-2), 81-87.
124. Connal, L. A.; Li, Q.; Quinn, J. F.; Tjipto, E.; Caruso, F.; Qiao, G. G. *Macromolecules* **2008**, 41, (7), 2620-2626.
125. Zimmerman, S.; Lemcoff, N. *Chemical Communications* **2004**, 2004, (1), 5-14.
126. Guan, G.; Liu, B.; Wang, Z.; Zhang, Z. *Sensors* **2008**, 8, (12), 8291-8320.
127. Wulff, G. *Chemical Reviews* **2002**, 102, (1), 1-28.
128. Haupt, K. *Nature Biotechnology* **2002**, 20, (9), 884-885.
129. Ye, L.; Haupt, K. *Analytical and bioanalytical Chemistry* **2004**, 378, (8), 1887-1897.
130. Asanuma, H.; Akiyama, T.; Kajiya, K.; Hishiya, T.; Komiyama, M. *Analytica Chimica Acta* **2001**, 435, (1), 25-33.
131. Osawa, T.; Shirasaka, K.; Matsui, T.; Yoshihara, S.; Akiyama, T.; Hishiya, T.; Asanuma, H.; Komiyama, M. *Macromolecules* **2006**, 39, (7), 2460-2466.
132. Kryscio, D. R.; Peppas, N. A. *Acta Biomaterialia* **2012**, 8, (2), 461-473.
133. Yang, K.; Zhang, L.; Liang, Z.; Zhang, Y. *Analytical and Bioanalytical Chemistry* **2012**, 403, (8), 2173-2183.
134. Li, H.; Li, D. *Journal of Pharmaceutical and Biomedical Analysis* **2015**, 115, 330-338.
135. Zhang, H.; Jiang, J.; Zhang, H.; Zhang, Y.; Sun, P. *ACS Macro Letters* **2013**, 2, (6), 566-570.
136. Sellergren, B.; Lepistoe, M.; Mosbach, K. *Journal of the American Chemical Society* **1988**, 110, (17), 5853-5860.
137. Yu, C.; Ramström, O.; Mosbach, K. *Analytical Letters* **1997**, 30, (12), 2123-2140.
138. Yu, C.; Mosbach, K. *The Journal of Organic Chemistry* **1997**, 62, (12), 4057-4064.
139. Yu, C.; Mosbach, K. *Journal of Molecular Recognition* **1998**, 11, (1-6), 69-74.
140. Farrington, K.; Regan, F. *Biosensors and Bioelectronics* **2007**, 22, (6), 1138-1146.
141. Takeda, K.; Kobayashi, T. *Science and Technology of Advanced Materials* **2005**, 6, (2), 165-171.
142. Yoshimatsu, K.; Yamazaki, T.; Chronakis, I. S.; Ye, L. *Journal of Applied Polymer Science* **2012**, 124, (2), 1249-1255.
143. Piletsky, S. A.; Karim, K.; Piletska, E. V.; Day, C. J.; Freebairn, K. W.; Legge, C.; Turner, A. P. F. *Analyst* **2001**, 126, (10), 1826-1830.
144. Yan, H.; Row, K. H. *International journal of molecular sciences* **2006**, 7, (5), 155-178.
145. Riahi, S.; Edris-Tabrizi, F.; Javanbakht, M.; Ganjali, M.; Norouzi, P. *J Mol Model* **2009**, 15, (7), 829-836.
146. Liu, J.-q.; Wulff, G. n. *Journal of the American Chemical Society* **2008**, 130, (25), 8044-8054.
147. Schweitz, L.; Andersson, L. I.; Nilsson, S. *Analytical Chemistry* **1997**, 69, (6), 1179-1183.
148. Pichon, V. r.; Haupt, K. *Journal of Liquid Chromatography & Related Technologies* **2006**, 29, (7/8), 989-1023.
149. Surugiu, I.; Danielsson, B.; Ye, L.; Mosbach, K.; Haupt, K. *Analytical Chemistry* **2001**, 73, (3), 487-491.

150. Ayela, C.; Vandeveld, F.; Lagrange, D.; Haupt, K.; Nicu, L. *Angewandte Chemie-International Edition* **2007**, 46, (48), 9271-9274.
151. Bompart, M.; Haupt, K. *Australian Journal of Chemistry* **2009**, 62, (8), 751-761.
152. Alexander, C.; Andersson, H.; Andersson, L.; Ansell, R.; Kirsch, N.; Nicholls, I.; O'Mahony, J.; Whitcombe, M. *Journal of Molecular Recognition* **2006**, 19, (2), 106-180.
153. Salian, V. D.; Vaughan, A. D.; Byrne, M. E. *Journal of Molecular Recognition* **2012**, 25, (6), 361-369.
154. Hattori, K.; Hiwatari, M.; Iiyama, C.; Yoshimi, Y.; Kohori, F.; Sakai, K.; Piletsky, S. A. *Journal of Membrane Science* **2004**, 233, 169-173.
155. Wang, H.; Kobayashi, T.; Fujii, N. *Journal of Chemical Technology & Biotechnology* **1999**, 70, (4), 355-362.
156. Titirici, M.-M.; Sellergren, B. *Chemistry of Materials* **2006**, 18, (7), 1773-1779.
157. Xu, S.; Li, J.; Chen, L. *Talanta* **2011**, 85, (1), 282-289.
158. Wei, X.; Li, X.; Husson, S. *Biomacromolecules* **2005**, 6, (2), 1113-1121.
159. Zu, B.; Zhang, Y.; Guo, X.; Zhang, H. *Journal of Polymer Science Part A: Polymer Chemistry* **2010**, 48, (3), 532-541.
160. Vaughan, A.; Sizemore, S.; Byrne, M. *Polymer* **2007**, 48, (1), 74-81.
161. Li, J.; Zu, B.; Zhang, Y.; Guo, X.; Zhang, H. *Journal of Polymer Science Part A: Polymer Chemistry* **2010**, 48, (15), 3217-3228.
162. Wulff, G.; Chong, B. O.; Kolb, U. *Angewandte Chemie International Edition* **2006**, 45, (18), 2955-2958.
163. Subrahmanyam, S.; Guerreiro, A.; Poma, A.; Moczko, E.; Piletska, E.; Piletsky, S. *European Polymer Journal* **2013**, 49, (1), 100-105.
164. Lu, C. H.; Zhou, W. H.; Han, B.; Yang, H. H.; Chen, X.; Wang, X. R. *Analytical Chemistry* **2007**, 79, (14), 5457-5461.
165. Pan, G.; Zu, B.; Guo, X.; Zhang, Y.; Li, C.; Zhang, H. *Polymer* **2009**, 50, (13), 2819-2825.
166. Liu, H.; Zhuang, X.; Turson, M.; Zhang, M.; Dong, X. *Journal of separation science* **2008**, 31, (10), 1694-1701.
167. Gonzato, C.; Pasetto, P.; Bedoui, F.; Mazeran, P.-E.; Haupt, K. *Polymer Chemistry* **2014**, 5, (4), 1313-1322.
168. Sonntag, M.; Kreger, K.; Hanft, D.; Strohrriegl, P.; Setayesh, S.; de Leeuw, D. *Chemistry of Materials* **2005**, 17, (11), 3031-3039.
169. Blanco-López, M. C.; Lobo-Castañón, M. J.; Miranda-Ordieres, A. J.; Tuñón-Blanco, P. *TrAC Trends in Analytical Chemistry* **2004**, 23, (1), 36-48.
170. Hoshino, Y.; Kodama, T.; Okahata, Y.; Shea, K. *Journal of the American Chemical Society* **2008**, 130, (46), 15242-15243.
171. Matsui, J.; Akamatsu, K.; Hara, N.; Miyoshi, D.; Nawafune, H.; Tamaki, K.; Sugimoto, N. *Anal. Chem* **2005**, 77, (13), 4282-4285.
172. Izenberg, N. R.; Murray, G. M.; Pilato, R. S.; Baird, L. M.; Levin, S. M.; Van Houten, K. A. *Planetary and Space Science* **2009**, 57, (7), 846-853.
173. Southard, G. E.; Van Houten, K. A.; Murray, G. M. *Macromolecules* **2007**, 40, (5), 1395-1400.
174. Nakayama, T.; Yamagishi, T.; Sekine, S. I.; Yoshimi, Y. In *Star shaped molecularly imprinted polymer working as a drug carrier*, 2006 AIChE Annual Meeting, San Francisco, CA, 2006; San Francisco, CA, 2006.
175. Yoshimi, Y.; Nakayama, T.; Sekine, S. I.; Piletsky, S. A. In *Star shaped molecularly imprinted polymer*, 55th Society of Polymer Science Japan Symposium on Macromolecules, Toyama, 2006; Toyama, 2006; pp 5404-5405.

176. Ban, L.; Han, X.; Wang, X.-H.; Huang, Y.-P.; Liu, Z.-S. *Analytical and Bioanalytical Chemistry* **2013**, 405, (26), 8597-8605.
177. Piletska, E. V.; Guerreiro, A. n. R.; Whitcombe, M. J.; Piletsky, S. A. *Macromolecules* **2009**, 42, (14), 4921-4928.
178. Ishizu, K.; Ochi, K. *Macromolecules* **2006**, 39, (9), 3238-3244.
179. Yamada, S.; Wang, Z.; Mouri, E.; Yoshinaga, K. *Colloid & Polymer Science* **2009**, 287, (2), 139-146.
180. Dasgupta, P. K. *Journal of Chromatography A* **2008**, 1213, (1), 50-55.
181. Nikitas, P.; Pappa-Louisi, A.; Papageorgiou, A. *Journal of Chromatography A* **2001**, 912, (1), 13-29.
182. Caballero, R.; Garcia-Alvarez-Coque, M.; Baeza-Baeza, J. *Journal of Chromatography A* **2002**, 954, (1), 59-76.
183. Kong, H.; Ye, F.; Lu, X.; Guo, L.; Tian, J.; Xu, G. *Journal Of Chromatography A* **2005**, 1086, (1), 160-164.
184. Felinger, A. *Analytical Chemistry* **1994**, 66, (19), 3066-3072.
185. Maeder, M.; Neuhold, Y. M., *Practical Data Analysis in Chemistry*. Elsevier Science: 2007.
186. Yang, X. M.; Qiu, K. Y. *Journal of Macromolecular Science, Part A* **1997**, 34, (2), 315-325.
187. Qin, S.-H.; Qiu, K.-Y. *Journal of Polymer Science Part A: Polymer Chemistry* **2001**, 39, (9), 1450-1455.
188. Zaremskii, M. Y.; Olenin, A. V.; Garina, Y. S.; Kuchanov, S. I.; Golubev, V. B.; Kabanov, V. A. *Polymer Science U.S.S.R.* **1991**, 33, (10), 2036-2045.
189. Ivanov, A.; Antzutkin, O., Natural Abundance <sup>15</sup>N and <sup>13</sup>C CP/MAS NMR of Dialkyldithiocarbamate Compounds with Ni(II) and Zn(II). In *New Techniques in Solid-State NMR*, Klinowski, J., Ed. Springer Berlin Heidelberg: 2005; Vol. 246, pp 271-337.
190. Guan, Z.; DeSimone, J. *Macromolecules* **1994**, 27, (20), 5527-5532.
191. Kongkaewa, A.; Wootthikanokkhana, J. *Science Asia* **1999**, 25, (1), 35-41.
192. Kongkaew, A.; Wootthikanokkhan, J. *Journal of Applied Polymer Science* **2000**, 75, (7), 938-944.
193. Otsu, T.; Yamashita, K.; Tsuda, K. *Macromolecules* **1986**, 19, 287.
194. Kannurpatti, A. R.; Lu, S.; Bunker, G. M.; Bowman, C. N. *Macromolecules* **1996**, 29, (23), 7310-7315.
195. Quirk, R. P.; Lee, B. *Polymer International* **1992**, 27, (4), 359-367.
196. Liu, P.; Landry, E.; Ye, Z.; Joly, H.; Wang, W.-J.; Li, B.-G. *Macromolecules* **2011**, 44, (11), 4125-4139.
197. Simmons, M. R.; Yamasaki, E. N.; Patrickios, C. S. *Polymer* **2000**, 41, (24), 8523-8529.
198. Li, Z.-J.; Ren, H.-Y.; Cui, M.-C.; Deuther-Conrad, W.; Tang, R.-K.; Steinbach, J.; Brust, P.; Liu, B.-L.; Jia, H.-M. *Bioorganic & Medicinal Chemistry* **2011**, 19, (9), 2911-2917.
199. Wu, Y.; Shi, Y.; Fu, Z. *Polymer* **2005**, 46, (26), 12722-12728.
200. Fazeli, N.; Mohammadi, N.; Taromi, F. A. *Polymer Testing* **2004**, 23, (4), 431-435.
201. Zhang, C.; Miao, M.; Cao, X.; An, Z. *Polymer Chemistry* **2012**, 3, (9), 2656-2664.
202. Mayadunne, R. T. A.; Jeffery, J.; Moad, G.; Rizzardo, E. *Macromolecules* **2003**, 36, (5), 1505-1513.
203. Baussard, J.-F.; Habib-Jiwan, J.-L.; Laschewsky, A.; Mertoglu, M.; Storsberg, J. *Polymer* **2004**, 45, (11), 3615-3626.
204. Biasutti, J. D.; Davis, T. P.; Lucien, F. P.; Heuts, J. P. A. *Journal of Polymer Science Part A: Polymer Chemistry* **2005**, 43, (10), 2001-2012.

205. Ferguson, C. J.; Hughes, R. J.; Nguyen, D.; Pham, B. T. T.; Gilbert, R. G.; Serelis, A. K.; Such, C. H.; Hawkett, B. S. *Macromolecules* **2005**, *38*, (6), 2191-2204.
206. Zhang, H. *European Polymer Journal* **2013**, *49*, (3), 579-600.
207. Lin, I. C.; Liang, M.; Liu, T.-Y.; Jia, Z.; Monteiro, M. J.; Toth, I. *Bioorganic & Medicinal Chemistry* **2012**, *20*, (23), 6862-6869.
208. Tran, N. T. D.; Truong, N. P.; Gu, W.; Jia, Z.; Cooper, M. A.; Monteiro, M. J. *Biomacromolecules* **2013**, *14*, (2), 495-502.
209. Zayas, H. A.; Truong, N. P.; Valade, D.; Jia, Z.; Monteiro, M. J. *Polymer Chemistry* **2013**, *4*, (3), 592-599.
210. Urbani, C. N.; Monteiro, M. J. *Australian Journal of Chemistry* **2009**, *62*, (11), 1528-1532.
211. Skrabania, K.; Miasnikova, A.; Bivigou-Koumba, A. M.; Zehm, D.; Laschewsky, A. *Polymer Chemistry* **2011**, *2*, (9), 2074-2083.
212. Chen, M.; Moad, G.; Rizzardo, E. *Journal of Polymer Science Part A: Polymer Chemistry* **2009**, *47*, (23), 6704-6714.
213. Cauët, S. I.; Wooley, K. L. *Journal of Polymer Science Part A: Polymer Chemistry* **2010**, *48*, (12), 2517-2524.
214. Zammit, M. D.; Davis, T. P.; Willett, G. D.; O'Driscoll, K. F. *Journal of Polymer Science Part A: Polymer Chemistry* **1997**, *35*, (11), 2311-2321.
215. Zeng, J.; Zhu\*, J.; Zhang, Z.; Pan, X.; Zhang, W.; Cheng, Z.; Zhu\*, X. *Journal of Polymer Science Part A: Polymer Chemistry* **2012**, *50*, (11), 2211-2218.
216. Li, J.; Jiang, T.-T.; Shen, J.-n.; Ruan, H.-M. *Journal of Membrane and Separation Technology* **2012**, *1*, (2), 117-128.
217. Zhou, W.; Yu, W.; An, Z. *Polymer Chemistry* **2013**, *4*, (6), 1921-1931.
218. Qiu, Q.; Liu, G.; An, Z. *Chemical Communications* **2011**, *47*, (47), 12685-12687.
219. Adkins, C. T.; Harth, E. *Macromolecules* **2008**, *41*, (10), 3472-3480.
220. Gao, H.; Tsarevsky, N. V.; Matyjaszewski, K. *Macromolecules* **2005**, *38*, (14), 5995-6004.
221. Wiltshire, J. T.; Qiao, G. G. *Australian Journal of Chemistry* **2007**, *60*, (10), 699-705.
222. Wei, S.; Mizaikoff, B. *Journal of Separation Science* **2007**, *30*, (11), 1794-1805.
223. Turiel, E.; Tadeo, J. L.; Cormack, P. A. G.; Martin-Esteban, A. *Analytist* **2005**, *130*, (12), 1601-1607.
224. Rathbone, D. L. *Advanced Drug Delivery Reviews* **2005**, *57*, (12), 1854-1874.
225. Huang, X.; Zou, H.; Chen, X.; Luo, Q.; Kong, L. *Journal of Chromatography A* **2003**, *984*, (2), 273-282.
226. Sueyoshi, Y.; Fukushima, C.; Yoshikawa, M. *Journal of Membrane Science* **2010**, *357*, (1-2), 90-97.
227. Chronakis, I. S.; Jakob, A.; Hagström, B.; Ye, L. *Langmuir* **2006**, *22*, (21), 8960-8965.
228. Chen, P.-Y.; Vittal, R.; Nien, P.-C.; Liou, G.-S.; Ho, K.-C. *Talanta* **2010**, *80*, (3), 1145-1151.
229. Duffy, D. J.; Das, K.; Hsu, S. L.; Penelle, J.; Rotello, V. M.; Stidham, H. D. *Journal of the American Chemical Society* **2002**, *124*, (28), 8290-8296.
230. Dai, C.-m.; Geissen, S.-U.; Zhang, Y.-l.; Zhang, Y.-j.; Zhou, X.-f. *Environmental Pollution* **2011**, *159*, (6), 1660-1666.
231. Yoshimatsu, K.; Reimhult, K.; Krozer, A.; Mosbach, K.; Sode, K.; Ye, L. *Analytica Chimica Acta* **2007**, *584*, (1), 112-121.
232. Hirayama, K.; Sakai, Y.; Kameoka, K. *Journal of Applied Polymer Science* **2001**, *81*, (14), 3378-3387.
233. Tamayo, F. G.; Casillas, J. L.; Martin-Esteban, A. *Analytica Chimica Acta* **2003**, *482*, (2), 165-173.

234. Sambe, H.; Hoshina, K.; Moaddel, R.; Wainer, I. W.; Haginaka, J. *Journal of Chromatography A* **2006**, 1134, (1–2), 88-94.
235. Mayes, A. G.; Mosbach, K. *Analytical Chemistry* **1996**, 68, (21), 3769-3774.
236. Liu, X.; Chen, Z.; Zhao, R.; Shangguan, D.; Liu, G.; Chen, Y. *Talanta* **2007**, 71, (3), 1205-1210.
237. Long, Y.; Philip, J. Y. N.; Schillén, K.; Liu, F.; Ye, L. *Journal of Molecular Recognition* **2011**, 24, (4), 619-630.
238. Wang, A. R.; Zhu, S. *Polymer Engineering & Science* **2005**, 45, (5), 720-727.
239. Jiang, J.; Zhang, Y.; Guo, X.; Zhang, H. *RSC Advances* **2012**, 2, (13), 5651-5662.
240. Zhao, M.; Zhang, H.; Ma, F.; Zhang, Y.; Guo, X.; Zhang, H. *Journal of Polymer Science Part A: Polymer Chemistry* **2013**, 51, (9), 1983-1998.
241. Yang, L.; Fan, Z.; Wang, T.; Cai, W.; Yang, M.; Jiang, P.; Zhang, M.; Dong, X. *Analytical Letters* **2011**, 44, (16), 2617-2632.
242. Zu, B.; Pan, G.; Guo, X.; Zhang, Y.; Zhang, H. *Journal of Polymer Science Part A: Polymer Chemistry* **2009**, 47, (13), 3257-3270.
243. Johnstone, A. C.; Lea, R. A.; Brennan, K. A.; Schenk, S.; Kennedy, M. A.; Fitzmaurice, P. S. *Journal of Psychopharmacology* **2007**, 21, (8), 888-894.
244. Yeap, C.; Bian, C.; Abdullah, A. *Health Environ J* **2010**, 1, (2), 38-50.
245. Elliott, S.; Smith, C. *Journal of analytical toxicology* **2008**, 32, (2), 172-177.
246. O'Byrne, P. M.; Kavanagh, P. V.; McNamara, S. M.; Stokes, S. M. *Journal of Analytical Toxicology* **2013**, 37, (2), 64-73.
247. Bell, C.; George, C.; Kicman, A. T.; Traynor, A. *Drug Testing and Analysis* **2011**, 3, (7-8), 496-504.
248. de Boer, D.; Bosman, I. J.; Hidvégi, E.; Manzoni, C.; Benkő, A. A.; dos Reys, L. J. A. L.; Maes, R. A. A. *Forensic science international* **2001**, 121, (1–2), 47-56.
249. Loeliger, J. R.; Witkowski, M. R. *J Forensic Sci* **2005**, 50, (2).
250. Wada, M.; Yamahara, K.; Ikeda, R.; Kikura-Hanajiri, R.; Kuroda, N.; Nakashima, K. *Biomedical Chromatography* **2012**, 26, (1), 21-25.
251. Waite, R. J.; Barbante, G. J.; Barnett, N. W.; Zammit, E. M.; Francis, P. S. *Talanta* **2013**, 116, 1067-1072.
252. Nikolova, I.; Danchev, N. *BIOTECHNOLOGY AND BIOTECHNOLOGICAL EQUIPMENT* **2008**, 22, (2), 652.
253. Elliott, S. *Drug Testing and Analysis* **2011**, 3, (7-8), 430-438.
254. Dickert, F. L.; Hayden, O. *Fresenius' journal of analytical chemistry* **1999**, 364, (6), 506-511.
255. Shimizu, K. D.; Stephenson, C. J. *Current Opinion in Chemical Biology* **2010**, 14, (6), 743-750.
256. McCluskey, A.; Holdsworth, C. I.; Bowyer, M. C. *Organic & Biomolecular Chemistry* **2007**, 5, (20), 3233-3244.
257. Wright, K. Towards the development of a benzylpiperazine specific molecular imprinted polymer. PhD Thesis, The University of Newcastle, 2010.
258. Pap, T. m.; Horvai, G. *Journal of Chromatography A* **2004**, 1034, (1–2), 99-107.
259. Rosenbaum, S. E., *Basic pharmacokinetics and pharmacodynamics: An integrated textbook and computer simulations*. John Wiley & Sons: 2011.
260. Schwarz, L.; Bowyer, M. C.; Holdsworth, C. I.; McCluskey, A. *Australian journal of chemistry* **2006**, 59, (2), 129-134.
261. Kemmer, G.; Keller, S. *Nat. Protocols* **2010**, 5, (2), 267-281.
262. Bai, F.; Yang, X.; Li, R.; Huang, B.; Huang, W. *Polymer* **2006**, 47, (16), 5775-5784.

263. Gonçalves, L.; Filho, J. D. N.; Guimarães, J. G. A.; Poskus, L. T.; Silva, E. M. *Journal of Biomedical Materials Research Part B: Applied Biomaterials* **2008**, 85B, (2), 320-325.
264. Cormack, P. A. G.; Elorza, A. Z. *Journal of Chromatography B* **2004**, 804, (1), 173-182.
265. Li, W.; Li, S., Molecular imprinting: A versatile tool for separation, sensors and catalysis. In *Oligomers-Polymer Composites-Molecular Imprinting*, Springer: 2007; pp 191-210.
266. Lanza, F.; Sellergren, B. *Analytical Chemistry* **1999**, 71, (11), 2092-2096.
267. Sellergren, B. *Die Makromolekulare Chemie* **1989**, 190, (11), 2703-2711.
268. Zander, Å.; Findlay, P.; Renner, T.; Sellergren, B.; Swietlow, A. *Analytical Chemistry* **1998**, 70, (15), 3304-3314.
269. Socrates, G.; Socrates, G., *Infrared and Raman characteristic group frequencies: tables and charts*. Wiley Chichester: 2001.
270. Petroski, J.; El-Sayed, M. A. *The Journal of Physical Chemistry A* **2003**, 107, (40), 8371-8375.
271. Pandiarajan, S.; Umadevi, M.; Rajaram, R. K.; Ramakrishnan, V. *Spectrochimica Acta Part A: Molecular and Biomolecular Spectroscopy* **2005**, 62, (1-3), 630-636.
272. Kuptsov, A. H.; Zhizhin, G. N., *Handbook of Fourier Transform Raman and Infrared Spectra of Polymers*. Elsevier.
273. Krishnakumar, V.; Seshadri, S. *Spectrochimica Acta - Part A: Molecular and Biomolecular Spectroscopy* **2007**, 68, (3), 833-838.
274. Kawaguchi, M.; Hayatsu, Y.; Nakata, H.; Ishii, Y.; Ito, R.; Saito, K.; Nakazawa, H. *Analytica Chimica Acta* **2005**, 539, (1-2), 83-89.
275. Spivak, D. A. *Advanced Drug Delivery Reviews* **2005**, 57, (12), 1779-1794.
276. Pichon, V.; Chapuis-Hugon, F. *Analytica Chimica Acta* **2008**, 622, (1-2), 48-61.
277. Dong, W.; Yan, M.; Liu, Z.; Wu, G.; Li, Y. *Separation and Purification Technology* **2007**, 53, (2), 183-188.
278. Bai, F.; Yang, X.; Huang, W. *European Polymer Journal* **2006**, 42, (9), 2088-2097.
279. Ye, L.; Weiss, R.; Mosbach, K. *Macromolecules* **2000**, 33, (22), 8239-8245.
280. Ha, M.; Lee, K.; Choe, S. *Polymer* **2008**, 49, (21), 4592-4601.
281. Shim, S. E.; Yang, S.; Choi, H. H.; Choe, S. *Journal of Polymer Science Part A: Polymer Chemistry* **2004**, 42, (4), 835-845.
282. Perrier-Cornet, R.; Héroguez, V.; Thienpont, A.; Babot, O.; Toupance, T. *Journal of Chromatography A* **2008**, 1179, (1), 2-8.
283. Sellergren, B.; Rückert, B.; Hall, A. J. *Advanced Materials* **2002**, 14, (17), 1204-1208.
284. Li, W.-H.; Stöver, H. D. H. *Journal of Polymer Science Part A: Polymer Chemistry* **1998**, 36, (10), 1543-1551.
285. Li, W.-H.; Li, K.; Stöver, H. D. H. *Journal of Polymer Science Part A: Polymer Chemistry* **1999**, 37, (14), 2295-2303.
286. Downey, J. S.; Mclsaac, G.; Frank, R. S.; Stöver, H. D. H. *Macromolecules* **2001**, 34, (13), 4534-4541.
287. Downey, J. S.; Frank, R. S.; Li, W.-H.; Stöver, H. D. H. *Macromolecules* **1999**, 32, (9), 2838-2844.
288. Baggiani, C.; Giraudi, G.; Giovannoli, C.; Tozzi, C.; Anfossi, L. *Analytica Chimica Acta* **2004**, 504, (1), 43-52.
289. Chen, Z.; Ye, L. *Journal of Molecular Recognition* **2012**, 25, (6), 370-376.
290. Yang, S.; Shim, S. E.; Lee, H.; Kim, G. P.; Choe, S. *Macromolecular Research* **2004**, 12, (5), 519-527.
291. Abouzarzadeh, A.; Forouzani, M.; Jahanshahi, M.; Bahramifar, N. *Journal of Molecular Recognition* **2012**, 25, (7), 404-413.

292. Jiang, M.; Zhang, J.-h.; Mei, S.-r.; Shi, Y.; Zou, L.-j.; Zhu, Y.-x.; Dai, K.; Lu, B. *Journal of Chromatography A* **2006**, 1110, (1–2), 27-34.
293. Fang, L.; Chen, S.; Zhang, Y.; Zhang, H. *Journal of Materials Chemistry* **2011**, 21, (7), 2320-2329.
294. Esfandyari-Manesh, M.; Javanbakht, M.; Atyabi, F.; Badiei, A.; Dinarvand, R. *Journal of Applied Polymer Science* **2011**, 121, (2), 1118-1126.
295. Garcia-Calzon, J.; Diaz-Garcia, M. *Sensors and Actuators B: Chemical* **2007**, 123, (2), 1180-1194.
296. Kim, H.; Kaczmarski, K.; Guiochon, G. *Chemical Engineering Science* **2006**, 61, (4), 1122-1137.
297. Okutucu, B.; Telefoncu, A. *Talanta* **2008**, 76, (5), 1153-1158.
298. Wang, J.; Guo, R.; Chen, J.; Zhang, Q.; Liang, X. *Analytica Chimica Acta* **2005**, 540, (2), 307-315.
299. Yang, Y.; Liu, X.; Guo, M.; Li, S.; Liu, W.; Xu, B. *Colloids and Surfaces A: Physicochemical and Engineering Aspects* **2011**, 377, (1–3), 379-385.
300. Ken, D. S., Binding Isotherms. In *Molecularly Imprinted Materials*, CRC Press: 2004; pp 419-433.
301. Guiochon, G.; Shirazi, D. G.; Felinger, A.; Katti, A. M., *Fundamentals of preparative and nonlinear chromatography*. Academic Press: 2006.
302. Cela-Pérez, M.; Castro-López, M.; Lasagabáster-Latorre, A.; López-Vilariño, J.; González-Rodríguez, M.; Barral-Losada, L. *Analytica chimica acta* **2011**, 706, (2), 275-284.
303. Umpleby li, R. J.; Baxter, S. C.; Rampey, A. M.; Rushton, G. T.; Chen, Y.; Shimizu, K. D. *Journal of Chromatography B* **2004**, 804, (1), 141-149.
304. Watabe, Y.; Hosoya, K.; Tanaka, N.; Kubo, T.; Kondo, T.; Morita, M. *Journal of Chromatography A* **2005**, 1073, (1–2), 363-370.
305. Umpleby, R. J.; Rushton, G. T.; Shah, R. N.; Rampey, A. M.; Bradshaw, J. C.; Berch, J. K.; Shimizu, K. D. *Macromolecules* **2001**, 34, (24), 8446-8452.
306. Muggli, D. S.; Burkoth, A. K.; Keyser, S. A.; Lee, H. R.; Anseth, K. S. *Macromolecules* **1998**, 31, (13), 4120-4125.
307. Allender, C. J.; Brain, K. R.; Heard, C. M. *Chirality* **1997**, 9, (3), 233-237.
308. He, J.-f.; Zhu, Q.-h.; Deng, Q.-y. *Spectrochimica Acta Part A: Molecular and Biomolecular Spectroscopy* **2007**, 67, (5), 1297-1305.
309. Haginaka, J.; Sanbe, H. *Journal of Chromatography A* **2001**, 913, (1), 141-146.
310. Holland, N.; Duggan, P.; Owens, E.; Cummins, W.; Frisby, J.; Hughes, H.; McLoughlin, P. *Analytical and Bioanalytical Chemistry* **2008**, 391, (4), 1245-1253.
311. Joshi, V. P.; Karmalkar, R. N.; Kulkarni, M. G.; Mashelkar, R. A. *Industrial & Engineering Chemistry Research* **1999**, 38, (11), 4417-4423.
312. Dong, C.; Li, X.; Guo, Z.; Qi, J. *Analytica Chimica Acta* **2009**, 647, (1), 117-124.
313. Yu, C.; Mosbach, K. *Journal of Chromatography A* **2000**, 888, (1-2), 63-72.
314. Spivak, D.; Gilmore, M. A.; Shea, K. J. *Journal of the American Chemical Society* **1997**, 119, (19), 4388-4393.
315. Turner, N. W.; Piletska, E. V.; Karim, K.; Whitcombe, M.; Malecha, M.; Magan, N.; Baggiani, C.; Piletsky, S. A. *Biosensors and Bioelectronics* **2004**, 20, (6), 1060-1067.
316. Yonker, C. R.; Zwier, T. A.; Burke, M. F. *Journal of Chromatography A* **1982**, 241, (2), 269-280.
317. Sellergren, B.; Shea, K. J. *Journal of Chromatography A* **1993**, 635, (1), 31-49.
318. Pascual, S.; Urbani, C. N.; Monteiro, M. J. *Macromolecular Reaction Engineering* **2010**, 4, (3-4), 257-263.

319. Sebakhy, K. O.; Kessel, S.; Monteiro, M. J. *Macromolecules (Washington, DC, U. S.)* **2010**, *43*, (Copyright (C) 2011 American Chemical Society (ACS). All Rights Reserved.), 9598-9600.
320. Jiang, J.; Zhang, Y.; Guo, X.; Zhang, H. *Macromolecules* **2011**, *44*, (15), 5893-5904.
321. Li, K.; Stöver, H. D. H. *Journal of Polymer Science Part A: Polymer Chemistry* **1993**, *31*, (13), 3257-3263.
322. Bonini, F.; Piletsky, S.; Turner, A. P. F.; Speghini, A.; Bossi, A. *Biosensors and Bioelectronics* **2007**, *22*, (9-10), 2322-2328.
323. Eun Shim, S.; Yang, S.; Choe, S. *Journal of Polymer Science Part A: Polymer Chemistry* **2004**, *42*, (16), 3967-3974.
324. Wang, H. Y.; Jiang, J. G.; Ma, L. Y.; Pang, Y. L. *Reactive and Functional Polymers* **2005**, *64*, (2), 119-126.
325. Li, P.; Rong, F.; Yuan, C. *Polymer International* **2003**, *52*, (12), 1799-1806.
326. Yan, Q.; Bai, Y.; Meng, Z.; Yang, W. *The Journal of Physical Chemistry B* **2008**, *112*, (23), 6914-6922.
327. Ansell, R. J.; Mosbach, K. *Journal of Chromatography A* **1997**, *787*, (1-2), 55-66.
328. Lu, Y.; Li, C.; Wang, X.; Sun, P.; Xing, X. *Journal of Chromatography B* **2004**, *804*, (1), 53-59.
329. Jin, Y.; Jiang, M.; Shi, Y.; Lin, Y.; Peng, Y.; Dai, K.; Lu, B. *Analytica chimica acta* **2008**, *612*, (1), 105-113.
330. Cheong, S. H.; McNiven, S.; Rachkov, A.; Levi, R.; Yano, K.; Karube, I. *Macromolecules* **1997**, *30*, (5), 1317-1322.
331. Navarro-Villoslada, F.; Vicente, B. S.; Moreno-Bondi, M. a. C. *Analytica Chimica Acta* **2004**, *504*, (1), 149-162.
332. Verma, A.; Murray, G. M. *Journal of Functional Biomaterials* *3*, (1), 1-22.
333. Liao, Y.; Wang, W.; Wang, B. *Bioorganic Chemistry* **1998**, *26*, (6), 309-322.
334. Kricheldorf, H. R.; Stoeber, O.; Luebbers, D. *Macromolecules* **1995**, *28*, (7), 2118-2123.
335. Heise, A.; Diamanti, S.; Hedrick, J. L.; Frank, C. W.; Miller, R. D. *Macromolecules* **2001**, *34*, (11), 3798-3801.
336. Roy, D.; Guthrie, J. T.; Perrier, S. *Macromolecules* **2005**, *38*, (25), 10363-10372.
337. Zhao, Y.-H.; Qian, Y.-L.; Pang, D.-X.; Zhu, B.-K.; Xu, Y.-Y. *Journal of Membrane Science* **2007**, *304*, (1-2), 138-147.
338. Liu, F.; Urban, M. W. *Progress in Polymer Science* **2010**, *35*, (1-2), 3-23.